Doctoral Thesis

Development and Application of Magnetically Controlled Optical Chemical Sensors

Günter Mistlberger

2010

Zur Erlangung des akademischen Grades
"Doktor der technischen Wissenschaften"
eingereicht an der

Technischen Universität Graz

Supervisor

Univ.-Prof. Dipl.-Chem. Dr.rer.nat. Ingo Klimant
Institute of Analytical Chemistry and Food Chemistry
Graz University of Technology

It is the tension between creativity and skepticism
that has produced the stunning and unexpected findings of science.

Carl Sagan

Statutory Declaration

I declare that I have authored this thesis independently, that I have not used other than the declared sources / resources, and that I have explicitly marked all material which has been quoted either literally or by content from the used sources.

Graz, April 20, 2010

Date

Signature

Acknowledgement

Now as the time to leave Graz is approaching faster than I am comfortable with, I would like to thank all people who helped to make the time truly unforgetable.

First of all, I would like to thank my supervisor Prof. Ingo Klimant. Ingo, you were inspiring and encouraging me but also cautious when I needed it. Working with you was a great pleasure and I will probably feed my whole scientific carrier on the things you taught me during this thesis.

A big "thank-you" also goes to the whole sensors group. You are all responsible for the fact that I have big troubles to imagine how it will be to work without you. In the working group, the "chemistry" was just perfect and I feel honored that I got the chance to spend time with everybody, both during and after work. I am especially thankful for the best diploma-students I can think of, Klaus, Daniel, Lisi and Birgit. Although I was far away from being a perfect supervisor, you always supported me with your enthusiasm whenever things worked out well and your casualness whenever things didn't work. The latter statement might not be entirely true but hopefully true enough for you to continue the great job you did! Klaus, you were my first victim and you had to carry out a lot of work I was unable to do because of my ambitious conference schedule. I greatly acknowledge your contribution to this work and also your social and "networking-oriented" life-style I often appreciated after work. Also a big thank-you to Birgit for willingly performing oxygen imaging experiments and especially for the nice conversations during the breaks. I was always desperately waiting for them. And, before I forget it, thanks for the great lasagne last Sunday. Daniel, you impressed me with your general and scientific knowledge as well as with your persistence when all the things I suggested just didn't work out they way they should. You did a great job! And finally Lisi, a big thank-you for the great discussions after work and for always having a smile on your lips, no matter how hopeless the scientific situation was which I lead you in to. You were also responsible for giving me back my faith into reproducibility of nanoprecipitations by helping me to perform hundreds of them. I would also like to thank Torsten for the numerous scientific discussions and the daily crash-course on bavarian swear-words, and Sergey for developing and providing the best sensor material in the world in exactly sufficient quanteties. Thanks also to Gunter, Kerstin and Wernfried for giving me such a warm welcome when I joined the group. Also thanks to the rest of the group: Tobi for cooking good food and for avoiding garlic from Sunday to Friday, Fabian for letting me win so often when we played squash together, Babsi N. for the nice "good morning" every day, Babsi E. for not forgetting to tell me whenever it was incredibly hot in our office and Spela, for always being interested in how things go in my life.

A special thank-you also to Herbert and Eveline. You always got the things done promptly. Eveline, you were a great person to ask for things that I never believed in being accomplished. You always knew the right people, the right stories and the perfect timing. Thanks for that.

During my thesis I was also working with people from other universities and I had a great time with all the cooperation partners abroad. I would like to thank Michael Kühl, Marc Staal and Lars Rickelt from the University of Copenhagen, where I performed oxygen imaging experiments on biofilms and aquatic microorganisms. To Jorge, Antonio, Angel and all the other members of the Department of Analytical Chemistry at the University of Granada: I had an incredible time in Granada because of you and I am very thankful for the nice welcome and fair-well you gave me! Finally, I would like to thank Eric Bakker and the people of his group (Ewa, Marcin, Debbie and Pengchao) for giving me such a nice time in Perth, both scientifically and by introducing me to the city and the nightlife of Perth.

The most intensive cooperation was, however, with the Institute for Electronmicroscopy. Thanks to Prof. Ferdinand Hofer, Dr. Peter Pölt and especially Dr. Armin Zankel for spending hours with me in the cellar looking at "Marillenknödel", as Armin used to call nano-MOSePs.

I am also especially greatful for all the friends that walked with me through the good times but didn't leave me in tough times. I would like to express my special thanks to Ute for never saying no to anything, to Sabine, for your nice presents and for loving Felix so much, and to Mango for the never ending, almost ruminant discussions on all kinds of topics including science. Thank you also for helping me with putting together the "flipper-device". I also would like to thank my friends in Bad Wimsbach, my home-village. It is good to know that we are still friends, although I seldomly find my way to the other side of the Alps.

A big thank-you also to my parents and my brother Gerald. It is always nice to come home and feel home because of your friendly and welcoming nature. Thank you also for the countless hours you spent working on our apartment, while I was sitting in Graz working on my thesis. I would also like to thank my (up-coming) parents in law, Grete and Walter for the nice Sundays in your house and all the other things you do to make Beate's and my life easier.

Finally, I am struggling for words when it comes to express my deep greatfulness for the love of my life, Beate. Thank you for completing my life the way you do. Also a big thank you to you, little Felix. You are the only person in the world that has a smile which makes me wake up happily every morning, even after just two hours of sleep.

Graz, April 20, 2010

Abstract

Monitoring metabolic parameters such as pH and oxygen is crucial for maintaining productive bioprocesses and for gaining knowledge about biological processes. For this purpose, optical sensors represent an attractive alternative to conventional, mostly electrochemical sensors. They are cheap, robust and easy to miniaturize. In this thesis, the concept of optical sensors was enhanced by equipping them with magnetic properties. Such magnetic sensors respond to a magnetic field and are therefore controllable and can be guided to a desired place. Moreover, they can be easily separated after usage. We report on the production of magnetic optical sensor systems with sizes ranging from 50 nm up to 5 mm. While the largest sensors were developed as remote-controlled, easy to use optical sensors for bioprocess monitoring and as quickly exchangeable sensor caps for dip-probes, particles in the micrometer range can also be used in smaller cavities and, to a limited extend, for imaging applications. Even smaller magnetic sensor particles with sizes around 100 nm were developed as multifunctional tools for imaging purposes and as platform for nanotherapeutics. The versatile matrix material with a mainly hydrophobic core and functional hydrophilic carboxyl groups on the shell enabled the modification with photosensitizers, optical sensors, polyelectrolytes, enzymes and stimuli responsive polymers. Finally, a review article outlines recent advances in the field of luminescent magnetic particles.

Keywords: magnetic optical sensor particles, oxygen sensor, imaging, drug targeting, bioprocess monitoring

Kurzfassung

Die kontinuierliche Messung von metabolischen Parametern, wie Sauerstoffkonzentration und pH-Wert ist unumgänglich für die Aufrechterhaltung effizienter Bioprozesse und für das bessere Verständnis von biologischen Vorgängen. Für diese Anwendungen stellen optische Sensoren eine attraktive Alternative zu konventionellen, meist elektrochemischen Sensoren dar. Optische Sensoren sind kostengünstig, robust und miniaturisierbar. Das Konzept von optischen Sensoren wurde durch die Ausstattung mit magnetischen Eigenschaften weiter verbessert. Magnetische optische Sensoren können in einem magnetischen Feld kontrolliert und positioniert werden. Darüberhinaus ist ihre Abtrennung nach erfolgter Messung einfach erreichbar. Magnetische Sensorpartikel im Größenbereich von 50 nm bis 5 mm wurden hergestellt, charakterisiert, und deren Anwendung wurde für die Messung von biologisch relevanten Parametern erprobt. Magnetische, optische Sensor-Kugeln zeigten sich nützlich als magnetisch-ferngesteuerte Sensoren für die Kontrolle von Bioprozessen. Magnetische Mikrosensoren konnten ebenfalls für die Kontrolle von Bioprozessen eingesetzt werden, erlaubten aber auch die Messung in engen Kavitäten und die Messung von Analytkonzentrationen auf Oberflächen von biologischen Materialien. Bildgebende Verfahren mit höherer Auflösung ließen sich mit magnetischen Sensorpartikeln im unteren Nanometerbereich (~ 100 nm) verwirklichen. Diese Partikel waren aufgrund ihrer einzigartigen Matrixeigenschaften auch für die Verwendung als multifunktionelles Werkzeug für Forschung und Medizin geeignet. Der hydrophobe Kern der Partikel wurde neben optischen Sensoren auch noch mit Singulettsauerstoff produzierenden Farbstoffen und einer Lichtsammelkaskade ausgestattet. Funktionelle Carboxylgruppen an der Oberfläche erlaubten die weitere Modifikation mit Luminophoren, Polyelektrolyten, Enzymen und Polymeren, die in Abhängigkeit von Umgebungsbedingungen wie Temperatur und pH-Wert ihre Ausdehnung ändern. Schlussendlich wurde ein Review-Artikel über lumineszente magnetische Partikel verfasst.

Stichwörter: Magnetische optische Sensorpartikel, Sauerstoffsensor, bildgebende Verfahren, gezielte Wirkstoff-Freisetzung, Bioprozesskontrolle

Contents

Part I

Introduction

1 Scope and outline of the thesis

Optical sensor particles equipped with a magnetic component have several attractive characteristics. Their position can be magnetically controlled and they might act as contrast agents for multimodal, medical imaging techniques. While optical sensor particles were known for a long time, the combination with magnetic compounds to form magnetic optical sensor particles (MOSePs) was new. In the beginning the main focus was put on the development of magnetically separable sensor particles for bioprocess monitoring. Such sensors can be merely added to a fermentation medium, collected at a vessel's wall by a magnetic separator and read-out with a fiber optical device. In this way, the advantages of dispersed sensor particles and fixed sensor spots are combined.

For the optimized separation of MOSePs at the sidewall, magnetic separators with an optical window were designed (chapter 3 on page 53). Magnetic field simulations revealed the construction of radially magnetized rings to be the ideal device for directing MOSePs towards the tip of an optical fiber. Due to the fact that conventional magnetization procedures are difficult to apply for the production of such rings, we developed simple separators that worked similarly but did not require special magnetization devices. Such separators collected MOSePs efficiently in the field of view of an optical fiber, which enabled sensing at ultra low particle concentration (chapter 4 on page 69).

In this thesis, magnetic sensor systems for sizes from $\sim 50\,\mathrm{nm}$ to $5\,\mathrm{mm}$ are described. The first MOSePs were sythesized *via* a bulk or emulsion polymerization in a Sol-Gel process (chapters 3 on page 53 and 4 on page 69). These sensors had sizes of $1-50\,\mu\mathrm{m}$ and were applied for monitoring dissolved oxygen in aqueous media. Later, spray-drying was used for the production of highly porous, organic polymer based MOSePs (section 4.3.3 on page 77). The incorporation of ultrabright oxygen optodes in the porous copolymer matrix yielded oxygen sensors with excellent brightness and dynamic range. Such sensors showed almost linear Stern-Volmer plots from $pO_2 = 0-1000\,\mathrm{hPa}$. Our first suspicion that spray-dried particles are hollow was confirmed by an extensive electron microscopy study in cooperation with the Institute for Electronmicroscopy, Graz University of Technology (chapter 5 on page 83). *In situ* ultra microtomy together with TEM and SEM images revealed the dimensions and porousity of the particles. Furthermore, the inorganic inclusions were visualized in material contrast images.

The applicability of the elaborated principles for other sensor systems was demonstrated in cooperation with the University of Granada. Together with Dr. Jorge F. Fernandez-Sanchez and Antonio L. Medina-Castillo from the Institute of Analytical Chemistry we developed magnetic molecular imprinted microparticles which can be used as optical sensors for fluorene, a model substance for polycyclic aromatic hydrocarbons (see also chapter 6 on page 95). The incorporation of magnetic nanoparticles was more complex than in plain optical sensors, because magnetic nanoparticles can influence the formation of binding sites, and because the luminescence intensity of the analyte is usually much weaker

than the luminescence of a distinct luminophore used for optical sensors. However, the final products simplified the measurement setup and a filtration cuvette plus a peristaltic pump were exchangeable for a simple fiber optical device. The versatility of molecular imprinting for the formation of specific recognition sites together with the simplified handling of magnetic particles might pave the way towards small, mobile devices for various bioanalytical applications.

In addition to the fact that we demonstrated the suitability of micrometer sized MOSePs for analyte monitoring at different scales, we aimed for a further optimization of their applicability for bioprocess monitoring. Further increasing the size of the sensors from micrometers to millimeters significantly improved magnetic retention strength, the signal intensity and the time required for capturing the sensor. Other aspects generally referred to as "handling" were also improved. We produced such magnetic sensor macrospheres (MagSeMacs) by spray-coating stainless steel spheres with a thin layer of a sensor cocktail (chapter 7 on page 115). In principle, such spheres are compatible with the sensor chemistry and read-out technology originally developed for sensor spots. MagSeMacs were applied for monitoring analyte concentrations in stirred liquids, rotating flasks, plug-flow reactors and 24-well plates. Furthermore, special magnetic separators were designed that enable the application of MagSeMacs as disposable, quickly exchangeable sensor caps for dip-probe type, optical fiber sensors.

Although MOSePs in the micrometer range are very attractive tools for monitoring analytes in bioprocesses, their applicability for analyte imaging with high spatial resolution is limited. The relatively large macrosizes of the particles negate imaging of small cavities in biological samples or the penetration into dense biological materials. Moreover, uniform film-formation on sample surfaces cannot be achieved. For this application, particles with sizes significantly smaller than the resolution of a luminescence microscope ($\sim 1\,\mu m$) are required.

We employed a nanoprecipitation method for the production of spherical MOSePs with sizes smaller than 500 nm (see also chapter 8 on page 131). The average sizes were tunable between 50 – 180 nm with a relatively narrow size distribution. After we demonstrated the basic oxygen sensing functionality, further modifications were introduced and studied in detail. The core was modified with a singlet oxygen producing trace oxygen sensor or a light harvesting cascade. The first yielded particles potentially suitable for simultaneous oxygen monitoring and photodynamic therapy. The latter increased the brightness of the optical sensor and enabled the excitation of the sensor with blue LEDs, which are known as one of the brightest currently available LEDs. The matrix material used for the MOSePs was an amphiphilic material that provided carboxyl groups at the surface of the final particles. These carboxyl groups ensured highly stable aqueous dispersions, but also enabled surface modifications for the introduction of further functionalities. The surface was modified with functional luminophores, polyelectrolytes, enzymes and stimuli responsive polymers.

Finally, a review article provides an overview of the versatile concept of luminescent magnetic particles and also represents an extended introduction of this thesis. Recent advances regarding applications of luminescent magnetic particles in different fields of science are discussed. Additionally, this review summarizes synthetic routes, the main components and resulting particle structures.

2 Luminescent Magnetic Particles: Multimodal imaging (Luminescence and MRI) and Analytical Applications

This chapter was prepared as a *Review Article* for the journal

Bioanalytical Reviews.

Authors:

Günter Mistlberger* and Ingo Klimant

Abstract Luminescent magnetic particles (LuMaPs) are attractive tools for life science applications such as multimodal imaging, analyte monitoring, nanotherapeutics and combinations thereof. LuMaPs consist of at least one magnetic and one luminescent component, which often are embedded in a matrix. A large variety of compounds exist for all three components of LuMaPs, however, a smart selection and combination is required for achieving useful tools. While the magnetic component mainly influences the response to a magnetic field, the luminophore can act as label, sensor or therapeutic agent. The matrix fulfills various tasks, such as stabilizing the embedded luminophore and magnetic compound, carrying useful functional groups on the surface and hosting smart drug delivery systems. Finally, surface modifications with, for instance, targeting ligands can greatly improve the suitability of LuMaPs for biomedical applications. Synthetic approaches towards LuMaPs are manifold and are often based on standard techniques. This review provides an overview of LuMaPs' components and structures. Moreover, routes towards LuMaPs are outlined, and potential as well as recently published applications are discussed.

2.1 Introduction

Magnetic particles are known for a long time and have been frequently used for life science applications including medical imaging and targeted therapy, but also for capturing pollutants from environmental samples. The final purpose determines the properties of a suitable particle. The particle size, for example, plays a crucial role for the separability or biocompatibility. While large magnetic particles can be quickly separated in an inhomogeneous magnetic field, magnetic nanoparticles might never separate from a dispersion and build a magnetic fluid, instead. Such small particles are, on the other hand, suitable for imaging applications where a homogeneous distribution of the contrast agent

in the tissue or biocompartment is highly desirable.

In particle technology, research focusing on combining magnetic properties with luminescence rapidly developed in recent years. Approximately two third of the articles on this topic were published from 2007 to 2010 and the number of new publications has increased every year. The possibility of controlling a luminescent reporter or label by a magnetic field attracted the interest of many research groups. Nowadays, the magnetic property of commercially available LuMaPs-products is simply used for magnetic separation, whereas in medical research the main focus is currently put on the development of multifunctional magnetic imaging probes and nanotherapeutics. Such tools can increase the contrast in MRI imaging during pre-operative diagnostics and enable real-time interoperative assistance for the surgeon by luminescence labeling. Moreover, LuMaPs can have a nanotherapeutic function such as heat generation for hyperthermia, singlet oxygen production for photodynamic therapy or targeted drug delivery to the affected tissue.

Recently, an optical chemical sensor function was included into LuMaPs. Currently, such tools are used for monitoring metabolic parameters in bioprocesses. However, with the availability of smaller particles biomedical applications might soon become more important. In any way, such multifunctional LuMaPs represent a significant step towards the ultimate medical nanoplatform with the following functions. It should be a contrast agent for MRI imaging, a label for luminescent imaging and a therapeutic agent. The latter can be achieved by generating heat, by releasing a drug or by producing toxic substances with light. Furthermore, such multifunctional particles should enable a magnetic enrichment in the tissue of interest. The targeting effect should be further improved by immunological interaction with cells in the affected tissue. Finally, the response of the organism to, for instance, a delivered drug should be monitored by an incorporate optical sensor. In reality, such an allrounder might never be available. The complexity of the system and potential cross-influences of the separate components might prevent a possible combination of all these functionalities into a single particle. Nevertheless, the realization of some functionalities in dedicated systems might allow the combined application without the necessity to have a single biomedical allrounder. Finally, the opposite size dependency of properties such as strong magnetic response and good tissue penetration negates the production of one perfect tool for all applications.

As a matter of fact, most LuMaPs developed nowadays are specialized for certain applications and do not claim the universal applicability. Fine-tuning properties *via* synthetic parameters and a careful selection of surface modifications are two crucial factors for making LuMaPs fit for their final purpose.

2.2 Components of luminescent magnetic particles (LuMaPs)

The type, structure and properties of the most important components of LuMaPs are discussed, namely the magnetic components, the luminescent components and the different matrix materials for LuMaPs. These compounds influence the LuMaPs' properties and a careful selection is crucial for achieving particles which are fit for their final purpose. Furthermore, optional but common modifications of LuMaPs are addressed. Exemplary structures of LuMaPs and the corresponding references are presented in table 2.1 and in

the figures 2.1–2.4.[a]

Table 2.1: Short description and references of the possible structures of LuMaPs depicted in the figures 2.1–2.4 on the following pages. The numbers of the structures are the same in the table and in the figures.

No.	Description	References
1	Homogeneous distribution of luminescent dyes or nanocrystals and magnetic nanoparticles.	1–29
2	Crosslinking of luminescent and magnetic nanoparticles.	30,31
3	Coating of LuMaPs with a reflective metal layer on one hemisphere.	32–35
4	LuMaPs coated with an extra matrix layer.	5,21,31,36–42
5	Luminescent dyes fixed to the magnetic core and protected with an extra matrix layer.	37
6	Magnetite doped inorganic phosphor as core with a protective matrix shell.	38,39
7	Manganese doped QDs which are magnetic and luminescent.	41
8	Heterodimer of MNP and QD coated with protective matrix shell.	43
9	Dyes or QDs directly adsorbed or covalently attached to a magnetic core.	44,45
10	Dyes or QDs covalently attached to a magnetic core with a linker.	46,47
11	Direct coating of a magnetic core with an inorganic luminescent shell.	48–50
12	Direct coating of a magnetic core with an inorganic luminescent shell and a protective matrix layer.	51,52
13	Coating of a magnetic core with a luminescent dendrimer.	53
14	Encapsulation of LuMaPs in a stimuli responsive matrix polymer.	54
15	Magnetic core in a matrix shell covalently modified with a luminescent moiety through a linker.	55–58
16	Magnetic core in a matrix shell directly coated with a luminescent moiety.	54,59–67
17	Magnetic particles in a matrix core, covalently modified with luminescent dyes or QDs through a linker.	64,68,69
18	Magnetic particles in a matrix core. Outer shell with incorporated dyes or QDs.	51,69–74
19	Single magnetic core with a protective matrix shell, where luminescent dyes are embedded.	75–89

Continued on next page

[a]The drawings in figures 2.1–2.4 are general schematic representations. In literature, combinations or extensions of the presented structures can be found. See the cited references for examples to each type of LuMaP.

Table 2.1 *(continued from previous page)*

No.	Description	References
20	Matrix core with both luminescent dyes or QDs and magnetic particles attached to the surface.	90
21	Matrix core with an outer matrix shell that encapsulates both luminescent dyes and MNPs.	91
22	Luminescent dyes or particles attached to a magnetic core in a non-core-shell like structure.	92,93
23	Heterodimer of an MNP and a QD.	94,95
24	Single crystalline magnetite, hollow capsule with a QD attached to the surface.	96
25	Multishell sytem with a matrix layer separating magnetic and luminescent moieties.	97,98
26	Magnetic core coated with polyelectrolytes and QDs by a layer-by-layer approach.	99
27	Magnetic matrix core coated with a dendrimer which is finally modified with luminescent dyes.	100
28	Magnetic core with multiple matrix shells, where every second shell has embedded QDs.	72
29	Hollow polyelectrolyte capsule with MNPs and one dye in the shell and the other in the core.	101
30	Hollow stimuli responsive polymer capsule with mobile luminescent and magnetic core inside.	102
31	Hollow polyelectrolyte capsule with MNPs and QDs in both the hollow core and the shell.	103
32	Hollow magnetic core with multiple shells of polyelectrolytes and QDs	104
33	Multiple compartment capsules from polyelectrolytes filled with MNPs and luminescent dyes or nanocrystalls.	105
34	Core of MNPs and QDs coated with a cross-linked block-copolymer.	106
35	Hollow silica capsule with a single hole and embedded luminescent and magnetic nanocrystals.	107
36	Hollow capsule with MNPs in the matrix and a luminescent moiety attached to the surface.	108
37	Porous matrix capsules with both MNPs and dyes embedded in the matrix.	14
38	Hollow magnetic capsule coated with QDs.	109
39	Hollow polyelectrolyte capsule with MNPs in the core and QDs in the shell.	110
40	Emulsifier stabilized droplet incorporating magnetic and luminescent moieties.	111,112

Continued on next page

Table 2.1 *(continued from previous page)*

No.	Description	References
41	Droplet stabilized by emulsifier-conjugates with gadolinium and luminescent dyes.	113
42	Droplet holding MNPs encapsulated in a polymer matrix. The luminescent component is embedded in the matrix shell.	114
43	Droplet containing MNPs stabilized by an emulsifier and emulsifier-dye-conjugates.	115
44	Matrix with embedded luminophores coated with MNPs *via* a covalent linker.	116
45	Matrix with embedded luminophores coated with gadolinium *via* a covalent linker.	117
46	Matrix with embedded luminophores coated with gadolinium in a cross-linked shell.	117
47	Silica coated QD modified with a PEG-emulsifier and lipid-gadolinium conjugates.	118

2.2.1 Magnetic components, their morphology and distribution in LuMaPs

The magnetic component of LuMaPs is responsible for different properties. It enables the LuMaPs' magnetic guiding, MRI contrast improvments and magnetically induced heat generation.

The incorporation of magnetic particles (MPs) in LuMaPs can be organized by the final structure. The main categories are:

1. Incorporation in a polymeric matrix by mainly hydrophobic interactions and/or by physical entrapment in the dense network (e.g. structure 1 in table 2.1).

2. Covalent or strong coordinative interactions between magnetic nanoparticles (MNPs) and the matrix (e.g. silica coating of MNPs, structures 4, 5, 8, 15 and 16 in table 2.1).

3. Electrostatic interaction with polyelectrolytes, luminescent dyes or semiconductor quantum dots (QDs) by a layer-by-layer encapsulation of MNPs (structures 26, 29, 31 and 32 in table 2.1).

4. Coating of MPs with small linkers, such as mercaptosuccinic acid[119] and consequent covalent linking of the luminescent compound to the resulting functional surface groups (e.g. structure 10 in table 2.1).

5. Direct inorganic synthesis of nanocomposites consisting of MNPs and inorganic luminescent phases, such as QDs and phosphores.

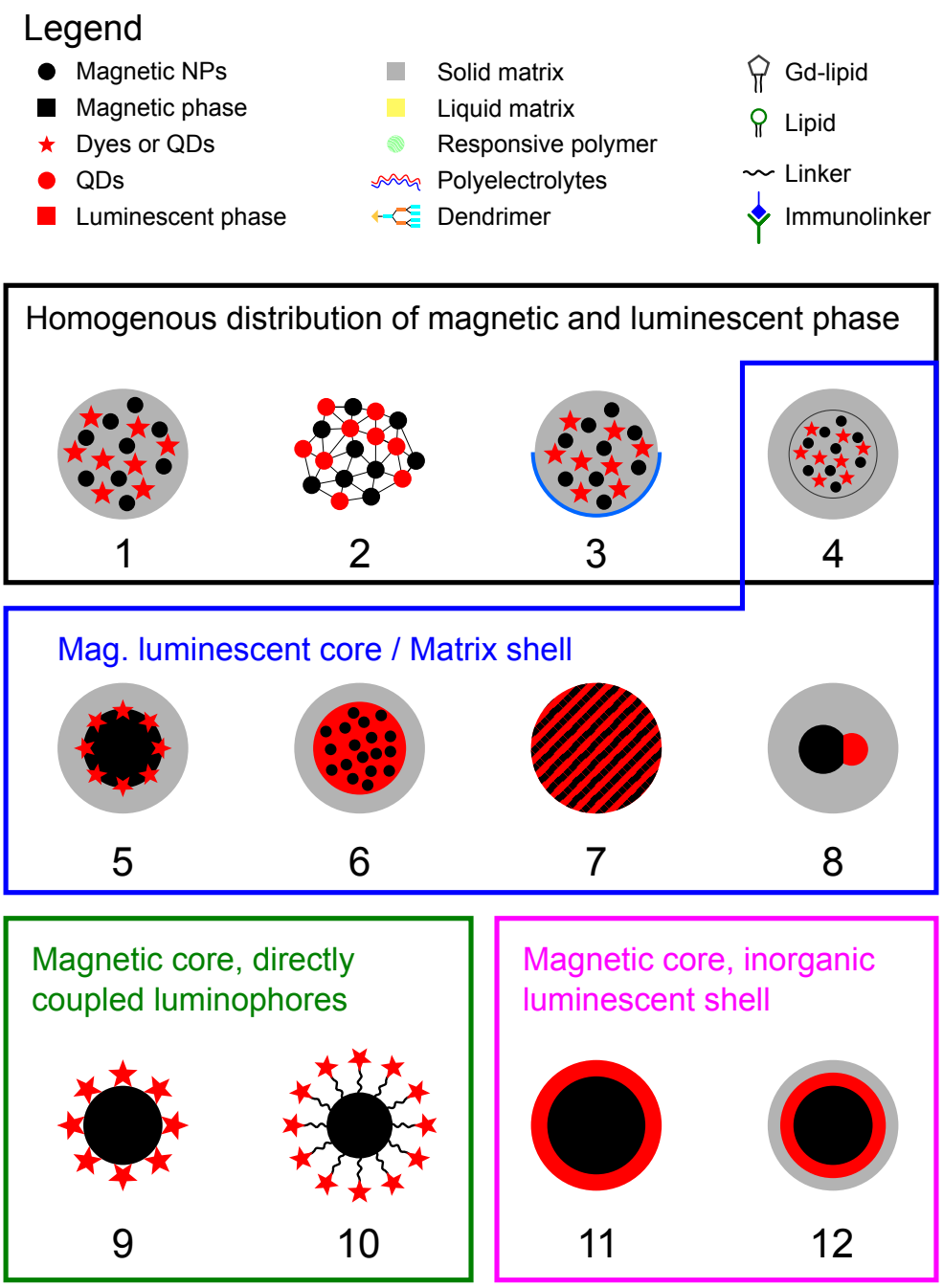

Figure 2.1: Structures of luminescent magnetic particles A (1–12). The legend provided in this figure is also valid for the figures 2.2, 2.3 and 2.4. Generally, all phases drawn with red color are luminescent, all phases drawn with black are magnetic and all gray phases represent a solid matrix material. The stars code for all types of luminescent components and can have other colors than red, if luminophores with different spectral properties are incorporated in the same particle. Linkers are presented as curled or straight lines. Short descriptions of all structures can be found in table 2.1 on page 7.

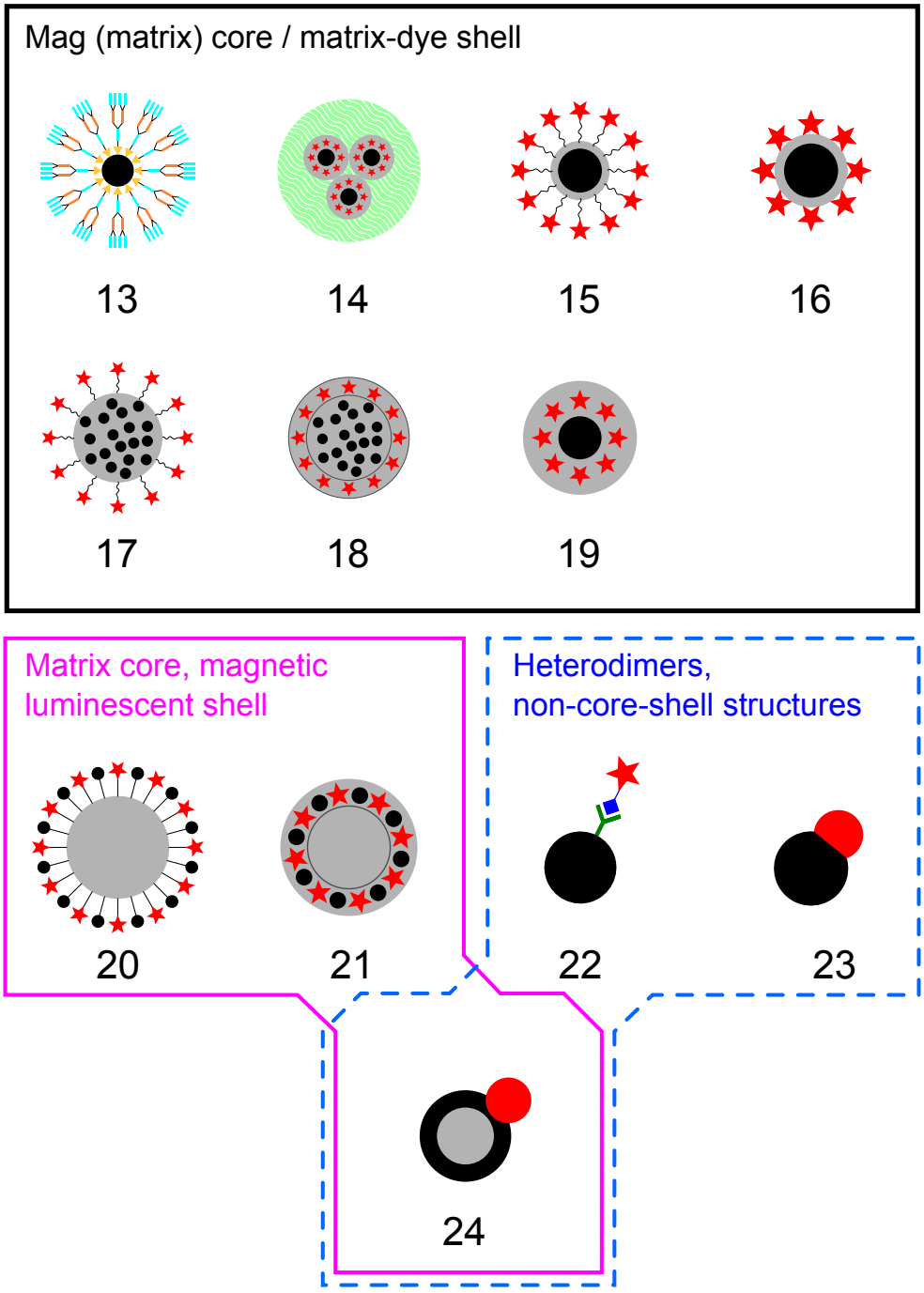

Figure 2.2: Structures of luminescent magnetic particles B (13–24). The legend for this figure is presented in figure 2.1 on the preceding page. Short descriptions of all structures can be found in table 2.1 on page 7.

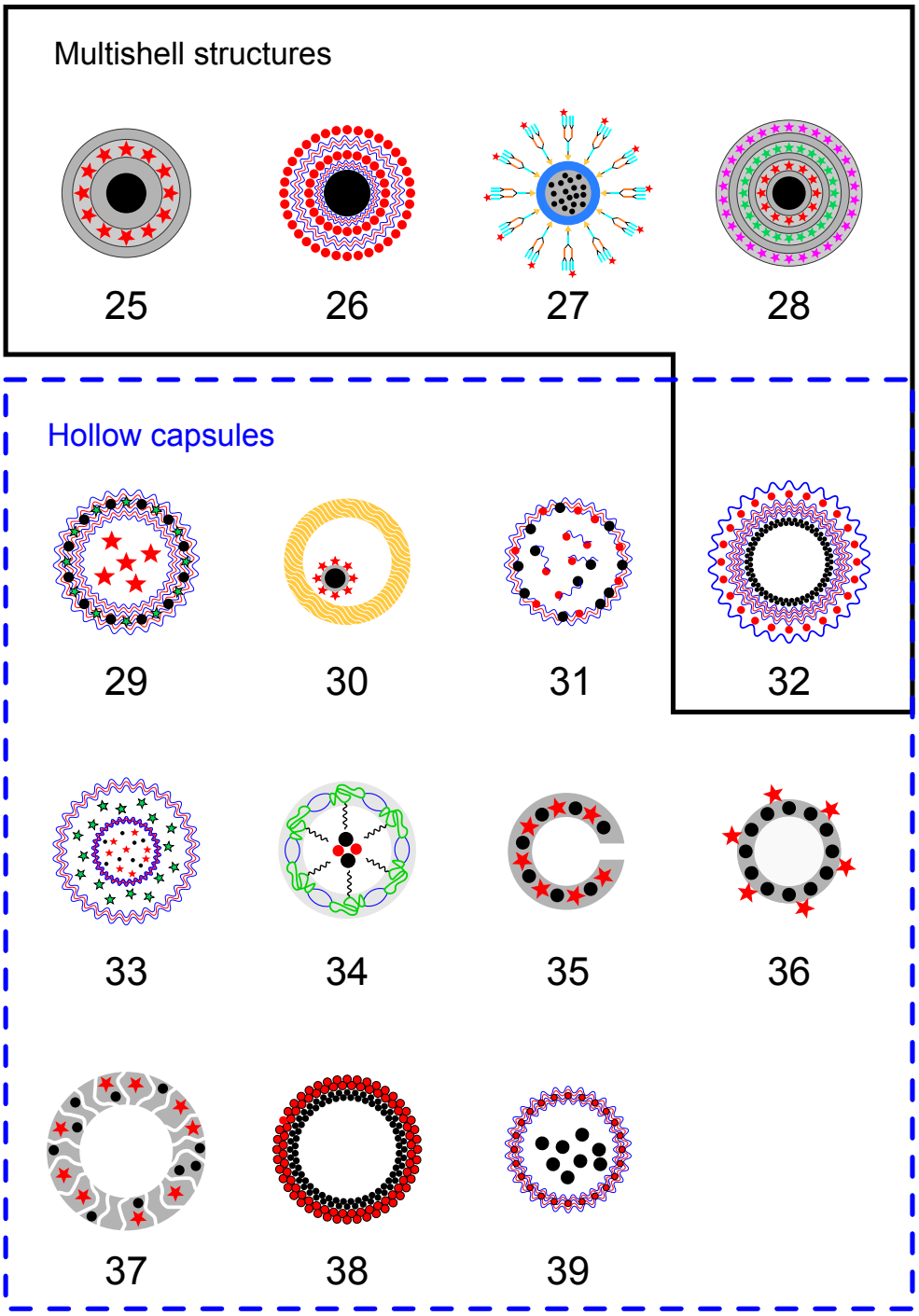

Figure 2.3: Structures of luminescent magnetic particles C (25–39). The legend for this figure is presented in figure 2.1 on page 10. Short descriptions of all structures can be found in table 2.1 on page 7.

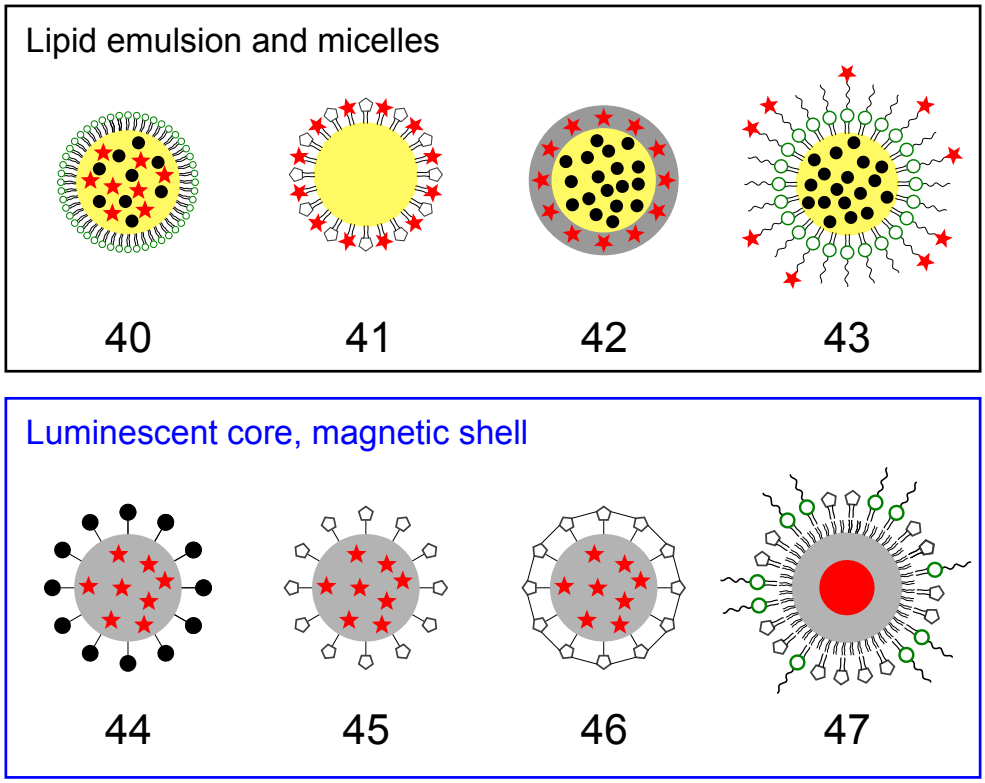

Figure 2.4: Structures of luminescent magnetic particles D (40–47). The legend for this figure is presented in figure 2.1 on page 10. Short descriptions of all structures can be found in table 2.1 on page 7.

2.2.1.1 Iron oxides or mixed iron oxides

Magnetite (Fe_3O_4) and maghemite (γ-Fe_2O_3) represent the most common magnetic components in LuMaPs. Actually, more than 60 % of the publications cited in this manuscript rely on these two components. This can be explained by the early discovery of the facile fabrication of magnetite by the coprecipitation of mixed iron(II) and iron(III) salts[120] and the peptization of the produced particles to form aqueous based ferrofluids.[121,122] Today, various companies supply high quality aqueous or organic solvent based magnetic fluids (e.g. FerroTec Inc.). Furthermore, iron oxide did not show toxic effects in *in vivo* applications.[123,124]

Virtually all iron oxide based LuMaPs contain superparamagnetic nanoparticles with sizes smaller than 30 nm. Unlike ferromagnetic materials in this size range, superparamagnetic nanoparticles do not show a residual magnetization above their blocking temperature.[125,126]

The tendency of untreated iron oxide MNPs to aggregate in both organic and aqueous solvents necessitates the application of stabilizing surface coatings prior to the incorporation of particles into a matrix and/or a biological application. Common surface modifications include surfactants, such as oleic acid or lecithin, electrostatically adsorbed

polyelectrolytes, poly(ethylene) glycol, polysaccharides, amphiphilic polymers and hyperbranched polymers.[127] Moreover, silica and organically modified silica phases are often used to produce biocompatible, stable magnetic nanoparticles. Silica enables further covalent surface modifications through functional groups.[76,88,128]

2.2.1.2 Metals and alloys

Metals and alloys are especially interesting due to their higher saturation magnetization resulting in a stronger response to a magnetic field gradient. However, their stability is usually lower and their toxicity higher compared to the thermodynamically stable maghemite.[127] High specific surface areas further increase the reactivity and toxicity of such nanoparticles. As a consequence, most metallic nanoparticles in LuMaPs are protected by a matrix which should reliably avoid the contact of the metallic core with the biological material. The most prominent metals and metal alloys used in LuMaPs are FeCo,[89,129] FePt,[50,83,95,128,130] iron or steel,[79,80,131] Co[48] and BaFe.[35]

2.2.1.3 Metal ions other than iron oxides

In this group of magnetic compounds, gadolinium is the most prominent one. Gd(III) chelate complexes are used as contrast agents in MRI imaging. Vuu et al.[113] used a Gd-lipid (Gd chelate with a lipid anchor) to produce a micelle with Gd ions and rhodamine dyes in the outer shell. After a photoinduced polymerization they obtained stable particles ready-to-use for *in vivo* MRI and luminescence imaging. For Gd very strong chelating agents are necessary because of the high cytotoxicity of free Gd-ions. Tan and Zhang[19] incorporated gadolinium diethylene triamine pentaacetate together with negatively charged QDs into a positively charged chitosan matrix. The resulting nanoparticles displayed comparable R_1 relaxivity to the pure Gd-complex. Bridot et al.[77,78] and Faure et al.[81] encapsulated a Gd_2O_3 core in a polysiloxane shell to avoid the toxic effect of Gd-ions. Dosev et al.[132] report on a one-step synthesis of Co:Nd:Fe_2O_3/Eu:Gd_2O_3 core-shell particles. Such particles were employed in a competitive immunoassay, where, most probably, the toxic effect of the ingredients was less critical. Rieter et al.[117] employed a crosslinking Gd-complex to form a paramagnetic shell around a dye-doped silica core. A lipid Gd-complex was arranged around a silica-coated QD-core to yield dual mode imaging agents.[118] A luminescent Eu or Tb doped Gd metal-organic framework (MOF) was published by Taylor et al.[133] Such nanoparticles were proposed as multimodal imaging agents. In another manuscript by the same group, Mn-based MOFs coated with a thin silica layer where presented. The silica layer enabled further functionalization with biomolecules or luminescent dyes.[57] A different LuMaP structure based on manganese as paramagnetic component was presented by Santra et al.[41] This group proposed ultrasmall Mn doped CdS:Mn/ZnS core-shell nanocomposites as dualmode imaging agents. To ensure high stability in a biological environment an additional surface coating with tetraethylorthosilicate and ATPS was established. The resulting surface amino groups were suitable for the modification with biomolecules such as a cell-targeting TAT-peptide.

2.2.1.4 Special cases

Recently, Fernandez et al.[93] and Galvez et al.[134] reported on the synthesis of LuMaPs with ferritin as magnetic component. Ferritin is an iron storage protein and consists of a magnetic, mixed iron oxide core and a protein shell. The shell protects the core and renders the magnetic particles water-dispersible.

A particularly interesting work, published by Maeda et al.[92] in 2009, reports on the production of bacterial magnetic particles with a genetically engineered biotin carboxyl carrier protein on their surface. Bacterial magnetic particles are produced by magnetotactic bacteria, such as *Magnetospirillum magneticum* AMB-1. Such bacteria naturally produce a chain of MNPs inside the cell which is used for navigation in a magnetic field. By a genetic modification of the bacteria, a biotin carboxyl carrier protein was directly synthesized and attached to the surface surface of the MNPs by the bacteria.

2.2.2 Luminescent components and their fixation in LuMaPs

2.2.2.1 Luminescent molecules

The most prominent luminescent components in LuMaPs are luminescent molecules, such as organic dyes and organic metal complexes. Organic dyes and metal complexes are commercially available with various functionalities, spectral and physical properties.

Incorporation strategies Except for the direct synthesis of an inorganic composite between QDs and MNPs, the linking mechanisms for luminescent substances in LuMaPs are the same for semiconductor quantum dots (QDs) and luminescent molecules. Organic dyes and metal complexes can be fixed *via* electrostatic interactions, covalent coupling *via* a linker and physical entrapment in a matrix. However, the generally much smaller size and higher mobility of dye molecules compared to QDs require a careful selection of the strategy to avoid any potential leaching. A covalent bond to the matrix or magnetic compound is often employed to ensure the reliable and longlasting incorporation of the dye into the LuMaPs.

The covalent linking strategy depends on the matrix. For silica, dyes are usually conjugated with aminopropyltriethoxysilane (APTS) to co-condense the luminescent moiety into the matrix during the Stöber process. To allow the binding of a dye to amino groups of APTS or amino groups present in the matrix polymer, the dyes are functionalized with an isothiocyanate group or a carboxy group. The latter is usually activated with N-hydroxysuccinimide (NHS) and 1-ethyl-3-[3-dimethylaminopropyl]carbodiimide hydrochloride (EDC) or dicyclohexylcarbodiimide (DCC), which increases the yield of the coupling reaction by stabilizing the intermediate product. Companies, such as Invitrogen supply a wide range of their dyes as ready-to-use, activated NHS esters. It is also possible to crosslink an amino group on a dye with an amino group on the matrix or magnetic moiety using glutaraldehyde by reductive amination. Other functionalities on dye molecules, such as epoxy and tosyl groups or monomeric residues occur less frequently but are also suitable for the reliable anchoring of the luminescent dye in the LuMaPs. The main advantage of such a strategy is the commercial availability of functionalized dyes for the whole spectral range.

Non-covalent but directed linking of dyes to magnetic particles can be achieved by immuno or "biotin/avidin" interactions. In this case, one partner (e.g. antibody or biotin) is linked to the matrix and the other partner (e.g. antigen or avidin, streptavidin, ...) is linked to the dye. These interactions are similar to a covalent binding because the orientation of the dye molecule is predictable. In contrast, the hydrophobic or electrostatic incorporation of a dye in a polymeric matrix usually results in a randomized orientation. Nevertheless, these interactions are also widely applied in the production of LuMaPs because of their simplicity and the absence of an extra linking step. A special case of a hydrophobic interaction yielding oriented binding of a dye to a particle is the application of lipid linkers on hydrophilic dye molecules. In this case, the directed incorporation into lipophilic membranes with the linker is predominant, while the hydrophilic part of the dye points out into the aqueous surrounding.[113]

Spectral properties Both emission and excitation characteristics of dyes in LuMaPs need to match the application. In recent years, *in vivo* multimodal imaging attracted the researchers' interest. For this purpose, excitation and emission wavelengths in the NIR are favored due to the increased penetration depths of NIR light and a reduced background due to scattering and autofluorescence. For imaging purposes, commercially available monofunctional dyes, such as NHS-activated Alexa Fluor 680 (NHS-Cy5.5) from Invitrogen, were coupled to magnetic amino functionalized nanoparticles[47,55,135] or *via* a lipid-PEG-NH_2 linker to a magnetic oil-droplet.[115] The above described considerations are valid for all dyes used for imaging. However, the combination of dyes with magnetic particles arises another problem, namely quenching or reabsorption of luminescence by dark colored MNPs.[70,97] Quenching is an issue concerning all luminescent components in combination with magnetic particles. Consequently, appropriate coatings or spacers between those compounds are considered as absolutely necessary to achieve high performance LuMaPs.[17,112,126] However, if the extra steps required for the production of such a core-shell or multishell structure are unreasonable, the LuMaPs' performance can be tuned by employing ultra-bright dyes[14] or by taking advantage of NIR dyes. Such dyes are exited in a spectral region where iron oxide nanoparticles, for instance, absorb significantly less light.[15] Finally, Chojnacki et al.[2] were able to increase the luminescence intensity of tris(4,7-diphenyl-1,10-phenanthroline)ruthenium(II) dichloride incorporated in an ormosil matrix with magnetic nanoparticles by the addition of TiO_2. They attributed the increased luminescence yield partly to an increased optical pathlength due to multiple scattering and partly to the shielding of iron oxide nanoparticles by titanium dioxide.

Functionalities of dyes Besides the predominant application of dyes as luminescent label for imaging or immunoassays, several other functions were reported in combination with LuMaPs. Dye-based LuMaPs were applied as optical chemical oxygen sensors,[2,13–15,79,80,136] pH sensors[2,15,35,80,101,136] and photodynamic therapy agents.[7,8,15,16,84,137,138] A detailed discussion of these applications can be found in section 2.4 on page 34.

2.2.2.2 QDs

Semiconductor nanocrystals (quantum dots, QDs) have been widely used in bioimaging applications.[139] Their main advantages are a high stability against photobleaching, narrow luminescence emission bands and wide absorption bands. These properties render them promising candidates for a wide range of applications, including bioimaging and encoding of luminescent spheres. However, the *in vivo* application of QDs is still under discussion due to the high inherent toxicity. Although the necessity of an adequate protecting matrix is known for a long time and various solutions for this issue have been presented in literature,[38,39,43,51,52] the question is if a component consisting of highly toxic elements (Cd, Hg, Se, Te, In, As, Pb) will ever be approved or widely accepted for *in vivo* medical applications. Nevertheless, QDs represent an excellent alternative to organic dyes in *in vitro* applications, where the unique QD-properties overcome common problems of organic dyes, such as photobleaching.

Despite the fact that both principles – QDs and magnetic nanoparticles – are know since the 1980s, it took almost twenty years until the number of publications on the application of nanocomposites combining both phases in single particles started to rise.

In 2004, four different structures of magnetic QD composites were published:

1. the incorporation of QDs in polyelectrolyte layers around a magnetic core,[99,103]
2. the direct inorganic synthesis of QD-MNP composites,[95]
3. the coating of thiol-modified MNPs with QDs[45] and
4. the entrapping of QDs into a polymeric matrix by hydrophobic interactions *via* a swelling method.[140]

These four principles (electrostatic interaction, direct inorganic composite, covalent coupling *via* a linker and physical entrapment in a matrix) were the basis for most of the QD-MNP composites reported in later publications. A few examples from over sixty publications of magnetic QD composites are described below.

A special case of a direct inorganic composite was presented by Santra et al.[41] Manganese doped CdS:Mn/ZnS QDs were both luminescent and paramagnetic and consequently suitable for luminescence and MRI imaging. Water dispersability of such particles was ensured by a phosphonate/silica coating.

Kim and Taton[106] reported on the coencapsulation of QDs and MNPs in micelles constructed from a polystyrene-*block*-poly(acrylic acid). The shell of this micelle was cross-linked which yielded stable polymer capsules.

Barcode LuMaPs were synthesized by Yan and co-workers[72] by the sequential coating of silica and QD layers onto a magnetic core. Three different mercapto trimethoxylsilane capped QDs with distinguishable spectral properties were covalently entrapped into the silica layers. FRET between the different QDs was avoided due to the coating of silica spacing layers between each luminescent layer.

Wang et al.[109] were the first to report the successful synthesis of Fe_3O_4/ZnS hollow, luminescent and superparamagnetic nanospheres by a so-called "corrosion-aided Ostwald ripening" process. Starting with monodisperse FeS nanoparticles, a mixture with zinc

acetylacetonate, poly(vinylpyrrolidone), ammonium nitrate, glycol, and water was prepared and then reacted at 150 °C for 10 h. This process resulted directly in hollow nanospheres with typical outer and inner diameters of 97 nm and 66 nm, respectively.

A structure where the QD-phase encapsulates the MNP was investigated by Yang et al.[51] An additional outer silica shell acted as protective layer. Such particles were obtained by a two-step process. Firstly, QDs were coated with silica and secondly, a reverse micelle route was employed to incorporate MNPs inside the hollow silica/QD capsules.

A particularly interesting approach was published by Hu et al.[96] This group generated a single crystalline magnetite shell around a drug loaded polymer capsule and, subsequently, modified the magnetic capsule with a single QD. Interestingly, the QD luminescence correlated with the rapture of the magnetic capsule, which was induced by an AC magnetic field.

2.2.2.3 Other inorganic dyes

Besides the dominantly used inorganic semiconductor QDs, other inorganic luminescent compounds were used in LuMaPs. Lanthanide doped inorganic phosphores represent the most common luminescent compounds in this category. Dosev et al.[132] and Nichkova et al.[49] successfully coated magnetic nanoparticles with europium-doped Gd_2O_3 by a spray pyrolysis process. The resulting composites emitted light at 620 nm upon excitation in the UV. After modification of the shell with antibodies, the phosphor was applied for a sandwich type immunoassay, where the luminescent coating acted as internal standard. Recently, the same group reported on the coating of iron oxide nanoparticles with an Eu:Y_2O_3 shell by a homogeneous precipitation method.[39] Surface modification with *p*-aminobenzoic acid yielded water-dispersible, functional LuMaPs.

Phosphores emitting in the NIR were prepared by coating $NaYF_4$ doped with different lanthanides (Nd, Er, Pr and Po). The luminescent nanocomposites were consequently coated with a thin silica layer, which rendered the LuMaPs biocompatible and stable. Yang et al.[141] coated YVO_4:Eu onto pores in mesoporous, magnetic silica particles. Such LuMaPs displayed an emission maximum at 615 nm upon excitation at 276 nm. The luminescence intensity was further correlated to the release rate of ibuprofen loaded into mesoporous silica and the authors suggested that this system would be useful for *in situ* monitoring of drug release. However, as suggested, the currently used luminophore is probably unsuitable for this purpose due to the limited penetration depth of the UV excitation light. A replacement by a NIR phosphore would be required, however, it is unknown if the same correlation with the drug release can be achieved.

Up-conversion (UC) phosphores are, for example, excitable with infrared light and emit light in the visible range. They are chemically stable, have higher quantum yields and are less toxic then their down-conversion counterparts, i.e. QDs. Moreover, using an NIR laser for excitation diminishes background auto-luminescence and biological tissue is not damaged by high energy UV light.[85] Already in 2004, Lu et al.[38] reported on the production of multifunctional magnetic UC-LuMaPs with streptavidin bound to a protecting silica-coating. The excitation with a 980 nm laser resulted in two emission peaks in the green (539 nm) and the red part (658 nm) of the visible spectrum. The conversion

of NIR excitation light to visible emission light enabled the readout of a magnetically assisted protein assay with a CCD chip. Liu et al.[85] incorporated UC nanoparticles in a silica shell surrounding a magnetic iron oxide single crystal and suggested the resulting material for the application in bioimaging, drug targeting and bioseparation. The same group that reported on the coating of pores in a mesoporous silica shell with YVO_4:Eu[141] succeeded in the production UC-LuMaPs by a similar procedure.[142] Replacing YVO_4:Eu with $NaYF_4$:Yb^{3+},Er^{3+}/Tm^{3+} resulted in particles emitting light with maxima in the range of 475-700 nm when excited at 980 nm. Moreover, the release rate of ibuprofen loaded in the pores could be correlated with the photoluminescence intensity.

Recently, Hyeon and co-workers reported on the production of upconverting nanoparticles as an optical imaging nanoprobe and MRI contrast agent.[143] They incorporated UC phosphores in a Gd-containing matrix. The resulting, highly monodisperse nanoparticles were further functionalized to be suitable for biological applications, i.e. the surface was coated with a PEG-phospholipid.

Finally, a hybrid organic-inorganic material for LuMaPs was investigated by Taylor et al.[133] They doped Gd-metal-organic frameworks with Eu or Tb, and received red (Eu^{3+}) and green (Tb^{3+}) luminescent particles.

2.2.2.4 Carbon nanotubes

The NIR luminescence of single-walled carbon nanotubes (SWNT) was utilized for the production of LuMaPs by Choi et al.[131] A SWNT was bound to a superparamagnetic Fe_2O_3 nanoparticle and wrapped with DNA (d(GN)15) to achieve a water dispersible dual-mode imaging probe. SWNTs are interesting luminescent labels, because they are completely photostable.

2.2.2.5 Proteins

To the best of our knowledge, so far no direct conjugate of fluorescent protein and a magnetic particle has been published. This might be explained by the relatively low stability of proteins compared to small organic dye molecules or inorganic luminophores. On the other hand, the application of such conjugates in life science could be a good alternative to systems based on toxic components, such as metal complexes and QDs.

An indirect approach towards the combination of magnetic particles with luminescent proteins was recently published. Kumar et al.[144] synthesized magnetic reporter particles carrying DNA that encoded for eGFP (enhanced GFP). Here, the original particle was non-luminescent, however, a plasmid DNA coding for eGFP expression was coupled to the magnetic particle. After injection of such particles into mice and magnetic guiding to the heart and the kidneys by an external magnetic field, the eGFP expression was monitored by whole-body fluorescence imaging. Interestingly, no targeting ligands were necessary to direct the particles towards their desired destination.

2.2.2.6 Luminescent polymers

An interesting application of a modified polythiophene in a PCR-free DNA sensor was presented by Dubus et al.[145] Polythiophene changes its luminescent properties depending

on the orientation of the subunits relative to each other. The conjugation with single strand DNA resulted in a planar, weak luminescent form. Unbound polythiophene or polythiophene bound to a double strand DNA twists the polymeric chain into a highly luminescent form.

Recently, Buathong et al.[53] reported on the successful controlled modification of maghemite nanoparticles with a luminescent mesomorphic oligo(phenylene vinylene)-based dendrimer. The spectral properties of such a dendrimer were controlled by extending the conjugated π-electron system with each dendrimer generation.

2.2.3 Matrix materials and morphologies

The LuMaPs' matrix highly influences their applicability in life science. The matrix can act as protecting layer, provider for functionalization, spacer between magnetic and luminescent compound, host that avoids leaching of the components, diffusion barrier in sensors, etc. The type of matrix needs to fit the purpose of the final application and the requirements of the included magnetic and luminescent components. Among all matrix materials, silica and organic polymer based materials are the most common ones. Both materials allow a high variability in properties and enable further modifications through covalent linking groups.

2.2.3.1 Silica based materials (silica, Ormosil)

The most prominent matrix material for LuMaPs is silica. This is mainly due to the following features:

- silica is relatively stable in biological environments,
- its chemical structure allows a versatile modification chemistry including co-condensation and post-synthesis modification,
- it is transparent (important for the inclusion of dyes),
- the synthesis from alkoxysilanes is well established,
- certain properties, such as gas permeability, can be tuned by co-condensation with organically modified silanes and
- silica can be generated with a mesoporous structure allowing the inclusion of drug molecules.

Depending on the synthesis procedure and the additional ingredients, silica in LuMaPs can be dense, meso- or nanoporous. While a dense structure provides optimal protection for the enclosed nanoparticles, porous structures are used for drug targeting or sensors, where analyte diffusion towards the indicator is required. The conventional Stöber method, i.e. the base-catalyzed condensation of tetraalkoxysilanes, usually leads to dense silica particles. Methoxy (TMOS) and ethoxy (TEOS) are the most common alkoxy groups in the educts. A porous structure can be achieved by adding porogens, such as cetyltrimethylammonium bromide (CTAB) during the TEOS condensation.[5,66,74,142] Another possibility used for

increasing the gas permeability of silica is the incorporation of organically modified alkoxysilanes. Such Ormosil-based particles were used as magnetically separable optical oxygen sensors.[2] Moreover, organo-alkoxysilanes can be used to modify the pore walls of mesostructured silica spheres.[146] Even the incorporation of controlled-release mechanisms based on nanovalves, nanoimpellers or enzyme-responsive snap-tops is possible.[147–149]

In an early work, Lu et al.[86] modified commercially available magnetite nanoparticles (5-15 nm, EMG304, Ferrofluids, Nashua) with silica shells of varying thickness (2-100 nm depending on the concentration of the sol-gel solution). Fluorescent dyes were conjugated with APTS and co-condensed into the silica shell. The resulting LuMaPs were magnetically responsive and luminescent.

Mesoporous silica particles with a single magnetic core and tunable size were reported by Kim et al.[66] Staining was achieved by the co-condensation of APTS-conjugates with fluorescein isothiocyanate (FITC) and rhodamine B isothiocyanate (RITC). The final particles were descrete, i.e. not cross-linked and monodisperse. Remaining CTAB (porogen) was removed by heating the particles at pH 1.4. Refluxing at lower pH (< 1) resulted in a dissolution of the iron oxide core and consequently in hollow mesoporous silica spheres. For biomedical applications, a PEG layer was coated onto the silica surface to increase biocompatibility.

In general, silica based LuMaPs smaller than ~ 150 nm are often internalized into cells. Moreover, the toxicity of magnetic mesoporous silica nanoparticles to cells is negligible.[146]

Inorganic monomeric matrices (non-luminescent, non-magnetic) Inorganic matrices other than silica, luminescent QDs and phosphores, or magnetic phases are rarely found in LuMaPs. Recently, one group reported on the coating of an Al_2O_3 layer onto silica encapsulated magnetic nanoparticles.[150] Reactive aluminium atoms in the shell provided a binding site for the luminophore morin. They concluded that the Al_2O_3 layer provides additional biocompatibility and the 60 nm spheres might be suitable as magnetically guidable luminescent label.

2.2.3.2 Organic polymers

The great variety of physical and chemical properties, that are achievable with organic polymers, is the main reason for their common usage for LuMaP-synthesis. Organic polymers can be adjusted seamlessly from hydrophilic to hydrophobic and their stability against solvents can be triggered by crosslinking reactions. Other properties (such as gas permeability) strongly depend on the type of polymer, the chain length, the crosslinking degree, the type of synthesis, etc. With the increasing popularity of various emulsion polymerization techniques, organic polymers gained importance in particle technology. Moreover, the availability of highly charged polymers (polyelectrolytes, PEL) enabled the predictable coating of small particles with alternating layers of polymers, charged nanoparticles or charged conjugates of dyes. In this way, particles can be designed to match the purpose in terms of components, size, functional groups and surface charge. The electrostatic interactions are usually strong enough to withstand the conditions in biological environments. Even the production of hollow capsules by coating PEL onto

melamine formaldehyde–[103,110] or $CaCO_3$–cores[105] and the subsequent dissolving of the core was shown.

Another way for precisely controlling the structure of LuMaPs is the dendrimerization of magnetic cores.[100] With a dendrimer that is also luminescent the spectral properties of the LuMaPs can be tuned by the number of dendrimer generations.[53]

Swelling of moderately cross-linked or linear polymer particles allows the entrapment of dyes and nanoparticles in the polymer network after the polymeric particles have been formed. This procedure is mostly used for the modification of commercially available magnetic particles.[26,140,151,152]

Especially in multifunctional LuMaPs, hydrogels and stimuli responsive polymers play a crucial role. Hydrogels are polymers that swell in water due to their hydrophilic and loose network structure. Common hydrogels are poly(acrylamide), poly(*N*-isopropylacrylamide) (pNIPAM) and poly(urethane) based materials. Poly(urethane) hydrogels (hydromed D4, Cardiotech) were used as host matrix for an optical pH sensor and coated onto stainless steel spheres.[80]

Poly(*N*-isopropylacrylamide) is the most studied stimuli reponsive polymer. It changes its structure and size reversibly with the temperature. Increasing the temperature above the lower critical solution temperature (LCST) changes the structure of a pNIPAM hydrogel network rapidly. Recently, optical sensor LuMaPs with a 130 nm pNIPAM shell around a 100 nm magnetic core were prepared using seeded radical polymerization.[80] These particles shrunk from 230 to 110 nm upon heating with an LCST of 33 °C. In an earlier work, Deng et al.[54] demonstrated that the LCST of pNIPAM coated LuMaPs can be adjusted by the amount of applied crosslinker (*N,N'*-methylene bisacrylamide). Doxorubicin (DOX) loaded into the spheres was released in two main steps. An initial burst release (42 %) of DOX adsorbed to the outer polymer shell was observed after dispersion in water. Above 35 °C the second half of DOX was released. During the second phase, water soluble DOX was pushed out from the pores together with the liquid located in the particle-pores. This was caused by the collapsing network.

2.2.3.3 Biopolymers

Polysaccharides Biopolymers, such as polysaccharides are frequently used as matrix for LuMaPs. The high biocompatibility and, in some cases, biodegradability enables new applications. The most prominent example of a polysaccharide in LuMaPs is chitosan. Chitosan is a β-(1-4)-linked D-glucosamine with randomly acetylated amino groups. The positive charges of the free amino groups can be utilized for electrostatic interactions between matrix and negatively charged inclusions. Moreover, the amino groups are suitable for covalent binding chemistry by reductive amination.

Tan and Zhang[19] reported on the production of 50 nm chitosan beads doped with QDs and a gadolinium diethyl triamine pentacetate complex. Interestingly, the CdSe/ZnS QDs showed a 10 % higher quantum yield in the chitosan matrix compared to non-incoporated QDs. The gadolinium complex acted as efficient MRI contrast agent in T_1-weighted images.

Chitosan beads incorporating QDs and MNPs for drug delivery were reported by Li et al.[9] The particles were cross-linked with glutaraldehyde and loaded with the hydrophilic

drug cefradine. Release rates of the drug depended on both the crosslinking time with glutaraldehyde and the pH value of the solution.

Another type of LuMaPs was produced by mixing methacrylic acid (MAA) with chitosan to achieve monomer-polymer pairs. Afterwards, MPA capped QDs and magnetite NPs were added to the chitosan-MAA mixture.[3] Radical polymerization of MAA and crosslinking of chitosan with glutaraldehyde yielded the final luminescent particles with sizes of approximately 100 nm.

In contrast to the linear chitosan, dextran is a branched polysaccharide consisting of glucose subunits. Charged groups at neutral pH are missing which limits the possibility of electrostatic interactions between matrix and charged inclusions. Nevertheless, Huang et al.[68] succeeded in the production of ~ 500 nm dextran based magnetic particles by a hydrothermal method and investigated their effect on cell proliferation and cell apoptosis of A375 cells, a human amelanotic melanoma cell line. Employing the same synthetic approach, they produced magnetic chitosan and poly(acrylic acid) based spheres and thereby extended the range of surface groups from $-OH$ to $-NH_2$ and $-COOH$. The modification of chitosan magnetic beads with fluorescein isothiocynate (FITC) yielded particles that were able to penetrate the plasma membrane and to deliver the fluorescent dye into the cytoplasm. FITC itself was not internalized into the cells.

Alginate, a polysaccharide consisting of 1,4-linked α-L-guluronate and β-D-mannuronate subunits, also found application in LuMaPs. The free carboxyl groups in alginate render the polysaccharide anionic and enable covalent modifications *via* the activated ester method. LuMaPs based on alginate were produced by emulsifying FITC modified alginate and meso-2,3-dimercaptosuccinic acid (MPA) modified maghemite NPs with the help of tensides.[12] Afterwards, remaining free carboxyl groups on the polysaccharide backbone were cross-linked by the addition of Ca^{2+}-ions in the form of a $CaCl_2$ solution.

Proteins and peptides A protein or peptide is a biopolymer that consists of different monomers (amino acids) linked *via* a peptide bond. The properties of proteins depend mainly on the amino acid composition but also on the 2D and 3D structure. For example, the adjustable charge of peptides was employed by Schellenberger et al.[153] They used a synthetic peptide consisting of an arginine rich, positively charged domain, followed by a FITC labeled domain and a cleaving site specific for a protease. This peptide was linked to an NHS-activated PEG chain *via* its terminal amino group and then attached to acid stabilized magnetic nanoparticles with its positively charged peptide domain. The resulting LuMaPs were stabilized by the PEG surrounding, however, protease activity resulted in the cleavage of the PEG residues and consequently a rapid aggregation of the remaining protein-coated LuMaPs.

An interesting way of modifying magnetic particles with a protein was presented by Maeda et al.[92] Here, genes coding for the biotin carboxyl carrier protein (BCCP) and protein G were introduced into *Magnetospirillum magneticum*, a magnetotactic bacterium that produces bacterial magnetic particles (BacMPs). Inside the bacterium, the BacMPs were directly modified by the two proteins. Later on, the binding sites for biotin and protein G sites on BCCP were modified with QD-labeled streptavidin and antibodies, respectively. This synthetic route is especially interesting, because it inspires to introduce

even more functionalities by simple genetic modification. The direct "bio-grafting" of fluorescent proteins or biologically active enzymes onto magnetic particles might be possible following this approach.

Ferritin is another example for a biologically obtained magnetic particle where protein is used as a cover. Such particles are very small (a few nanometers), water dispersible and covalently linkable by primary amino groups present on the protein surface.[93]

2.2.3.4 Monomeric organic matrices (emulsions, liposomes, micelles)

Alternatively, magnetic and luminescent compounds can be encapsulated or dissolved in monomeric organic substances in the form of tenside stabilized emulsions, liposomes or micelles. For instance, Mandal et al.[112] prepared oil-in-water emulsions with lipophilic MNPs and QDs in the oil phase to investigate the dependency of the luminescence intensity on the QD:MNP ratio. In this experiment, the QD-luminescence decreased by one order of magnitude in droplets containing 5 % MNPs and 150 µM QDs compared to droplets without MNPs. Soybean oil droplets with tunable sizes from 30 to 95 nm incorporating oleic acid coated iron oxide nanoparticles were stabilized with a Cy5.5 modified PEG-phospholipid-conjugate.[115] The resulting nanoparticles had a narrow size distribution and a high MNP load.

Magnetic luminescent micellar structures lacking an oil phase were prepared by Vuu et al.[113] and Roullier et al.[111] In the first publication, rhodamine and Gd-complex modified lipids were mixed with other phospholipids and ultrasonicated to form water dispersible, magnetic luminescent micelles. In the latter, Roullier et al.[111] reported on micelles containing QDs and maghemite NPs. The stabilizing agents were synthesized by the group and consisted of $COOH-PEG-C_6H_2-(OC_{11}H_{23})_3$ or $NH_2-PEG-C_6H_2-(OC_{11}H_{23})_3$ molecules. These tensides had a hydrophilic PEG group and three hydrophobic undecanoyl aliphatic chains. In addition, the tensides added carboxyl and amino groups to the surface at an adjustable ratio.

2.2.3.5 Structures of LuMaPs without a matrix material

A number of LuMaPs is known were the linkage between the luminescent and the magnetic component was accomplished either directly or *via* a non-polymeric linker.

Direct linkage In this group, heterodimers or core-shell systems of both inorganic magnetic and luminescent phases are predominant.

Already in 2004, Gu et al.[95] successfully synthesized FePt@CdSe core/shell particles that reorganized themselves at elevated temperature to a heterodimeric structure. This reorganization was explained by the different lattice spacings and phase transition temperatures of FePt and CdSe. The initially amorphous CdSe shell transformed to a crystalline state at the temperature of 280 °C. A layer of ZnS deposited onto Fe_3O_4@CdSe core/shell nanoparticles improved the quantum yield from 2-3 % to 10-15 % by passivation.[154] Quite differently, Wang et al.[109] achieved hollow magnetic capsules consisting of single magnetite nanospheres and coated with fluorescent ZnS nanospheres with a so-called "corrosion-aided Ostwald-ripening" process. Recently, Zhou et al.[50] published

a synthesis method for coating 3.3 nm FePt cores with a fluorescent 10.3 nm ZnO layer in a sequential process. First, a zinc-oleylcomplex was adsorbed onto FePt nanospheres. Then, slowly increasing the temperature to 260 °C decomposed the zinc complex under formation of ZnO which coated onto the FePt particles. According to the authors, the sequential heating was important, because a direct injection of the zinc complex into the heated solution would yield individual ZnO and FePt particles. Although the heating rate was strictly controlled the formation of individual FePt particles or heterodimeric structures was not be completely suppressed.

Small linker molecules Luminescent molecules were coupled to magnetic particles with standard coupling reactions between EDC/NHS activated carboxyl groups from citric acid[44] or 5-hydroxy-5,5-bis(phosphono)pentanoic acid[46] and amino groups on rhodamine B or amino fluorescein. Gu et al.[138] first coupled a porphyrin to an activated dopamin derivative, which binds tightly to iron oxide surfaces *via* M-O bonds.[155] This bond also withstands elevated temperatures and makes the resulting nanocomposite ready for hyperthermia. Sulfhydryl groups on magnetic nanoparticles introduced *via* dimercaptosuccinic acid were coupled to activated rhodamine B and fluorescein derivatives.[119] Octaaminopropylsilsesquioxane was used as linker between magnetic nanoparticles and a porphine.[156] Finally, Thakur et al.[31] reported on the crosslinking between mercaptopropionic acid (MPA) capped QDs and (3-mercaptopropyl)trimethoxysilane (MPS) modified iron oxide nanoparticles resulting in LuMaPs with a relatively broad size distribution.

2.2.4 Optional surface modifications

In order to increase the functionality of LuMaPs a range of surface modifications was developed. An overview on the most common modifications is given in figure 2.5 on the following page.

2.2.4.1 Modifications for increased biocompatibility

Especially *in vivo* applications of LuMaPs require highly biocompatible particle surfaces. Biocompatibility can be defined as an increased dispersion stability or blood circulation time. A high blood circulation time is required for biomedical applications such as drug delivery and imaging applications, because it reduces the required amount of LuMaPs and, consequently, the burden on the organism. Avoiding the formation of big particle aggregates inside the body is, however, not only beneficial for the application but absolutely necessary. Aggregates that reach the brain, for example, might cause a stroke and have to be avoided.

The most common coating for ensuring a high biocompatibility of LuMaPs is poly(ethylene glycol) (PEG).[58,64,78,89,111,118,129,157] This polar molecule is commonly used to ensure highly hydrophilic surfaces, the prerequisite for low fouling and high biocompatibility of surfaces. Moreover, PEG was used in an amino-modified form as linker to dyes and cell targeting molecules[47] or membrane anchors.[43] Linking of biomolecules, such as antibodies, *via* a PEG spacer might increase the binding efficiency due to a flexible orientation.

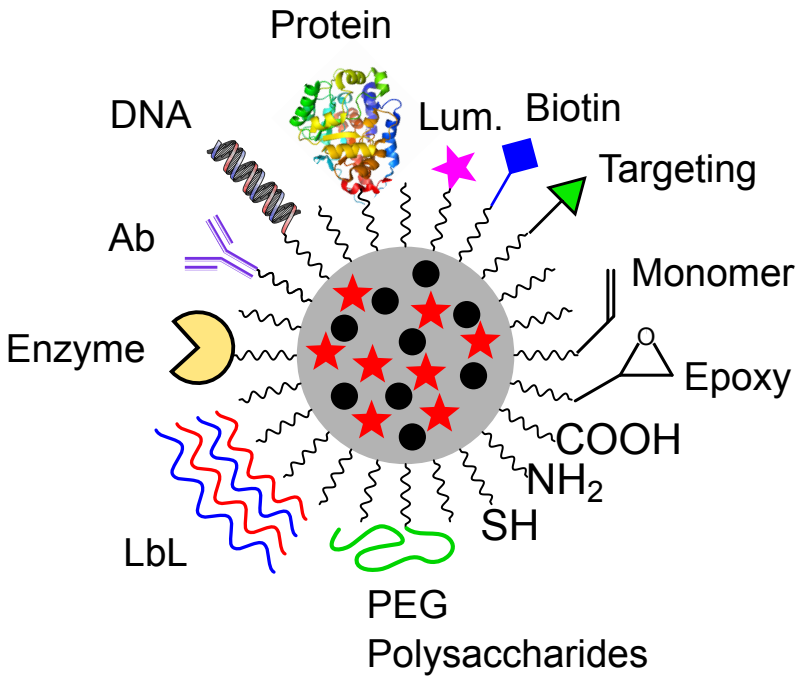

Figure 2.5: Potential surface modifications of LuMaPs. The surface modifications outlined in this figure are commonly found in combination with most of the particles' structures provided in figures 2.1 – 2.4.

Schellenberger et al.[153] reported on magnetic particles, stabilized with PEG which is linked *via* a vulnerable peptide sequence. Upon cleavage of this peptide, the PEG cover is lost and the initially small individual paricles (25 nm) form aggregates with sizes probably in the micrometer range. Despite the fact, that the authors encountered problems in estimating the size of the aggregates in *in vitro* experiments due to a fast sedimentation after peptide cleavage, they suggested these probes to be used as protease specific contrast agents for *in vivo* MRI imaging. Depending on the location and the spatial control of such aggregates inside the organism, this might lead to a decreased biocompatibility and blood circulation time or the formation of clots.

Interestingly, modified PEG influences not only the clearance or blood circulation time of LuMaPs inside the body, but also the biodistribution. Faure et al.[81] investigated the biodistribution of PEGs with different chain lengths (250 vs. 2000 $g\,mol^{-1}$) and termination groups (PEG−COOH, PEG−NH_2, PEG−OCH_3) and found that LuMaPs coated with the shortest derivative (PEG250−COOH) conferred the longest blood circulation time.

Other macromolecules ensuring hydrophilic, biocompatible surfaces of LuMaPs are polysaccharides and DNA. Choi et al.[131] reported on the DNA-coating of a nanocomposite consisting of a magnetic particle attached to a single wall carbon nanotube (SWCNT). In *in vitro* applications, the highly hydrophobic SWCNT would quickly aggregate, adsorb to proteins and stick to tissue, respectively. DNA, however, ensured a hydrophilic surface of the composite and thereby increased the dispersability in a biological environment.

More recently, Jiang and co-workers[158,159] developed ultra low fouling surfaces based

on carboxy betain polymers. In addition to a high wettability, such materials also provide alternating charges. Such alternating charges can also be found in bovine serum albumin (BSA), another agent frequently used as coating material to increase the biocompatibility of surfaces. Although this type of coating seems to be especially promising for the coating of LuMaPs, up to now, nothing has been published.

2.2.4.2 Molecular recognition components

Molecular recognition or immuno components, such as antibodies and aptamers are often conjugated to the surface of LuMaPs. Antibodies help to attach LuMaPs to specific cells for therapeutic applications, cell labeling,[89,92,116] cell capturing,[21,89] or act as recognition element in magnetically assisted immunoassays.[36,49,132,140,160,161]

Aptamers are oligo nucleotides selected for an optimal binding to a target molecule. They represent an attractive alternative to antibodies due to their lower production cost and higher chemical stability. LuMaPs modified with aptamers were employed to collect and detect different cancer cell lines by Smith et al.[18]

2.2.4.3 Components for cell targeting and cellular uptake

Biomolecules that trigger the uptake of particles into cells or bind to recognition sites on the cell surface are also used as coatings of LuMaPs. Funovics et al.[55] modified LuMaPs with a peptide that selectively binds to E-selectin. Upon binding, E-selectin mediated the internalization into endothelial cells and cancer cells. A different peptide which enhances the binding efficiency to endothelial cells is the RGD-peptide. This peptide was covalently attached to the surface of LuMaPs by Koole et al.[118] and Taylor et al.[57] Finally, Stelter et al.[56] grafted the transfection agent HIV-1 TAT onto commercially available LuMaPs and investigated the biodistribution of the resulting nanocomposites over time.

Another prominent cancer cell targeting molecule is folic acid (FA). FA binds to the folic acid receptor, a glycoprotein which is overexpressed in various human tumor cells.[25]

2.2.4.4 Coupling groups

Coupling groups are widely-used modifications of LuMaPs that enable their covalent modification with biomolecules, polymers, dyes or other functional groups. They include $-$COOH (carboxy),[4,15,28,46,106,162] $-NH_2$ (amino),[23,30,39,60,63] $-$SH (thiol),[162] $-$CHO (aldehyde), epoxy and polymerizable groups.

For strong, non-covalent coupling of ligands, the surface of LuMaPs is often modified with biomolecules such as avidin,[21] streptavidin[38,92,163,164] and biotin.[21,39,111] These biomolecules strongly interact with each other (avidin or streptavidin with biotin) and are used to specifically connect biomaterials, molecules and all types of particles labeled with e.g. streptavidin to the counterpart labeled with biotin.

2.3 Synthetic strategies

Synthetic strategies towards LuMaPs are manifold and a comprehensive discussion of all methods would be beyond the scope of this article. Therefore, some general principles are

discussed and a few selected examples are mentioned in this section. A combination of two or more techniques is common and further complicates the description of a general route towards LuMaPs. Similar to the relation between particle properties and particle structures or components used for particle production (chapter 2.2 on page 6), the synthesis method also needs to be selected in relation to the desired particle properties.

The functionality, suitability and quality of the final particles are defined by properties such as the stability of the matrix polymer (physical, chemical), the particle surface (polarity, functional groups, targeting groups), the magnetization, the particle size and the brightness and spectral range of the luminophores, respectively. The synthetic route often determins these properties and a careful selection of the appropriate strategy is inevitable.

2.3.1 Modification of commercially available particles

Due to the cumbersome optimization of the myriad of synthesis parameters during the production of multi-component systems such as LuMaPs, commercially available particles sometimes represent a better choice as starting point. Various suppliers provide ready-to-use luminescent magnetic particles. An overview of available LuMaPs with corresponding sizes, matrix materials and surface modifications is given in table 2.2.

Table 2.2: Commercially available LuMaPs.

Manufacturer	Sizes / µm	Surface functionality	Matrix material	Reference
Bangs Labs	$0.5 - 8$	$-$COOH	Polymeric	165
Chemicell	$0.5 - 1$	n.a.	Polysaccharide	166
Magnamedics	n.a.	n.a.	Silica	167
Micromod	6	n.a.	Silica	168
Micromod	2, 30, 100	n.a.	Poly(lactic acid)	168
Micromod	2	n.a.	BSA	168
Polysciences	6	$-$COOH, streptavidin	n.a.	169
Spherotech	$1 - 10$	$-$COOH, $-NH_2$	Polystyrene	170

Such particles can be modified for the application in immunoassays and bioseparations. Magnetically assisted immunoassays are a common procedure and various suppliers produce kits for this application. LuMaPs simplify the handling and reduce the time required for necessary separation steps. A more detailed discussion on this topic can be found in section 2.4.2.1 on page 39. For a different type of application, Kopelman and co-workers[32–34] deposited a reflecting metal layer onto LuMaPs. In this case, the LuMaPs were permanent magnetic with a fixed magnetization direction. The metal coating on one hemisphere resulted in so-called MagMOONs.

Modification of non-luminescent, magnetic particles Due to the enormous variety of luminescent dyes, suppliers usually also provide magnetic particles without a luminescent label. In this case, strategies were elaborated to stain such particles with dyes that perfectly match the final purpose of the LuMaPs. Up to now the following coupling

strategies have been reported: covalent coupling of the luminescent moiety to the magnetic particle,[56,171] coupling *via* immuno interactions[160,172] and streptavidin/biotin coupling of a dye to commercially available magnetic particles.[161]

The incorporation of dyes into magnetic particles by swelling the matrix polymer in an organic solvent containing the desired dye is both a versatile and simple approach. In 2004, Mulvaney et al.[140] investigated different organic dyes and QDs and analyzed their incorporation efficiency into magnetic microspheres from Seradyn Inc. and Bangslabs Inc. A spectral encoding scheme for multiplexed sedimentation arrays was accomplished *via* swelling of polymeric magnetic particles from Micromod GmbH.[151,152] It is important to mention that this route can only be successful for matrices fulfilling certain requirements. The crosslinking degree has to be high enough to avoid dissolving in the applied solvent but low enough to allow swelling. Moreover, the polarity of the dye and the matrix should match and the magnetic component of the particle should not leach during the swelling process.

2.3.2 Polymerization techniques

The most common strategies for the production of LuMaPs are based on conventional bulk-, precipitation-, emulsion-, miniemulsion-, microemulsion- and inverse microemulsion polymerization techniques. These techniques are extensively explained in various textbooks such as Elaissari[173] to which we kindly redirected our readers. Both silica and organic polymer based LuMaPs can be produced by these syntheses in large size range and with different matrix structures. While organic polymers are most often achieved by a radical polymerization, the Stöber process,[174] a base catalyzed polycondensation of tetraalkoxysilanes, is predominant for silica based LuMaPs.

The seeded polymerization is a common variant of conventional polymerization techniques. Here, a mostly monodisperse core particle is used as a template for the subsequent polymerization step. The resulting magnetic particles have a narrow size distribution. This is a key requirement for applications such as flowcytometry but is also important for a reproducible and predictable clearance from organisms after *in vivo* applications.

2.3.3 Layer-by-layer techniques

A versatile, facile and predictable strategy for coating the components of LuMaPs onto a core particle is the so-called layer-by-layer (LbL) technique. Usually positively and negatively charged species are coated onto a charged template in alternating manner. Thereby, the surface charge can be adjusted to fit the requirements of the particles and to allow adsorption of charged species such as drug molecules or functional nanoparticles. Polyelectrolytes, such as negatively charged poly(styrene sulfonate)[15,99,103,110,175] or poly(acrylate)[104] and positively charged poly(allylamine hydrochloride),[99,103,110,175] poly(diallyldimethylammonium chloride), poly(ethyleneimine)[176] or chitosan,[104] are most commonly used as matrix material applying this method. However, also charged nanoparticles such as thioglycolic acid capped QDs[99,103,104,110,175] and charged magnetic ironoxide nanoparticles can be arranged in layers on oppositely charged surfaces.

The thickness of the coatings can be adjusted by the number of layers. On the one hand,

this method seems to be ideal for the study of distance dependent phenomenons such as quenching or energy transfer between magnetic core and luminescent shell. On the other hand, no reports employing polyelectrolytes for this purpose exist in literature so far. In studies which describe that a spacing layer between magnetic and luminescent components reduced the quenching, silica was mainly employed as polymeric material.[97,98,177] Wang et al.[72] reported on LuMaPs where silica spacing layers between multiple shells that incorporated different QDs were used to minimize the resonance energy transfer between the different luminophores.

2.3.4 Spray-drying or aerosol spray technique

Spray-drying of cocktails containing lipophilic magnetic nanoparticles, a matrix polymer, a luminophore and a solvent with relatively high vapor pressure results in LuMaPs with a usually broad size distribution. This method was successfully applied for the production of oxygen sensitive LuMaPs.[14] Advantages of this production method are the predictable distribution of the components similar to the distribution in a spin- or knife-coated foil and the direct and emulsifier-free production of the final particles. Moreover, a low-cost equipment, such as a conventional air-brush and a heated beaker, was sufficient for the production of LuMaPs. Of course, the particle size distribution would be narrower and the particle size might be tuned easier applying a dedicated spray-drying device.

In contrast to solid sensor films, the spray-dried oxygen sensitive LuMaPs showed highly linear calibration characteristics.[14] The authors were able to attribute these characteristics to a highly porous structure of the resulting particles which ensures similar environments for all sensor dye molecules.[178] Moreover, the response time of such sensors is usually fast due to short diffusion distances.

In a similar approach, Li et al.[11] employed a houshold ultrasonic humidifier for the production of an aerosol with droplets containing TEOS, MNPs, a triblock copolymer, rare earth chloride salts, hydrochloric acid, ethanol and water. The acid catalyzed condensation reaction occured inside the droplets and the resulting silica matrix incorporated both magnetic and luminescent components.

2.3.5 Solvent evaporation

Similar to spray-drying techniques, cocktail droplets can be generated in a liquid phase instead of in a gas phase. By the aid of conventional emulsion techniques droplets of an organic solvent containing all required LuMaP-components can be produced. The solvent needs to be immiscible with water. The emulsification is assisted by the application of high-energy mechanic shear forces and emulsifiers dissolved in the continuous phase.

Zhang et al.[29] used this technique to incorporate different QDs together with MNPs inside a methacrylic acid based triblock copolymer matrix which was modified with octylamine to better encapsulate the lipophilic nanoparticles. The resulting LuMaPs had sizes between 40 and 280 nm. The sizes depended on the ratio of QD to polymer and the authors mentioned that controlling the average size was relatively easy while controlling the size distribution was difficult. To narrow the originally broad size distribution, filtration and fractional precipitation by centrifugation at different speeds were used.

Similarily, Kim et al.[6] incorporated QDs or MNPs together with the anti-cancer drug doxorubicin (DOX) into a biodegradable poly(D,L-lactic-co-glycolic acid) (PLGA) matrix. The resulting particle suspension was also filtered in order to remove big aggregates. The surface was further functionalized with poly(L-lysine)-poly(ethylene glycol)-folate to increase the cell internalization efficiency. Although the authors found that PLGA nanospheres with encapsulated MNPs are almost non-toxic compared to the DOX loaded particles, the cytotoxicity of QD containing biodegradable particles should be investigated separately. QDs consisting of highly toxic components will be released from the spheres upon degradation and their effect on the organism is unpredictable.

Recently, this method was employed for the production of magnetic pH and oxygen sensor particles.[179] In contrast to the nanoprecipitation method[15] described in section 2.3.6, this allowed a higher variability of the matrix polymers and significantly increased the particle production rate.

2.3.6 Nanoprecipitation or solvent displacement

The so-called nanoprecipitation or solvent displacement method for the production of LuMaPs differs from the previous mentioned methods (sections 2.3.4 and 2.3.5) in this way that the solvent is removed differently from the cocktail. While evaporation is the main process of solvent removal in spray-drying and solvent evaporation, here, the solvent is highly soluble in the precipitant. In a nanoprecipitation process, the cocktail consists of magnetic nanoparticles, a luminophore, a matrix polymer and a solvent which is miscible with the precipitant. The precipitant can be any organic or waterbased liquid that is miscible with the cocktail solvent but is not a solvent for the other matrix components. While this method is relatively flexible considering the type of solvent and matrix polymer for the production of non-magnetic particles,[180] only limited combinations are possible for the production of LuMaPs. This is due to the requirement of a stable MNP dispersion in the solvent while maintaining the miscibility with the precipitant. Successfully employed combinations for the production of MOSePs (magnetic optical sensor particles) are THF or THF/acetone mixtures as solvent together with water, methanol or ethanol as precipitant.[15] The authors reported highly reproducible, tunable hydrodynamic diameters in the submicron range by varying precipitation parameters, such as flow rate, polymer concentration, MNP concentration, precipitant polarity, precipitation direction, molecular weight and polarity of the polymer. In general, the PDI values for most precipitations were low (i.e. < 0.1), however, electron microscopic investigations revealed a trend towards increasing polydispersity with increasing average particle diameters.

A combination of precipitation and emulsion technique was presented by Liu et al.[12] Here, tenside stabilized micelles containing FITC labeled alginate and dimercaptosuccinic acid stabilized MNPs were produced by ultrasonication and subsequently cross-linked by the addition of Ca^{2+} ions. The particle diameters were tunable between approximately 3 and 35 µm by changing precipitation parameters such as the stirring rate, the $CaCl_2$ dripping rate, the hydrophilic-lipophilic balance or the MNP concentration.

2.3.7 Monomeric emulsions

For the production of LuMaPs, emulsions are frequently used starting points of different polymerizations techniques. However, LuMaPs were also described that exclusively consist of low molecular weight, non-polymerizable components. Here, the matrix material consists either of an oil phase (oil-in-water emulsions) or of a water based solution using reverse emulsions. The matrix molecules are usually not cross-linked and the emulsion droplets are stabilized by emulsifiers. The luminescent compound is either linked to an emulsifying molecule and therefore attached to the surface of the droplet,[113,115] or dispersed together with the magnetic nanoparticles in the particle core.[111,112] Emulsification often requires strong shear forces. Such mechanic stress can be generated by ultrasonication, high-speed stirring devices and high pressure homogenizers. On the contrary, microemulsions usually do not require the input of energy to stabilize the droplets as they are thermodynamically stable. The droplets of microemulsions are non-scattering and stable under defined conditions. A detailed summary of important factors influencing microemulsions such as stabilizers and co-surfactants can be found elsewhere.[173,181]

2.3.8 Other frequently used techniques

Other techniques for the production of LuMaPs are less frequently used but still highly interesting due to their simplicity and, in some cases, flexibility with respect to the LuMaPs' components and the output volume.

2.3.8.1 Swelling

The same procedure used for staining commercially available magnetic polymer beads (section 2.3.1 on page 28) was succesfully applied for the incorporation of both magnetic nanoparticles and QDs inside cross-linked polymer beads. The resulting nano-[25] or microparticles[28] retained their load inside the porous hydrophobic network.

2.3.8.2 Dip- or spray-coating of magnetic spheres

Increasing sizes of the magnetic particles require different methods for binding or incorporating luminescent compound. In the extrem case of magnetic spheres with diameters between $\sim 500\,\mu m$ and several millimeters, simple coating procedures can be applied. Ergeneman et al.[79] dip-coated, for instance, magnetic spheres with a cocktail containing polystyrene and an oxygen indicator dye. Very recently, Mistlberger et al.[80] applied a spray-coating procedure for the production of magnetically remote-controlled optical sensor spheres (MagSeMacs). This high throughput coating method resulted in thin and mechanically stable coatings. Linear polymers and hydrogels were employed as matrix material. By this one-step process, indicator dyes sensitive to oxygen or pH were incorporated into the matrix. In the case of the pH-sensor, a reference dye embedded in virtually impermeable nanoparticles was co-encapsulated in the hydrogel matrix.

2.3.8.3 Coupling of the luminescent component to a magnetic core *via* linker molecules

The direct binding of a luminescent dye to a magnetic core is possible with the help of bi-active linking molecules. One end of the linker should strongly coordinate with the magnetic particle while the other end ususally carries a functional group, such as a carboxyl-, amino-, thiol-, or epoxy-groups. Sahoo et al.[44] coupled a rhodamine 110 through its amino group to citric acid stabilized MNPs. The carboxy groups on the MNPs, provided by the citric acid, where activated with EDC/NHS. This is a common way to link amino groups with carboxyl groups. In a similar approach, Bertorelle et al.[119] used dimercaptosuccinic acid as stabilizer for maghemite NPs and coupled modified rhodamine B and fluorescein to the sulfhydryl groups at the MNP surface. The disadvantage of such direct linking procedures is, however, the missing protection by a potential matrix, which usually encloses the dye and the magnetic particle. All coupled moieties are directly exposed to substances in the medium that can cause spectral interferences, quenching or degradation of the dyes and magnetic components, respectively. Moreover, a zero-length crosslinking procedure also increases the possibility of luminescence quenching induced by the dark colored magnetic core. This problem might be circumvented by using longer spacing molecules, such as PEG derivatives or dendrimers.

2.3.8.4 Spray pyrolysis

An interesting method for the production of inorganic magnetic/luminescent core/shell particles was recently reported.[49,132] In a first step, Nd:Co:Fe_2O_3 precursors were produced by spraying an ethanol solution containing $Fe(NO_3)_3$, $Co(NO_3)_2$ and $Nd(NO_3)_3$ into a hydrogen diffusion flame. The resulting precursor particles were then dispersed in an ethanol solution containing $Eu(NO_3)_3$ and $Gd(NO_3)_3$ and again sprayed into the hydrogen flame to form the final Nd:Co:Fe_2O_3@Eu:Gd_2O_3 nanocomposites. Coating such nanoparticles with different capture antibodies resulted in multiplexed immunoassay probes with an internal reference dye.

2.3.8.5 Thermal decomposition

A two-step process for the production of core/shell Co/CdSe particles was reported by Kim et al.[48] In the first step, cobalt nanocrystals were produced *via* a high-temperature thermal decomposition of an organometallic $Co_2(CO)_8$ precursor. The resulting Co nanocrystals of 11 nm were then coated with a 2-3 nm CdSe shell to form the final nanocomposite. The authors emphasized that the relatively low reaction temperature of 140 °C during the second step had been crucial for the formation of the core/shell structure. While at this temperature, the fraction of non-coated Co nanocrystals and non-magnetic QDs was relatively low, a reaction temperature above 200 °C resulted exclusively in unassociated CdSe QDs and Co nanocrystals.

2.3.8.6 Microfluidic assisted synthesis

Reproducibility in size, shape and composition is one of the most important points regarding the production of LuMaPs. The application of microfludic devices that produce cocktail-droplets with predictable size and composition is one potential way of avoiding the sometimes cumbersome procedure of adjusting an existing particle synthesis protocol to fit the required purpose. Recently, Yang et al.[27] reported on a microfluidic device that produces cocktail droplets containing polycaprolactone, MNPs, CdTe-QDs, tamoxifen anticancer drugs and chloroform as water-immiscible solvent. The continuous phase contained poly(vinyl alcohol) which acted as crosslinking agent and stabilized the resulting nanospheres in aqueous dispersion. During the curing process, in which chloroform was evaporated, the morphology of the initially perfectly spherical droplet altered to slightly distorted but still spherical capsules. The final particle sizes depended mainly on the flow rates of dispersed (cocktail) and continuous phase.

The flexibility and the possibility of predictable upscaling by parallelization of multiple devices renders the microfluidic approach a promising route for the future production of LuMaPs and other particle based explorers.

2.3.8.7 Direct growth of SWCNT on MNP

A side product of the so-called HiPco (high-pressure carbon monoxide) process for the production of single walled carbon nanotubes (SWNTs) are SWNTs attached to magnetic iron oxide nanoparticles. Choi et al.[131] coated this nanocomposite with DNA to improve the biocompatibility and dispersability in aqueous media, respectively. The NIR fluorescence of SWNT together with the MRI contrast enhancement by superparamagnetic MNPs enabled multimodal biomedical imaging.

2.4 Applications of LuMaPs

The main components of LuMaPs which are a matrix, a magnetic and a luminscent compound (outlined in chapter 2.2 on page 6) suggest applications for which luminescent emission and/or magnetism of such particles is beneficial. These applications can be roughly organized into three categories: 1) imaging, 2) (semi-)quantitative analyte determination and 3) therapeutic applications.

The most prominent application of LuMaPs is multimodal imaging combining an enhanced MRI contrast and luminescent properties of the probes. However, the wide variety of surface modifications, matrix materials and particle structures also allows other imaging techniques, such as cell labeling, cellular uptake for imaging, visual particle tracking and the magnetic manipulation of cells labeled with LuMaPs.

Quantitative analyses achieved by either chemically sensitive dyes or immunoassays are often assisted by the magnetic properties of LuMaPs. Frequently required separation steps are simplified by the potential automatization of steps and/or require less time compared to filtration or sedimentation techniques.

Finally, the magnetic properties of LuMaPs allow targeted therapeutic applications. Here, the luminescent component can either allow a visual tracking of the drug delivery

vehicles, quantitatively monitor a drug release or act as therapeutic agent itself. Singlet oxygen producing photosensitizers are the most prominent example for luminescent dyes with therapeutic properties.

All of the above mentioned categories and their subcategories overlap and combinations of different applications are often found in literature. Nevertheless, in the following, different principles will be discussed separately for the sake of clarity.

2.4.1 Imaging

2.4.1.1 Multimodal imaging (MRI, luminescence)

Multimodal imaging is by far the most prominent application of LuMaPs. This is reflected by the large number of publications dealing with LuMaPs as multimodal imaging agents.[5,8,11,12,21,43,46,58,70,72,74,81,83–85,109,118,119,128,129,138,156,157,182–184] Most commonly, MRI and luminescent imaging techniques are combined. While the enhanced contrast in MRI images induced by the magnetic component of LuMaPs supports a preoperative *in vivo* diagnosis, the luminescent component is useful for intraoperative visualization of a labeled target tissue.[126,135] A few interesting examples of such multifunctional imaging probes were selected and are discussed below in chronological order.

In one of the first reports on LuMaPs as multimodal imaging agents published in 2005, Tan and Zhang[19] discribed the successful encapsulation of QDs and gadolinium diethylene triamine pentaacetate in chitosan particles (50 nm). The biopolymer based LuMaPs were luminescent and increased the MRI contrast by decreasing T_1. The magnetic contrast effect was dependent on the Gd-concentration.

One year later Lee et al.[116] found out that binding small magnetic nanoparticles (9 nm) to the surface of 30 nm silica spheres resulted in a significant improvement of the T_2-weighted MR images. This change was attributed to the synergistic magnetism of multiple magnetite satellites surrounding a single core silica nanoparticle. Moreover, the rhodamine incorporated in the silica core allowed simultaneous luminescence imaging. Apparently, the dark colored MNP coating still permitted the luminescence light, coming from the particle core, to penetrate the shell in sufficient amounts.

In 2007, Rieter et al.[117] investigated LuMaPs with a silica core and a gadolinium (trimethoxysilylpropyl)diethylenetriaminetetraacetate or bis(silylated) gadolinium diethylenetriaminepentaacetate shell. The first monofunctional agent binds to the surface of the silica spheres and therefore limits the Gd loading. The bifunctional Gd-complex allowed higher Gd loading by self-crosslinking in the shell. They succeeded in demonstrating the *in vitro* imaging of monocyte cells with both MRI and confocal laser scanning microscopy.

A highly interesting architecture for a multimodal imaging probe was presented by Choi et al.[131] Single walled carbon nanotubes (SWNT) attached to iron oxide NPs and wrapped in DNA were synthesized by a HiPco process followed by a coating with DNA. The DNA cover rendered the SWNT/MNP composite water dispersible and biocompatible. While the MNP acted as MRI contrast agent, the CNT was successfully used as NIR luminescent probe and thereby enabled dualmode imaging of macrophage cells.

In the same year, Bridot et al.[77] reported on Gd_2O_3@polysiloxane core-shell particles with a high longitudinal proton relaxivity and fluorescent properties. The small silica

coated Gd_2O_3 particles moved freely in the bloodstream without accumulation in lungs and liver. Later the same group employed similar particles not only for dual mode imaging but also for neutron capture therapy.[78]

The synthesis of mesoporous monodisperse silica particles with magnetic cores and co-condensed fluorescein and rhodamine dyes was reported by Kim et al.[66] in 2008. Such silica based LuMaPs were successfully employed for *in vivo* multimodal imaging in mice.

Biodegradable PLGA spheres encapsulating MNPs and doxorubicin were presented as multimodal imaging probes and drug delivery vehicles by Kim et al.[6] The MNPs resulted in an increased contrast in MRI imaging whereas the doxorubicin acted as anticancer drug and as fluorescent label for confocal laser scanning microscopy (CLSM) imaging. At the same time, Schellenberger et al.[153] reported on specially designed particles that changed there MRI contrast properties in presence of a protease. This change in MRI contrast was achieved by a special coating of the magnetic cores that triggered an aggregation of the particles upon contact with a protease. The stabilizing PEG chains were linked to the cores with a peptide containing a protease specific cleavage sequence. In this way, MRI was used for achieving quantitative information about the *in vivo* concentration of an enzyme.

In 2009, Jarzyna et al.[115] succeeded in the production of soybean oil emulsions with different droplet sizes that contained lipophilic MNPs and were conjugated with an NIR fluorescent dye (Cy5.5). They showed the accumulation of such droplets in subcutaneous human tumors in nude mice with both *in vivo* MRI and fluorescence imaging. In another interesting publication, Li et al.[104] reported on the production of hollow magnetite core, QD shell particles by a layer-by-layer technique. In addition to being luminescent and a T_2-weighted contrast agent, such particles were loaded with a model drug (cefradine) whose release rate was pH-dependent.

Recently, Stelter et al.[56] produced trifunctional imaging probes. Such particles were suitable for *in vivo* MRI, fluorescence imaging and positron emission tomography (PET). They modified commercially available PEG and amino coated magnetic particles (100 nm) with radio nucleotides (Ga-68 for *in vivo* applications, In-111 for *in vitro* applications) to allow PET and cell targeting peptides (TAT) to specifically deliver the particles to cancer cells.

2.4.1.2 Labeling cells *via* recognition sites or non-specific interactions

A number of publications reported on the application of LuMaPs for fluorescently labeling target cells for luminescence imaging.[8,54,116] Compared to non-magnetic luminescent particles, LuMaPs have the advantage of being magnetically controllable towards the target tissue and, after binding to the target cells, they allow the manipulation of the labeled cells by an external magnetic field.

Using LuMaPs equipped with targeting ligands enables the recognition of and binding to specific cells in a whole pool of cells. Wang et al.[21], for instance, used antibody modified LuMaPs for binding to an antigen present on apoptotic cells. By this, such cells could be visually sorted and magnetically manipulated or even separated from a suspension. Much effort was put into the development of LuMaPs that automatically target cancer cells. Such particles allow the localization of the targeted cells *in vivo*, but at the same

time enable a targeted therapeutic action against specific cells. Damaging healthy cells, a common side effect of conventional chemotherapeutic agents, is thereby limited. Moreover, operative removal of malignant tissue might be assisted by a better visualization of the affected cells in both MRI and luminescence images.

A simple modification for transforming LuMaPs into cancer cell targeting agents is the binding of folic acid (FA) to the particle surface. FA binds strongly to the folic acid receptor which is highly overexpressed in a variety of human tumors, especially epithelial cells. Xie et al.[25] modified LuMaPs with FA which enabled them to bind, track and magnetically manipulate cancer cells. In 2006, Chu et al.[59] reported on LuMaPs equipped with an epidermal growth factor that binds specifically to human breast cancer MDA-MB-435S cells. Thereby, these cells were labeled and could be separated from a suspension. Such smart materials might have the potential to track and remove metastatic cancer cells, an otherwise extremely difficult task. An antibody specific for leukemia cells was attached to LuMaPs by Yoon et al.[89] Floating SP2/0 cells were tracked down by the CD-10 specific antibody on the LuMaPs and the cells could be magnetically manipulated under visual control with fluorescence microscopy. More recently, Maeda et al.[92] reported on bacterial magnetic particles modified with a QD and an antibody specific for lung cancer cells. These nanocomposites were able to fluorescently label the target cells and separate them from a suspension in a magnetic field. Very small LuMaPs ($< 20\,\mathrm{nm}$) consisting of a magnetic core, a QD shell and a BSA protection on the outside were conjugated with antibodies.[61] The particles were successfully used as label for HeLa cells. The authors suggest the usage of such nanocomposites for magnetically guiding and optically tracking the delivery of drugs.

In a similar approach, Smith et al.[18] used aptamers specific for certain cancer cell lines instead of antibodies. Aptamers are a type of artificial antibodies consisting of an oligonucleotide. They are usually cheaper than monoclonal antibodies and their chemical stability is higher. Magnetic particles modified with specific aptamers selectively bound and separated the cancer cells. In a second step, luminescent particles were bound to the cells and used for visualization and quantification, respectively.

Later, Selvan et al.[43] reported on LuMaPs modified with a so called "bio-anchored membrane", which is an oleyl group bound *via* a PEG spacer to the amino group at the LuMaPs-surface. This surface modification targets cell membranes. Due to the biocompatibility, such particles are useful for imaging of live cells.

2.4.1.3 Cellular uptake and imaging

LuMaPs can either be modified to favor a specific uptake by target cells[41,47,58] or internalized *via* non-specific processes.[3,12,68,82,156] In many cases, the increased metabolism of, for example, cancer cells leads to an increased uptake efficiency without the necessity of targeting ligands at the particle surface.

LuMaPs coated for specific or triggered cellular uptake Most agents enhancing the cellular uptake efficiency are based on peptides. Funovics et al.[55], for example, modified amino functionalized MNPs with a tumor E-selectin binding peptide. This resulted in the specific uptake of these particles by the target cells. Similarily, Wu et al.[24] prepared

LuMaPs modified with transferrin, which induces endocytosis by binding to the transferrin receptor on HeLa cells. Incubation with unmodified LuMaPs showed no unspecific uptake of the nanoparticles by the cells. They also found that the transferrin-transferrin receptor interaction is weak due to sterical hindrance. Binding transferrin *via* a flexible linker would solve this problem. Another endocytosis based uptake system was presented by Lu et al.[87] Here, 50 nm LuMaPs were internalized by human stem cells *via* clathrin and actin dependent endocytosis. The labeled cells were not affected by the LuMaPs in terms of viability, proliferation and differentiation capacity. Cells encapsulating the modified LuMaPs were imaged with MRI and luminescence imaging techniques. Finally, Lim et al.[107] tracked dendritic cells *in vivo* after injection with NIR fluorescence imaging. For the delivery of the LuMaPs into HeLa cells, the particles were modified with a derivative of the TAT-peptide.

LuMaPs without targeting ligands As mentioned above, LuMaPs can also be taken up by cells *via* unspecific mechanisms. The magnetic pre-concentration of LuMaPs in the vicinity of living breast cancer cells significantly increased the unspecific uptake efficiency, as demonstrated by Zebli et al.[110] This is explained by a high local concentration of the capsules. Vuu et al.[113] performed *in vivo* MRI tumor imaging and detailed histological experiments of tumor tissue by employing the luminescent functionality of gadolinium-rhodamine based, micellar LuMaPs. Two tumors were grown with unlabeled and labeled cells, respectively, in one test animal and imaged seven days after the subcutaneous inoculation. Luminescence imaging showed that a signal was only generated in the tumor grown with the labeled cells. Yoon et al.[64] let cells simply grow in the presence of LuMaPs. The resulting cancer cells were magnetically manipulable and directed along a magnetic field gradient. Luminescent imaging was used to observe this process.

Although the ligands of LuMaPs made for unspecific cellular uptake do not trigger specific mechanisms for cellular internalization, the surface properties still influence the uptake efficiency. Holzapfel et al.[4] could correlate the cellular uptake efficiency with the number of carboxyl groups on the surface of LuMaPs. Very low acrylic acid concentrations during the particle preparation resulted in a low number of carboxyl groups on the surface and, consequently, low ingestion rates of LuMaPs into different cell lines. Bertorelle et al.[119] could selectively bind LuMaPs to the cell membrane or internalize them into the endosomes of the cells by incubation at different temperatures. The internalization pathway of HeLa cells is inhibited at 4 °C and therefore only a particle-membrane interaction can occure. Upon heating to 37 °C, the internalization pathway is restored and the LuMaPs are efficiently taken up by the cells. Luminescence imaging elucidated the possibility of magnetic manipulation of endosomes with incorporated LuMaPs.

The cytotoxicity of nanoparticles due to their small size and large specific surface area is currently topic of many discussions. While toxic components, such as QDs, obviously need to be shielded and should not get in contact with the body, the effect of untoxic components, such as iron oxide, on organisms is still not clear. Lin et al.[185] reported on silica LuMaPs that internalize into NIH 3T3 cells without being cytotoxic up to a LuMaPs-concenctration of 200 $\mu g\,mL^{-1}$. Wu et al.[62] investigated the uptake efficiency of mesoporous silica LuMaPs into rat bone marrow stromal cells (rMSCs) and NIH 3T3

fibroblast cells. At particle concentrations $> 60\,\mu g\,mL^{-1}$ close to 100 % of the cells were labeled and the cell viability remained at values above 90 %. Despite these reports, the cytotoxicity of LuMaPs, especially in the nanometer range, will be topic of many future studies. This is because a full understanding of the LuMaPs' actions *in vivo* is crucial for their approval by the agencies.

Imaging of very small Gd_2O_3 particles labeled with various dyes and coated with a PEG layer in a naked nude mouse by reflectance fluorescence imaging was carried out by Bridot et al.[77] The particles coated with PEG accumulated in kidneys and bladder (renal excretion) whereas uncoated particles were found in the liver and the lungs. This indicates the importance of a carefully selected surface coating for *in vivo* applications of LuMaPs. In a later work, Faure et al.[81] investigated the faith of LuMaPs with different PEG coatings, varying in chain length and terminal groups, after injection into the blood circle of a test animal. They found that the investigated coatings resulted in different *in vivo* biodistributions of the particles. One of the tested polymers ($PEG2000-OCH_3$) favored the accumulation of the particles in the tumor, which is desired for targeted therapy. The missing group for functionalization could be introduced by mixing the polymer with PEG terminated by amino or carboxyl groups. PEG250−COOH ensured high blood circulation times without accumulation anywhere but in the natural excretion organs, the kidneys and the bladder.

2.4.1.4 Tracking particles *in vivo*

In vivo particle tracking allows a simplified investigation of the particle accumulation in certain organs[81] or the tracking of drug delivery vehicles. In this way, the efficiency of magnetic drug targeting can be visually controlled. An interesting approach was published by Kumar et al.[144] They coupled a plasmid coding for EGFP (enhanced green fluorescent protein) to magnetic particles. Inside the body, the particles were then visible, whenever the plasmid-DNA was translated into EGFP. The particles were directed towards specific organs by a simple magnetic field without targeting ligands on the particle surface.

2.4.2 Quantitative or semi-quantitative analyte sensing

Obtaining quantitative information with LuMaPs is an attractive extension of pure imaging and tracking applications. While magnetic and optical imaging is usually still possible with quantitative LuMaPs, such particles also acquire quantitative information of their surrounding. The quantitative information can be manifold and different principles have been developed in recent years. Starting with magnetically assisted immunoassays, the application of LuMaPs has lately been extended to the field of magnetically controlled sensors. Generally, the luminescent component is responsible for acquiring the quantitative data, whereas the magnetic component of LuMaPs is mainly used in order to facilitate handling.

2.4.2.1 Fluorescence based immunoassays

In fluorescence based immunoassays the common separation step can be simplified by the aid of magnetic particles.[10,36,140,186,187] Kits for LuMaPs-based immunoassays including

necessary separators are commercially available. Fluorescence based immunoassays usually start with non-fluorescent magnetic particles with an immuno-targeting compound attached to the surface. Then the luminescence is only introduced after binding of a secondary, labeled antibody to the target molecule captured by the antibody which is attached to the LuMaP. A few reports exist however, where the luminescent label of the magnetic particle acts as an internal standard.[49,132]

The first application of LuMaPs for immunoassays was published in 1995 by Scheffold et al.[188] This group reported on a 100-1000 fold increased sensitivity by the application of magnetic luminescent liposoms conjugated to a hapten specific antibody. A combination of magnetic manipulation and immunoassays was achieved by capturing luminescent particles that carried an antigen, by magnetic particles conjugated to the corresponding antibody.[189] The conjugates were then deflected by a magnetic field inside a microfluidic channel. This enabled the separation of analyte carrying particles from non-magnetic luminescent particles and the guiding to a spatially separated read-out spot.

A completely different approach for an increased signal-to-noise ratio was proposed by Anker et al.[33] Here, permanent magnetic LuMaPs were coated on one hemisphere with a reflecting metal layer. This enabled the modulation of the luminescence of the magnetic immunoprobes with a rotating magnetic field (MagMOONs).

In 2006, Wellman and Sepaniak[161] published a magnetically assisted immunoassay with evanescent wave enhanced fluorescence detection. Besides the sensitive detection system, the washing steps were reduced by the aid of magnetic particles. Inorganic phosphores with a magnetic core and modified with different antibodies were employed for multiplexed immunoassays with an internal calibration signal.[49]

Magnetic handling of the luminescent particles also enables a certain degree of automation in immunoassays. Examples in literature report on a high-throughput automated immunoassay for 3-phenoxybenzoic acid[190] or toxins.[191] Such systems are interesting for unattended measurements or whenever analyses are carried out by untrained operators.

Sandwich type immunoassays with magnetic particles were developed for the quantification of Dengue virus[192] or for drugs in fingerprints.[193] In the latter application, first a fingerprint was incubated with magnetic immuno-particles. After the removal of unspecifically adsorbed particles with a magnetic brush, a luminescent label with a secondary antibody was applied. Interestingly, the interaction force between particles and analytes was strong enough to withstand the force induced by the magnetic brush.

In a recent work, Dupont et al.[194] developed a silicon chip for a single bead immunoassay. The readout was established with a highly sensitive avalanche photo diode. The authors suggested their device for miniaturized, mobile devices.

2.4.2.2 DNA-binding assays

Similar to antibody based immunoassays, magnetic beads simplify handling procedures in DNA-binding assays, a type of assay frequently used for the identification of specific DNA sequences.

A method called “BEAMing” was developed by Dressman et al.[195] BEAMing allowed the identification and quantification of mutations in a pool of DNA fragments. This was achieved by generating an inverse microemulsion, where statistically only one magnetic

particle (modified with an oligonucleotide primer) and one DNA fragment were located in the same droplet. When a PCR was performed with this microemulsion, the DNA fragment located in the droplet was amplified and attached to the magnetic beads. After the PCR, each magnetic bead had $\approx 10^5$ copies of the same DNA fragment at its surface. The sequence differentiation was established by incubating these beads with differently labeled oligonucleotides, which selectively bound to one or the other amplified DNA strand. To further amplify the signal, a cascade of fluorescently labeled antibody-antigen interactions was used. Finally, the beads were analyzed using a flow cytometer.

Later, Dubus et al.[145] reported on a highly interesting approach for PCR-free detection of DNA. A polythiophene was used to detect the hybridization of DNA molecules. Polythiophene has a planar and a twisted conformation, where the subunits are oriented perpendicular to each other. While the planar structure is only weakly luminescent, the twisted one strongly emits at 525 nm. Also the absorption spectra change. Interestingly, polythiophene can hybridize with both, single stranded (ssDNA) and double stranded DNA (dsDNA). With ssDNA, the planar conformation is predominant. Upon formation of a dsDNA the thiophene changes its structure to the twisted form and emits light upon excitation at 421 nm.

Sandwich type DNA assays with QDs and magnetic particles, both modified with DNA fragments, were also presented.[163,196]

Another interesting approach for very low detection limits was presented by Danielli et al.[164] A biotinylated DNA probe, that was modified with a luminescent label and a quencher (on opposite ends), was coupled to streptavidin coated magnetic beads. Upon successfull PCR, the quencher was detached from the fluorescent label and a signal was generated. The very low detection limits (3×10^{-14} M) were achieved by modulating the emission light by moving the beads in and out of the laser beam. Thereby, the background signal was eliminated.

2.4.2.3 Multiplexing and encoding of LuMaPs

Encoding of magnetic beads with luminescent labels enables multiplexed DNA- or immunoassays in combination with suspension and sedimentation arrays, respectively. The magnetism again speeds up the necessary sedimentation steps in arrays and simplifies handling.

Moser et al.[152] and Mayr et al.[151] developed an interesting encoding scheme by combining the luminescence decay time, the luminescence intensity and the particle size as encoding parameters. They calculated the possible number of clearly distinguishable encoded magnetic bead groups to be 140 and demonstrated the suitability of this concept in a DNA hybridization assay. Here, the target strand was captured by the corresponding encoded bead and the double strand formation was detected by a specific staining. Encoding of LuMaPs was also accomplished by incorporating two luminophores in different ratios,[11,17] QDs in different concentrations[28] or by producing silica layers doped with different QDs around a magnetic core.[197] The latter approach resulted in particle sizes below 40 nm. In a different, non-luminescent encoding procedure, Nichkova et al.[49] coated their LuMaPs with antibodies specific for different proteins enabling multiplexed immunoassays. The constant luminescent label of the spheres acted as internal reference.

2.4.2.4 Screening for peptides on cells, and magnetically capturing of cells

Cells often display a specific pattern of peptides and other biomolecules on their surface. Using LuMaPs modified with antibodies that specifically bind to such peptides enables capturing and manipulating of cells. Moreover, if a secondary antibody with a luminescent label is applied, a quantitative result can be achieved.

Yeung and Wittrup,[172] for instance, performed a screening of a surface-displayed polypeptide library with antibody modified Dynabeads and a luminescently labeled secondary antibody. Magnetic cell separation and luminescent detection with QD-coated magnetic nanoparticles, that were modified with a mouse anticycline E antibody, were reported by Wang et al.[45] A similar procedure specific for apoptotic cells was presented by Shi and co-workers.[21] Binding antibody modified LuMaPs to such cells enabled their visual sorting and manipulation with a magnetic field.

More recently, Smith et al.[18] developed an assay which specifically captured and preconcentrated different cancer cells with aptamer conjugated magnetic particles. In a second step, luminescent particles bound to the cell-particle conjugates to form the final hybrid. This enabled both, detection of the cancer cell type and the quantification of cancer cells.

Although antibodies are the predominant immuno-compound in these assays, other recognition mechanisms were used for cell capturing. Xie et al.[26] published the modification of LuMaPs with lectins for capturing cells *via* the glycoconjugates presented on the cell surface.

2.4.2.5 Oxygen sensors

A relatively young field of research is dealing with the combination of optical chemical sensors with magnetic properties. In such systems, the luminescence emission light changes its properties depending on the analyte concentration in the surrounding of the sensor. Despite the fact that particle based optical sensors and magnetic particles are long known and applied for different purposes, it was only recently that these two principle were combined to generate a novel tool for analyte monitoring in life science.

One of the most important parameters for bioprocess monitoring is the dissolved oxygen concentration. Most bioprocesses rely on an efficient oxygen transfer from gasphase to solution, because the solubility of oxygen in aqueous media is relatively low (260 µM at 25 ℃ under atmospheric pressure). Therefore, a continuous control of the concentration is necessary to maintain an efficient bioprocess.

In contrast to LuMaPs with the purpose of being only luminescent and magnetic, but without a sensing functionality, chemically sensitive LuMaPs have two more requirements. Firstly, the dye must have an indicator function, and secondly, the matrix must be designed so that the analyte can access the sensitive dye. Magnetically controlled, optical sensor particles were first mentioned by Anker et al.[136] and Chojnacki et al.[2] Kopelman and co-workers[136] developed magnetic sensor particles by modifying PEBBLEs, an optical nanosensor platform invented earlier by this group. They used magnetic tweezers and found sensitive LuMaPs forming particle spots which were called “Sensor Swarms”. Such sensor swarms have a higher intensity and respond faster to moving magnetic tweezers

than single particles. Chojnacki et al.[2] synthsized magnetic ormosil particles with an incorporated oxygen sensor *via* a bulk or emulsion polymerization. The resulting sensors were employed for monitoring dissolved oxygen inside a cultivation vessel with a fiber optic device through the side wall. In this way, the advantages of dispersed sensors (flexible, facile handling) were combined with the advantages of fixed sensor spots (high intensity, no interference with the surrounding medium).

The problem of collecting the magnetic particles directly in the field of view of an optical fiber was solved later on by the construction of magnetic separators with an optical window.[13] Here, block magnets were positioned around an optical fiber with their like poles pointing against each other. This produces a strong magnetic field gradient towards the tip of the optical fiber and traps the LuMaPs reliably in the optimal readout position. Due to the quantitative and efficient collection, very low amounts of sensing material were necessary to achieve sufficiently high signals.[14]

The same group reported on the production of magnetic optical sensor particles (MOSePs) by a facile spray-drying process.[14] A sensor cocktail containing a matrix polymer, lipophilic magnetic nanoparticles and an iridium coumarin based, ultrabright oxygen indicator[198] was sprayed into hot air by a conventional airbrush. The resulting sensor particles showed highly linear calibration curves from 0 to 1013 hPa of oxygen partial pressure (or 0 to $\sim$1.2 mM at 25 °C in pure water under normal pressure). Later, a detailed study on the structure of spray-dried MOSePs revealed a highly porous structure. As a consequence, all dye molecules inside the porous structure became equally accessibility.[178]

Recently, the concept of magnetically controllable sensors was further improved for the suitability in bioprocess monitoring. Mistlberger et al.[80] used magnetic stainless steel spheres with millimeter sizes and coated them with an optical chemical sensing layer. A similar system was presented earlier as a prototype for intraocular oxygen measurements. However, their suitability for bioprocess monitoring has not yet been discovered. By increasing the size of the sensors from micrometers to millimeters the handling was improved tremendously. Such magnetic sensor macrospheres (MagSeMacs) were immediately captured by a magnetic separator, they followed a movement of the separator without delay, the intensity was high and, finally, sensor chemistry and technology could be directly transferred from fixed sensor patches to the spheres. MagSeMacs were used as mobile sensor inside rotating flasks, 24-well plates, stirred cultivation vessels, tube reactors and as disposable sensors for optical fiber dip-probes.

Via a versatile nanoprecipitation method[180] the production of multifunctional MOSePs with submicron size was accomplished by Mistlberger et al.[15] Due to the bifunctional copolymer matrix with a lipophilic core and a hydrophilic shell with carboxy-groups, both the core and the surface could be equipped with versatile functionalities. The core included various oxygen sensors differing in spectral properties such as emission from the visible to the NIR range. A light harvesting system[199] in the core further increased the brightness of the sensors and extended their excitation range into the blue region, where low-cost, high-intensity light sources are available. The authors also mentioned that such particles were suitable for oxygen imaging at the surface of biological samples, such as biofilms.

2.4.2.6 pH-sensors

The same group that reported on the first magnetic optical oxygen-sensing particles also included a pH sensing functionality.[2,136] Anker et al. monitored pH by moving a LuMaPs-sensor swarm through a pH-gradient.

A different particle construction was presented by Kreft et al.[101] Multiple polyelectrolyte layers formed a capsule around a pH-indicator (SNARF) which was bound to dextrane. In the shell of the capsule, magnetic nanoparticles were immobilized. Such micro sensor particles allowed imaging of the pH in biological samples. Even intracellular measurements were performed after endocytosis of a capsule by a cancer cell.

Guo et al.[3] discovered that mercaptopropionic acid (MPA) stabilized QDs incorporated in chitosan/poly(methacrylic acid) beads changed their luminescence intensity between pH 7 and 4 non-linearly but reversibly. They attributed this change to the "pull-out" of MPA (the complexing agent) from the QD-surface upon protonation, leading to a higher number of surface defects. The cellular uptake of the nanosensors was increased by the application of a magnetic field. Li et al.[11] obtained pH sensitive LuMaPs by the incorporation of pH indicators together with MNPs in silica spheres during an ultrasonic assisted spray drying process.

Magnetic pH-sensors with sizes in the millimeter range were produced and investigated by Mistlberger et al.[80] The spray-coating of stainless steel spheres with a dual-lifetime-referenced pH-sensor resulted in mobile pH-MagSeMacs (magnetic sensor macrospheres). Similarly to the oxygen MagSeMacs, these spheres were strongly but reversibly attached to the tip of an optical fiber and could be controlled inside a vessel with a magnetic separator positioned at the outside of the vessel.

The same group produced pH-sensitive magnetic optical sensor particles (MOSePs) by covalently coupling a fluorescent pH-indicator to the magnetic polymer cores.[80] This concept was later improved by copolymerizing a functional pH indicator into a hydrogel shell around the same magnetic core. In this way, the cross-sensitivity to ionic strength was greatly decreased.[200]

If a modulated light source is not an option for background reduction, the principle of magnetically modulated optical nanoexplorers (Mag-MOONs) also enables the differentiation of a modulated analyte signal from an unmodulated background signal.[32,201] This principle was used by Roberts et al.[35] to produce pH-sensitive, magnetic sensor particles.

2.4.2.7 Physical parameters (viscosity, temperature)

Mag-MOONs (MOdulated Optical Nanoexplorers)[32,201] are luminescent microspheres with two properties that differ from conventional LuMaPs. Firstly, they are permanent magnetic, i.e. they orient themselves in a magnetic field. Secondly, one hemisphere is coated with a reflective metal layer while the other is not. Thereby, light emitted by a luminescent dye which is encapsulated in the transparent matrix can be modulated by a rotating magnetic field. The particle rotation speed is reflected by the blinking frequency and depends on the rotation speed of the external magnetic field. However, at a certain frequency the particles are unable to follow the driving magnetic field and start to slip. This slipping frequency depends on physical parameters, such as the viscosity

and indirectly the temperature of the surrounding medium. Optical sensors for physical parameters that rely on this principle were reported in literature.[33,34]

Other temperature sensors are achievable by the incorporation of temperature sensitive luminescent dyes into polymer matrices with low cross sensitivity to other substances such as oxygen or salt. Basically, all luminescent chemical sensors are cross sensitive to temperature. As a consequence, the measurements must either be carried out at a constant temperature or a temperature reference sensor must be included in the setup. Although the incorporation of temperature sensitive dyes in magnetic polymeric particles is obvious, to the best of our knowledge up to now, no publications have been dedicated to this topic.

2.4.2.8 Enzyme activity monitoring

Recently, LuMaPs were employed for monitoring enzyme activity. Kreft et al.[105] produced multishell capsules similarly to the magnetic pH-sensors developed by the same group. Different enzymes were located in different compartments of the capsules. Such a system allows spatially confined enzymatic reactions. As an example, they encapsulated glucose oxidase (GOX) and peroxidase (POX) in different capsules and followed the enzymatic reactions

$$\text{glucose} + \text{O}_2 + \text{H}_2\text{O} \xrightarrow{\text{GOX}} \text{gluconolactone} + \text{H}_2\text{O}_2$$
$$\text{H}_2\text{O}_2 + \text{Amplex Red} \xrightarrow{\text{POX}} \text{H}_2\text{O} + \text{resorufin} + \text{CH}_3\text{COOH}$$

detecting the luminescent product resorufin.

Enzyme activity based MRI contrast imaging was published by Schellenberger et al.[153] A PEG stabilizing chain was linked to MNPs *via* a protease cleaving site. When the enzyme was active, the stabilizing chain was removed from the particles surface and aggregation occured. This led to a changing MRI contrast. Finally, Mistlberger et al.[15] succeded in measuring the activity of enzymes coupled to the surface of MOSePs with a sensor dye incorporated in the same particle's core.

2.4.2.9 Other analytical applications

Detection principles and applications of LuMaPs other than the ones mentioned in the sections above include magnetophoresis, affinity capillary electrophoresis and electro chemiluminescence (ECL). Two examples are known about the application of LuMaPs in magnetophoresis. After attaching magnetic particles to cells or incorporating them into cells, magnetophoresis can be applied to concentrate the cells[192] or to measure the efficiency of particle uptake *via* the velocity of the cells.[119] Okamoto et al.[171] presented a combination of capillary electrophoresis and magnetic preconcentration. The LuMaPs were coated with a dextran-sulfate layer that binds the analyte. Nonbinding impurities were traveling on, while the target analyte was kept until the magnetic field was switched off.

In an early work, Namba et al.[160] reported on a magnetically assisted sandwich type immunoassay with a ruthenium(II)-tris-bipyridine-NHS labeled antibody. The lumines-

cence of the label was excited *via* electric energy. More recently, Zhang et al.[73] published a ECL sensor for polyamines. Amines were directly oxidized by $Ru(bpy)_3^{2+}$ in its excited state. The magnetic properties of the nanoparticles facilitated the production of the ECL-nanoparticle modified electrode.

An interesting system with LuMaPs acting as markers for a broken blood purification system was presented by Ettenauer et al.[202] In this system, LuMaPs were mixed to a blood purification liquid to introduce an emergency stop after membrane rupture. In case of a broken membrane, the particles entered a detector where they were captured by strong magnets and detected *via* their fluorescent properties. An immediate shutdown of the pumps was triggered upon positive particle detection.

In a recent publication, Gai et al.[142] reported on a system for *in situ* druge release monitoring. They used mesoporous silica particles with a magnetic core and upconversion nanoparticles adsorbed to the pores. After loading of the pores with ibuprofen the drug release was monitored by a changing upconversion luminescence. The increasing signal upon drug release allowed a quantitative information about the progress of drug delivery.

2.4.3 Therapeutic applications

The application of LuMaPs in medicine is a fast growing field. Diagnosis and imaging, however, only represent a part of their potential. Recently, various magnetic luminescent particle platforms were reported as tools for actively affecting the tissue by means of drug delivery or direct interaction.

2.4.3.1 Drug targeting

A smart selection of the matrix material allows a drug to be loaded into a LuMaP. The magnetic properties then enable a targeted delivery of the drug to the affected tissue.[144] As mentioned above, luminescent imaging can be used to trace the particles after injection or it can be used for monitoring a drug's release.[142]

NIPAM A well know matrix polymer for targeted drug delivery is the stimuli responsive poly-*N*-isopropylacrylamide (NIPAM). Delivery vehicles based on NIPAM were already reported in 2005.[54,102,182] NIPAM is temperature responsive and shrinks with increasing temperatures (T). When T reaches the lower critical solution temperature (LCST), a sharp decrease in size can be seen. Consequently, a drug release can be triggered in dependency on the temperature.

Mesoporous silica A second prominent drug delivery matrix is mesoporous silica (MS). MS is generated by a Stöber-process in the presence of a porogen. The pores can be loaded with a drug which is passively released into the target tissue. Due to the high stability of the material and the potential surface modifications an increasing number of papers based on this principle appeared in the past few years.[5,7,11,66,74,85,141,142,146] Kim et al.[7] reported on magnetic mesoporous silica particles loaded with a zinc-phthalocynine (for PDT) and ibuprofen for drug delivery. Liong et al.[74] delivered a water-insoluble anticancer drug into cancer cells. The silica support enabled the transport of the hydrophobic drug through

the hydrophilic medium. Folic acid conjugated to the surface of the particles mediated the cellular uptake. The same particles were also used for MRI and luminescence imaging.

Poly-saccharide shells A drug delivery system based on a stimuli responsive chitosan network with co-encapsulated magnetic nanoparticles and QDs was presented by Li et al.[9] The drug release rate depended on the pH of the medium and the crosslinking degree. Wang and Sun[22] presented dextran/poly(allylamine hydrochlorid)-based LuMaPs and demonstrated the release of methylorange, a model drug.

Biodegradable polymers Another possibility to release a drug from particles is the application of biodegradable polymers. Such a matrix is degraded inside the organism either unspecifically, by enzymes present virtually everywhere, or at distinct positions. The latter can only be accomplished with a material that is stable in most environments, but prone to degradation by an enzyme which is located at a distinct position inside the body. Kim et al.[6] reported on the inclusion of doxorubicin, together with QDs or MNPs in poly(D,L-lactic-*co*-glycolic acid) particles by a miniemulsion/solvent-evaporation process. This polymer was degraded inside the human body. A problem of this approach might be the release of all other substances that were also encapsulated in the matrix. Yang et al.[27] used a microfluidic device to load tamoxifen, MNPs and QDs into polycaprolactone micro capsules. The size of these delivery vehicles was important for the degradation and release kinetics. The microfluidic device allowed a highly uniform size distribution and fine-tuning by adjusting the flow rates of cocktail and shear fluid.

Other systems A common and versatile approach for loading drugs to LuMaPs is the layer-by-layer technique. Li et al.[104] produced hollow capsules applying this technique and loaded them with cefradine by a simple diffusion process. The release rate of cefradine from the hollow core was pH dependent. A highly interesting drug delivery system was presented by Hu et al.[96] The drug was loaded into single crystalline magnetite capsules. At high frequency magnetic fields the capsules broke and released the drug. They could also attach a QD to the magnetite capsule. The luminescent properties of the QDs correlated with the release rate of the drug.

2.4.3.2 Cancer therapy

Cancer therapy is one of the hottest topics in current research. Recently, also LuMaPs found their way into this lucrative field of research. The properties of multifunctional nanoparticles attracted the interest of scientists due to the multitude of possibilities in medical research, diagnosis and therapy. While the production of highly cytotoxic substances is usually unproblematic, the biggest challenge is to limit the damage of healthy cells. In other words, to produce the ideal anti-cancer drug.

Photodynamic therapy (PDT) In photodynamic therapy, cytotoxic oxygen species are generated from molecular oxygen by so-called photosensitizers. Such photosensitizers are luminescent dyes that use the energy of light to transform non-toxic $^3O_2$ to a toxic,

reactive oxygen species. Frequently, research groups report on the incorporation of photosensitizers into magnetic particles.[7,8,15,16,84,137,138] Such particles allow targeted photodynamic therapy and limit damages to healthy tissue. Gu et al.[138] observed apoptosis (controlled cell death) of HeLa cells after the uptake of porphyrin modified MNPs and illumination. Due to the magnetic properties of the nanocomposites, the group also mentioned the possibility of hyperthermia, a different cancer therapy that will be discussed later. Lai et al.[84] also treated HeLa cells with PDT-functional LuMaPs. The particles contained a singlet oxygen producing iridium complex. In addition to PDT, such nanotherapeutics are suitable as MRI contrast agent and for phosphorescent imaging. Recently, Mistlberger et al.[15] reported on the production of magnetic polymer particles that incorporated a trace-oxygen sensor dye which also produced singlet oxygen. These particles were multifunctional, and they acted as a magnetically controllable vehicle for an oxygen sensor and for a PDT agent. The production rate of singlet oxygen in nanoparticles is especially high, due to the short diffusion distances and the high specific interaction area with the surrounding.

Magnetically induced cancer therapy Due to the magnetic properties of LuMaPs they are often employed for hyperthermia induced by AC magnetic fields.[137] Jarzyna et al.[115] and Mistlberger et al.[15] mentioned that hyperthermia combined with drug release might have synergistic effects and might increase the efficiency of a cancer treatment. Another group reported on "Nanoclinics" that induced cell lysis by the application of a DC magnetic field.[37] This is noteworthy, because all other cancer therapeutic applications of magnetic particles use an AC magnetic field to generate heat locally. Here, ferromagnetic particles with a cancer cell targeting ligand (LH-RH) entered cancer cells and induced lysis upon a DC magnetic field. Such a DC magnetic field might originate from an MRI instrument.

Magnetic separation of labeled cancer cells Since the introduction of magnetic particles for cancer treatment, it has always been a dream to send smart magnetic particles out into the body, let them find and capture free floating cancer cells and filter them in an external device by a magnetic field from the blood stream. However, only few reports on successful labeling and separation of cancer cells with magnetic particles exist.[59,92] There will probably be an emphasis on this field of research in the near future, because it is especially difficult to treat cancer cells after entering the metastatic stage. LuMaPs represent a promising tool for this purpose providing the possibility to monitor the process simultaneously.

Neutron capture therapy Other cancer therapies are less commonly reported in relation with LuMaPs. In 2007, Bridot et al.[77] presented FITC labeled, Gd_2O_3 particles as a tool for multimodal imaging and neutron capture therapy of cancer. They attributed the high neutron capture cross-section of their particles to the presence of ^{157}Gd, an isotope with an approximately 20 % natural abundance. The 66 times higher neutron-capture cross section of ^{157}Gd compared to ^{10}B allowed the destruction of a tumor loaded with biocompatible Gd_2O_3 particles under the irradiation with a harmless thermal neutron beam.

2.4.3.3 Anticoagulant

Qiu et al.[40] reported on the coupling of heparin to the surface of LuMaPs. The anticoagulant activity was tested and the particles were magnetically guided to a desired place and traced *via* their fluorescence. Such particles might act as tool for magnetically guided anticoagulation of blood clots inside blood vessels.

2.4.4 Environmental or life science applications

The magnetic properties of LuMaPs are often employed for the magnetic manipulation of cells or molecules that are recognized by the particles through a targeting agent. As an example, magnetic separation of target cells might be useful for enhancing the signal in an analyte assay, but also for therapeutic applications.[59] Moreover, by specific targeting agents on the LuMaPs-surfaces, a visual cell sorting is possible.[21] Recently, Jang and Lim[69] reported on magnetic particles for such different applications as capturing proteins from a solution or for the extraction of heavy metal ions (Cu, Cd, Co, and Pb) from solutions by EDTA modified LuMaPs.

2.5 Conclusion and outlook

Research on luminescent magnetic particles (LuMaPs) with sizes ranging from a few nanometers up to several millimeters will be a major topic in research. Due to the multitude of possibilities introduced by the combination of functional luminophores with magnetic materials, applications in virtually all fields of science are thinkable. LuMaPs act as nanoexplorers, nanotherapeutics, imaging- and bioprocess monitoring tools, and most of these functions can be spatially restricted to a region of interest by magnetic control. Especially the combination of optical sensors with drug delivery vehicles is promising for biomedical applications.

Part II

Publications in peer-reviewed journals

3 Magnetic sensor particles – An optimized magnetic separator with an optical window

This chapter was published as *Full Paper* in

Journal of Physics D: Applied Physics, 2008, 41, 085003, (9pp)

doi: 10.1088/0022-3727/41/8/085003

Authors: Günter Mistlberger, Paweł Chojnacki and Ingo Klimant

Abstract Magnetically separable optical sensor particles represent a good alternative for conventional electrochemical and fibre-optical oxygen and pH sensors. Further improving the suitability of magnetically separable optical sensor particles, we reconstructed the separation adapters. Computer simulations of magnetic fields, indicated that an assembly of radially magnetized rings is preferred. We investigated different materials and dimensions of adapters and improved commercially available, axially magnetized rings using a magnetically soft iron cone together with the rings. Adapters simulating a radially magnetized ring were constructed out of several block magnets arranged like a star around an optical fibre. These adapters collected the sensor particles exactly in the field of view (FOV) ensuring high efficiency and, on top of that, showed a higher resistance of the resulting sensor spot against shear forces in stirred liquid. All adapters were characterized in a stirred flask recording signal intensity versus stirrer speed plots.

3.1 Introduction

Monitoring of chemical parameters in biological samples is of major interest in such different fields as food technology, pharmaceutical industry, biotechnology, waste water treatment and bio-engineering. Whether it is fermentations in large-scale bioreactors or micro-scale deep well plates, knowledge of oxygenation and pH-value is of great interest during the whole process.[203–205] While the electrochemical sensors for these parameters are well established and widely used in industry, they especially lack an easy way of miniaturization, which is very important for the use in high throughput methods. Cultivation of bacteria and other cell cultures in very small volumes (e.g. deep well-, or microtiter plates) and monitoring of various parameters in parallel provides new possibilities for high-throughput investigation of culture-growth and metabolic parameters.

But not only the size and complexity of sensors play a crucial role for high-throughput techniques, also the costs become more and more important. This is where optical sensors can score. They are cheap, small and in principal only sight contact is required for signal-readout. During the last years especially modified particles became more and more important as versatile and highly flexible sensors for a variety of analytes.

The use of modified magnetic micro particles as optical sensors for oxygen was recently published.[2] The magnetic sensor particles could also be in the submicrometer range, as long as the size and magnetite content ensure reasonable separability. The presented magnetic optical sensor particles combine the advantages of pre-immobilized sensor spots and dissolved indicator dyes or sensor particles. On one hand, they are easily added to and autoclaved with the fermentation media, and, on the other hand, they can be magnetically collected at a certain region and optically measured from outside the flask or vessel. Moreover, also recycling is easily achieved due to the possible magnetic separation of the sensor-particles. Thus, for the use as optical sensors, magnetic optical micro particles provide major advantages compared to their non-magnetic counterparts.

The sensing principle the sensor particles used in this work are based on is dynamic luminescence quenching. In this particular case the luminescence of the dye is quenched by oxygen. This leads to a phase shift of the emission light which can be measured with a phase fluorimeter and correlated to an oxygen concentration.

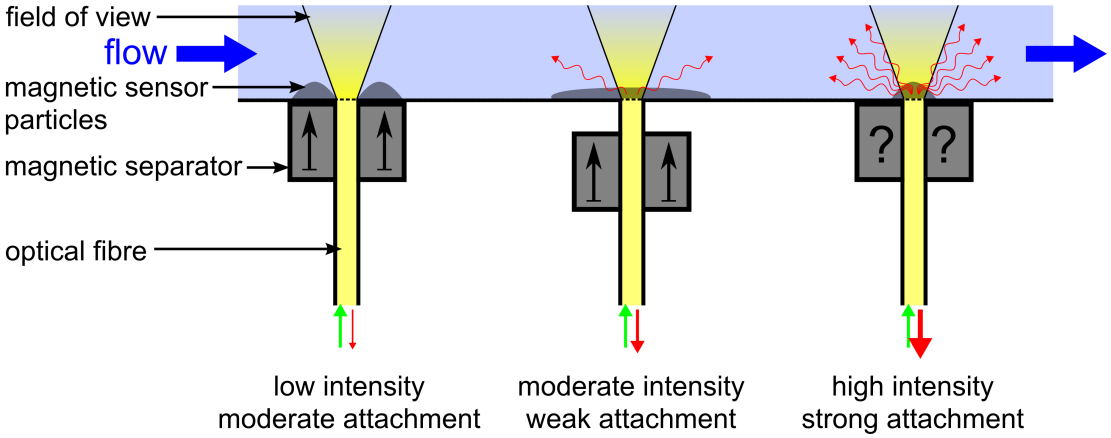

Figure 3.1: Simultaneous sensor collection and signal readout. The available axially magnetized adapters either collect the particles very inefficiently or completely at the wrong place. A desired adapter would collect the optical sensor particles exclusively in the FOV, which results in high intensity and most efficient usage of the sensor material.

However, one problem remained during the first approaches published by Chojnacki *et al.*:[2] Due to the use of axially magnetized rings with the optical fibre in their centre, the particles were not exclusively collected in the field of view (FOV), but tended to drift to the point of maximum magnetic field density at the poles, which were located just around the optical fibre. Until now, the situation was improved by positioning the axially magnetized ring magnets further away from the particle spot (3-4 mm). This led to the accumulation of particles in a wide spread area including the whole ring surface and the inner circle.

Drawbacks of this setup are the necessity to employ a large amount of particles and in addition, magnetic forces acting on the particles are low (figure 3.1). Generally, magnetic particles drift along a gradient in a magnetic field towards points with maximal flux density. The steeper the gradient, the faster move the particles. However, as usually a certain maximal flux density at some point can be reached, a steeper gradient towards this point also results in a smaller interaction volume between magnet and magnetic particles. The magnet "sees" less particles. Consequently, it is required to consider all three parameters, when designing an optimized magnetic separator, namely the absolute maximal field strength, the gradient steepness of the field and the shape and expansion of the magnetic field, respectively.

In this study we present a solution to these problems employing specially designed magnetic separators. Magnetic field simulations showed good evidence that radial magnetization could result in major improvements. High gradient magnetic separators were previously used for different applications including biotechnology, waste water or air treatment, magnetic bead handling on micro chips and even medical applications such as drug targeting in cancer therapy.[45,206–212] Also repulsive-mode magnetic separators were constructed for separating magnetic particles from suspensions with high efficiency.[213–215] However, these separators have only limited suitability for optical magnetic sensor particles, because usually no optimal sight contact to the sensor spot is given. With our new setup it was possible to focus the magnetic sensor particles exactly in the field of view of an optical fibre. This provided the possibility to look at the collected particle spot without inserting the fibre in the media itself. At the same time, negative effects like disturbance of the signal by turbid media or the magnet itself were avoided. The particles were collected much more efficiently and even the magnetic field strength was up to 200 % higher resulting in higher resistance against shear forces.

3.2 Experimental

3.2.1 Simulations

The magnetic field simulations were carried out by finite element methods provided by the free software FEMM (Finite Element Method Magnetics).[216] As magnetic material, the predefined values in the “Materials Library” for NdFeB37 (Neodymium Iron Boron magnet) with a maximum energy product (B*H) of 294 kJ*m^{-3} were used. Various magnet-geometries and arrangements were simulated (figure 3.2) and based on the results of these simulations, the practical experiments were designed.

3.2.2 Materials

The NdFeB ring and block magnets were all of grade N38 and purchased from Chen-Yang Technologies (Erding, Germany). As axial ring magnet, a stack of three magnets with $Do = 8\,\text{mm}$, $Di = 2\,\text{mm}$, $d = 2\,\text{mm}$ (each) with a total volume of 283 mm^3 (“AX8”) was employed. Since currently no radially magnetized ring magnets are available, adapters were constructed fixing block magnets in a Teflon cylinder so that they are positioned like a star around the centre provided for the optical fibre with their like poles pointing

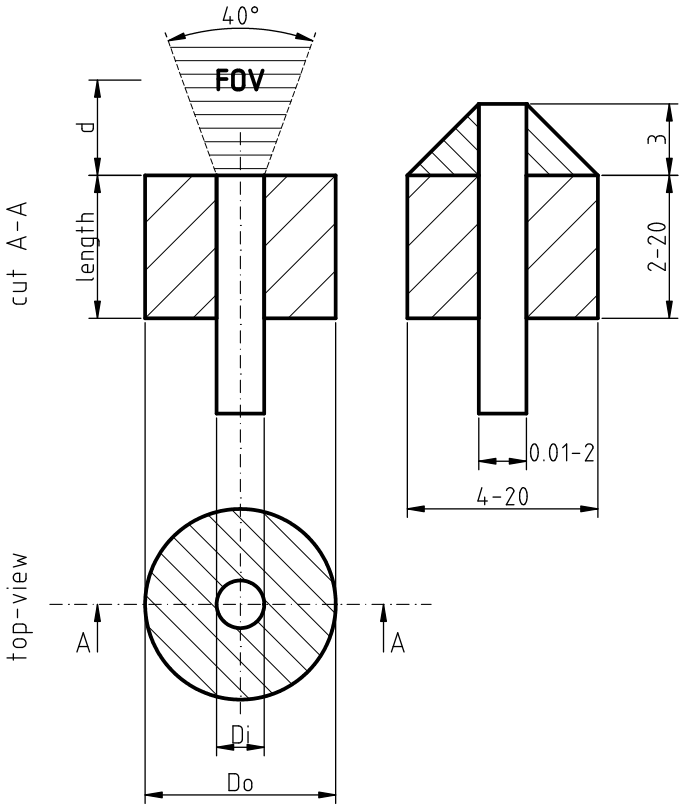

Figure 3.2: Sketch of the simulated adapters (dimensions in mm). The parameters varied in the simulations are the vertical distance d from the magnets, the length of the magnets, the inner diameter Di of the hole and the outer diameter Do of the magnetic ring. The right part of the sketch shows the setup of the simulation with a magnetically soft iron-cone on top. In addition, the ranges of all values are given.

against each other. For this purpose adapters with 4 ("RAD4"), 6 ("RAD6") and 8 ("RAD8") block magnets were constructed (see figure 3.9). The single block-magnets were all squared (6*6 mm) with gauges of 2, 1.5 and 1 mm for the 4, 6 and 8 block adapters, respectively. The names of the single adapters stated in brackets were used as reference in the results and discussion section. The minimal inner distances (distance between two facing block magnets) and their volumes are 2.0 mm with $V = 288\,\mathrm{mm}^3$ (RAD4), 2.6 mm with $V = 324\,\mathrm{mm}^3$ (RAD6) and 2.4 mm with $V = 288\,\mathrm{mm}^3$ (RAD8), respectively.

3.2.3 Particle synthesis

Tetramethoxysilane, methyltrimethoxysilane and iron-(II/III)-oxide nanopowder were of grade purum and purchased from Sigma. TiO_2 was purchased from Kemira (Helsinki, Finnland). Ruthenium(II)-tris-4,7-diphenyl-1,10-phenanthroline dichloride was synthesized in our lab as described elsewhere.[217] All other chemicals were purchased from Carl Roth (Karlsruhe, Germany) and used without further purification.

The particles were synthesized in our lab according to the procedure for aspherical

particles described by Chojnacki *et al.*[2] yielding particles with approximately 20 µm and wide size distribution. Briefly, 15 mL of each tetramethoxysilane, methyl trimethoxysilane and double distilled water were mixed with 100 µL of 0.1 M HCl, and homogenized by sonification for 30 seconds ("hydrolyzed Sol"). 1 mL of hydrolyzed Sol was mixed with 200 µL of ruthenium(II)-tris-4,7-diphenyl-1,10-phenanthroline dichloride solution in ethanol (25 mg mL^{-1}) and 700 µL of an aqueous suspension containing 70 mg of TiO_2 nanoparticles and 200 mg magnetite nanopowder. Subsequently, 200 µL of an ammonia solution (0.25% w/w) were added followed by vigouros vortexing for 3 min. The mixture was left over night, then the monolith was wet ground in a mortar. Prior to the measurement unbound magnetite crystals were removed from the sensor particles by magnetic separation and the resulting suspension was further homogenized by sonication.

All measurements were performed with one and the same batch of particles. Only the magnetic adapters were exchanged during the measurement, which makes the results totally comparable.

3.2.4 Measurements and experimental setup

In order to provide experimental proof of the performed simulations, magnetic ormosil micro-sensors were dispersed in water at a concentration of 12 µg mL^{-1} and stirred using a mechanical stirrer (EUROSTAR digital, IKA-Werke GmbH & CO. KG, Staufen, Germany) with a moon-shaped stirrer blade (50*18*3 mm, Bohlender GmbH, Germany) in a 250 mL Erlenmeyer-flask with a wall thickness of 1.7 mm. The particles were collected on the bottom part of the side-wall with the various permanent-magnetic adapters mentioned above. The signal intensity of the collected particles was measured by a phase-fluorimeter (pH-Mini, PreSens GmbH, Germany) with the corresponding 2 mm optical fibre purchased from PreSens.

3.3 Results and discussion

3.3.1 Simulations

3.3.1.1 Principal considerations

The setup and results of the simulation can be seen in Figure 3.3. Throughout this publication the field of view (i.e. the optically accessible region, "FOV") in flux-density plots will be indicated by a gray shaded background. All sensor particles within this box are available for signal readout. Three ring magnets with an outer diameter (Do) of 8 mm, an inner diameter (Di) of 2 mm and a height of 2 mm were used for this simulation. This results in a total volume of 283 mm^3. Ring magnets with this dimension are commercially available with axial magnetization and magnetized through the diameter of the ring. However, as mentioned above, vendors for radial magnetized rings have not been found so far. Nevertheless, the simulation of a radial magnetization is not problematic at all. In a magnetic field super paramagnetic particles tend to move along a magnetic field gradient to places with maximal magnetic flux density and avoid regions with less magnetic flux. With axially magnetized rings, the flux density ran through a minimum exactly at the centre of the ring's hole and was maximal right in front of the ring's surface at a vertical

distance of 1 mm away from the magnet. In a radial magnetized ring with one pole (e.g. N) on the inner and the other one (e.g. S) along the outer perimeter, the magnetic flux lines are rejected out of the centre and are therefore "compressed" at the outlets of the ring system. This resulted in a maximum magnetic flux density right in front of a non magnetic fibre in the hole of the ring. While most of the magnetic sensor particles are spoiled in the optically useless region with the axial setup, now the maximum of the flux density is located exactly in the field of view (FOV).

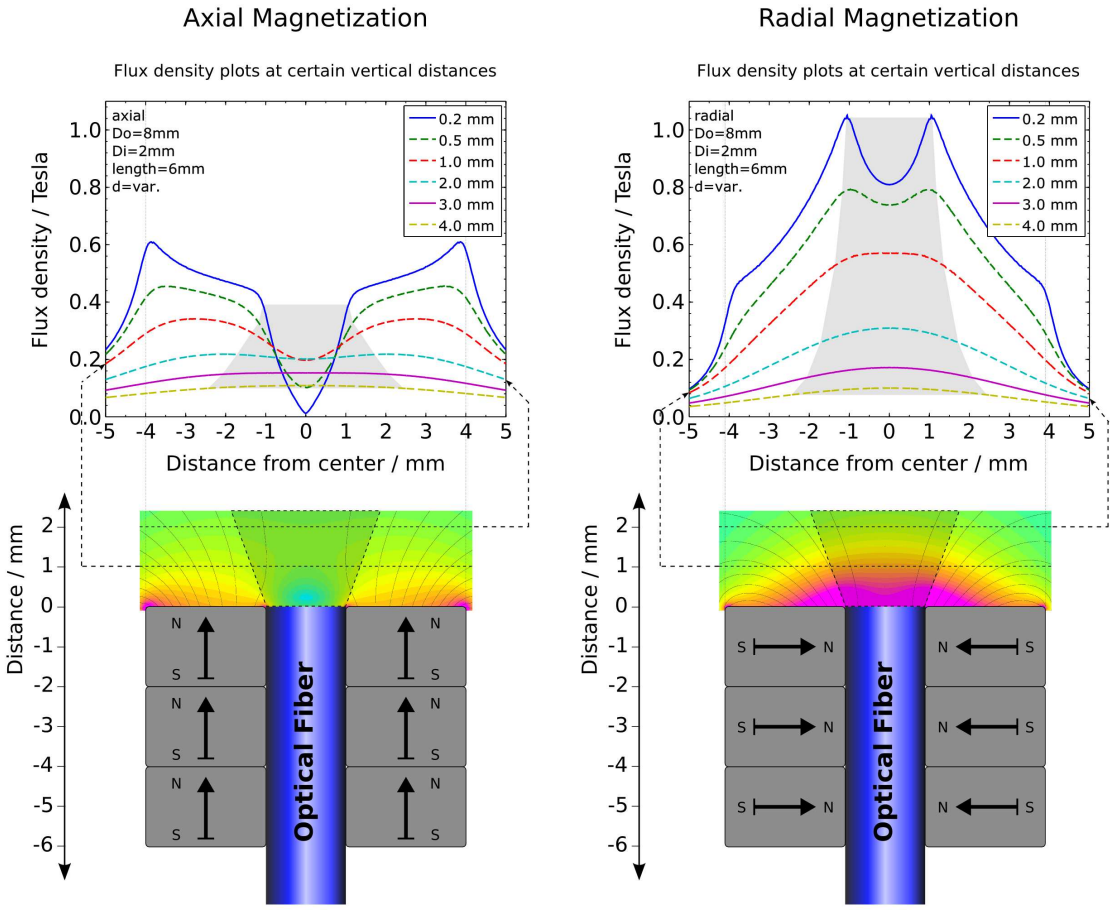

Figure 3.3: Simulation of the magnetic flux density above the end of an optical fibre, when using ring magnets with different magnetization direction. The gray shaded area indicates the field of view (FOV) at the stated distances, meaning particles located inside this area are available for signal readout. Axial magnetization: The magnetic flux density passes through a minimum at the centre of the ring magnet. Radial magnetization: The density at a certain distance is the highest exactly in the FOV of the optical fibre, which allows optimal signal read-out. Furthermore, the same volume of permanent-magnetic material results in a higher absolute flux density at a given distance ensuring a higher stability against shear forces.

3.3.1.2 Different magnetic materials

The importance of choosing the right magnetic material is illustrated in Figure 3.4. While in an axial magnetized ring (a) the results were "equally bad", a more than 10 times higher flux density in the FOV was achieved in the case of radial magnetization using NdFeB37 as magnetic material over Alnico5 (b). Especially the slope of the plot outside the FOV is worth mentioning, because it displays the gradient in flux density and therefore the force acting on the sensor particles along this line.

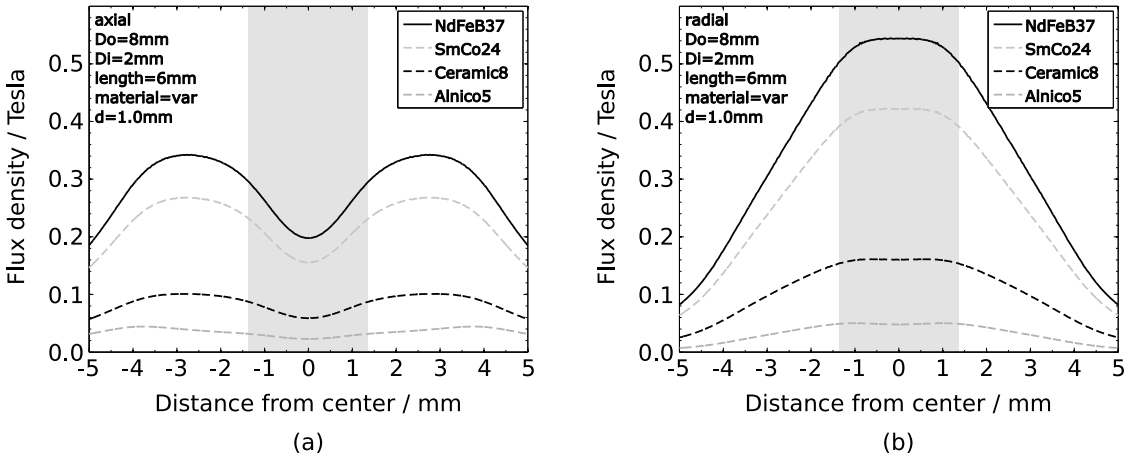

Figure 3.4: Material dependancy of the flux density. Axial magnetization (a): the negative effect of the magnetization direction got worse with an increasing magnetic strength of the material, i.e. the difference between the core and the outer regions was higher with NdFeB37 compared to Alnico5. Radial magnetization (b): improved ratio $B_{NdFeB37}/B_{Alnico5}$ of approximately 10.

3.3.1.3 Different geometries

To find out the limitations and possibilities by changing the geometries of the magnets, different outer diameters (at fixed lengths), different lengths (at fixed diameters) and finally, variable inner diameters (at fixed length and volume) were simulated. Figure 3.5a shows that an increasing outer diameter had opposite effects in axial and radial cases. Axial magnetization was most efficient when the magnetic material was located as close as possible to the perimeter of the optical fibre. Compared to the periphery, in the FOV the realtive amount of magnetic flux increased with decreasing amount of magnetic material (i.e. smaller outer diameter). Additionally, the absolute field strength of a ring with $Do = 4\,\text{mm}$ exceeded the one of a 20 mm ring. In case of radial magnetization (figure 3.5b), the employment of magnetic material was actually also most efficient at lower outer diameters considering the integral of flux density inside and outside the field of view. However, the absolute flux density in the FOV depended significantly on the outer diameter until saturation was reached.

The impact of a change in length is illustrated in figure 3.6. Again, at a distance of 1 mm (figure 3.6a and b) from the magnet, the radial magnetization was beneficial

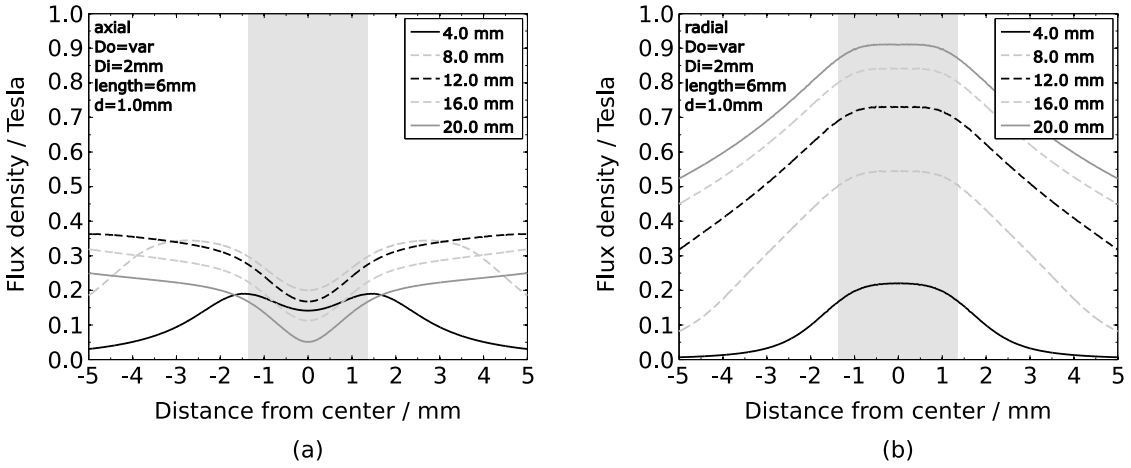

Figure 3.5: Increasing the volume of the permanent magnet *via* the outer diameter (Do) favored clearly the use of smaller *Do* with axial magnetized rings (a). The smallest *Do* was also the best in case of radial magnetization (b) considering the ratio between the outside and inside of the FOV. However, a higher absolute value of flux density in the centre was reached increasing the Do.

for the particle collection at all lengths. However, the gain in absolute flux density was negligible above 6 mm. In contrast, at a vertical distance of 4 mm some of the benefits of radial magnetization disappeared. Regarding the FOV, the gradient from the outside to the inside was still significantly higher at radial magnetization, but the absolute flux density was lower than the one achieved by axial magnetization at lengths above 2 mm. This revealed the only real weakness of the radial magnetization concept: It only works efficiently in a certain distance-range.

In all the previous simulations the inner diameter was left unchanged, because the aim of this study was to develop an adapter for the use of 2 mm optical fibres. To top results off, we investigated diameters from 0.01 to 2 mm with radial magnetized rings (figure 3.7). Axial magnetized rings with very small holes in the centre are not shown, because they behave almost like stick magnets. For this series of simulations, the volume and the length was kept constant, the outer diameter was changed to fulfil these requirements at a given inner diameter.

As a result of the repelling poles coming closer together, the valley in flux-density plots disappeared. At 0.2 mm vertical distance, there was no minimum in flux density anymore, a real apex appeared in the plot in front of a virtual optical fibre. At a vertical distance of 2 mm from the magnet, however, almost no difference in the peak shape throughout the range of simulated diameters was seen.

Due to the lack of commercially available radial magnetized rings, we tried to find alternatives. One approach towards a radial magnetization was the previously mentioned adapter with block magnets with like poles around the perimeter of the fibre. Another way was to improve the axially magnetized rings. This was realized by simply adding a magnetically soft iron cone with a hole in its centre (for the fibre) to the top of the ring magnet stack. Doing so resulted in flux density plots which were similar to the ones of a radially magnetized ring with the same volume (figure 3.8b). Compared to a radial

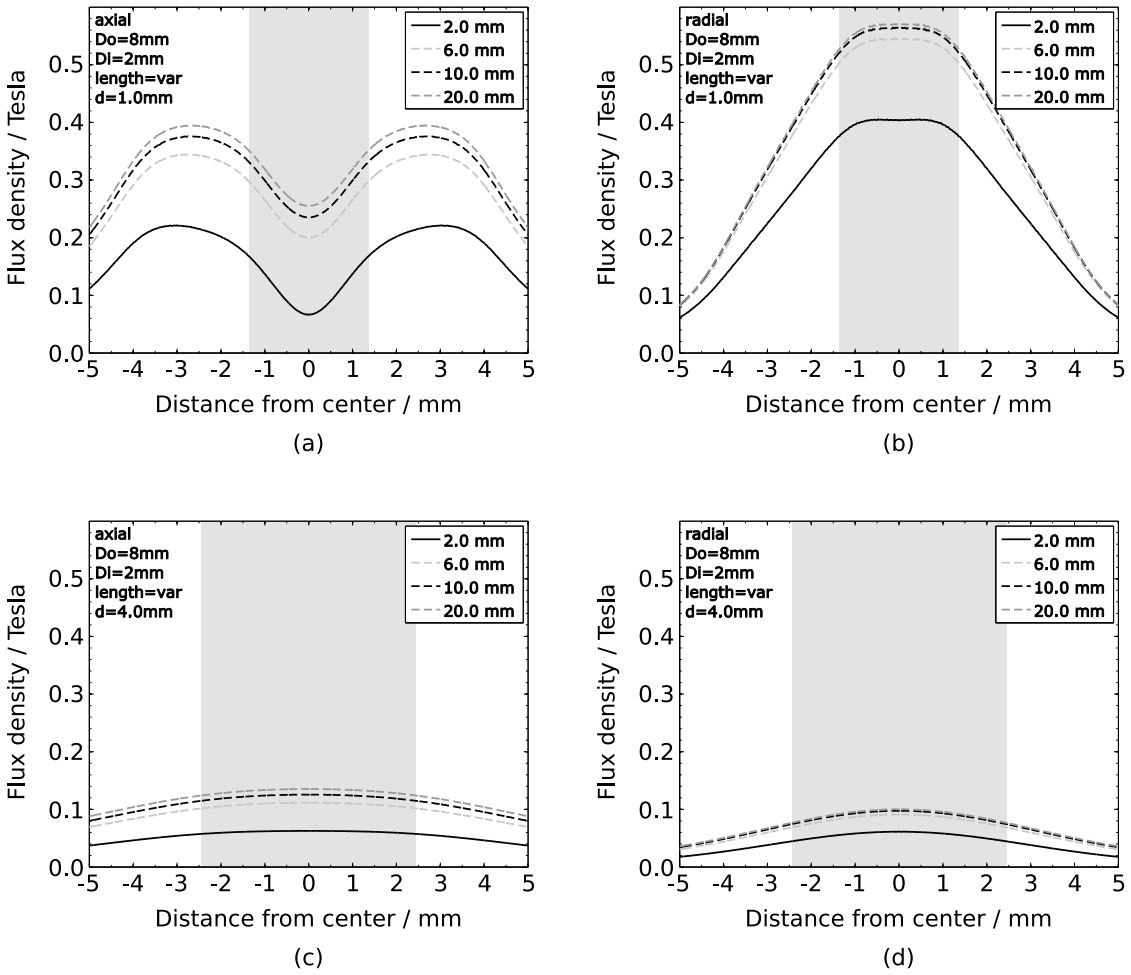

Figure 3.6: Changed lengths of the rings had negligible effects on the shape of flux density plots using the axial setup (a). For the radial magnetization (b) all curves exhibited a comparably valuable slope outside the FOV and the absolute flux density inside the FOV was saturating above adapter lengths of 10 mm. Interestingly, the differences between axial (c) and radial (d) magnetization became much less significant at a vertical distance of $d = 4\,\text{mm}$.

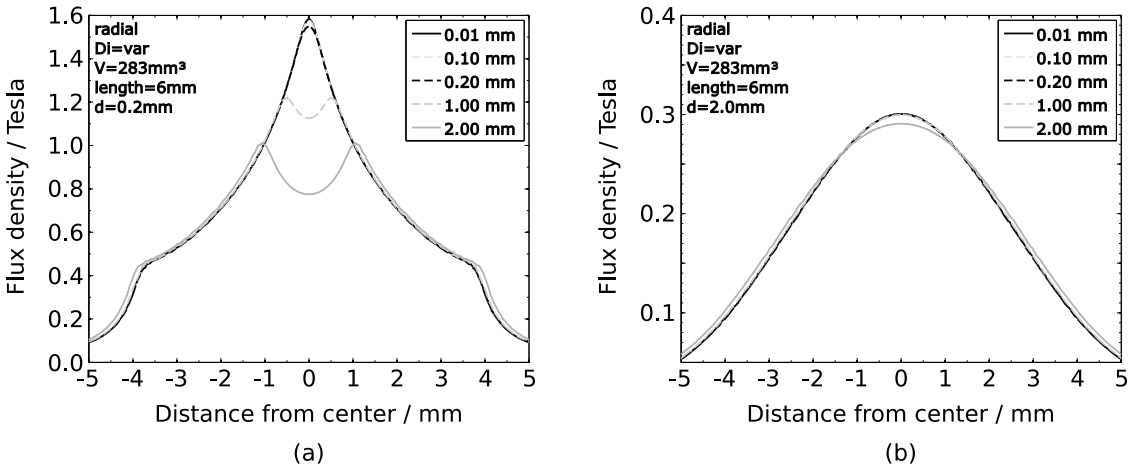

Figure 3.7: Decreasing inner diameters (Di) for radial magnetized rings at constant volume resulted in a better concentration of flux density at low vertical distances ($d = 0.2\,\mathrm{mm}$), meaning that the usual valley disappeared. At $d = 2\,\mathrm{mm}$ this positive effect diminished almost completely.

magnetization without this magnetically soft iron tip (figure 3.8c), the flux densities were still much lower and also the relative densities within and outside the FOV were worse. Nevertheless, an improvement compared to axial magnetization (figure 3.8a) was achieved. Applying the magnetically soft cone to a radially magnetized ring was not beneficial.

3.3.2 Adapter characterization

3.3.2.1 Visualizing collection behaviour

The superior separation behaviour of our newly designed adapters is visualized in figure 3.9.

Magnetic sensor particles were collected on the bottom of a Petri dish by five different adapters. While the axial magnetized rings left a hole of sensor particles at the centre, the radial adapters collected the majority of the provided sensors exactly in front of the adapter's hole. Another result, which was not directly expected after the simulations, was the collection of particles at the outer edges of the block magnets. This can be explained by the fact that high magnetic field densities and gradients always occur at edges and especially spikes and corners of the magnetic material. In case of the simulated radially magnetized rings, there is only one continuous edge at the outer perimeter, while in case of the block magnets two corners and one edge are located very close to each other. The relative loss of sensor material due to this behaviour is in any case much lower than the loss with axial magnetization. Additionally, a further improvement of the adapters can be achieved applying real radial magnetized rings or adapters built of cylinder segments and arcs, respectively. Furthermore, dipolar interactions between different magnets should be considered for separator design. They might contribute to some unpredicted collection behaviour when the outer edges of the block magnets are located closer to each other (e.g. RAD8 in figure 3.9).

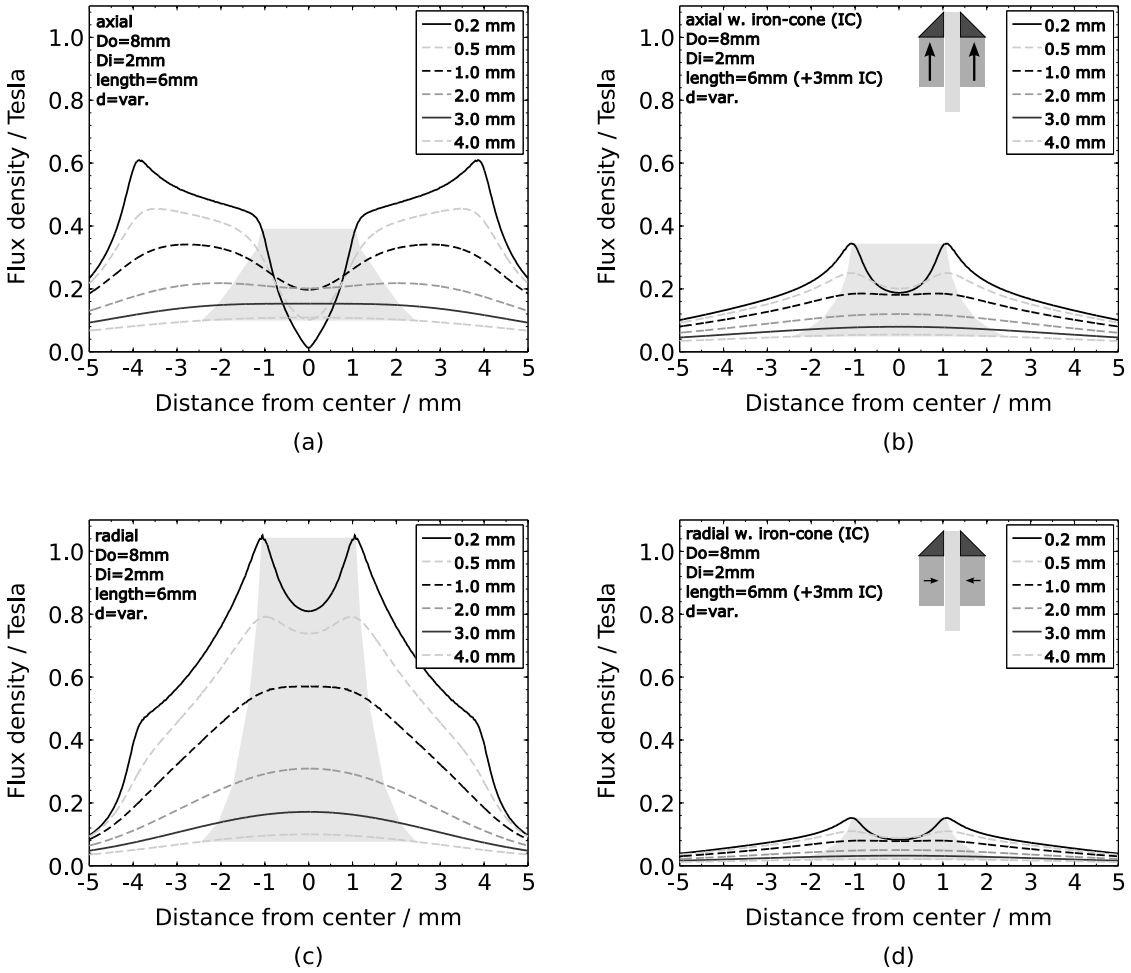

Figure 3.8: The use of a magnetically soft iron cone with axial magnetized ring magnets (b) could very much improve the behaviour of the standard setup (a). A higher relative flux density inside the FOV could be obtained, which guarantees a particle spot formation in the FOV. The absolute value correlating with the "attachment force" remained unchanged in the FOV and actually decreased outside the FOV. This is the reason, why the novel radial magnetization (c) is still much better than the improvement with the iron cone. Applying the cone to a radial magnetized ring did not improve the results (d).

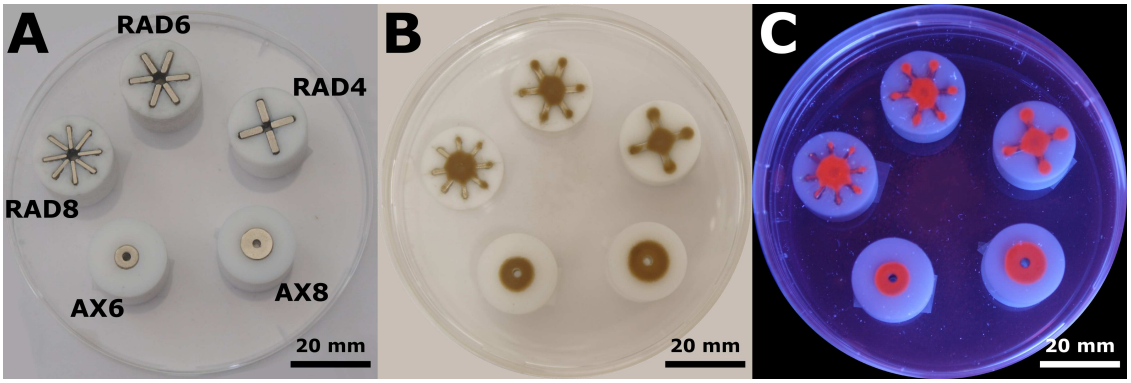

Figure 3.9: Images comparing the separation behaviour of the different adapters. In (A) the adapters are shown in top-view without sensor particles in the Petri dish above. (B) and (C) display the particles collected in a plane 0.7 mm above the adapters. While (B) depicts a normal light image, in (C) the sensors were illuminated with a UV-lamp and the image was recorded in dark with 30 s exposure time. In case of the novel radial adapters, the luminescent magnetic particles were collected at the perfect site with only a minor amount remaining outside of the FOV, while the axially magnetized rings left a hole in the particle spot in the FOV. It is also clearly visible that the better the setup resembles the shape of a ring (RAD8 compared to RAD4) the less particles are lost at the outer corners of the block magnets.

3.3.2.2 Luminescence intensity in stirred flask

To further visualize the importance and suitability of the novel adapters for lab application, we measured the luminescence intensity of collected particle spots on the side wall of a flask bearing a mechanically stirred suspension of 12 $\mu g\,mL^{-1}$ sensor particles in water. To simplify the discussion, the adapters will be referenced throughout this part in the way stated in section Materials.

The outermost curvature of the flask was identified to be the preferred measuring site providing the highest signal and consequently the highest signal/noise ratio. In figure 3.10 the luminescence intensity (amplitude of signal) was plotted against time. Stirred speeds were first increased and then decreased again. Here, it has to be mentioned that the phase shift, (i.e. the actual employed measuring signal for phase fluorimetric measurements) reaches a stable value much earlier, because in principal it does not dependent on the intensity (intrinsic parameter, valid above a certain minimal level).[218] Two different approaches were investigated: a bottom-up (from lower to higher stirrer speeds) and a top-down (from higher to lower stirrer speeds) approach. The first 30 minutes of the bottom-up approach (0-75 min) were intended to show the collection behaviour at very low stirrer speed (75 min^{-1}). After 30 min the stirrer speed was increased every 5 min in steps of 50 min^{-1} to investigate the strength of particle entrapment in the FOV.

In the top-down approach (75-110 min) additional, interesting information about the heterogenity of the sensor-particles concerning the magnetite content and size can be achieved. The higher the magnetite content, the easier the particles get trapped using higher stirrer speeds and the lower is the intensity due to light absorption by the magnetic compound.

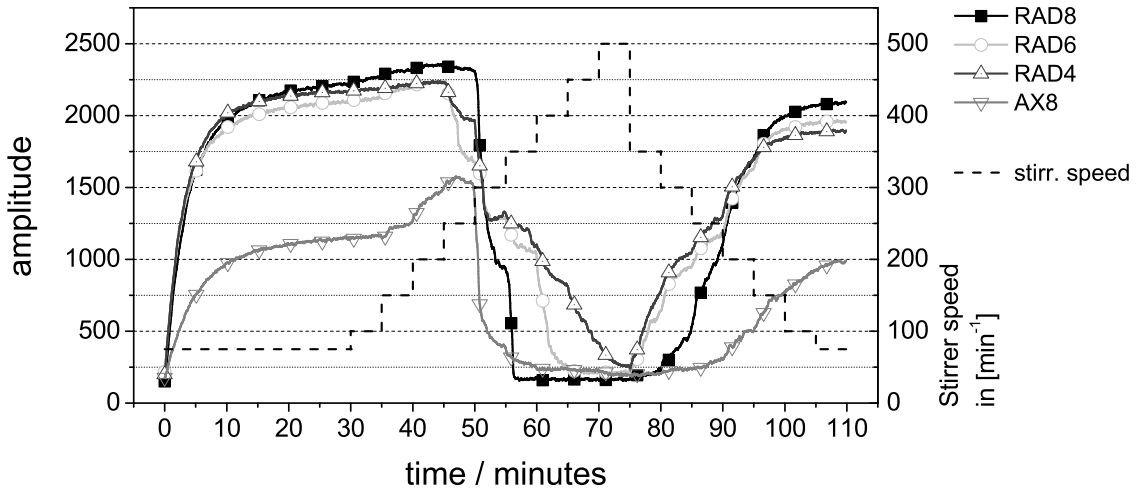

Figure 3.10: Signal intensities plotted against time. The bottom-up approach (0-75 min) displays the differences between the single adapters. All radial ones (RAD4, RAD6 and RAD8) show a higher response than the axial one (AX8). AX8 displays the unwanted effect of particle-collection outside the FOV resulting in weak signals. Higher stirrer speeds lead to the decomposition of the collected particle spots. After 75 min the stirrer speed was reduced. Due to the primary collection of high magnetite content particles, the resulting maximum intensities were slightly lower than the ones of the bottom-up approach, because the magnetite was absorbing the excitation light significantly. With axially magnetized ring magnets this effect is lowered because the particles with higher magnetite content were collected at the poles, outside the FOV.

3.3.2.3 Radial adapters

The radial adapters (RAD8, RAD6 and RAD4) showed only negligible differences in their signal intensity after 30 min, as well as in their collection curves. Up to a speed of 250 min^{-1} all three adapters showed slightly elevated signals. This can be explained by a migration of particles collected at the edges of the built-in block magnets into the centre of the FOV. Shear forces caused by the stirred liquid let the particle-spot slightly drift in the direction of the liquid movement. However, they were not strong enough to completely flush away the particles. The high shear-force resistance of the particle spot formed by the RAD4 adapter is probably due to the optimal distance between the like poles. A Di of 2 mm was the lowest among the radially magnetized adapters. Additionally, the real amount of permanent magnetic material might differ a little bit due to the production process. The block magnets were delivered with a protecting Ni-layer with given final dimensions. The thinner the blocks are, the higher is the ratio of coating to magnetic material, explaining the possibly lower field strength of the RAD8.

3.3.2.4 Axial Adapters

In general, the axial adapter AX8 collected less sensor particles in the FOV than all investigated radial adapters. As already seen during simulations, the particles were collected around the FOV. This explains also the fact that the intensity was increasing until a speed of 200 min^{-1}. Two effects may have contributed to this result. Firstly, as

explained before, the ring of sensor particles around the FOV was drifting slightly into the FOV giving a higher signal, and secondly the sensor ring may have acted as a small protector against shear forces, reducing the liquid speed inside the ring and therefore, leaving more particles in this actually low magnetic field region. It has to be mentioned that keeping the stirrer speed at a higher level for a longer time led to a complete loss of the sensor spot (data not shown).

3.3.2.5 Comparison axial-radial

Comparing the adapters with a comparable volume of magnetic material, which are AX8, RAD8 and RAD4 in figure 3.10 (0-75 min), the radial magnetization resulted in an approximately 100% higher signal intensity compared to the axial ones. Also the stability of the particle spot against the shear forces of the liquid was much higher with the novel adapters.

In the top-down approach (figure 3.10 / 75-110 min), the signal intensities of all 4 adapters are plotted against the time with decreasing stirrer speeds in steps of $50\,\mathrm{min}^{-1}$ every 5 min. Again, the adapters showing the highest resistance against the shear forces (RAD4 and RAD6) in the bottom-up approach, started collecting particles first (at $350\,\mathrm{min}^{-1}$), followed by RAD8 at 300-250 min^{-1}. Finally, the axial adapter started collecting at $200\,\mathrm{min}^{-1}$. The little difference between the final intensities in the bottom-up and top-down approaches can be explained by heterogenities of the employed sensor particles. In case of higher stirring speed, particles with higher magnetite content are collected first and are therefore located as the first layer in the FOV. This leads to a higher light absorption effect by the magnetite and consequently slightly lower intensities. However, this effect does not have any influence on the comparability of the results, because one and the same batch of particles was used during all the experiments and only the adapters were changed after each step. Additionally, these results indicated the suitability of this device for magnetic sorting of heterogeneous particles according to their separability. The results of this experiment should be considered as direct comparison between the different adapters.

3.3.3 Improvement of the AX8 adapter with a magnetically soft iron tip

As already indicated by the simulations depicted in figure 3.8, an improved collection behaviour can be expected adding a magnetically soft iron tip on top of the magnetic ring stack. A measurement with such a device placed at a stirred flask was carried out and the results for the AX8 adapter are shown in figure 3.11. Compared to the plain AX8, the AX8IT (with magnetically soft iron tip) resulted in a 50% higher intensity after 30 min of particle collection. Although this easily accomplished alteration of the commercially available axially magnetized rings displays a significant improvement, the novel radial adapters are still two steps higher on the way to the optimal solution. Especially the lower attraction force induced by this kind of adapter results in an early decomposition of the sensor spot. Nervertheless, the AX8IT adapter performed better in all respects than the plain AX8 adapter.

The key values of all adapters are summarized in Table 1.

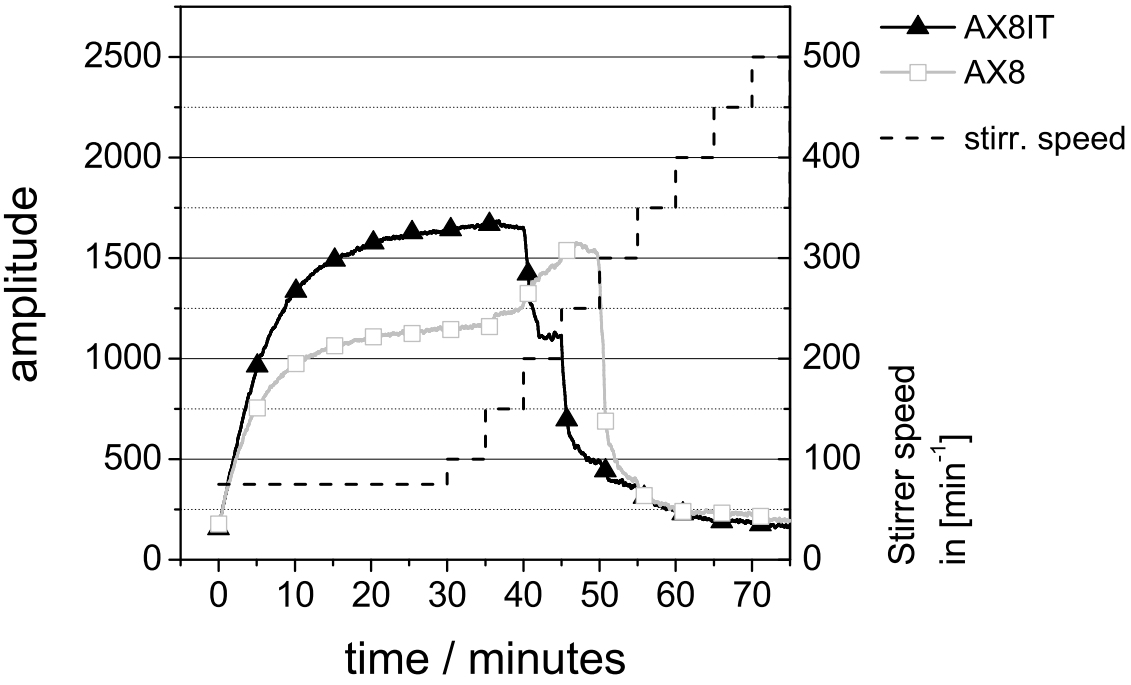

Figure 3.11: The effect of an magnetically soft iron cone with a hole in the centre for the optical fibre. A 50% higher signal was measured after a collection time of 30 min using the bottom-up approach. However, due to the lower magnetic field density with the iron tip, the resistance against decomposition was less than without the tip.

Table 3.1: Key values of all adapters. V is the volume of magnetic material, I_{30min} is the intensity after 30 min in bottom-up approach, t_{99} and t_{90} are the times needed to reach 99% and 90% of I_{30min}, respectively, and n_{break} and n_{re} are the stirrer speeds when the signal broke down (n_{break}, bottom-up approach) or when particles were collected again (n_{re}, top-down approach).

Adapter	V [mm^3]	I_{30min}	t_{99}/t_{90} [min]	n_{break}/n_{re} [min^{-1}]
RAD4	288	2170	21.4/8.6	250-450/350
RAD6	324	2101	22.6/9.5	250-400/350
RAD8	288	2191	22.9/10.6	300-350/300-250
AX8	283	1153	27.3/13.4	300/200-150
AX8IT	283	1636	25.1/14.4	200-250/250-200

3.4 Conclusion

Employing radial magnetized adapters rather than axial rings improves the signal intensity, the collection efficiency and the strength of particles spot attachment. Simulations of magnetic fields elucidated the parameters vertical distance and inner diameter to have the highest impact on the flux densities in the FOV of an optical fibre. The novel adapters constructed and employed instead of radially magnetized rings, which are not commercially available yet, performed outstandingly well in all experiments. Maximum signal intensity, stability against shear forces and also collection efficiency were improved. Finally, the employment of a magnetically soft iron cone improved the behaviour of axially magnetized rings significantly. Beyond the application of the herein described principle for monitoring chemical parameters in shaking flasks, micro plates or flow-through system, it is also very useful whenever sight contact to a magnetically trapped particle spot is required. One of many possible applications is e.g. working with light sensitive, stimuly responsive magnetic particles for drug delivery.

4 Enhancing performance in optical sensing with magnetic nanoparticles

This chapter was published as *Full Paper* in

Sensors and Actuators B: Chemical, 2009, 139(1), 174

doi: 10.1016/j.snb.2008.11.008

Authors: Günter Mistlberger*, Sergey M. Borisov and Ingo Klimant

Abstract Magnetic optical sensor particles (MOSePs) allow *in situ* sensor spot formation by separating the dye-loaded particles in the field of view (FOV) of e.g. an optical fiber. In order to further improve the suitability of magnetic optical sensors, we constructed optimized magnetic separators with an optical window. The combination of these new separators with the concept of magnetic sensor particles enabled oxygen sensing at particle concentrations below $1\,\mathrm{mg\,L^{-1}}$. In addition to the application in a stirred flask, we demonstrated the concept of magnetic separation for *in situ* sensor spot formation in 24-well plates by modifying a commercially available SensorDish reader. Finally, we introduce in this article a new technique for the low-cost production of MOSePs, i.e. spray-drying. With this, we produced MOSePs with 100 times increased brightness and almost linear Stern-Volmer correlation between $pO_2 = 0$ and 1013 hPa.

4.1 Introduction

Real-time measurements of chemical parameters in biological samples are crucial for process control and for performing in-depth studies of the metabolism of involved organisms. The degree of oxygenation and the pH-value, particularly, are of great interest in such different fields as food technology, pharmaceutical industry, biotechnology, waste water treatment and generally, in life-sciences.[203–205,219,220] In these fields applications are encountered with volumes ranging from several microliters up to several $100\,\mathrm{m^3}$.

Electrochemical sensors (such as the Clark-electrode for oxygen or the glass-electrode for pH-sensing) are well established and robust measuring systems. However, they can not be efficiently miniaturized and the costs, handling, recalibration and autoclavation can be drawbacks these systems. In these aspects, the optical sensors represent a very efficient alternative. Today, sensor patches attached inside the sample vessel or reactor are most commonly used as optical sensors.[221] These solid sensor spots minimize interferences with

the components of the media and can even be optically isolated to avoid disturbances by background fluorescence. However, their production and attachment in the flask and vessel, respectively, have to be done long before the measurement and require additional production effort.

MOSePs (**M**agnetic **O**ptical **Se**nsor **P**articles) represent an excellent alternative to these patches.[2,101,136] They can merely be added to the cultivation media and collected at the sidewall by a magnetic field. After this *in situ* sensor spot formation, readout can be principally performed with the same optical techniques originally developed for solid sensor spots. The remaining challenge of optimally separating the particles to form an ideally shaped particle spot was recently investigated in our lab. The problem of ineffecient collection by commercially available, axially magnetized ring magnets was resolved by the construction of special separators simulating radially magnetized ring magnets.[13] These separators focus the maximum magnetic flux density exactly in front of an optical fiber, which is located in the center of the separator, and avoid particle loss due to trappment in optically unaccessible areas (figure 4.1). Moreover, they produce more than the double field strength compared to their axial counterparts ensuring high stability of the sensor spots against shear forces induced by moving liquids.

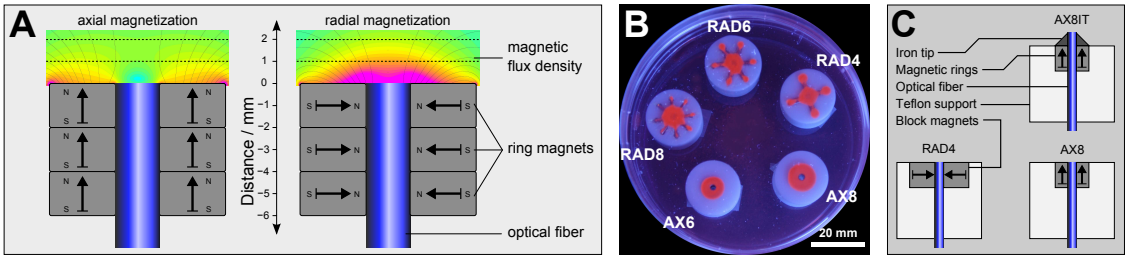

Figure 4.1: Scheme illustrating the superior collection efficiency of our radial magnetic separators. In (A) computer simulated flux densities of axially and radially magnetized rings are shown. In case of radial magnetization the flux density is concentrated in front of the optical fiber exactly in the field of view. This was experimentally proven by supplying a suspension of magnetic phosphorescent particles in a petri dish on top (B). The radial separators (RAD4-RAD8) collected the particles right in the centre while the axial ring magnets (AX6,AX8) left a hole where the optical fiber would be located. (C) shows schematic cross sections of the employed separators.

Herein, we investigated the influence of the sensor particle concentration on the time required for sensor spot formation and the maximum reachable intensity. Furthermore, we pushed the setup in order to identify the minimum amount required for achieving suitable signal strength for oxygen monitoring. For demonstrating the usability of magnetic sensor particles for oxygen monitoring in 24-well plates, we modified a SensorDish Reader (SDR) from Presens GmbH (Germany) with simple block magnets and trapped the magnetic sensor particles on the bottom of the plates, where otherwise solid sensor spots would be located. Finally, spray-drying with a conventional air-brush is introduced as a method for the production of oxygen sensitive MOSePs with enhanced brightness and a highly linear Stern-Volmer correlation.

4.2 Experimental

4.2.1 Materials

Tetramethoxysilane, methyltrimethoxysilane, poly(styrene-*co*-maleic anhydride) (PSMA, maleic anhydride 7 % $^{w}/_{w}$) and iron(II/III)oxide nanopowder were of grade purum and purchased from Sigma. Sodium hydroxide, glucose monohydrate, dichloromethane and ethanol (all purchased from Carl Roth GmbH, Germany) and glucose oxidase from *Aspergillus niger* (GOX, Fluka) were used without further purification. TiO_2 was purchased from Kemira (Helsinki, Finnland). Ruthenium(II)-tris-4,7-diphenyl-1,10-phenanthroline dichloride (RuDPP) and iridium(III)((benzothiazol-2-yl)-7-(diethylamino)-coumarin))$_2$(acetylacetonate) (Ir(C_S)$_2$(acac)) were synthesized in our lab as described elsewhere.[198,217]

The lipophilic, magnetic nano-particles (stabilized by oleic acid) were synthesized according to a procedure described by Ramírez and Landfester[222] and will be referred to as LMNP.

Nitrogen and oxygen (all of 99.999 % purity) were purchased from Air Liquide, Austria.

Absorption spectra were measured at a Cary 50 UV-Vis spectrophotometer (Varian Inc., USA). Emission spectra were acquired on a Hitachi F-7000 fluorescence spectrometer (Hitachi Inc., www.inula.at) equipped with a red-sensitive photomultiplier R 928 from Hamamatsu (www.hamamatsu.com). Microscopic images were acquired using a PCO SensiCam (PCO Computer Optics GmbH, Kelheim, Germany) digital camera mounted onto a Zeiss (Göttingen, Germany) Axiovert 25 CFL inverted fluorescence microscope.

All NdFeB permanent magnets (magnetized through the length, grade N38) were purchased from Chen-Yang Technologies (Erding, Germany).

4.2.2 Particle synthesis

The ormosil particles where synthesized as described by Mistlberger *et al.*[13] Briefly, 15 mL of each tetramethoxysilane, methyl trimethoxysilane and doubly distilled water were mixed with 100 µL of 0.1 M HCl, and homogenized by sonication for 30 seconds ("hydrolyzed Sol"). 1 mL of hydrolyzed Sol was mixed with 200 µL of a RuDPP solution in ethanol (25 mg mL^{-1}) and 700 µL of an aqueous suspension containing 70 mg of TiO_2 nanoparticles and 200 mg magnetite nanopowder (Aldrich). Subsequently, 200 µL of the ammonia solution (0.25% w/w) were added followed by vigorous mixing on a vortexer for 5 min. The mixture was left overnight, then the monolith was wet ground in a mortar. Prior to the measurement unbound magnetite aggregates were removed from the sensor particles by magnetic separation and the resulting suspension was further homogenized by sonication.

For the spray-dried particles, a 2 % ($^{w}/_{w}$) solution of PSMA in dichloromethane was prepared. To this solution, 2 % Ir(C_S)$_2$(acac) and 25 % LMNP (all $^{w}/_{w}$ polymer) were added. This cocktail was then applied to a conventional air brush and sprayed into a pre-heated 5 liter beaker. The particles were dispersed in ethanol and – after magnetic concentration – hydrolyzed for 6 min in a 1 M sodium hydroxide solution in the ultra sonic bath. Afterwards, the particles were magnetically separated, washed three times with water and dispersed in water to a final concentration of 1 % ($^{w}/_{w}$).

4.2.3 Calibration

The calibration of the spray-dried particles was carried out in 4 mL of an aqueous dispersion of the particles. The suspension was purged with different ratios of nitrogen and oxygen adjusted by a gas mixing device (MKS Instruments, Germany) at a flow rate of 200 µL min^{-1}. The particles were collected at the bottom of the vial with the RAD4 separator and the phase shifts were recorded with a 2 mm optical fiber and a phase fluorimeter (PreSens GmbH, Germany) equipped with a blue LED (470 nm) for excitation and a 550 nm long-pass filter for the emission. The modulation frequency was adjusted to 20 kHz.

4.2.4 Measurement setup

MOSePs (Ormosil based) were dispersed in 154 mL of water at concentrations ranging from 0.77 to 40 mg L^{-1} and transferred to a 300 mL-Erlenmeyer flask. The suspension was stirred using a mechanical stirrer (EUROSTAR digital, IKA-Werke GmbH & CO. KG, Staufen, Germany) with a moon-shaped stirrer blade (50*18*3 mm, Bohlender GmbH, Germany) at 100 min^{-1}. For particle collection the RAD4, AX8 and AX8IT separators were used. A detailed description of these separators is given in.[13] Briefly, the RAD4 separator consists of 4 block magnets arranged like a star around an optical fiber with like poles pointing against each other. The AX8 separator consists of axially magnetized rings with an outer diameter of 8 mm and an inner diameter of 2 mm. The AX8IT has an additional iron-cone on top of the magnetic rings with a hole in the center for the optical fiber (figure 4.1C). The separators were fixed to the sidewall at the position of maximum intensity. Optical signal readout was established with a 2 mm optical fiber and a phase fluorimeter (PreSens GmbH, Germany). The modulation frequencies where adjusted to 44.6 kHz for RuDPP and 20 kHz for $Ir(C_S)_2(acac)$ (figure 4.2).

For online monitoring of oxygen in a 24-well microtiter plate, magnets of the size 17*6*1 mm (L*W*H) were taped with their like poles pointing against each other on top of a SensorDish reader device (SDR, PreSens, Germany). The readout spots were not covered by the magnets (figure 4.3). This enabled the collection of magnetic sensor particles at the positions, where otherwise solid sensor spots would be located. The phase shift was then measured at a modulation frequency of 20 kHz.

4.3 Results and discussion

4.3.1 Separator characterization

As reported previously,[13] radial magnetized separators are an attractive alternative to the commercially available, axially magnetized rings. They ensure higher signal intensity, collection efficiency and sensor spot stability. Considering the complexity of the separator construction, we discovered that the simple setup of the RAD4 device with 4 block magnets pointing against each other is the best tradeoff between construction effort and collection efficiency. For massproduction it would be possible to construct better magnetic separators at a reasonable price by using specially fabricated ring segments fixed

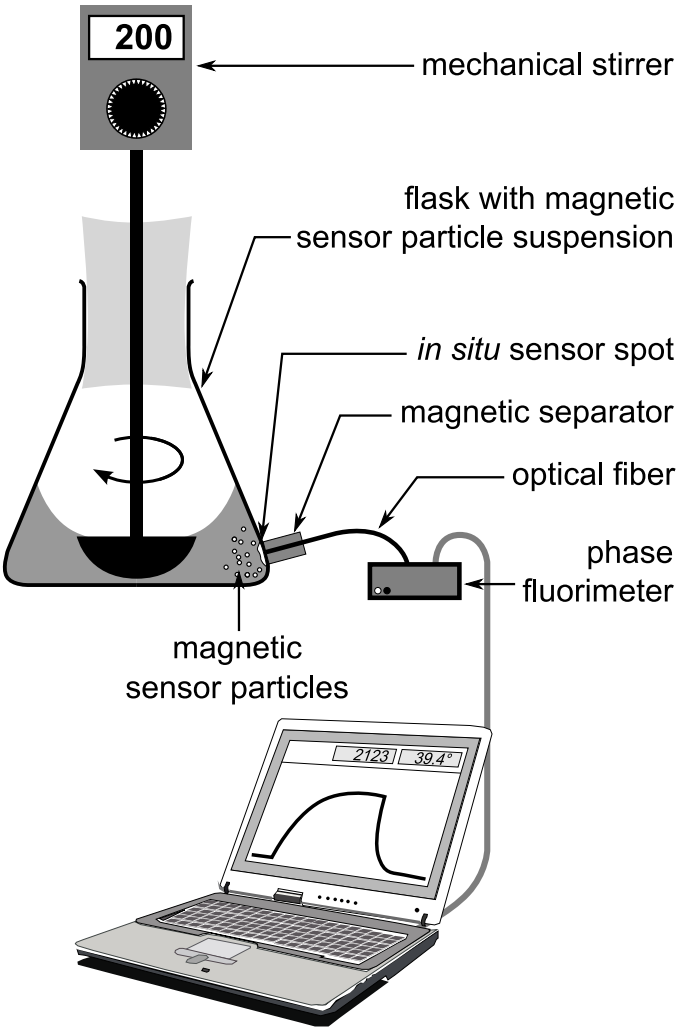

Figure 4.2: Measurement setup. The magnetic particles were magnetically trapped from a stirred suspension and read out by a phase fluorimeter from the outside.

in a ringshaped mantle. However, for demonstrating the suitability of this technique for practical applications, the setup with block magnets was considered to be sufficient.

In figure 4.4, relative signal intensities of collected ormosil particles (with RuDPP as the oxygen indicator) are plotted against the collection time. This correlation already demonstrates that magnetic sensor particles alone cannot enable sensing at ultra low sensor concentrations. All three applied separators completely separated the MOSePs from the medium. However, only separators with optimized geometry and magnetization direction allowed the efficient readout of the particle sensor spots. This indicated that the combination of both concepts – the unique properties of MOSePs and the optimized magnetic separators – was crucial to reveal the full potential of the technique.

The great advantage of the novel radial separators is their capability of quickly forming the particle sensor spot in the FOV, whereas common axially magnetized rings waste more

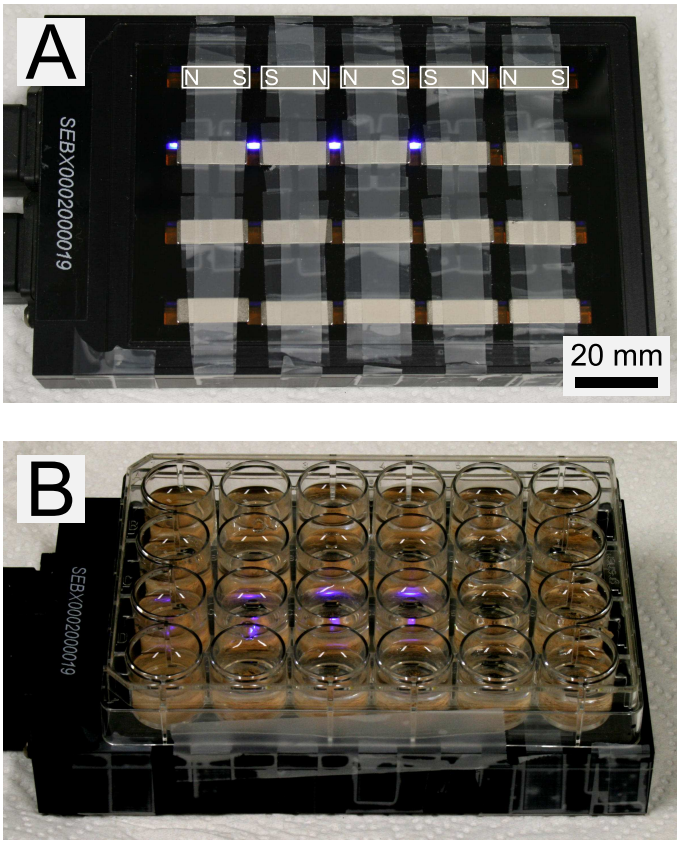

Figure 4.3: Images of the modified SDR with magnets on top for particle collection (A) and with a 24-well plate filled with sensor particle suspension on top (B).

than 80 % of the particles' potential due to collection outside of the optically accessible area.

The characteristics of the different separators are visualized by three parameters (figure 4.5): firstly, the maximum signal intensity achieved at a certain concentration of particles, secondly t_{90}, which is the time required to get 90 % of the maximum signal intensity and finally t_{crit}, defined as the time necessary for reaching a signal intensity (amplitude) sufficient for a stable phase signal in the phase-fluorimeter.

The maximum intensity plot (figure 4.5A) already elucidates the great separation charactaristics of the novel radial separators. When using the AX8 separator the signal already dropped to below 20 % at sensor particle concentrations of $10\,\mathrm{mg\,L^{-1}}$, while the RAD4 separator had its maximum intensity at the same concentration and still showed more than 30 % of its maximum intensity at a concentration of $0.75\,\mathrm{mg\,L^{-1}}$. At very high particle concentrations ($40\,\mathrm{mg\,L^{-1}}$) the highly light absorbing magnetite diminished the advantage of the radial magnetization. Due to a slight inhomogeneity of the magnetite content in the particles, a layer of particles with high magnetite content was formed in front of the optical fiber. This dense layer only occurs, when lots of particles are available. In case of axially magnetized rings, these particles were collected outside of the FOV,

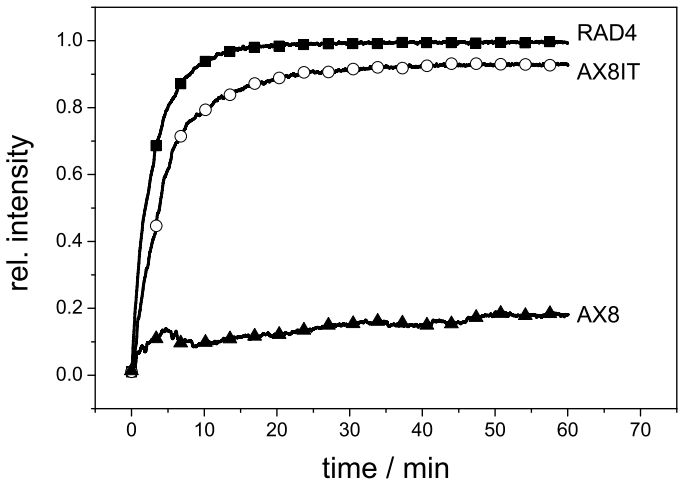

Figure 4.4: Relative signal intensity during sensor spot formation at a particle concentration of $10\,\mathrm{mg\,L^{-1}}$. While the modified separators (RAD4 and AX8IT) collected the sensor particles efficiently in the field of view of the optical fibre, the unmodified axially magnetized separator collected the particles outside of the illuminated area, i.e. around the perimeter of the optical fiber. This was in good agreement with the results from the magnetic field simulation (figure 4.1A).

which resulted in a slightly higher signal compared to the modified separators.

The time required to achieve 90 % of the individual intensity maximum, can be used as a parameter to describe the promptness of the response. The shorter this time is the faster an equilibrium will be achieved. Herein, again the RAD4 separator performed best, although in average the AX8IT only needed 40 % longer to achieve I_{90} (figure 4.5B). In contrast, the AX8 separator only produced enough intensity for evaluation down to a concentration of $10\,\mathrm{mg\,L^{-1}}$. However, as can be seen in figure 4.4, at this concentration the signal intensity is very noisy.

Probably the best parameter for charactarization is the time t_{crit}, required to achieve a stable phase shift in a phase fluorimeter depending solely on the analyte concentration. After this point, the amplitude of the signal may still be increasing, but the phase shift and therefore the measured oxygen concentration or pH value does not change anymore at a constant analyte concentration. The unmodified axial adapter (AX8, figure 4.5C) was only able to establish this critical particle amount in the FOV at concentrations $>20\,\mathrm{mg\,L^{-1}}$. The performance of this adapter was greatly improved by the application of a soft iron cone on top. As shown elsewhere, this iron cone reduces the magnetic field at the outer edges of the ring while keeping it high, close to the FOV. Consequently, the gradient towards the FOV directs magnetic particles into the center. This easily accomplished modification reduced the minimum particle concentration, which is necessary to reach the critical intensity, to $2\,\mathrm{mg\,L^{-1}}$, a factor of 10. The only separator still beeing able to reach the critical intensity at $0.75\,\mathrm{mg\,L^{-1}}$ ormosil particles was again the RAD4 separator. This equals a RuDPP concentration of $6.8\,\mu\mathrm{g\,l^{-1}}$ or an absolute amount of 1 µg RuDPP (116 µg ormosil sensor particles) in the measurement volume.

Apart from the minimum concentration, the time required to reach the critical intensity

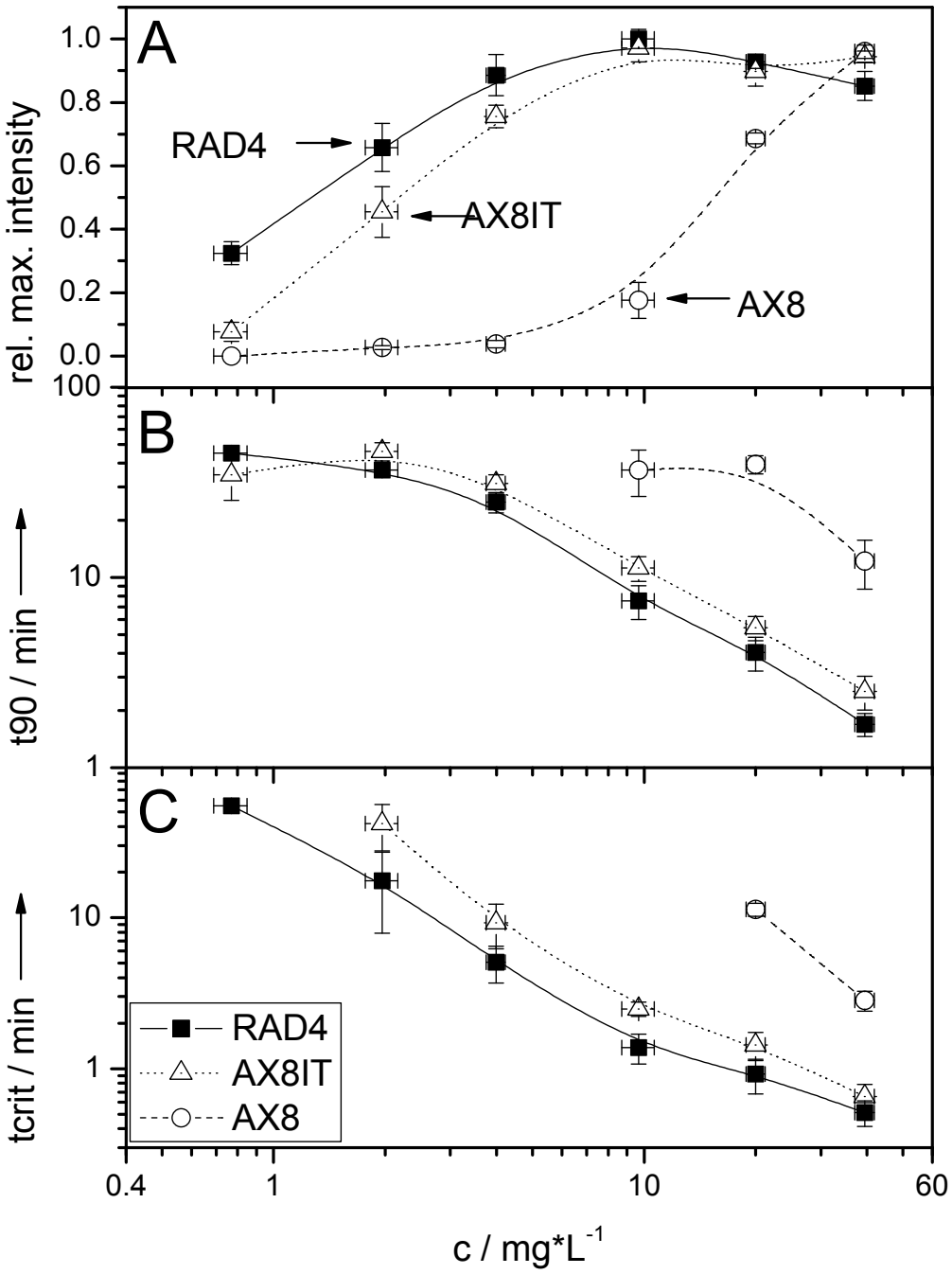

Figure 4.5: Separator characteristics. (A) Maximum signal intensities at certain concentrations demonstrate the ability of the RAD4 separator to utilize ultra low sensor particle amounts. In (B) the time required to reach 90 % of the individual maximum intensity is plotted vs. the particle concentration. (C) The time (t_{crit}) to reach a signal intensity at which a phase shift is solely depending on the analyte concentration is one of the most important characteristics of a separator. Here the novel RAD4 adapter performed again outstandingly well.

for a measurement should also be considered for everyday application. At a $20\,\mathrm{mg\,L^{-1}}$ particle concentration, the sensor spot was formed more than 12 times faster in case of the RAD4 separator than with the AX8 separator. A collection time of less than a minute is more than sufficient for most applications.

Concluding, both the RAD4 and AX8IT separator, collected the magnetic sensor particles much more efficiently than the AX8. The advantage of the RAD4 over the AX8IT separator is significant with respect to all evaluated parameters. However, due to the logarithmic scale of the plots in figure 4.5 the difference seems rather small. Nevertheless, the biggest advantage of the RAD4 over the AX8IT is the much higher field strength acting on the particles in the spot, which ensures highly stable sensor spots.[13]

4.3.2 Parallel oxygen monitoring with magnetic particles employing a SensorDish reader

In addition to the use of magnetic sensor particles for oxygen monitoring in shake flasks and bioreactors, we tested the application in 24-well micro dishes. For this purpose, a 24-well SensorDish reader (SDR) from PreSens (Germany) was modified with a layer of magnetic separators between the sample-well and the reader itself (figure 4.3). This allowed effective trapping of our magnetic micro sensors in the FOV of the SDR.

For a proof of priniple, 1 mg of the ormosil sensor particles were suspended together with 21 U of GOX in 3 mL water and filled into each well of the plate. Starting at $t = 0\,\mathrm{min}$, 20 µmol glucose were added and mixed with a pipette. The phase increased immediately after mixing due to the rapid consumption of the dissolved oxygen by the enzyme (figure 4.6). After approximately 20 hours of reaction the GOX had converted the glucose completely and therefore stopped to consume the oxygen diffusing into the liquid. This led to a slow re-oxygenation and consequently to a drop in phase shift to its starting value. The differences in the time profiles are due to different positions of the wells on the plate. Two wells located close to each other displayed similar time profiles (A4/A5 vs. D3/D4).

4.3.3 Magnetic micro sensor particles with enhanced brightness

Due to the high light absorption of the dark colored magnetite, we investigated the usability of new ultra bright oxygen indicator dyes based on iridium(III)-coumarin complexes[198] for our purposes. Namely, we incorporated $\mathrm{Ir(C_S)_2(acac)}$ in completely different matrices (PSMA) and evaluated spray-drying with a conventional air brush as a simple method for the preparation of oxygen-sensing MOSePs. The chemical structure and the absorption and emission spectra of the dye and can be seen in figure 4.7A. Directly after the spray-drying process the particles exhibited only weak dispersibility in water, because the anhydride groups were not yet hydrolyzed. After hydrolysis in ethanolic 1 M sodium hydroxide solution, the surface properties changed from rather hydrophobic to hydrophilic (figure 4.7B). The phosphorescence image of the as prepared particles elucidated particle sizes in the range of 3 to 30 µm (figure 4.7C).

The results of the calibration at different oxygen concentrations can be seen in figure 4.8A. In this plot the two values τ_0/τ and I_0/I were plotted versus the partial pressure of

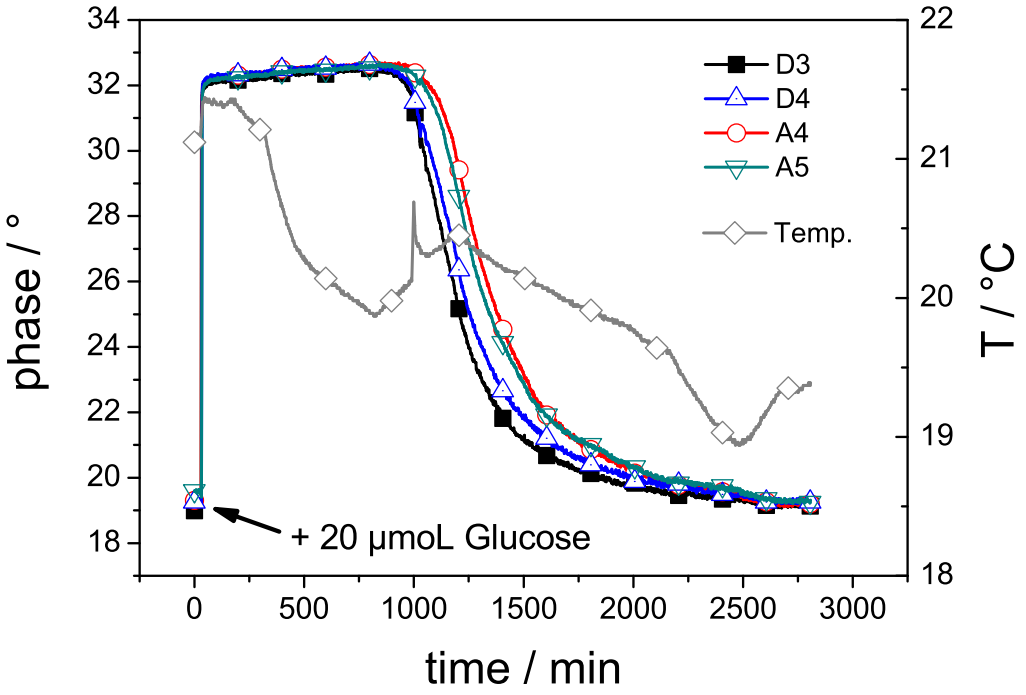

Figure 4.6: Oxygen monitoring with an SDR device and magnetic particles in a 24-well plate. 20 µmol of glucose were added to a glucose oxidase solution with suspended magnetic sensor particles. The phase responded immediately to the addition and was then stable until the glucose was consumed by the GOX. Afterwards slow aeration occured at rates depending on the location of the wells on the plate.

oxygen in solution. The luminesence intensities were calculated from the signal amplitude by correction with the modulation ratio.[218] Surprisingly, both plots display almost the same linear correlation and slope throughout the whole calibration range from $pO_2 = 0$ to 1013 hPa ($K_{SV} = 0.0019\,\mathrm{hPa}^{-1}$, $\tau_0 = 8.5 * 10^{-6}$ s)). This is a really rare phenomenon in solid state oxygen optodes. The perfect correlation is usually only expected dyes in solution and means that nearly all indicator molecules are equally accessible and quenchable by oxygen. It is likely that this behavior is caused by a combination of the unique material properties and the production process. On the contrary, in bulk optodes the Stern-Volmer plots are non-linear and can be only fitted adequately using a two-site model.[223]

To prove the ability of the new particles for oxygen monitoring in a stirred flask, $15\,\mathrm{mg\,L}^{-1}$ particles were dispersed in water and the particles were collected with the RAD4 separator on the sidewall. The continuously monitored phase shift reached a stable value within a few minutes and was then solely depending on the oxygen concentration in the flask (figure 4.8B). After approximately 60 min, glucose was added to the flask and after another 5 min, glucose oxidase was added to deoxygenate the solution. Here, the lifetime immediately increased due to the absence of quenching components, in this case oxygen.

Comparing the absolute signal intensities of the ormosil-RuDPP-particles and the PSMA-Ir-coumarin particles, the new matrix and dye resulted in an approximately 100

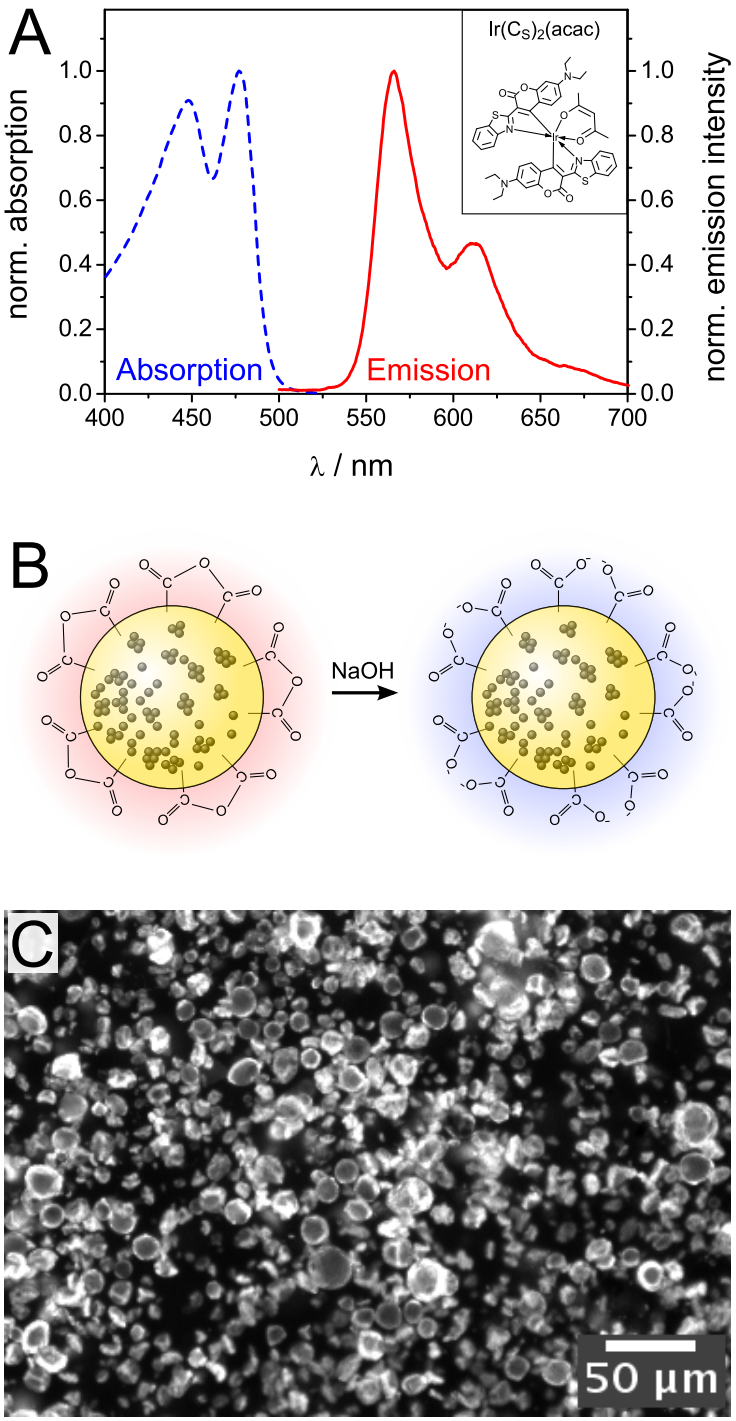

Figure 4.7: Brightness enhanced oxygen sensing MOSePs prepared using a spray-drying technique. (A) Absorption and emission spectra of the sensor dye $Ir(C_S)_2(acac)$ and structure thereof (insert). (B) During hydrolysis of the maleic anhydrid groups, the surface properties switch from hydrophobic to hydrophilic. (C) Phosphorescence microscope image.

times higher signal.

4.3.4 Future outlook

Although, the presented combination of magnetic sensor particles with the novel magnetic separators represents a perfectly usable setup for a range of applications,[2] some parameters can be even further improved. These aspects will be discussed in the following.

First of all, the separators can be further optimized by the use of magnetic ring segments replacing the block magnets. This mimics the real radially magnetized ring – which we proposed to be the perfect separator for this purpose – even better than the current setup. Further pushing the geometry to its limits, it is also possible to use optical fibers with a smaller diameter. This allows the use of a smaller diameter of the separator and consequently also the particle spot will be smaller. Simulations with a distance of 0.2 mm between two like poles of magnets indicated that it would be possible to achieve particle spots with diameters smaller than 0.3 mm by this technique. This would reduce the required amount of particles again by a factor of approximately 300. This potential is however strictly limited by the distance between separator and particle spot, as discussed elsewhere.[13]

Another aspect concerns the magnetic sensor particles themselves. Firstly, the magnetite content is of course a crucial factor for the separability of the sensor particles. The more magnetic material incorporated in the sensor particles the faster they will separate from the medium when a magnetic field gradient is applied. On the contrary, the high absorbance of magnetite affects the luminesence of the indicator. This requires either a compromise between the two effects or a different solution, which can be e.g. optical isolation of the magnetic and the optical sensor compound, the incorporation of scattering components, such as TiO_2, or the use of sensor dyes with higher brightness. For the latter, ultrabright oxygen optodes based on cyclometalated Ir(III) coumarin complexes were reported recently.[198] These dyes were incorporated in the spray-dried particles presented here.

To obtain optical isolation of the magnetite and the sensor dye, a core-shell structure with a magnetic core, followed by an optically isolating and scattering layer (e.g TiO_2-filled polymer) and finalized with a layer incorporating the sensor dye is desired. If required, an outer layer for adjusting surface properties (charge, hydrophobicity) or with linker groups allowing covalent coupling of e.g. anti-bodies is feasible.

4.4 Conclusion

The combination of MOSePs with optimized magnetic separators enabled optical sensing at ultra low sensor concentrations. Due to the enrichment of the sensor dye in the field of view of an optical fiber by particle separation, the sensor material is utilized much more efficiently than with dissolved indicators or non magnetic particle suspensions. It was also demonstrated that only the combination of optimized separators and magnetic particles provides access to the full potential of this technique. The suitability of MOSePs for parallel cell culture monitoring in multi-well plates was shown by modifying a commercially available SensorDish reader with repulsive-mode magnetic separators. The new, low-cost

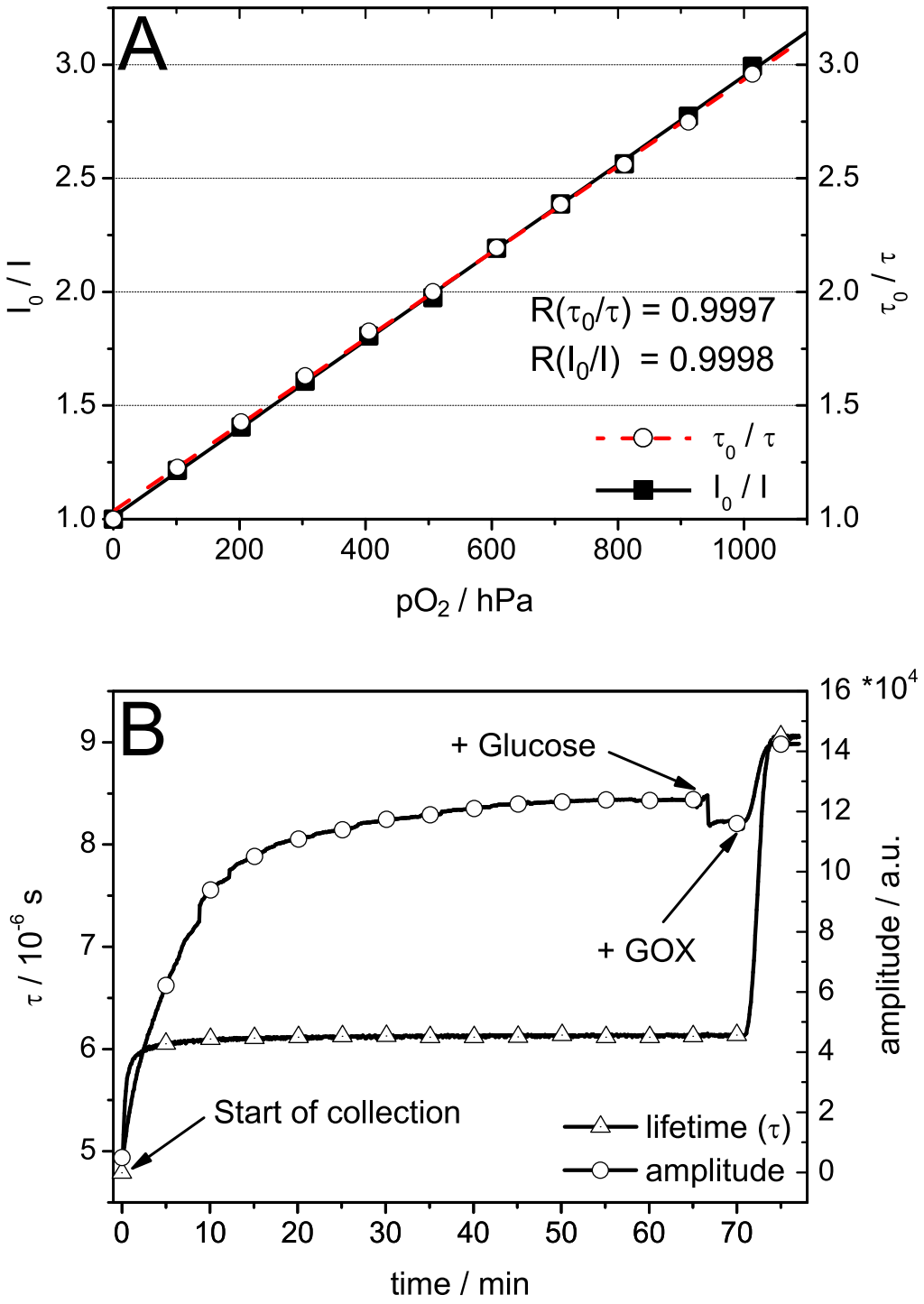

Figure 4.8: Magnetic optical oxygen sensor particles by spray-drying technique of PSMA. (A) Calibration curves I_0/I and τ_0/τ vs. pO_2. The very uncommon linear correlation of both parameters is a major improvement of oxygen sensing materials. (B) Amplitude and phosphorescence lifetime vs. time plots: Upon addition of glucose and glucose oxidase the lifetime increased immediately.

spray-drying method for producing MOSePs resulted in sensors with 100 times enhanced brightness and a highly linear Stern-Volmer correlation from 0-100 % oxygen saturation (pO_2 = 0–1013 hPa).

Acknowledgement

We gratefully thank PreSens GmbH for providing the necessary equipment for performing the measurements on the SensorDish reader.

5 Characterization of micrometer-sized magnetic optical sensor particles produced via spray-drying

This chapter was published as *Full Paper* in

Monatshefte für Chemie - Chemical Monthly, 2010, in press.

doi: 10.1007/s00706-010-0262-z

Authors: Klaus Koren, Günter Mistlberger*, Daniel Aigner, Sergey M. Borisov, Armin Zankel, Peter Pölt and Ingo Klimant

Abstract We investigated the correlation between optical sensing performance and morphology of micrometer-sized magnetic optical sensor particles (MOSePs). Oxygen-sensitive MOSePs were produced via spray-drying, a technique suitable for particle production from polymers in various solvents. A common problem of precipitation and polymerization techniques is the inhomogeneous distribution of dispersed nanoparticles. In spray-drying, this phenomenon is suppressed by fast solvent evaporation. The resulting sensor particles responded to changing analyte concentration within seconds, their Stern-Volmer calibration was highly linear, and they were magnetically controllable. The sensor characteristics resulted from the porosity of the matrix polymer, which enabled fast analyte diffusion towards the sensitive dye. Diffusion distances were further reduced by the formation of hollow particles. This was caused by the sequential drying of the polymer-solution droplet from the outside to the inside. Finally, the suitability of different polymers and magnetic nanoparticles for the production of MOSePs via spray-drying was evaluated.

5.1 Introduction

Optical sensors are tools for monitoring analytes by correlating their concentration with light properties.[224] Since the introduction of optical sensors, they have constantly gained importance in industry and research laboratories.[225] Among others, physiologically important parameters such as oxygen and pH can be monitored using optical sensing systems.[226] For biological applications involving small objects of interest (e.g., cells, tissues or biofilms), miniaturized sensors are needed.[227] For this purpose, micro-optodes

and particle-based sensors are state of the art.[228] Micro- and nanometer-sized sensor particles have been produced using various polymerization methods, as well as grinding and precipitation techniques.

Recently, great efforts have been applied to the functionalization of nano- and micro-particle-based sensors with magnetic particles, quantum dots, and antibodies.[229] The encapsulation of magnetic nanoparticles resulted in magnetically controllable optical sensor particles. As a result, novel applications of optical sensors (e.g., in situ sensor spot formation inside cultivation vessels or the formation of a "sensor swarm"[2,136]) are possible.

In contrast to methods such as nanoprecipitation[180] and emulsion polymerization, spray-drying tolerates a variety of solvents, polymers, and additives. The composition of the obtained particles only depends on the mixture used for spraying. The rapid solvent evaporation suppresses inhomogeneities regarding the resulting nanoparticle distribution. The equipment required is cheap and simple (i.e., a conventional airbrush and a beaker). Spray-drying works without emulsifiers or other additives, which minimizes necessary purification steps. These aspects make spray-drying a straightforward concept towards micrometer-sized optical sensor particles.

Here, we present spray-drying as a versatile method for production of magnetic optical sensor particles (MOSePs). We report on the sensor characteristics and morphology of spray-dried magnetic optical sensor particles (sd-MOSePs). Comparing the sensor characteristics of sd-MOSePs with sensor films obtained by knife-coating demonstrated increased linearity of the Stern-Volmer correlation. The remarkable sensor characteristics are explained by detailed morphological studies.

5.2 Results and discussion

Oxygen-sensitive micrometer-sized particles consisting of poly(styrene-co-maleic anhydride) (PSMA), lipophilic magnetite nanoparticles (LMNPs), and cyclometalated iridium(III) coumarin complex ($Ir(C_S)_2(acac)$[198]) were produced via spray-drying and subsequent hydrolysis of anhydride groups on the surface (Figure 5.1).

Spray-drying is a high-throughput method for polymer particle production. It tolerates different polymers, solvents, and additives such as inorganic nanoparticles. In contrast to most emulsion polymerization techniques, the produced particles are emulsifier free and, depending on the matrix polymer, ready to use right after production. Finally, the equipment required for spray-drying is simple and cheap, in the current case, an airbrush and a 10 dm^3 beaker.

Prior to spraying, all components were dissolved and dispersed, respectively, in highly volatile dichloromethane. This mixture will be referred to as "cocktail" throughout the manuscript. The cocktail was nebulized through an airbrush into a preheated beaker. Upon contact with the hot gas phase, the cocktail droplets are transformed into particles due to rapid solvent evaporation. As previously reported,[14] particles consisting of PSMA are dispersible in aqueous media due to the hydrophilic surface groups. The suitability of several polymers (Table 5.1) and LMNPs (Table 5.2) for spray-drying was tested. Particle morphology was characterized by scanning and transmission electron microscopy, and

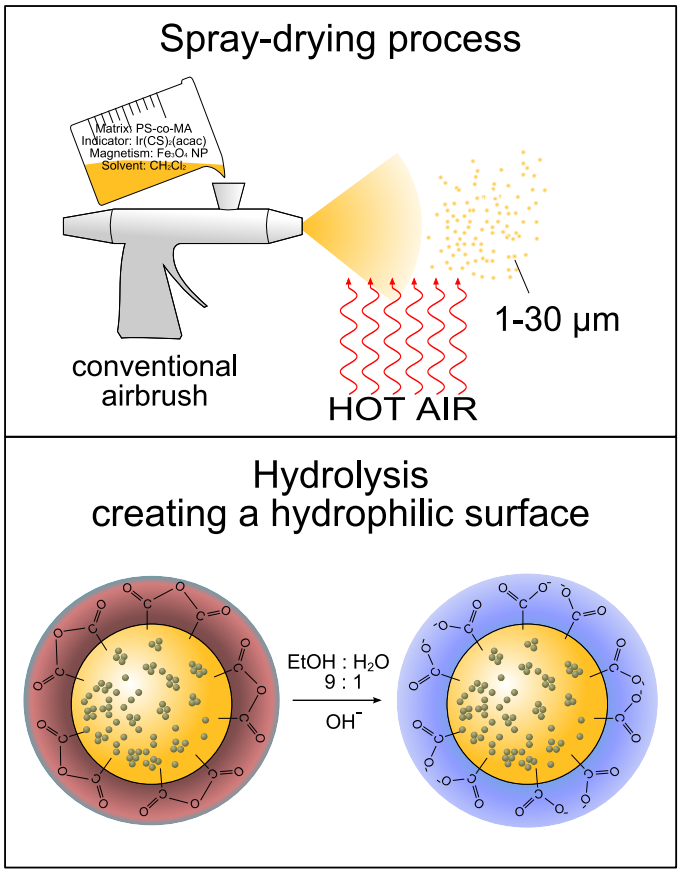

Figure 5.1: Synthetic pathway towards micrometer-sized MOSePs. Polymer, indicator, and magnetite particles are dissolved and dispersed, respectively, in dichloromethane and are sprayed into a hot atmosphere using an airbrush. The obtained particles had sizes ranging from approximately 1 to 30 µm. Subsequent hydrolysis of the particles resulted in a hydrophilic surface.

fluorescence and light microscopy, and sensor characteristics were determined by phase fluorimetric measurements at varying analyte concentrations.

5.2.1 Sensor characteristics

In contrast to the calibration plots observed for 5-µm-thick sensor films, spray-dried MOSePs showed a highly linear calibration behavior from $pO_2 = 0$ to 1,013 hPa (Figure 5.2a).

Highly linear calibration curves are rare, especially for optical sensors with a working pO_2 range of 0–1,013 hPa. Nonlinear calibration curves can be explained by the so-called two-site model from Carraway et al.[223], suggesting that some dye molecules are less quenchable by the analyte than others. Therefore two different Stern-Volmer constants (K_{SV1} and K_{SV2}) and a distribution coefficient P are added to the classical Stern-Volmer

Table 5.1: Applicability of polymers with varying maleic anhydride (MA) content and molecular weight (MW) for spray-drying.

Polymer	MA (wt%)	MW ($g\,mol^{-1}$)	Suitability for spray-drying	Sensor performance	K_{SV} (hPa^{-1})
PSMA93	7.0	224,000	+	++	0.00181
EF 80	11.1	14,400	+	+	0.00135
EF 60	14.3	11,500	+	–	NA
PSMA75	25.0	1,900	–	– –	NA
PS	0.0	220,000	NA	NA	0.00420

Table 5.2: Properties of magnetite nanoparticles (surface coating, dispersibility, and price) and their applicability for spray-drying

Magnetite type	Synthesis	Coating	Suitability for spray-drying	Price
CP-LMNP	Coprecipitation	Oleic acid	++	++
TD-LMNP	Thermal decomp.	Oleic acid	+	+
EMG1200	Commercial	Fatty acid	+	-
EMG1300	Commercial	Polymeric	++	-
EMG1400	Commercial	Hydrophobic	-	-

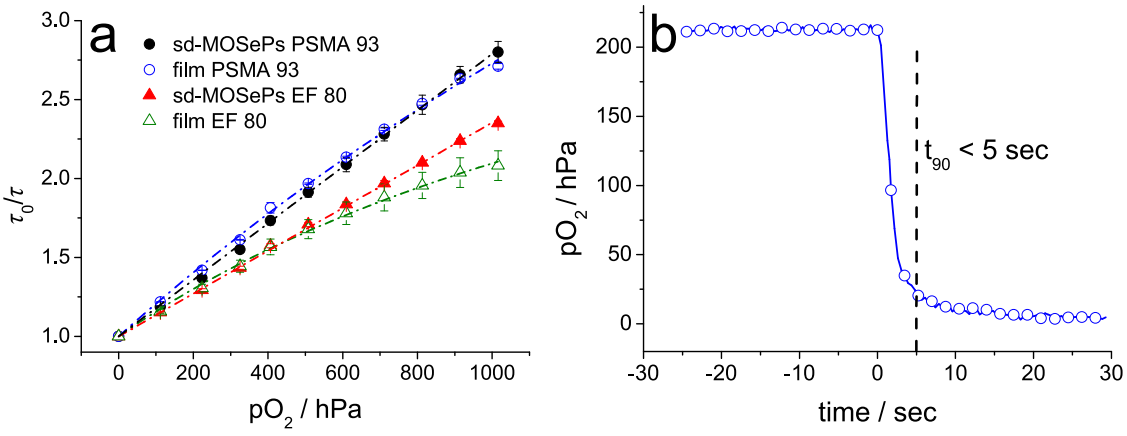

Figure 5.2: a) Comparison of the calibration curves (Stern-Volmer plots) of 5-µm-thick sensor films and spray-dried particles. While the calibration curves of the sensor films were fitted using the two-site model, sensor particles (10 mg Poly / g Solv; 100 mg Mag / g Poly) showed a highly linear Stern-Volmer correlation. K_{SV} values decreased with increasing polarity of the matrix. b) The response time of the MOSePs to changing oxygen concentration is fast enough for monitoring most biological processes ($t_{90} < 5\,s$).

equation.

$$\frac{\tau}{\tau_0} = \frac{P}{1 + K_{SV1} pO_2} + \frac{1 - P}{1 + K_{SV2} pO_2} \tag{5.1}$$

This equation can be simplified by the assumption that one portion of the dye is virtually unquenchable, i.e., K_{SV2} =0 hPa^{-1}.[230]

$$\frac{\tau}{\tau_0} = \frac{P}{1 + K_{SV1} pO_2} + 1 - P \tag{5.2}$$

Microheterogeneity of the polymeric matrix yields environments with different permeability and consequently different quenching behavior.

The Stern-Volmer constant K_{SV} decreased with increasing maleic anhydride content[198] (Table 5.1; Figure 5.2a). The higher matrix polarity induced by maleic anhydride resulted in decreased lifetime of the indicator's excited state and consequently in decreased sensitivity. While the calibration curves of the sensor films are nonlinear (e.g., $R^2 = 0.969$), linear fits with $R^2 = 0.999$ or higher were obtained for the studied sd-MOSePs. Hence, the two-site model is required to fit the obtained curves ($R^2 > 0.998$). The estimated response time t_{90} (the time required to achieve 90 % of the signal change) is less than 5 s (Figure 5.2b), which is sufficiently fast for measurements of most biological growth processes.

As demonstrated below, structural investigations explain this unexpectedly high linearity of the sd-MOSePs calibration curves.

5.2.2 Fluorescence and light microscopy

Particle specific surface area and dimensions dramatically influence analyte diffusion towards the sensitive dye. Therefore, we determined the size distribution of the produced particles based on light and fluorescence microscopy images. Figure 5.3 shows polydisperse particles with sizes ranging from 1 to 30 µm. Although uniform particles are beneficial for certain applications, monodispersity is usually not essential. As shown here, the performance of MOSePs in oxygen monitoring is unaffected by the different particle sizes. The reason is the unique matrix structure, as described in the following section.

Furthermore, not all the observed particles were perfectly spherical and the luminescence intensity was not equally distributed over the entire particle. Assuming a homogeneous distribution of the indicator dye in the polymeric matrix, the high luminescence intensities at the edges indicate a hollow particle structure. However, the same effect might have resulted from an inhomogeneous distribution of the dye in the particle. Therefore, the particle morphology was further investigated by electron microscopy.

5.2.3 Scanning electron microscopy

The scanning electron microscopy (SEM) images in Figure 5.4a indicate a porous surface structure of the particles. A nanoporous structure favors short response times because of decreased analyte diffusion distances. The average diameter of the pores of the particle in Figure 5.4a was 160 ± 60 nm. The fragment of a broken sensor sphere depicted in

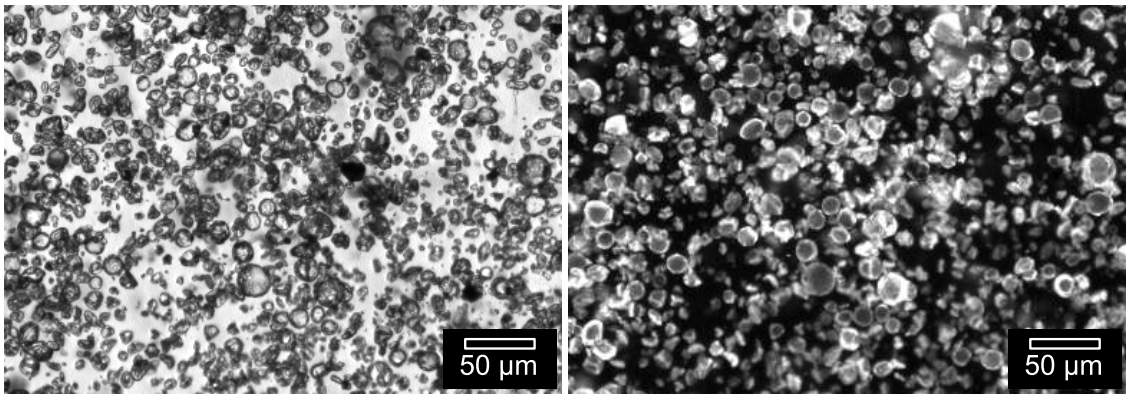

Figure 5.3: Light (*left*) and fluorescence (*right*) microscopy images of sd-MOSePs (20 mg Poly / g Solv PSMA93; 300 mg Mag / g Poly LMNP) indicate a broad size distribution with average diameter of 5-7 µm.

Figure 5.4b gives deeper insight into the structure of sd-MOSePs. Firstly, the spheres were obviously hollow, and secondly the pores seemed to penetrate the polymeric shell connecting the outside with the hollow particle core. These morphological features are important and explain both the sensor characteristics and the particle formation steps.

The particle formation process can be separated into three steps: (1) the shear gas stream forms cocktail droplets at the nozzle of the airbrush and ensures rapid transport of the droplets to the hot gas phase in the beaker. (2) Temperatures above the solvent's boiling point and the high vapor pressure of the solvent ensure fast drying around the outside of the droplets. Thereby, a solid polymer film encloses the cocktail droplets. (3) During sequential drying from the outside to the inside, the solvent disrupts the outer polymer shell, forming pores. In this final phase, the cocktail components precipitate and stick to the initially formed polymer film. Depending on the polymer properties and the rigidity of the initial outer layer, the spheres either keep their spherical shape and initial droplet diameter (Figure 5.4a) or collapse during phase 3. The result is a folded structure similar to a compressed paper bag (Figure 5.4c). The molecular weight of the polymer is a crucial factor for the rigidity of the initial shell. The tendency of the spheres to collapse during phase 3 increased with decreasing molecular weight (MW) of the tested polymers, as can be seen in Figures 4a (MW = 224,000 $g\,mol^{-1}$) and 4c (MW = 14,400 $g\,mol^{-1}$).

The SEM images reveal the porous structure of sd-MOSePs and suggest a hollow particle core. However, they do not provide insight into the distribution of pores and magnetite in the shell. In addition, the shell thickness remains unknown. This information is available from TEM images of a particle's thin section achieved by ultramicrotomy.

5.2.4 Transmission electron microscopy

Sectioning of particles by ultramicrotomy enabled visualization of the particle interior via TEM. A cross-section through an sd-MOSeP is shown in Figure 5.5. This image confirms the assumption of a structure with a hollow core and a polymeric shell. A particle of 28 µm diameter is relatively large, and a bulk sensor with this thickness responds slowly to

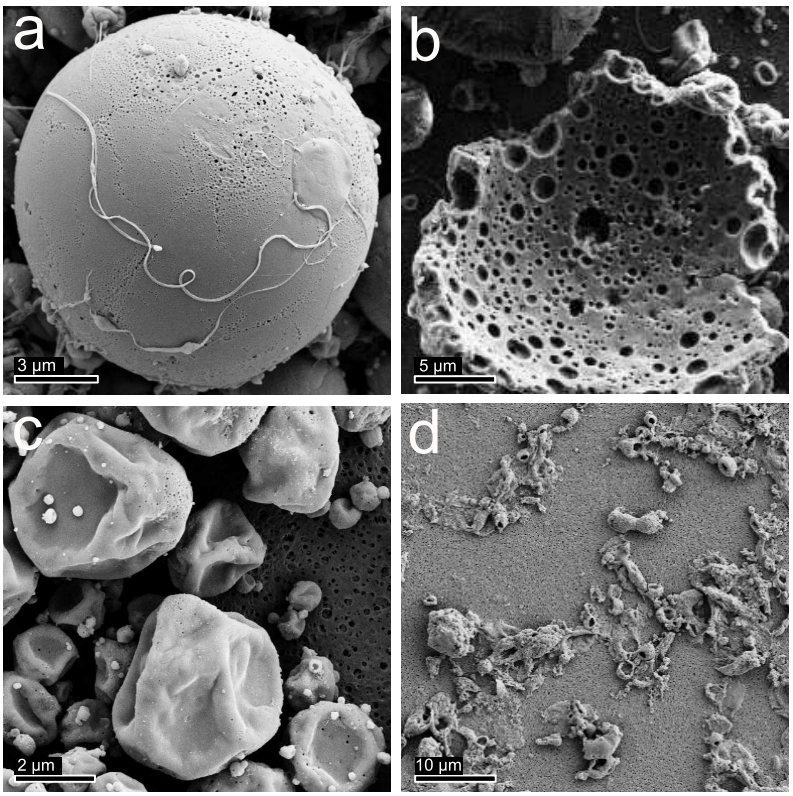

Figure 5.4: SEM images of different sd-MOSePs (all particles with 20 mg Poly / g Solv and 300 mg Mag / g Poly LMNP). a) Spherical particles with a nanoporous matrix were obtained using PSMA93. b) The porous shell structure is seen in a particle fragment (PSMA93). c) Low-molecular-weight polymers (EF80 and EF60) yielded partly collapsed, nonspherical particles. d) No particles were found when using the polar, low-molecular-weight matrix PSMA75.

changing analyte concentration. However, the thin shell of the particle reduces diffusion distances and consequently the sensor's response time. The shell thickness in sd-MOSePs is usually $\sim 1/10$ of the particle diameter (e.g., 1-4 µm in Figure 5.5). Moreover, the thickness of the shell reveals the ratio between pores and bulk material of the particle. The pore volume in the shell can be estimated with the following assumption. Based on the particle formation process outlined above, the particle diameter should be roughly constant during the drying process ($d_{\mathrm{Particle}} = d_{\mathrm{Droplet}}$). In this case, the pore ratio R in percent can be calculated by

$$R = 1 - \frac{d^3 c}{\rho(d^3 - (d - 2t)^3)} \times 100, \tag{5.3}$$

where d is the droplet diameter, c is the concentration of the solids in the cocktail in $\mathrm{kg\,m^{-3}}$, ρ is the average density of the solid phase, and t is the shell's thickness. The evaluation of this equation for the particle shown in Figure 5.5 results in a pore fraction in the shell of more than 95 %. Even if 80 % of the solvent evaporates before the particle reaches its final size, the pore fraction is still approximately 80 %. Such a high porosity

further decreases diffusion distances and response times. Analyte diffusion, a common factor limiting the response time of optical sensors, is very fast in a material with high specific surface area and thin bulk structures.

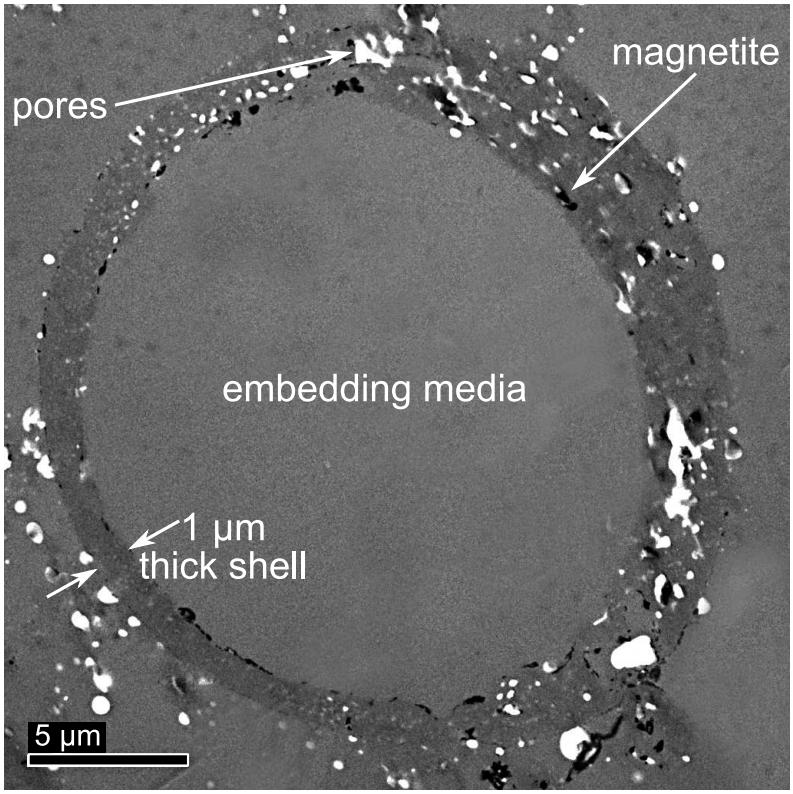

Figure 5.5: TEM image of a thin-sectioned particle (20 mg Poly / g Solv PSMA93; 300 mg Mag / g Poly LMNP) indicates a hollow structure. Magnetite particles aggregate inside the polymeric shell (black regions). While the particle diameter is 28 µm, the polymeric shell is only 1-4 µm thick. Analyte diffusion towards the sensitive dye is favored by the porous structure (white holes).

Moreover, the porous structure provides an explanation for the linear Stern-Volmer correlation. Due to the high porosity, the polymer structure is amorphous since thin polymeric layers can hardly crystallize. Microheterogeneities resulting in varying permeability are therefore prevented, and all indicator molecules are equally accessible for the analyte.

Finally, TEM revealed the structure of the magnetic nanoparticles in the matrix polymer. The black regions inside the polymeric shell (Figure 5.5) originate from magnetite aggregates. During the drying of the particles, the lipophilic magnetic nanoparticles change from a homogeneous dispersion in the cocktail to an aggregated state in the final particles. This might cause the inhomogeneous magnetite distribution over the particle population. However, aggregation also reduces the contact surface between magnetite and luminophore. As a result, luminescence quenching and the inner filter effect are minimized and this increases the signal intensity.

5.2.5 Material studies

The preparation of sd-MOSePs was successful using three different polymers and four different LMNPs. The most hydrophilic PSMA75 with the smallest molecular weight (1,900 g mol^{-1}) yielded aggregates rather than defined particles (Figure 5.4d). Due to the low molecular weight the matrix structure was less stable and the high polarity caused partial solubility in the alkaline EtOH/water hydrolysis medium. The trend that low-molecular-weight polymers formed less stable structures was supported by the EF60 and EF80 results. Spraying cocktails with these matrix polymers resulted in collapsed spheres (Figure 5.4c). On the contrary, particles from PSMA93, the polymer with the highest molecular weight in this study, retained the spherical shape of the droplet with a hollow core (Figs. 5.4a, 5.5).

The suitability of a polymer for particle formation is necessary but not sufficient for applicable optical sensor particles. In order to achieve water-dispersible sensor particles a substantially hydrophilic surface is required. This is achieved by polar matrix groups (maleic anhydride) that are hydrolyzed to carboxyl groups after particle formation. On the other hand, strong hydrophobic interactions between the nonpolar indicator dyes and the matrix are required. While both EF80 (11.1 wt% MA) and EF60 (14.3 wt% MA) yielded particles, only EF80 was suitable for production of MOSePs. In case of EF60, the polarity was too high to keep the $Ir(C_S)_2(acac)$ – the oxygen-sensitive dye – inside the matrix. As a consequence, the dye leached out into the ethanolic hydrolysis medium and the final particles were virtually nonluminescent.

The influence of the polymer concentration in the cocktail on the particle size and structure was also studied. A 10 mg polymer per gram solvent (mg Poly / g Solv) cocktail was optimal for the production of sensor particles. Higher concentrations ($\geq$ 20 mg Poly / g Solv) – especially of high-molecular-weight polymers – favored aggregation and fiber-like structures. Lower concentrations increased the solvent consumption without significant impact on particle size (Table 3). As mentioned above, the spray-drying process is versatile and suitable for different classes of polymers and molecular weights. However, the cocktail composition requires optimization for each new polymer-solvent system. Hence, it is difficult to propose a universal recipe.

Table 5.3: Size distribution d (from light microscopy) of sprayed particles with different polymers and polymer concentrations c in the cocktail

Polymer	$\boldsymbol{c}$ (mg Poly/g Solv)	$\boldsymbol{d(\pm s)}$ (µm)
PSMA93	5	5 (±2)
PSMA93	10	7 (±3)
PSMA93	20	6 (±3)
EF80	5	7 (±2)
EF80	20	5 (±3)

In addition, three commercial and two self-prepared LMNPs were tested for sd-MOSePs. The most important property of the LMNPs was good dispersibility in the solvent, here dichloromethane. The dispersibility decreased from EMG1300 (perfectly dispersible)

to EMG1200, TD-LMNP, and CP-LMNP (dispersible in smaller concentrations), and finally to EMG1400, which was not dispersible at all. CP-LMNPs were prepared by coprecipitation followed by surface coating with oleic acid.[222] Thermal decomposition of Fe oleate also yielded magnetic nanoparticles (TD-LMNP).[231] A key problem of the latter method was the presence of strongly attached organic impurities which represented the main component of the resulting precipitate. Although both self-made LMNPs were successfully incorporated into sd-MOSePs, the current study was carried out with commercial EMG1300 to ensure highest reproducibility of the results.

The LMNP content in the cocktail accounts for the magnetic separability of the resulting sensor spheres. Higher magnetite content results in faster response to a changing magnetic field and in the strong attachment to a magnetic separator. On the contrary, the dark magnetite efficiently absorbs light from both excitation and luminescent emission and therefore decreases the signal intensity. As a result, the concentration required optimization and we found 100 mg per gram polymer (mg Mag / g Poly) to be a good trade-off between magnetic separability and optical signal intensity. The filter effect of magnetite caused a 50 % signal reduction when increasing the concentration from 100 mgMag/gPoly to 300 mg Mag / g Poly. A concentration below 100 mgMag/gPoly reduced the particle yield during washing due to low collection efficiency.

Sensor stability and measurement reproducibility are important factors regarding the applicability of an optical sensor. The performance of the spray-dried particles presented herein did not change after several months of storage in the dark. This indicates that the structure of the particles did not change over time. Nonetheless it has to be mentioned that bleaching of the indicator dye occurs. Dye bleaching is the only process affecting the sensor stability and performance over time.[198] This problem might be overcome by using dyes with increased photostability.

5.3 Conclusion

We present spray-drying as a versatile and straightforward method to produce magnetic polymer microparticles with optical sensor properties. Starting from a dispersion and solution, respectively, of all desired compounds in a volatile solvent, the sensor particles were formed directly and without emulsifier. Compared with other particle production methods, spray-drying is highly flexible regarding polymers, solvents, and additives in the cocktail. The oxygen-sensitive sd-MOSePs displayed a linear Stern-Volmer correlation from $pO_2 = 0$ to 1,013 hPa, a rare property of optical oxygen sensors. Morphological studies revealed the reason for this linearity. The particles were found to be hollow and to contain a thin shell which was highly porous. This led to fast responding sensors and finally ensured that all indicator molecules were located in the same environment, explaining the linear calibration curves.

5.4 Materials and methods

5.4.1 Materials

Polystyrene (PS) and poly(styrene-co-maleic anhydride) (PSMA) polymers were purchased from different suppliers: PSMA93 and PS from Sigma-Aldrich, both EF80 and EF60 from Sartomer (www.sartomer.com), and PSMA75 from Scientific Polymers (www.scientificpolymer.com). Sodium hydroxide, dichloromethane, and ethanol were purchased from Carl Roth (www.carl-roth.de). Magnetite nanoparticles were either prepared by thermal decomposition[231] or coprecipitation followed by surface modification.[222] The Nanoparticle Developer Kit including EMG1200, EMG1300, and EMG1400 was purchased from FerroTec, Inc. (www.ferrotec.de). The O_2-sensitive dye $Ir(C_S)_2(acac)$ was prepared in our laboratory as described elsewhere.[198] Oxygen and nitrogen were of 99.999 % purity and purchased from Air Liquide (www.airliquide.at).

5.4.2 Particle production

MOSePs were prepared using a spray-drying process. Typically, 100 mg polymer and 1.5 mg $Ir(C_S)_2(acac)$ were dissolved in 10 g dichloromethane. Magnetite nanoparticles (10 mg) were added to the solution and dispersed by sonication. This cocktail was sprayed into a preheated 10 dm^3 glass beaker using a conventional airbrush (HP 120 with nozzle diameter of 0.2 mm, www.conrad.at). After spraying, the particles were dispersed in 100 cm^3 ethanol. Then 10 cm^3 of a 10 M NaOH solution were added to hydrolyze the anhydride groups on the surface under sonication for 15 min. The MOSePs were magnetically separated and washed with water until neutral. The particles were redispersed in water to final concentration of 10 mg mL^{-1}.

5.4.3 Sensor characterization

The sensor characteristics of oxygen-sensitive MOSePs were investigated using a phase fluorimeter (pH-Mini, PreSens GmbH, Germany). The modulation frequency was adjusted to 20 kHz. The sensor particles were collected in front of an optical fiber with the help of a specialized magnetic separator.[13] Different ratios of oxygen and nitrogen required for the calibration were adjusted with a gas mixing device (MKS, www.mksinst.com). As reference, 5-µm-thick PSMA films containing 1.5 wt% $Ir(C_S)_2(acac)$ were used.

5.4.4 Microscopy

Light-microscopic images were acquired using a PCO SensiCam (PCO Computer Optics GmbH, Kelheim, Germany) digital camera mounted onto a Zeiss (Göttingen, Germany) Axiovert 25 CFL inverted fluorescence microscope. SEM images were collected using a Zeiss Ultra55 microscope (www.smt.zeiss.com). The particles were dried on a polymeric support [polytetrafluoroethylene (PTFE) filter membrane] and sputtered with Au/Pd. For TEM investigations MOSePs were embedded and cut using ultramicrotomy. TEM images were collected at a Tecnai 12 transmission electron microscope (www.fei.com).

Acknowledgments

The authors thank S. Fladischer, C. Mayrhofer, and E. Ingolic from the Austrian Centre for Electron Microscopy and Nanoanalysis for their technical support.

6 Novel strategy to design magnetic, molecular imprinted polymers with well-controlled structure for the application in optical sensors

This chapter was published as *Full Paper* in

Macromolecules, 2010, 43 (1), 55-61.

doi: 10.1021/ma902095s

Authors: Antonio L. Medina-Castillo, Günter Mistlberger*, Jorge F. Fernandez-Sanchez*, Antonio Segura-Carretero, Ingo Klimant and Alberto Fernandez-Gutierrez

Abstract The incorporation of magnetic properties allows the in situ formation of sensor spots by magnetic separation and, consequently, optical readout from the outside. Several magnetic MIPs have been synthesized and characterized, highlighting that both the amount and distribution of magnetite are essential for producing a good material. This work also shows that well-organized structures must be obtained for designing magnetic MIP which can be used as optical sensors phases. Thus, in this work we propose a novel strategy to design well-organized, highly magnetic MIP particles to be used as optical sensing phases. The obtained magnetic MIP is the first one that has been used for optical sensing. It shows highly magnetic properties with high sensitivity (detection limit of $20\,\mathrm{ng\,mL^{-1}}$), good imprinting effect (MIP/NIP ratio of 2.4), and high selectivity. This strategy may be further extended for implementing optical sensing phases in portable devices that can control a broad variety of analytes in different matrices (water, organic solvent, etc.) and may be used to improve sensitivity in other magnetic optical sensors.

6.1 Introduction

Molecular imprinting is a method of inducing molecular recognition properties in synthetic polymers in response to the presence of a template species during formation of the three-dimensional structure of a polymer.[232] The history of molecular imprinting is usually traced back to the experiments of Dickey in the 1940s and 1950s,[233,234] who was inspired to create affinity for dye molecules in silica gel by a theory of Linus Pauling as to how

antibodies are formed.[235] Molecular imprinted polymers (MIPs) have been employed in a wide area.[236,237] Successful applications of MIPs were, e.g., in liquid chromatography, as material for solid-phase extraction, in membrane technology, for sensors, as artificial antibodies, in catalysis, in biotransformation processes, and as diagnostic tools for drug assays.[238] The main advantages over their natural competitors (i.e., antibodies) are their resistance to organic solvents and their stability over time, while maintaining the ability for molecular recognition. However, the application of MIPs for optical sensors was only successful in a few cases.[239–243] The three main reasons for this are (1) if the analyte is not fluorescent, it is challenging to find a good transducer, (2) the low sensitivity in many cases, and (3) the difficulty to implement the resulting MIPs in optical sensors.

While it is still difficult to find a transducer system for nonfluorescent analytes, the fixation of MIPs for luminescent analytes has been partly solved in the past with the following strategies. The first approach is based on the design of micro- or nanoparticles of MIPs and complex flow cells in which these particles are immobilized. This results in a sensor spot inside the cell which allows optical readout from the outside. However, sometimes fixing of the sensing material inside a cell can be cumbersome or even impossible. Alternatively, an additional polymer which works as a glue between MIP and fiber can be used, but it may change its optical and adsorption properties and thus its sensitivity and selectivity. All these problems can be minimized by the incorporation of magnetic properties into the sensing material. It allows the in situ formation of sensor spots by magnetic separation and, consequently, optical readout from the outside or an easy way to fix a MIP at the tip of an optical fiber[2,13,14] Therefore, the incorporation of magnetic properties to MIPs by using paramagnetic magnetite (Fe_3O_4) nanobeads will simplify the readout of micro- or nanoparticles of MIPs with fiber-optic devices solving some of the previously mentioned drawbacks.

Several magnetic MIPs have been developed,[244,245] but none of them were proposed as optical sensor because, as we will demonstrate, the dark color of magnetite can cause severe problems in optical sensors. Magnetite is responsible for the filter effect and self-absorption of luminescence emission, decreasing the sensitivity or, in some cases, even annulling it.[2]

In this work, we evaluated three strategies for the preparation of magnetic MIPs (Mag-MIPs) for pyrene as model analyte. We show the relevance of the amount and the distribution of magnetite in MIPs for the performance of MIP-based optical sensors and propose a new strategy for designing highly magnetic, sensitive, and selective Mag-MIPs which can be used as magnetic optical sensors by measuring the intrinsic fluorescence of the target analyte; the analyte is selectively retained in the Mag-MIP and concentrated for readout by sensor spot formation.

6.2 Experimental

6.2.1 Reactives

Methyl methacrylate (MMA; 99 %), divinylbenzene (DVB; 98 %), ethylene glycol dimethacrylate (EDMA; 80 % in meta/para isomers), 4-vinylpyridine (4-VP; 95 %), 2,2′-azobis(isobutyronitrile) (AIBN), potassium persulfate (KPS), oleic acid (OA; 90 %), sodium dodecyl sulfate (SDS; minimum 98.5 % GC), and poly(vinyl alcohol) (PVA) were purchased

from Sigma-Aldrich. Iron(II) chloride tetrahydrate ($FeCl_2 \cdot 4\,H_2O$) and iron(III) chloride hexahydrate ($FeCl_3 \cdot 6\,H_2O$) were obtained from Merck. Pyrene, acenaphthene (ACE), anthracene (ANT), fluorene (FLU), benzo[a]anthracene (BaA) and benzo[a]pyrene (BaP) were obtained from Fluka.

Magnetite coated with oleic acid was prepared according to the procedures described elsewhere.[14,246]

6.2.2 Chloroform ferrofluid

It was prepared dispersing 2 g of magnetite coated with oleic acid in 40 mL of chloroform. This mixture was sonicated for 20 min, and then it was centrifuged at 6000 rpm for 15 min. The supernatant was further concentrated until the required concentration of magnetite was reached. Mag-MIPs Prepared by Solution Polymerization (sMIP) A mixture containing 0.75 mL of a mixture of 83.5 mol% DVB, 16.5 mol% 4-VP, 26 mg of pyrene, 18 mg of AIBN, and 3 mL of chloroform ferrofluid with different weight of magnetite with respect to the weight of polymeric mixture (DVB and 4-VP) were placed in a glass vial. The mixtures were cooled with ice and purged with nitrogen for 3 min. The polymerization (65 ℃, 24 h) resulted in a monolithic polymer which was ground in a ball mill, sieved through a 20 µm sieve, and washed several times with chloroform to extract the template. Mag-MIPs Prepared by Emulsion Polymerization (eMIP) The discontinuous phase was based on a mixture of 0.75 mL of a mixture of 83.5 mol% DVB, 16.5 mol% 4-VP, 26 mg of pyrene, 18 mg of AIBN, and 3 mL of chloroform ferrofluid with different amounts of magnetite. The continuous phase was formed by 180 mg of PVA solved in 10 mL of Milli-Q water. The discontinuous phase was dispersed in a double-necked flask containing the continuous phase by vigorous mechanical stirring. It was purged with nitrogen, and the polymerization was carried out at 65 ℃ under a gentle stream of nitrogen for 24 h.

6.2.3 Magnetic hybrid nanoparticles encapsulated by EDMA/MMA (EDMA/MMA-Fe_3O_4-OA)

2 g of lipophilic magnetic nanoparticles were dispersed in 5 mL of n-heptane and added to 400 mL of Milli-Q water containing 250 mg of SDS. The ice-cooled mixture was sonicated for 20 min in a high-energy sonifier (BRANSON, S-450D) at 70 % amplitude. The resulting miniemulsion was transferred slowly (under mechanical stirring) to a double-necked flask containing 1.5 mL of 40 wt% MMA and 60 wt% EDMA. The mixture was stirred for 2 h at room temperature. Then, 180 mg of KPS was added to start the polymerization, and the reaction system was heated to 65 ℃ under a gentle stream of nitrogen. After a polymerization time of 24 h the resulting product was washed 6 times with Milli-Q water, 5 times with acetone, and 5 times with chloroform in order to eliminate surfactant and unreacted compounds.

6.2.4 Magnetic microparticle of MIP containing EDMA/MMA-Fe_3O_4-OA prepared by precipitation polymerization (pMIP)

0.75 mL of a mixture containing 83.5 mol% DVB, 16.5 mol% 4-VP 83, 26 mg of pyrene, and 18 mg of AIBN was mixed with 3 mL of a 6.5 % (w/w polymer) methanolic dispersion

of EDMA/MMA-Fe_3O_4-OA. The mixture was then placed in an ice-cooled glass vial and purged with nitrogen for 3 min. The polymerization was carried out at 65 °C for 24 h with continuous mechanical stirring.

6.2.5 Setup

The setup for the optical measurements consisted of a 1.5 mm diameter optical fiber probe (Varian Iberica, Spain) coupled with a special magnetic separator with an optimized geometry as described elsewhere.[13] Briefly, the separators consisted of four block magnets arranged like a star around the optical fiber with their like poles pointing against each other. The optical fiber probe was connected to the luminescence spectrometer (Varian Eclipse) by using a Varian fiber adapter. The Supporting Information shows a picture of the used setup (see Figure 6.6).

6.2.6 Measuring protocol

Samples were prepared by adding 0.7 mg of sensing material to a conventional quartz cuvette which contained 2 mL of the sample. The cuvette was shaken for 10 s prior to each measurement. The magnetic separator collected the Mag-MIPs at the tip of the optical fiber probe, and therefore, the luminescence intensity of the analyte bound to the Mag-MIPs was read out very efficiently (ESI shows an example for the data evaluation of the acquired measurements; see Figure 6.7). As blank value (I_0) the same amount of particles was measured in 2 mL of solvent (water or acetonitrile/water mixture) without analyte. The analytical signal was obtained by subtracting I_0 from I_x. To renew the sensing material, it was washed twice with 2 mL of acetone.

6.3 Results and discussion

The incorporation of magnetic properties has been done by adding magnetite coated with oleic acid (Fe_3O_4-OA) which was prepared as described elsewhere.[14,246] 4-Vinylpyridine (4-VP) has been selected as functional monomer because it has a certain hydrophilic character and allows the dispersion of the material in water, and in addition, it favors the $\pi - \pi$ interactions during the formation of the prepolymerization complex with the template pyrene.[247] Divinylbenzene (DVB) has been used as cross-linker and chloroform as porogen and solvent. In order to test how the amount and distribution of magnetite affects the optical recognition of pyrene, Mag-MIPs with different amounts of Fe_3O_4-OA (1, 2, and 5 wt%) were prepared by solution polymerization (sMIP) and emulsion polymerization (eMIP), and then they were evaluated. Nonimprinted polymers (NIP) were also prepared to distinguish between specific and unspecific interactions. The Fe_3O_4-OA distribution was studied by field-emission scanning electron microscopy with electron backscattering diffraction (FESEM-EBSD) in order to get a higher material contrast in the images (5 wt% Fe_3O_4-OA sMIP corresponds with Figure 6.1A and 5 wt% Fe_3O_4-OA eMIP with Figure 6.1B). The images elucidate an aggregation of the magnetite (white spots) in both cases. However, while in the sMIP the resulting magnetite clusters are evenly distributed in the particle, in the eMIP the clusters seem to be concentrated on the particles' surface. This

morphology may be the result of a thermodynamic incompatibility between the employed polymeric phase and the magnetic ferrofluid. The low affinity between oleic acid coating of the magnetic nanoparticles (Fe_3O_4-OA) and the cross-linked polymer phase induces the phase separation between both.[248] Thus, the system organized itself to reach the most thermodynamically favored state corresponding to the minimum free energy for which the interfacial tensions between main phases were the lowest.[249,250] figure

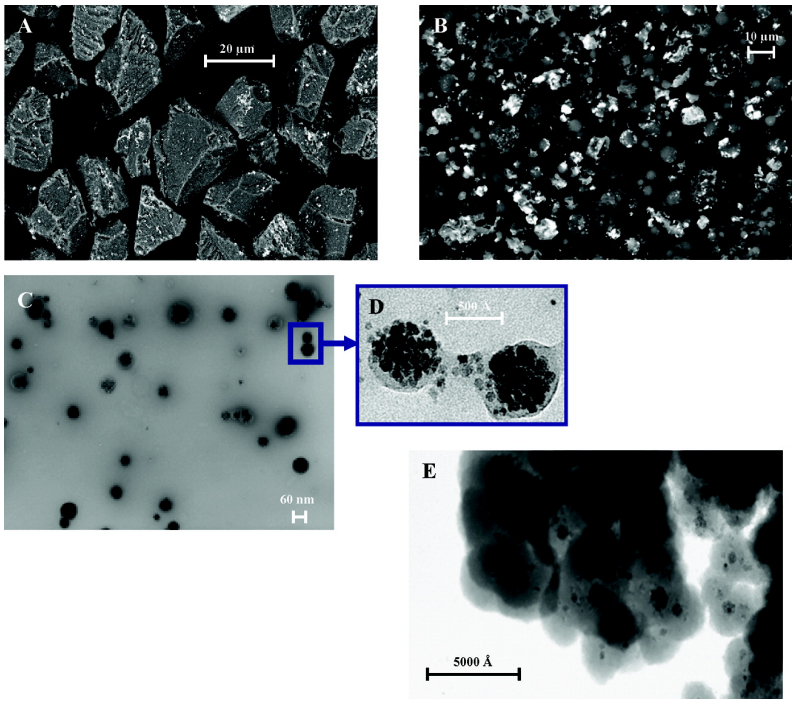

Figure 6.1: FESEM-EBDS pictures of (A) 5 wt% Fe_3O_4-OA sMIP and (B) 5 wt% Fe_3O_4-OA e-MIP. (C) TEM and (D) HREM pictures of EDMA/MMA-Fe_3O_4-OA nanoparticles. (E) HREM image of pMIP.

While the sMIP particles show a homogeneous distribution along their entire surface, the distribution of the Fe_3O_4-OA aggregates in eMIP particles is more heterogeneous, obtaining some particles with a high and others with a low amount of magnetite. Moreover, the fraction of magnetite which is located close to the outer surface of the particles is even higher in eMIPs. Thus, the increased phase separation in eMIP compared to sMIP has an even more drastic effect on the optical sensitivity as we will show later. ESI shows the SEM pictures of 5 wt% Fe_3O_4-OA sMIP (Figure 6.8) and 5 wt% Fe_3O_4-OA eMIP (Figure 6.9). There are three potential reasons for the increased phase separation between magnetite and polymer in eMIPs compared to sMIPs: (1) chloroform is a good dispersant for Fe_3O_4-OA nanoparticles, and the polymerization of sMIP was done in closed vials avoiding the chloroform evaporation while the eMIP polymerization was done under a gentle N2 stream, making chloroform (the magnetite dispersant) evaporate faster; (2) the use of surfactant in the synthesis of the eMIP may increase the Fe_3O_4-OA diffusion to the contact surface with the aqueous medium, and therefore the separation of phases

is more effective; and (3) the contact surface between the continuous phase (containing water and surfactant) is very large in emulsion polymerizations. Therefore, the chances for magnetite to aggregate on the surface of the particles is higher, and once the magnetite found the thermodynamically more stable position at the surface, it will not drift back into the particle's interior. All the Mag-MIPs containing 5 wt% Fe_3O_4-OA were highly magnetic and consequently collected very fast (within 2 min). Lower amounts of magnetite resulted in Mag-MIP which required more time for sensor spot formation. In addition, when the amount of magnetite is lower than 5 wt%, a lot of material is lost during the necessary washing steps. In contrary, the absorption of the luminescence emission by the magnetite made the use of 5 wt% of Fe_3O_4-OA in pyrene sensitive Mag-MIPs impossible. 1 wt% Fe_3O_4-OA sMIP showed a response with pyrene which was not observed for higher percentages of magnetite, and in the case of eMIP, it was not possible to detect a response signal to pyrene at any percentage of (Fe_3O_4-OA) (see Figures 6.2 and 6.3b). As mentioned above, this was caused by the heterogeneous interparticle distribution of the magnetite and the high fraction of magnetite located at the outer surface of the particles (Figure 6.3b). Particles with a higher amount of Fe_3O_4-OA were collected faster in the field of view of the optical fiber and created a highly absorbing layer which did not allow the coupling of luminescence light into the optical fiber. figure

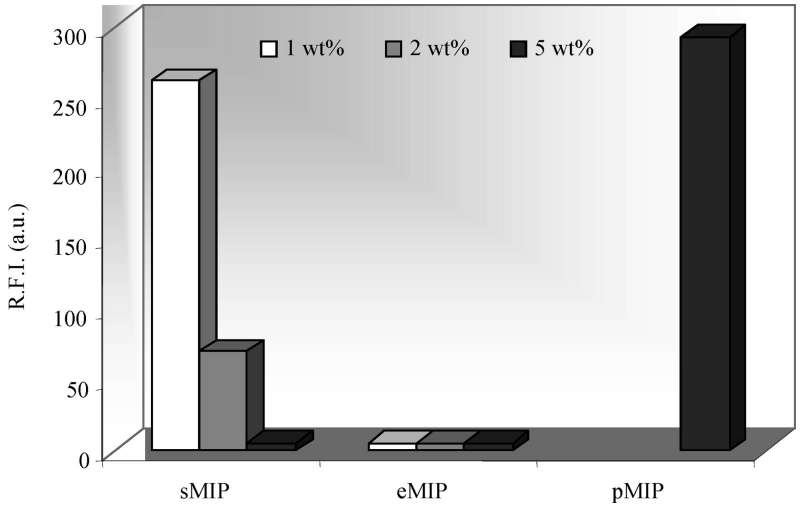

Figure 6.2: Effect of the Fe_3O_4-OA content on the optical sensitivity.

In conclusion, for obtaining appropriate magnetic properties at least 5 wt% Fe_3O_4-OA were necessary. Magnetite had to be homogeneously distributed among the single particles, the phase separation had to be avoided, and the Fe_3O_4-OA had to be isolated from the MIP in order to avoid filter effects and self-absorption of luminescence emission.

Bearing in mind these conclusions, we propose the synthesis of new magnetic microparticles of MIPs in which the magnetite is located inside the particle, and the MIP is covering these magnetic cores. It allows the use of a higher amount of magnetite, and the isolation between magnetite and sensing material reduces the negative side effect of the magnetite on the sensitivity and selectivity of the MIP.

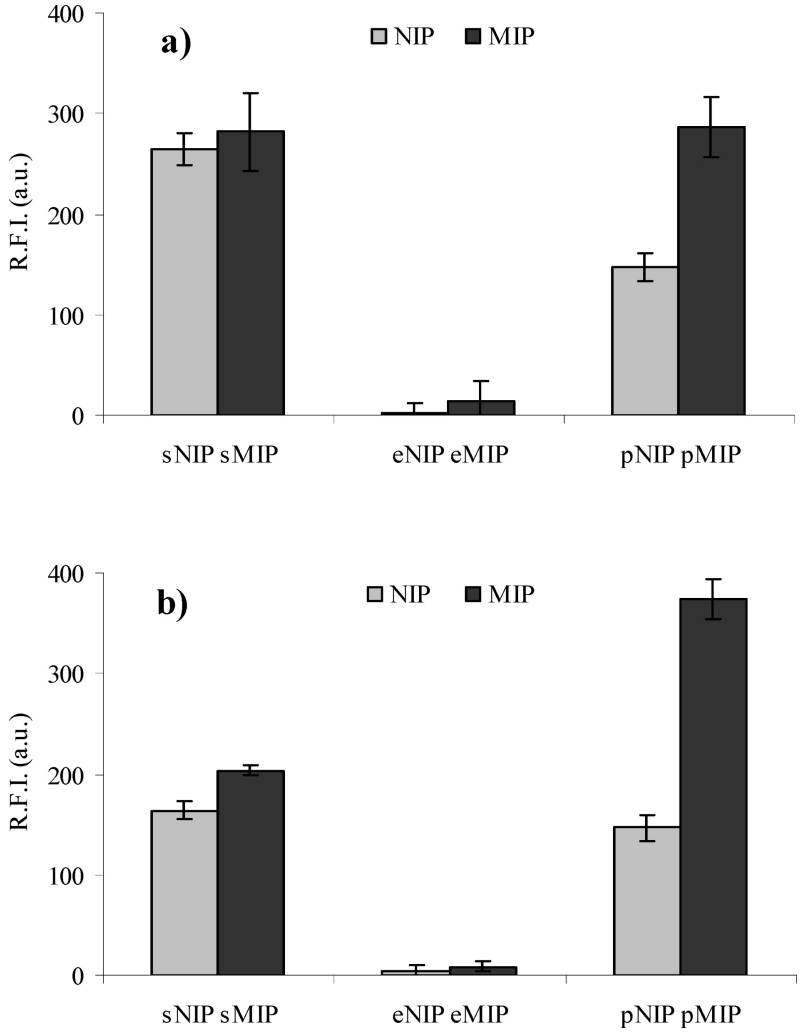

Figure 6.3: Relative fluorescence intensity (RFI) of pyrene immobilized in 1 wt% Fe_3O_4-OA s- and e-, MIP and NIP and microparticles of pMIP and pNIP (5 wt% Fe_3O_4-OA) in (a) pure water, [pyrene] = 60 ng mL^{-1} and (b) 60 vol% acetonitrile/water mixture, [pyrene] = 1000 ng mL^{-1}.

Figure 6.1E shows a HREM picture of this novel material (see Supporting Information, Figure 6.10, which shows the size of the magnetic hybrid nanoparticles encapsulated by a cross-linked polymer into pMIP and also the SEM picture of pMIP). It was prepared in two steps. First, magnetic nanoparticles of Fe_3O_4-OA were encapsulated in a cross-linked polymer (EDMA/MMA) by a miniemulsion polymerization[251] (magnetic hybrid nanoparticles, see Figure 6.1C,D). Then, these magnetic particles were embedded into the structure of a MIP which was prepared by precipitation polymerization.[252] The resulting microparticles will be called pMIP (see Figure 6.1D). Nonimprinted polymer (pNIP) was prepared following the same protocol but in the absence of the template molecule pyrene.

The first step was the preparation of the magnetic hybrid nanoparticles encapsulated by a cross-linked polymer with specific features: small size (nanometer scale), high magnetite content[253–255] (between 80 and 90 wt%), and an appropriately cross-linked, polymeric matrix.

The cross-linked, polymeric matrix, which has to encapsulate the magnetic Fe_3O_4-OA nanoparticles, must be selected very carefully because interactions with the template, such as $\pi - \pi$ forces, must be avoided. A good choice of polymeric coating minimizes high background signals caused by irreversibly bound template molecules at the interface between the magnetic hybrid nanoparticles and the covering MIP.

In addition, these magnetic hybrid nanoparticles encapsulated by a cross-linked polymer must be dispersible in the medium in which the polymerization of the MIP will be carried out and have to have a high affinity to the MIP matrix in order to avoid the phase separation during the MIP formation in the second step.[256]

Methyl methacrylate (MMA) and ethylene glycol dimethacrylate (EDMA) were selected to encapsulate magnetic hybrid nanoparticles (40 wt% MMA-60 wt% EDMA) for the following reasons: they do not show $\pi - \pi$ interactions with pyrene, they provide a polymer which is dispersible in methanol, and the resulting cross-linked polymer has good affinity to the pMIP.

Parts C and D of Figure 6.1 show the TEM and HREM images of these magnetic hybrid nanoparticles encapsulated by EDMA/MMA (EDMA/MMA-Fe_3O_4-OA). They have a z-average of 63.7 nm with a polydispersity index (PDI) of 0.114 measured by dynamic light scattering. The estimated amount of iron oxide by electron microscopy in these nanoparticles is approximately between 75 % and 90 % (v/v) as can be seen in Figure 6.1C,D.

The second step was the preparation of MIP microparticles by precipitation polymerization in the presence of the EDMA/MMA-Fe_3O_4-OA nanoparticles prepared in the first step. MIP was prepared with 6.5 wt% of EDMA/MMA-Fe_3O_4-OA nanoparticles which corresponded approximately with a 5 wt% of Fe_3O_4-OA if an average Fe_3O_4-OA content of 80 % is assumed in the EDMA/MMA-Fe_3O_4-OA nanoparticles. The yield in magnetic, molecular imprinted microparticles after several washes with chloroform in an ultrasonic bath was 92 %.

Figure 6.1E shows the structure of the pMIP. The EDMA/MMA-Fe_3O_4-OA nanoparticles are homogeneously distributed in the pMIP. Thus, the surface of the resulting microparticles is free of magnetite. The phase separation is avoided by the adequate polarity of the EDMA/MMA-Fe_3O_4-OA nanoparticles which renders the free energy of the separation process along the polymerization process.

This new and well-organized material combines a high magnetite content (5 wt%) and adequate optical properties making it highly sensitive and selective. Figures 6.2, 6.3, and 6.4 show the analytical characteristics of pMIP. The time required for achieving a stable signal depends only on the speed of particle separation and, consequently, the magnetite content in the Mag-MIPs. The time required for analyte diffusion (response time) is much faster than the particle collection, and therefore its contribution to the overall equilibration time is negligible. This assumption is corroborated by the decreasing equilibration time from 1 wt% Fe_3O_4-OA sMIP to 5 wt% Fe_3O_4-OA pMIP (see Supporting Information, Figures 6.11a and 6.11c) and also by magnetization study at room temperature of pMIP and 1 wt% Fe_3O_4-OA sMIP (see Figure 6.5). It shows that the magnetic properties of pMIP are 3 times higher than of 1 wt% Fe_3O_4-OA sMIP.

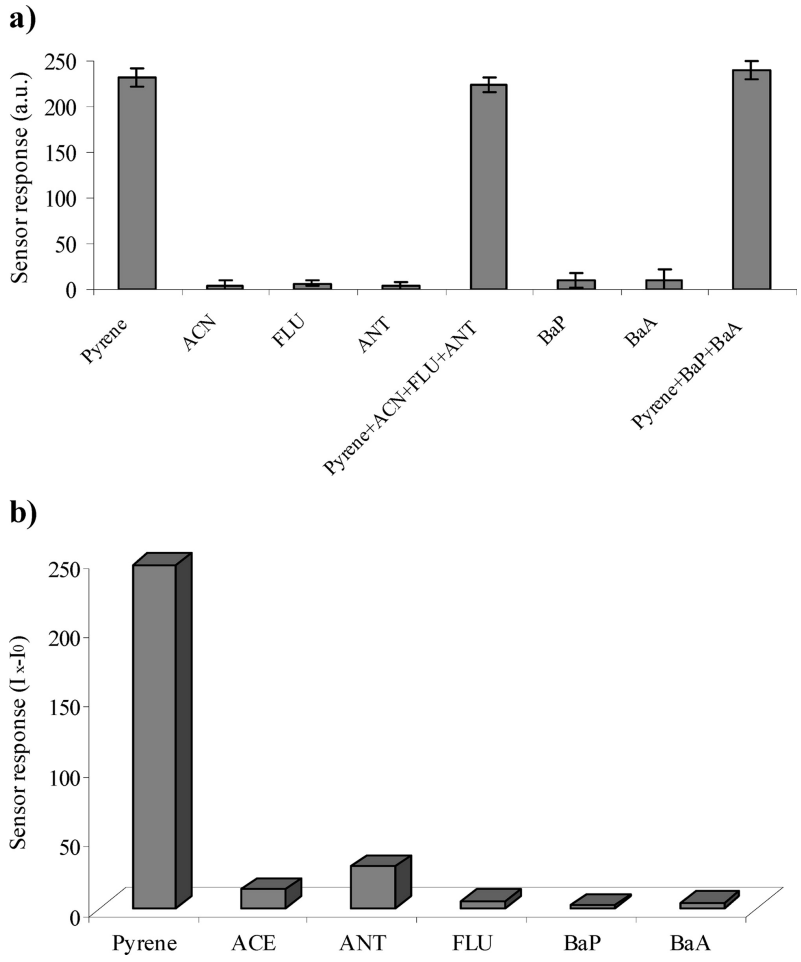

Figure 6.4: Optical interference study. (a) Study 1: sensing response ($I_x - I_0$) of pMIP in the presence of [pyrene] = [ACN] = [FLU] = [ANT] = 40 ng mL^{-1} and [BaA] = [BaP] = 1 ng mL^{-1} at the excitation and emission wavelengths of pyrene ($\lambda_{ex/em}$ = 340/396 nm). (b) Study 2: sensing response ($I_x - I_0$) of pMIP in the presence of [pyrene] = [ACN] = [FLU] = [ANT] = 40 ng mL^{-1} and [BaA] = [BaP] = 1 ng mL^{-1} at their respective excitation and emission wavelengths (see Table 6.6 for the wavelengths).

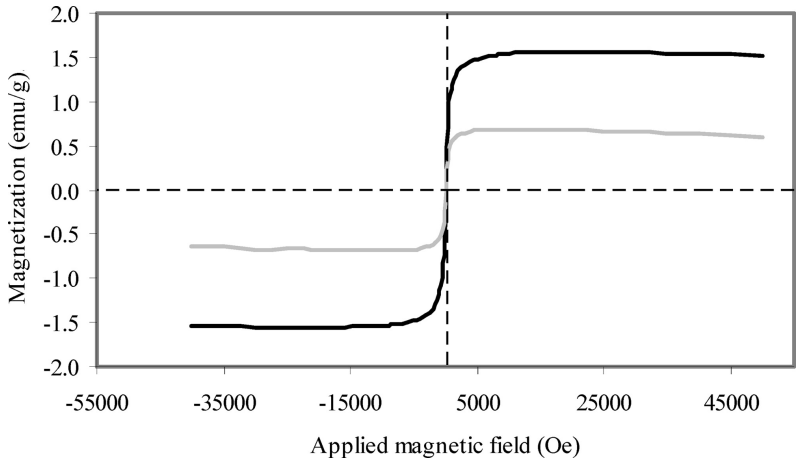

Figure 6.5: Magnetization curves at room temperature of pMIP (black line; S saturation magnetization is 1.52 emu g^{-1}) and 1 wt% Fe_3O_4-OA sMIP (gray line; saturation magnetization is 0.61 emu g^{-1}).

Another big advantage of the novel pMIP is its higher sensitivity. Although pMIP contains 5 times more magnetite, the signal intensity of pMIP was higher than 1 wt% Fe_3O_4-OA sMIP at the same pyrene concentration. This was unexpected because the dark colored magnetite is absorbing light efficiently, and one would expect a decreasing intensity with an increasing magnetite concentration. The explanation is most probably a better optical isolation of the magnetite in pMIP from the fluorescent analyte. pMIP showed a signal of 295 au for 65 ng mL^{-1} of pyrene in pure water while 1 wt% Fe_3O_4-OA sMIP provided only 262 units (see Figure 6.3a).

The new material also showed a good MIP/NIP ratio, i.e., the imprinting process was very effective: the MIP/NIP ratio in the determination of 1 mg L^{-1} pyrene solved in 60 wt% acetonitrile-water was 2.41 for pMIP compared to 1.30 for 1 wt% Fe_3O_4-OA sMIP (see Figure 6.3b) and 2.0 compared to 1.0 for 65 ng mL^{-1} pyrene in pure water (see Figure 6.3a). In the Supporting Information also the MIP/NIP ratio can be seen (Figure 6.12). The increase of unspecific interactions in water was because water increases the unspecific hydrophobic interactions, mainly van der Waals forces, between pyrene and polymer. Thus, comparing MIP/NIP ratios of pMIP and sMIP, it is possible to suggest that phase separation and superficial distribution of Fe_3O_4-OA clusters during MIP formation might affect the imprinting phenomena in the MIP surface. This is more effective in a polymer with the surface free of Fe_3O_4-OA such as pMIP. The phase separation is a dynamic process which may adversely affect the adequate formation of molecular imprinting cavities during the polymerization: i.e., destroying the specific cavities and absorption of the template in the clusters of Fe_3O_4-OA.

To determine the sensitivity of pMIP to pyrene, a standard linear calibration graph was drawn according to recommended procedures (Figure 6.13 shows the experimental results of the analytical calibration). The wide linear range, the small standard deviation, and the correlation coefficient close to unity indicate a good suitability of the obtained Mag-MIPs for analytical applications. The detection limit was determined using the IUPAC method (LOD = $3s_b/m$) where sb is the standard deviation for 10 blank samples and m the slope

of the calibration curve. The detection limit of $7\,\mathrm{ng\,mL^{-1}}$ shows the surprisingly high sensitivity of this magnetic optical sensor MIP.

In addition, the newly designed magnetic MIP microparticles were very selective to pyrene. Two different studies were developed. First, the signal of pyrene and the interference substances in pMIP were measured at the excitation and emission wavelengths which are optimal for pyrene. The plots in Figure 6.4a show that the optical signal of pyrene in pMIP was not affected by the presence of other luminescent PAHs such as acenaphthene (ACE), fluorene (FLU), anthracene (ANT), benzo[a]pyrene (BaP), and benzo[a]anthracene (BaA), and therefore it can be determined in the presence of these analytes (see also Supporting Information Figure 6.14).

Second, the luminescent intensities of pyrene, ACE, FLU, ANT, BaP, and BaA were recorded at their respective excitation and emission wavelengths (see Table 6.2). Figure 6.4b shows that the signals of the interferents (ACE, FLU, ANT, BaP, and BaP) were negligible, and therefore the selectivity of the sensing Mag-MIP was due to the imprinting phenomena and not caused by the spectroscopic characteristics of the analytes (see also Figure 6.15). Thus, it is possible to conclude that the pMIP is highly selective to pyrene.

The affinity, capacity, and heterogeneity of pMIP have also been studied using the Freundlich isotherm-affinity distribution analysis. The aim of this study was double: on the one hand, to corroborate the high selectivity of pMIP by showing the affinity and capacity of pMIP to different PAHs; and on the other hand, to demonstrate the imprinting phenomena by analyzing the differences between pMIP and pNIP.

Because of the different hydrophobic character of PAHs (Supporting Information shows the solubility of the compounds under study, Table 6.3), only three PAHs (FLU, ANT, and ACE) whose water solubility is higher than $50\,\mathrm{ng\,mL^{-1}}$ can be used to develop the cross-reactivity study because only they have the adequate solubility to be compared in the same range of affinities with pyrene (see Supporting Information for the linear ranges of these compounds in 60 vol% acetonitrile-water, Table 6.4). The experimental binding data for this study were modeled with the Freundlich isotherm (FI) equation (see equation 6.1), which is a power function of concentration according to

$$B(C) = aC^m \tag{6.1}$$

where B and C are the concentrations of bound and free analyte, respectively, and a and m are fitting constants that have physical meaning.[257] The constant m is particularly interesting, as it is the heterogeneity index. Its value ranges from 0 to 1 and increases as heterogeneity decreases. The broad applicability of the FI to noncovalent MIPs has been demonstrated recently.[258]

Two additional binding parameters can be calculated:[259–263] the number of binding sites per gram of material ($N_{K_{\min}-K_{\max}}$; see equation 6.2) and the apparent average association constant ($K_{\min} - K_{\max}$; see equation 6.3) where a and m are equivalent to Freundlich parameters:

$$N_{K_{\min}-K_{\max}} = a * (1 - m^2) * (K_{\min}^{-m} - K_{\max}^{-m}) \tag{6.2}$$

$$K_{\min} - K_{\max} = \left(\frac{m}{m-1}\right) * \left(\frac{K_{\min}^{1-m} - K_{\max}^{1-m}}{K_{\min}^{-m} - K_{\max}^{-m}}\right) \tag{6.3}$$

The values for these parameters can be calculated for any range of binding affinities within the limits of the Kmin and Kmax being equal to the reciprocal corresponding concentrations $K_{\min} = 1/C_{\min}$ and $K_{\max} = 1/C_{\max}$. Comparisons of $N_{K_{\min}-K_{\max}}$ and values are valid if the range of affinities considered in the calculation of these values are the same for all compared cases.[259,263]

All the isotherms were acquired in a 50 vol% mixture of acetonitrile and water, using 6 mg of polymer per 5 mL of solution of the target compound. The measurements were done after 1 h because the equilibrium was reached in 3 min due to the fast diffusion of the compounds into the pMIP (see Supporting Information Figure 6.11c).

Table 6.1: Freundlich fitting parameters, weighted average affinity, and number of sites for pyrene in pMIP and pNIP and ANT, FLU, and ACE in pMIP.

	m	a $[(\mu g\, g^{-1})\ (L\, mg^{-1})^m]$	r^2	$N_{K_{\min}-K_{\max}}$ [a] $[\mu mol\, g^{-1})] \times 10^{-3}$	$K_{K_{\min}-K_{\max}}$ [a] $[L\, mol1] \times 10^{-8}$
pyrene in pMIP	0.73 ± 0.02	331.82 ± 2.80	0.999	168.0 ± 1.0	12.0 ± 0.9
pyrene in pNIP	0.92 ± 0.04	214.31 ± 3.86	0.996	32.5 ± 0.6	11.0 ± 0.9
ANT in pMIP	0.95 ± 0.02	152.57 ± 3.29	0.999	14.4 ± 0.3	10.0 ± 0.9
FLU in pMIP	0.96 ± 0.01	162.19 ± 1.50	0.999	12.3 ± 0.1	9.0 ± 0.9
ACE in pMIP	0.99 ± 0.03	99.91 ± 1.90	0.998	1.9 ± 0.0	8.0 ± 0.8

[a] Calculated for a concentration range $\log K = 1 - 0.53\,(mg\, L^{-1})$.

Here, it can be seen that the value of pyrene adsorbed on pMIP particles is slightly higher than for the interferents, and consequently, the interaction pyrene–pMIP is the most effective one of the studied analytes. This means the prepared Mag-pMIP contains steric cavities with adequate geometry for pyrene. The small differences between the values of indicate a low binding energy of the prepolymerization complex due to the low energy forces (i.e., $\pi - \pi$ interactions) involved in the formation of the steric binding cavities.(9) For this reason, pMIP can be cleaned very easily by only two washing steps with acetone.

The data also show that $N_{K_{\min}-K_{\max}}$ of pyrene in pMIP is 5 times higher than in pNIP. This means that the number of sites with adequate geometry and good accessibility to pyrene is higher in pMIP than in pNIP, demonstrating the imprinting phenomenon. In addition, $N_{K_{\min}-K_{\max}}$ of pyrene in pMIP was 89, 14, and 12 times higher than ACE, FLU, and ANT in pMIP, respectively. Therefore, pMIP particles were highly selective to pyrene and the steric cavities formed in pMIP had adequate geometry to pyrene, which was experimentally confirmed by optical interference measurements where none of the PAHs tested interfere with the selective determination of pyrene and none of them are observed at their maxima excitation and emission wavelengths (see Figure 6.4).

6.4 Conclusions

We have demonstrated a new synthetic route to a well-controlled magnetic imprinted material based on a two-step process: first, the incorporation of the magnetite into a

matrix which does not negatively influence the molecular imprinting phenomenon and, second, the embedding of these magnetic nano precursors in the MIP structure which can be used for optical sensing. To the best of our knowledge, this is the first time that a magnetic MIP can be used as optical sensor. The preparation of these microparticles is simple and provides a sensing material which is highly magnetic (content of 5 wt% Fe_3O_4-OA approximately) and sensitive (detection limit of 7 ng mL^{-1}). In addition, this material shows a very high affinity characteristic to pyrene which was the imprinted molecule (ratio MIP/NIP of 2.41, the highest and NKmin-Kmax of pyrene in pMIP 5, 89, 14, and 12 times higher than pyrene in pNIP and ACE, FLU, and ANT in pMIP) and, therefore, very high selectivity. None of the tested luminescent PAHs (ACE, FLU, ANT, BaP, and BaA) interfered with the determination of pyrene. Lastly, this novel strategy to design MIPs with well-controlled structure for the usage as optical sensors with adequate magnetic and optical properties may be further extended for implementing optical sensing phases in portable devices that can control a broad variety of analytes in different matrices (water, organic solvent, etc.) and may be used to improve sensitivity in other magnetic optical sensors.

Acknowledgments

The authors thank the Spanish Ministry of Education (FPU grant reference AP2006-01144 and Project CTQ2008-01394) and the Regional Government of Andalusia (Excellence projects P07-FQM-02738 and P07-FQM-02625) for their financial support.

6.A ESI for the manuscript: Novel strategy to design magnetic, molecular imprinted polymers with well-controlled structure for the application in optical sensors

This chapter was published as *Supporting Information for the Full Paper* in

Macromolecules, 2010, 43 (1), 55-61.

doi: 10.1021/ma902095s

Authors: Antonio L. Medina-Castillo, Günter Mistlberger*, Jorge F. Fernandez-Sanchez*, Antonio Segura-Carretero, Ingo Klimant and Alberto Fernandez-Gutierrez

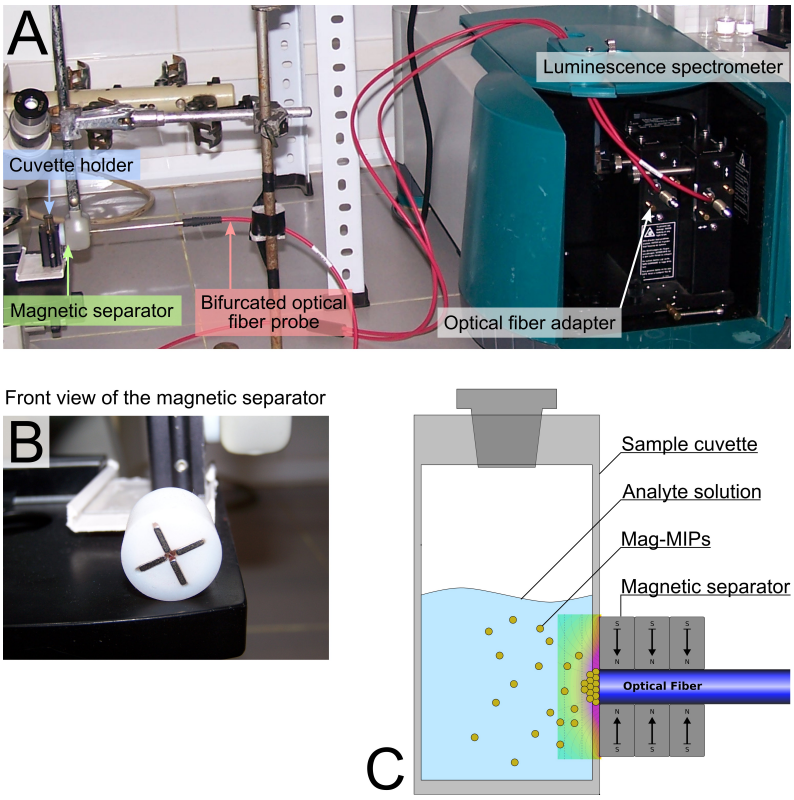

Figure 6.6: Pictures of the measuring setup and the magnetic separator.

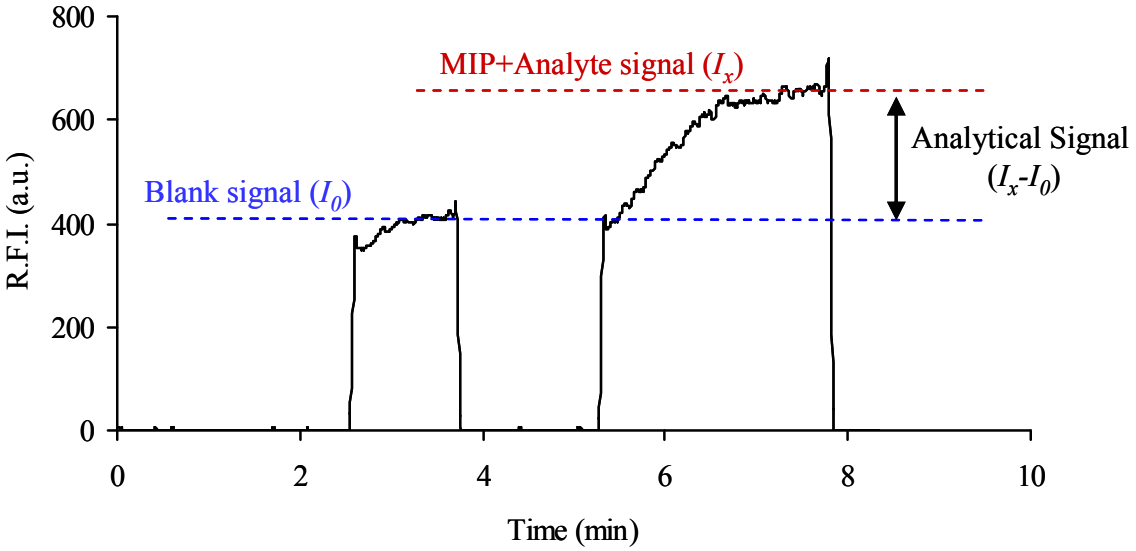

Figure 6.7: Calculation of the analytical signal.

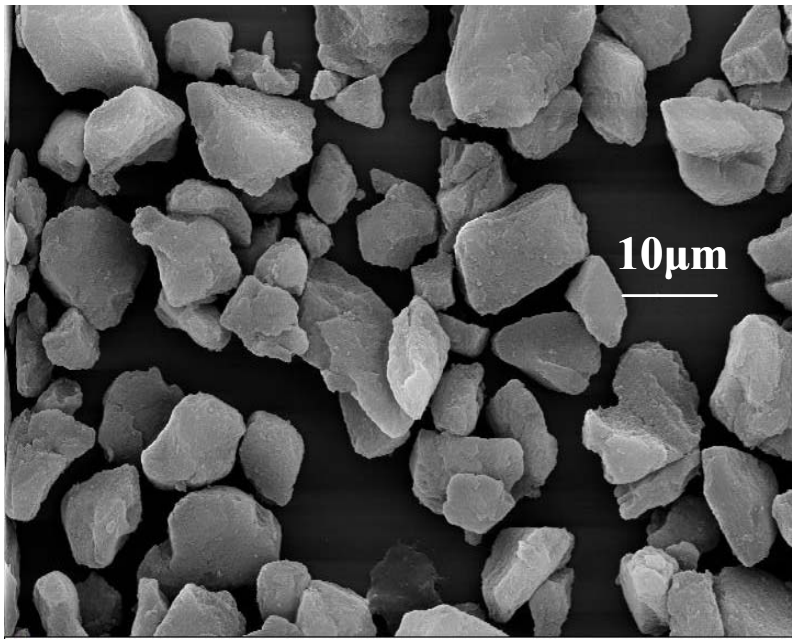

Figure 6.8: SEM image of 5 wt% Fe_3O_4-OA sMIP sieved at 20 µm.

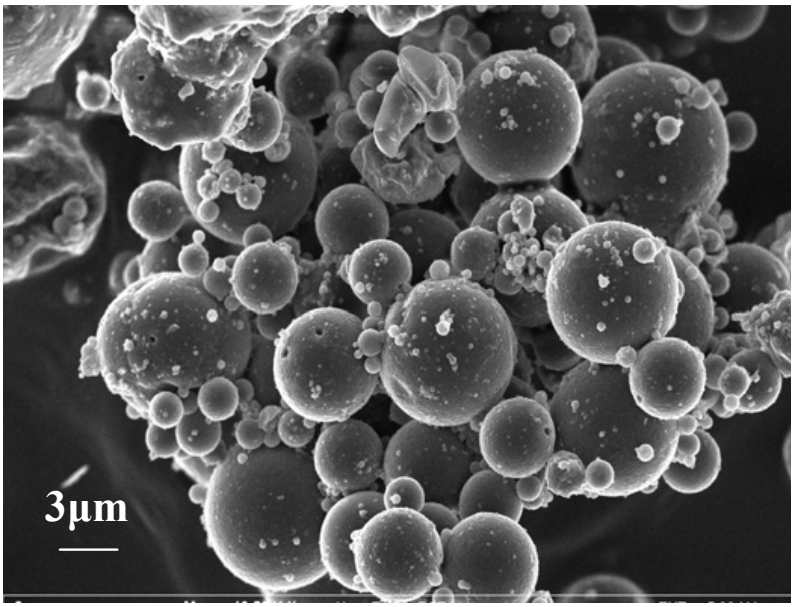

Figure 6.9: SEM image of 5 wt% Fe_3O_4-OA eMIP.

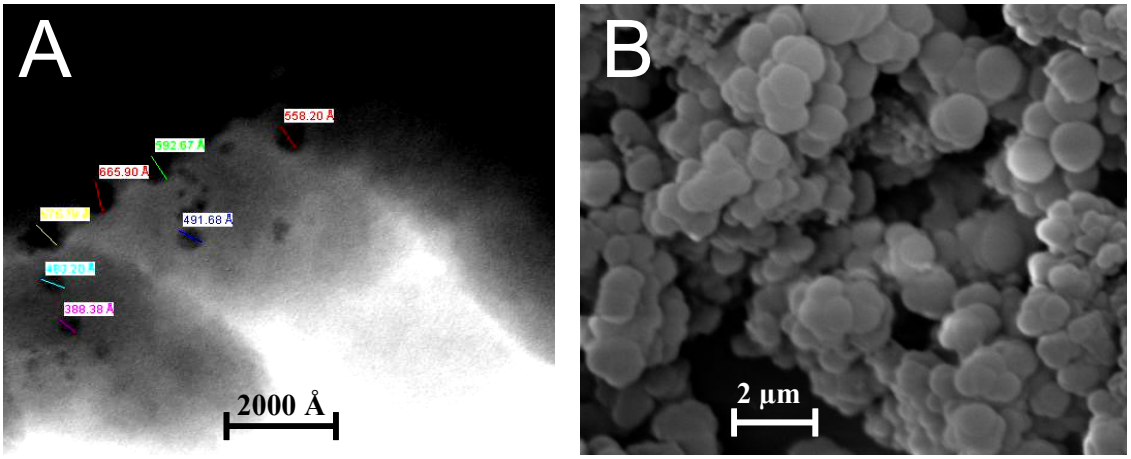

Figure 6.10: Images of HREM (A) which shows the size of the EDMA/MMA-Fe_3O_4-OA nanoparticles incorporated into the structure of pMIP, and a SEM picture (B) of pMIP to observe the size of the designed particles.

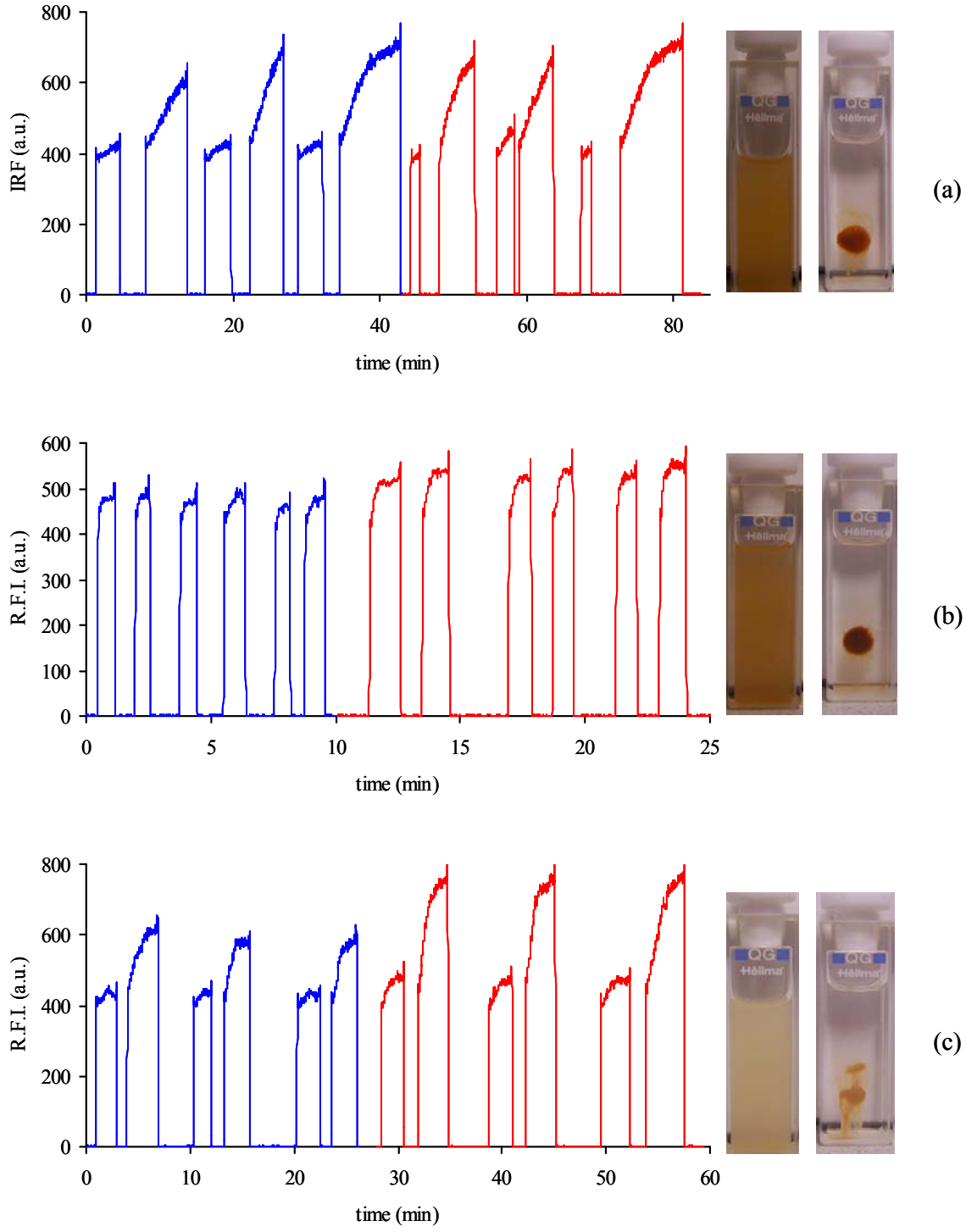

Figure 6.11: Relative fluorescence intensity (R.F.I.) of 65 ng mL^{-1} PYR in pure water in a) 1 wt% Fe_3O_4-OA sMIP (red) and sNIP (blue), b) 1 wt% Fe_3O_4-OA eMIP (red) and eNIP (blue), and c) 5 wt% Fe_3O_4-OA pMIP (red) and pNIP (blue). To the right of the intensity plots the sensor spot after the measurement can be seen. The images elucidate that the color of pMIP particles was much brighter than the one of eMIP and sMIP, although 5 times more magnetite was embedded.

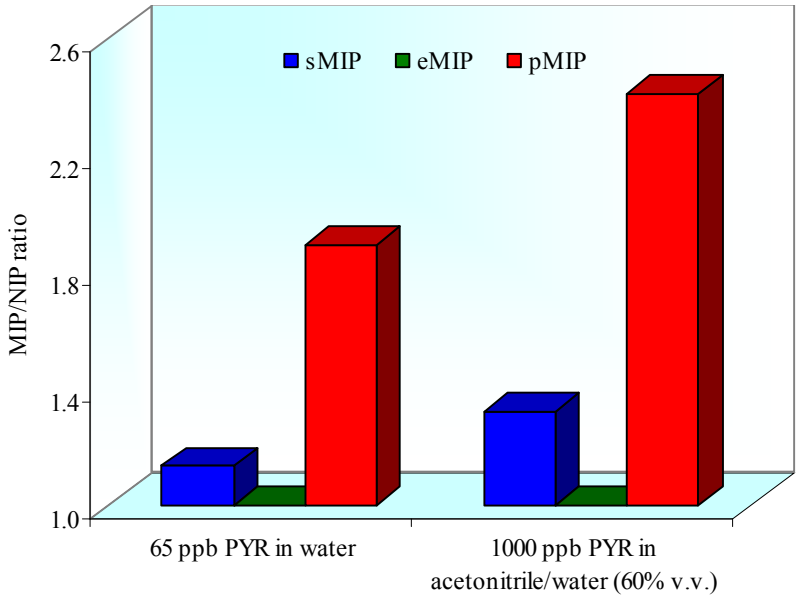

Figure 6.12: MIP/NIP ratio for 1 wt% Fe_3O_4-OA sMIP, 1 wt% Fe_3O_4-OA e-MIP and 5 wt% Fe_3O_4-OA pMIP with 65 ng mL^{-1} of PYR in pure water and 1000 ng mL^{-1} of PYR in a mixture of acetonitrile/water 60/40 % (v/v).

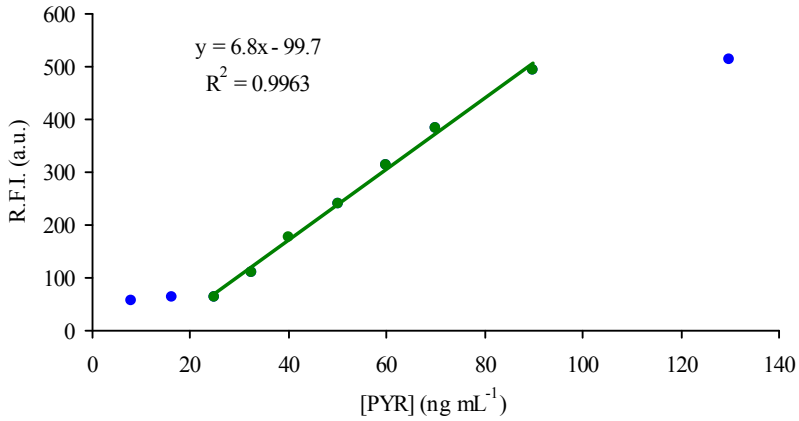

Figure 6.13: Standard calibration curve of pMIP with PYR in pure water ($\lambda_{ex/em}$ = 340/396 nm, excitation and emission slit width 5 nm, detector voltage 1000 V).

Table 6.2: Spectroscopic characteristics of the PAHs under study.

	λ_{ex} (nm)	λ_{em} (nm)
PYR	340	396
FLU	300	318
ANT	286	388
ACE	290	322
BaA	286	388
BaP	390	406

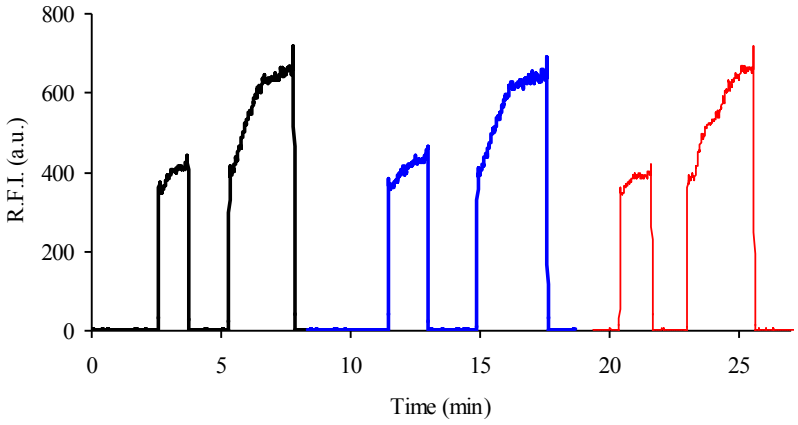

Figure 6.14: RFI recorded for 40 ng mL^{-1} PYR into pMIP (black), 40 ng mL^{-1} PYR + 40 ng mL^{-1} ACE + 40 ng mL^{-1} FLU + 40 ng mL^{-1} ANT into pMIP (blue); 40 ng mL^{-1} PYR + 1 ng mL^{-1} BaA + 1 ng mL^{-1} BaP into pMIP (red).

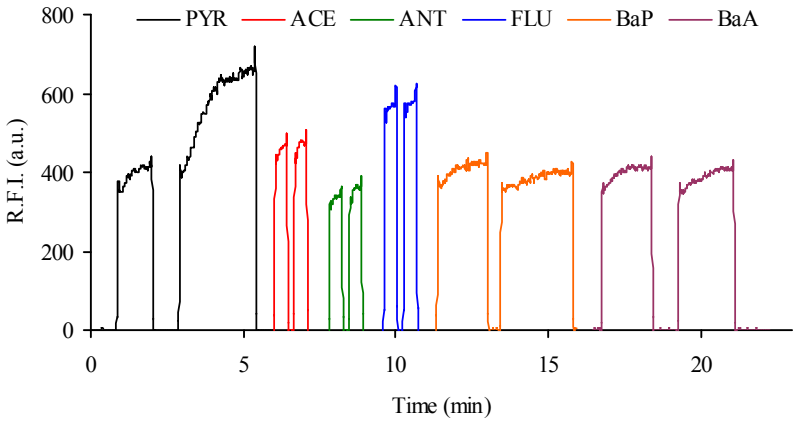

Figure 6.15: Signal of PYR, ANT, FLU, ACE, BaA and BaP into pMIP at their maxima excitation and emission wavelengths. [PYR]=[ACE]=[FLU]=[ANT]= 40 ng mL^{-1}, [BaA]=[BaP] 1 ng mL^{-1}.

Table 6.3: Water solubility of polycyclic aromatic hydrocarbons.

	PYR	**FLU**	**ANT**	**ACN**	**BaP**	**BaA**
Water Solubility [µg mL^{-1}]	0.06	17	0.09	2.9	0.0013	0.0063

Table 6.4: Linear ranges used for calculating the free equilibrium concentrations (C).

	Linear range [mg L^{-1}]	R^2
PYR	0.05-1.5	0.999
FLU	0.05-0.90	0.999
ANT	0.05-0.35	0.999
ACN	0.05-0.90	0.999

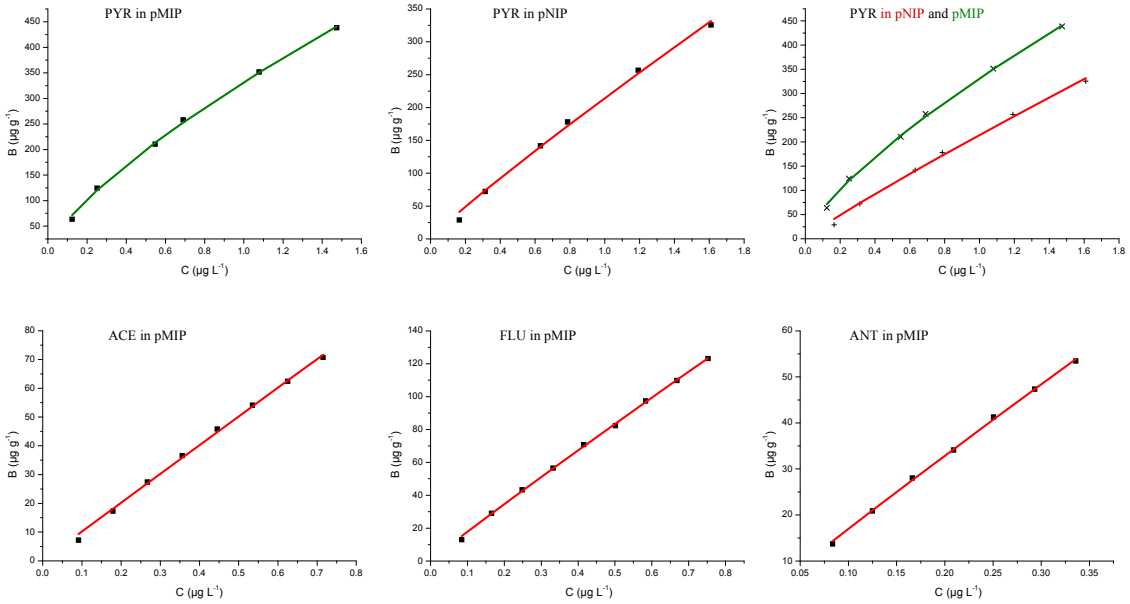

Figure 6.16: Adsorption isotherms for pMIP and pNIP and their corresponding experimental Freundlich isotherms. Binding conditions: quantity of polymer MIP or blank polymer NIP: 6 mg, volume: 5 mL, binding time: 1 h in a mixture of acetonitrile/water 60/40 % v/v.

7 Magnetically remote-controlled, optical sensor spheres for monitoring oxygen or pH

This chapter was published as *Technical Note* in

Analytical Chemistry, 2010, 82, 2124-2128

doi: 10.1021/ac902393u

Authors: Günter Mistlberger*, Klaus Koren, Sergey M. Borisov and Ingo Klimant

Abstract Magnetic sensor macrospheres (MagSeMacs), i.e. stainless steel spheres coated with optical chemical sensors, are presented as an alternative to existing optical sensor patches and fiber-optical dip-probes. Such spheres can either be reversibly attached to the tip of an optical fiber (dip-probe) or trapped inside a vessel for read-out through the side wall. Moving the magnetic separator at the exterior enables measurements at varying positions with a single sensor. Moreover, the sensor's replacement is rapid and contactless. We measured dissolved oxygen or pH in stirred liquids, rotating flasks, and 24-well plates with an SDR-device for parallel cell culture monitoring. In these applications, MagSeMacs proved to be advantageous over conventional sensor patches and magnetic optical sensor particles because of their magnetism, spherical shape, reflectance and size. These properties resulted in strong but reversible fixation, magnetic remote-controllability, short response times, high signal intensities and simplified handling.

7.1 Introduction

Bioprocess developments rely on the strict control of process parameters, such as pO_2, pH, temperature and metabolite concentrations.[219,264–267] For process monitoring, optical sensors represent a reliable, robust and cheap alternative to conventional, mostly electrochemical or physical sensors. Among optical sensors, sensor patches fixed in transparent reaction vessels or coated onto optical fiber probes (micrometer or millimeter scale) have been used most frequently.[220,226,268–273] Although sensor patches are wide-spread they have some limitations. (1) Price: Photobleaching and biofouling of the sensors require periodical exchanges of vessels as well as fiber-optic probes. (2) Time: The sensor-spots need to be fixed long time before the measurement. (3) Mobility: Once a sensor patch is fixed, its position cannot be changed. Consequently, measurement information can

only be acquired at a single position. The identification of concentration gradients would require many sensor spots or the application of a dip-probe.

Measuring analyte concentrations at different positions with mobile sensors was recently solved by applying magnetic optical sensor particles (MOSePs).[2,136] With MOSePs, sensor spots can be formed *in situ* in front of an optical fiber by using special magnetic separators.[13] The brightness and inducible magnetic force of such "sensor swarms" is higher compared to single particles.[136] Despite the suitability of MOSePs for complex applications, where fixed sensor patches fail, further improvements are essential for bioprocess monitoring. Stability against shear forces and time required for sensor spot formation play a crucial role for the sensor performance and are difficult to control with micro- and nanoparticles. Nelson and co-workers recently reported on wireless optical sensors as MEMS prototypes for intraocular oxygen measurements.[79] Focusing the sphere in a certain distance from the magnets, however, resulted in a relatively complex setup.

This paper describes the spray coating of stainless steel spheres with polymeric matrices and sensor dyes for the production of highly ferromagnetic, user-friendly, remote-controlled, optical sensor macrospheres (MagSeMacs) in transparent vessels (7.1). These spheres can also be used as disposable sensors for dip-probes. The response times and calibration curves of two types of MagSeMacs (pH or oxygen sensitive) were measured. Their suitability as alternative but also as extension to currently available sensor patches is discussed. Finally, magnetic separators are described which enabled the application of MagSeMacs as dip-probes and remote-controlled sensors.

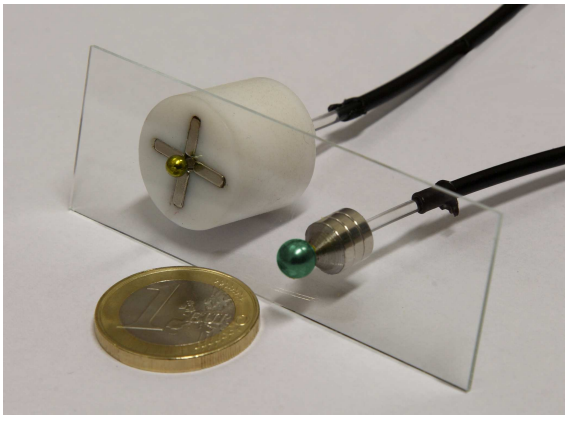

Figure 7.1: Magnetic sensor macrospheres captured in front of an optical fiber with a radial (left) or axial (right) separator.

7.2 Experimental section

7.2.1 Chemicals and materials

Polysulfone (MW 35,000; Sigma), polystyrene (PS, MW 250,000; Acros Organics), poly(vinylidene chloride-co-acrylonitrile) (PViCl-PAN; 20% (w/w) polyacrylonitrile; MW 150,000; Polysciences), polyurethane hydrogel D4 (Cardiotech), glucose oxidase from

Aspergillus niger (GOx, Fluka), trichloromethane, ethanol, glucose monohydrate, phosphate and citrate buffers (all purchased from Carl Roth GmbH, Germany) were used as received without further purification. Iridium(III)((benzothiazol-2-yl)-7-(diethylamino)-coumarin))$_2$(acetylacetonate) (Ir(C_S)$_2$(acac)),[198] 1-hydroxypyrene-3,6,8-*tris*-*bis*(2-ethylhexyl)sulfonamide (HPTS(DHA)$_3$)[274] and platinum(II)-tetraphenyltetrabenzoporphyrin (PtTPTBP)[275] were synthesized in our lab as described in literature. Spectra and structure of the dyes can be seen in Figure 7.6 on page 125 in the Supporting Information (section 7.A). Magnetic steel spheres (stainless steel or class 3 DIN5401) with diameters of 2, 3.2, 4 and 5 mm, respectively, were purchased from Kugel Pompel (www.kugelpompel.at). NdFeB block and ring magnets were purchased from ChenYang Technologies (www.cy-magnetics.com).

7.2.2 Magnetic separator design

The magnetic separators were designed as described elsewhere.[13] Dip-probes for magnetically fixed MagSeMacs had additional barriers around the sphere in order to avoid the sphere's accidental wiping off from the fiber tip (7.2).

7.2.3 Sensor preparation

Steel spheres were coated by spraying a solution of dye and polymer in organic solvent ("cocktail") with an airbrush on rapidly shaking spheres. One hundred stainless steel spheres (d = 3.2 mm) were heated in a crystallizing dish to 70 °C with a heat gun. The crystallizing dish was fixed to a vibrating device (Vibramax 100, Heidolph) with double-faced adhesive tape and shaken at 1000 min^{-1} (shaking orbit 3 mm) in order to avoid the sticking of the spheres to the dish and to each other, respectively.

For oxygen sensitive MagSeMacs, a cocktail of 14.6 mg polystyrene or polysulfone, 0.22 mg of an indicator dye (PtTPTBP or Ir(C_S)$_2$(acac)) and 0.732 g (0.5 mL) CH_3Cl was sprayed onto the preheated spheres from a distance of 30 mm with a cocktail flow-rate of 1.6 mL*min^{-1} and a shear gas pressure of 3 bar. The airbrush was moved in circles above the crystallizing dish to additionally agitate the spheres and to avoid their sticking to the dish.

A dual lifetime referencing (DLR) system[276,277] was utilized for the production of pH-sensitive MagSeMacs. We incorporated HPTS(DHA)$_3$ as pH-sensitive, and Ir(C_S)$_2$(acac) as a reference dye in D4 hydrogel (7.3 and Figure 7.7 on page 126 in the Supporting Information, section 7.A). In order to avoid cross-sensitivity of Ir(C_S)$_2$(acac) to oxygen, this reference dye was first incorporated in PViCl-PAN nanoparticles, which is a gas-impermeable material.[180] For the spraying procedure, the cocktail consisted of 116 mg D4, 1.4 mg HPTS(DHA)$_3$, 14.6 mg PViCl-PAN nanoparticles containing 0.15 mg Ir(C_S)$_2$(acac), 5 g ethanol and 0.5 g deionized water. One milliliter of this cocktail was used for spray-coating.

The oxygen sensing performance of MagSeMacs, a sensor patch, dispersed nanoparticle sensors and magnetic optical sensor particles (MOSePs) was compared. Except for MagSeMacs, these sensors were previously employed for monitoring the analyte concentration in multi-well plates with a SensorDish-reader device. We used a 4 µm thick PS-foil

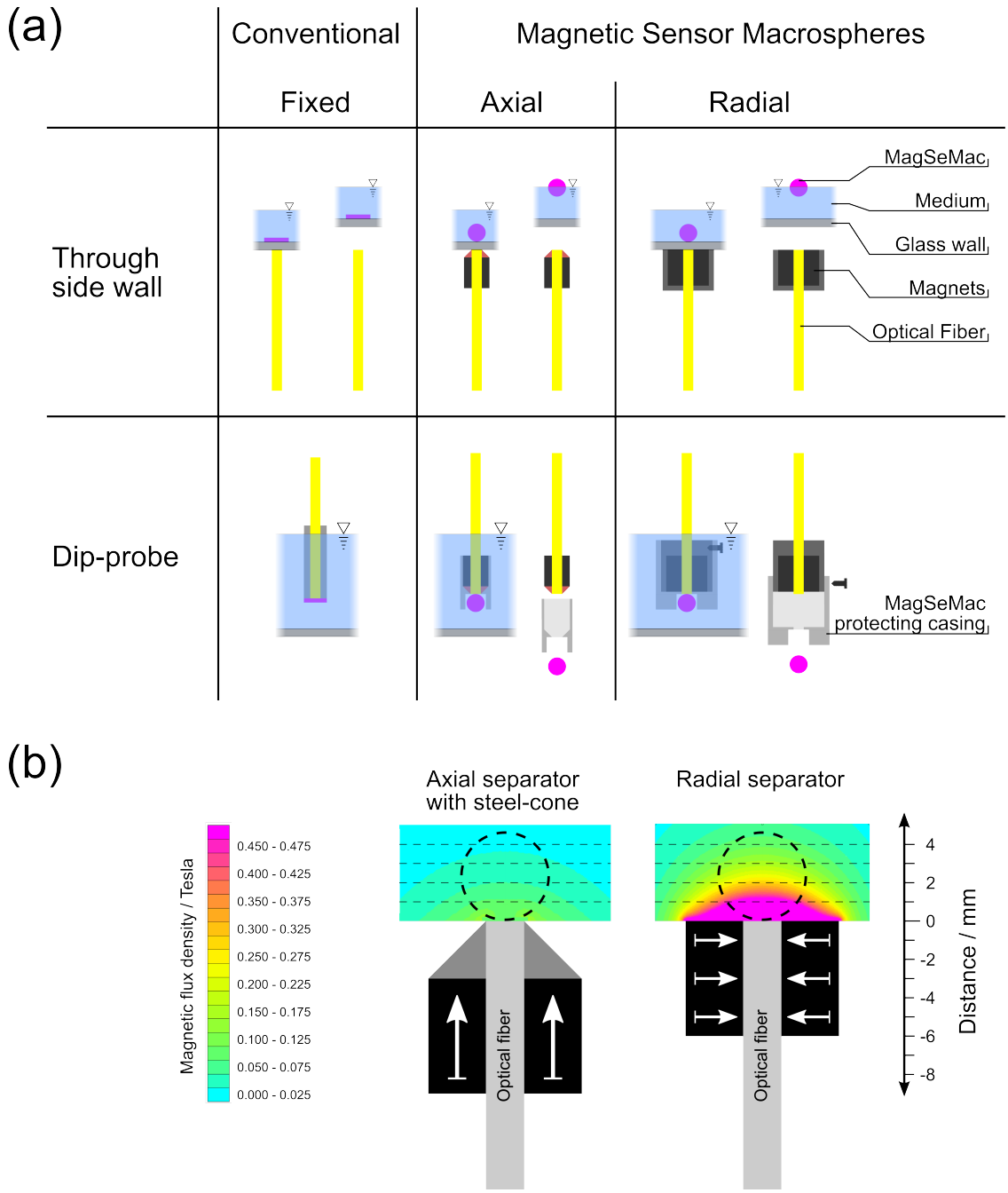

Figure 7.2: (a) Overview of possible sensor configurations with MagSeMacs (right) compared to fixed sensor patches (left). MagSeMacs can replace both fixed sensor spots on glass walls and coated fiber optical dip-probes. (b) The employed magnetic separators ensure a reliable localization of the magnetic sphere in the field of view of the optical fiber. The radial magnetization results in a higher magnetic field density and, consequently, in a stronger attraction of the sphere by the separator.

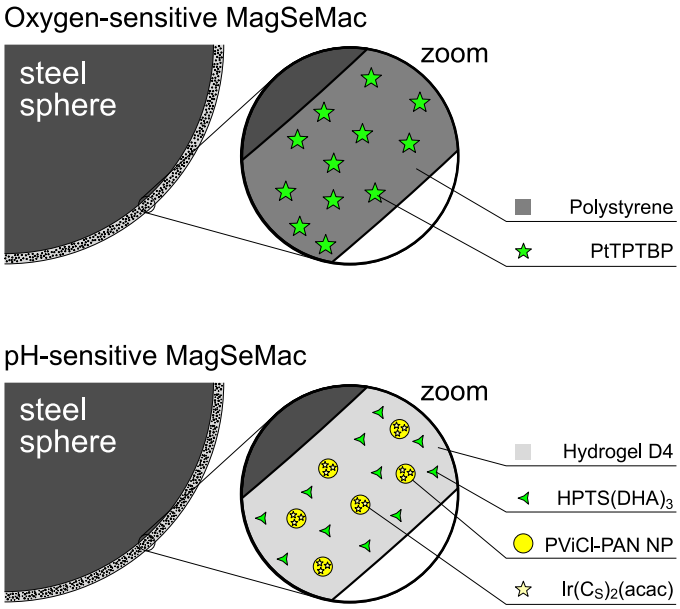

Figure 7.3: Schematic representation of the chemically sensitive coatings of MagSeMacs.

containing 2 % $Ir(C_S)_2(acac)$ as sensor patch. Non-magnetic nanoparticles (PSPVP-NP)[228] and MOSePs[14] were prepared in our lab as described elsewhere.

7.2.4 Measurement setup

MagSeMacs were placed in a 10 mL glass vial (calibration) or a 200 mL beaker (response time) and trapped with the above mentioned magnetic separators. The luminescence phase shift was read out with a 2 mm optical fiber and a phase fluorimeter (pH-Mini, PreSens GmbH, Germany). Alternatively, for PtTPTBP a 625 nm LED (Roithner Laser Technik, www.roithner-laser.com) was modulated with a two-phase lock-in amplifier (SR830, Stanford Research Inc., www.thinksrs.com). A bifurcated fiber bundle was used to guide the excitation light (filtered through a Calflex X filter, Linos) to the MagSeMac and the luminescence back to the detector after being filtered through an RG9 (Schott) glass filter. Luminescence was detected with a PMT (H5701-02, Hamamatsu, www.sales.hamamatsu.com). The modulation frequencies were adjusted to 5 kHz for PtTPTBP and 20 kHz for $Ir(C_S)_2(acac)$. For the measurements in a 24-well plate, a SensorDish® reader device (PreSens GmbH, Germany) was modified with magnets as described elsewhere[14] and the modulation frequency was adjusted to 20 kHz, which is the ideal frequency for $Ir(C_S)_2(acac)$. Gas mixtures for pO_2-calibration were obtained using a gas mixing device (MKS Instruments, www.mksinst.com). Nitrogen, synthetic air and oxygen were purchased from Air Liquide. Calibration of pH-MagSeMacs was carried out in 20 mM phosphate or phosphate-citrate buffers (ionic strength adjusted to 100 mM with NaCl) with pH-values from 3.69 to 11.9. The response time was measured upon rapid mixing of two solutions with analyte concentrations in the dynamic range of the sensors. Here, dip-probe type separators were employed.

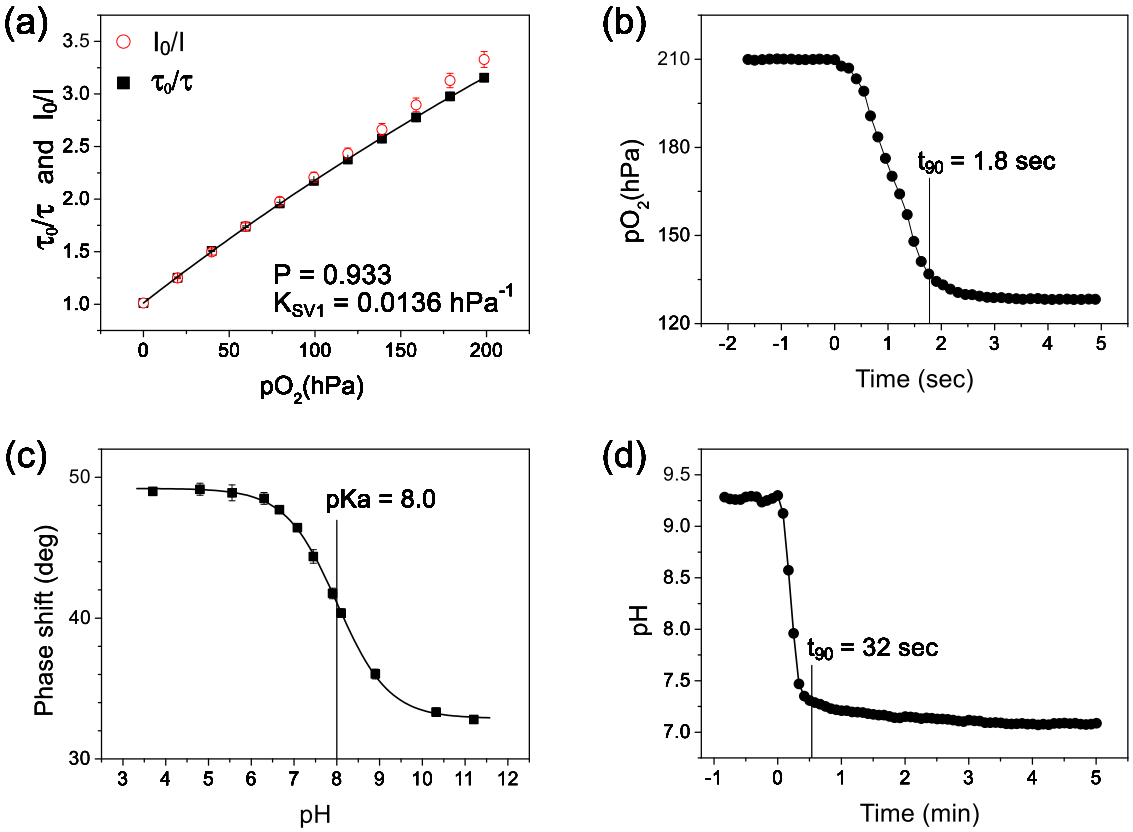

Figure 7.4: Calibration and response curve of an oxygen sensitive, PtTPTBP-stained MagSeMac (a,b) and pH-sensitive MagSeMacs (c,d).

7.3 Results and discussion

Magnetic stainless steel spheres were coated with an optical sensor by spray-painting. This high-throughput method resulted in fast responding, bright and mechanically stable coatings. Stainless steel was necessary to avoid signal changes due to corrosion. Oxygen and pH-sensitive MagSeMacs, respectively, were prepared and their response times as well as their sensor characteristics were investigated. The Stern-Volmer plot of PtTPTBP-stained MagSeMacs (7.4a) shows a good correlation with the simplified two-site model of Carraway and Demas,[223] where one fraction of the dye molecules is assumed to be unquenchable, i.e. its $K_{SV2} = 0$ (see equations 8.1 and 8.2).[230]

$$\frac{\tau}{\tau_0} = \frac{P}{1 + K_{SV1} * pO_2} + \frac{1 - P}{1 + K_{SV2} * pO_2} \tag{7.1}$$

$$K_{SV2} = 0 \Longrightarrow \frac{\tau}{\tau_0} = \frac{P}{1 + K_{SV1} * pO_2} + 1 - P \tag{7.2}$$

The quenchable fraction of the dye (93 %) has a K_{SV1} of 0.014 hPa^{-1}.

The response time of oxygen-sensitive MagSeMacs ($t_{90} = 1.8$ s, 7.4b) is sufficiently fast

Table 7.1: Intra- and inter-sphere variations of the analyte signal of oxygen (PtTPTBP-stained) or pH-sensitive MagSeMacs.

	$\tau_0/\tau_{air} \pm s$	s_{rel} (%)	$\tau_0 \pm s$ (10^{-6} s)	s_{rel} (%)	pH$\pm s$	s_{rel} (%)
Intra sphere	3.28 ± 0.03	1.0	47.3 ± 0.2	0.3	7.16 ± 0.04	0.6
Inter sphere	3.28 ± 0.07	2.1	47.5 ± 0.4	0.7	7.0 ± 0.1	1.8

for real-time monitoring of most biological processes. As a consequnce of the small contact area between sphere and wall, the analyte exchange at the sensing spot is rapid and the diffusion distance is reduced to the thickness of the sensor coating. Finally, the signal is enhanced by doubling the optical path length and yield of luminescence light by the reflective surface of the stainless steel spheres.

To further characterize the applicability of such sensors, we tested the variability of the analyte signal by repeated release and collection cycles of a single sensor-sphere ("intra-sphere"). In addition, the signal of different spheres was compared ("inter-sphere"). The summarized data can be seen in 7.1. The intra-sphere variation of τ_0/τ_{air} of an oxygen sensitive MagSeMac given as the relative standard deviation of 15 measurements was 1 % which equals 3 hPa error in oxygen determination. The inter-sphere variation at air saturation was 2.1 % (6.3 hPa). Variations of τ_0 were below 1 % in both cases. These results suggested that a one-point calibration at air saturation is sufficient for each sphere and that no recalibration is required whenever the same sphere is released and trapped again. MagSeMacs sensitive to pH also showed little variation in both intra- and inter-sphere measurements (0.04 and 0.1 pH units, respectively).

Due to the intrinsic or self-referenced detection principle, the analyte signal was not affected by slightly inhomogeneous coatings. The variable thickness among different spheres ($8 \pm 2\,\mu$m) resulted in a varying signal intensity ($I = 40 \pm 20$ mV), whereas the values for τ_0/τ_{air} changed only marginally (Table 7.1).

Bioprocess-monitoring applications usually require sterile sensor spheres. Polystyrene is unsuitable due to its low glass transition temperature of approximately 105 °C. Therefore, we produced MagSeMacs coated with polysulfone and $Ir(C_S)_2(acac)$ incorporated as oxygen sensor. The ratio τ_0/τ of such sensors did not change significantly upon autoclaving, i.e. less than the intra-sphere variability. The decreased sensitivity ($\tau_0/\tau_{air} = 1.37$ compared to 1.62 for $Ir(C_S)_2(acac)$ in PS) might be overcome by using PtTPTBP as oxygen indicator. Another potential problem of using MagSeMacs for bioprocess-monitoring are strong magnetic field gradients in close proximity to the sphere. Such fields might capture the sensor irreversibly. Moreover, moving MagSeMacs might damage fragile adherent cells.

MagSeMacs with a pH sensing capability were accomplished with a dual lifetime referencing (DLR) system.[277] We incorporated $HPTS(DHA)_3$ as pH-sensitive component and $Ir(C_S)_2(acac)$ as reference dye in a polyurethane hydrogel matrix. To avoid oxygen cross-sensitivity of the reference dye, we incorporated the dye in virtually gas-impermeable PViCl-PAN nanoparticles.[180] The emission spectra of the reference dye and the pH-indicator in its basic form match perfectly (Supporting Information Figure 7.7 on page 126), which is a prerequisite for DLR.[277] The calibration curve (7.4c) shows an apparent pKa-value of 8.0, a typical value for sensors applied in marine biology but also suitable under

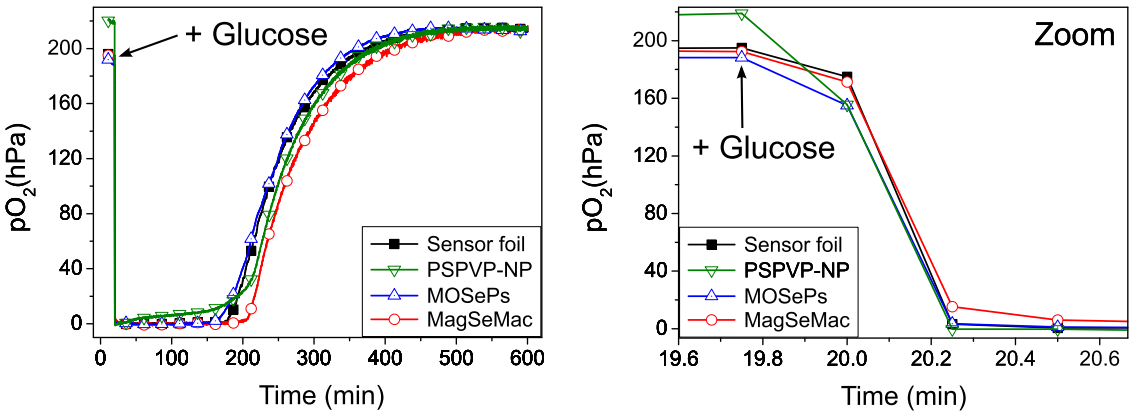

Figure 7.5: Dissolved oxygen concentration monitored by a sensor foil, a dispersed optical nano sensor (PSPVP-NP), magnetic, optical sensor particles (MOSePs) and MagSeMacs. The addition of 5 µmol glucose to the solution containing 25 U*mL^{-1} GOx was followed by a steep drop in oxygenation. After all glucose was consumed, the medium was slowly reoxygenated. The right plot represents a zoom into the time frame in which the glucose was added to the solution. All tested sensors equilibrated within two data points.

physiological conditions (pH 7.4). The pKa value is in good agreement with the results reported previously.[274] Such a high apparent pKa value for the sulfonamide derivative results from the localization of the indicator in apolar regions of the hydrogel. The formation of charged species upon dissociation of the hydroxyl group is not favored in such an environment. As a consequence, the pKa value increases significantly compared to the aqueous solution (pKa = 5.6 for 8-hydroxypyrene 1,3,6-trisdimethylsulfonamide)[278] and more polar materials such as poly(vinylpyrrolidone) (pKa = 6.9).[274] The response time (t_{90} = 32 s, 7.4d) was significantly higher than the one for oxygen-MagSeMacs, but still in an acceptable range for most biological systems.

Finally, we evaluated MagSeMacs for oxygen monitoring in a commercial SensorDish-Reader suitable for simultaneous monitoring in standard 24-well microplates (see Figure 7.11 on page 130e in the Supporting Information). To compare the performance of MagSeMacs with other sensor systems, we measured the oxygen level in a solution of glucose oxidase upon addition of glucose with four different systems: a fixed sensor patch, a dispersion of dye doped PSPVP nanoparticles,[228] spray-dried MOSePs[14] and the here presented MagSeMacs. For all sensors, the Ir-coumarin dye was chosen as an oxygen indicator due to the spectral compatibility with the SensorDish-reader. All sensors reflected the steep drop in oxygen concentration upon mixing and the slow reoxygenation (7.5).

7.4 Conclusion

Magnetic sensor macrospheres (MagSeMacs) were prepared for monitoring analyte concentrations in both solution and gas phase. Sphere sizes in the milimeter range ensure strong and rapid magnetic retention of MagSeMacs. This enables analyte monitoring in stirred

liquids, rotating and shaking vessels and along gradients in plug-flow reactors. The size of the spheres also allows to retract the sensor from the medium without a contamination of the sample. Sensor chemistry and readout equipment of sensor patches can be used for MagSeMacs without major modifications.

In summary, we successfully extended the concept of magnetically guided, optical sensors[2,136] to millimeter sized, highly ferromagnetic sensor spheres. Such MagSeMacs are suitable as versatile remote-controlled sensors and as exchangeable sensor caps for dip-probes.

Acknowledgement

The authors thank PreSens GmbH, Germany, for generously providing the SensorDish-Reader device and pH-Mini phase fluorimeter used in this work, and the FELMI-ZFE Graz for providing the equipment for acquiring the scanning electron micrographs.

Supporting information

Structures and spectra of the used dyes, surface images of MagSeMacs and a discussion on potential applications of MagSeMacs (including schematic drawings and movies) can be found in the Supporting Information.

7.A ESI for the manuscript: Magnetically remote-controlled, optical sensor spheres for monitoring oxygen or pH

This chapter was published as *Supporting Information for the Technical Note* in

Analytical Chemistry, 2010, 82, 2124-2128

doi: 10.1021/ac902393u

Authors: Günter Mistlberger*, Klaus Koren, Sergey M. Borisov and Ingo Klimant

7.A.1 Spectra and structures of the dyes

Chemical structures, emission and excitation spectra of iridium(III) acetylacetonato-bis(3-(benzothiazol-2-yl)-7-(diethylamino)-coumarin) ($Ir(C_S)_2(acac)$), 1-hydroxypyrene-3,6,8-*tris*-*bis*(2-ethylhexyl)sulfonamide ($HPTS(DHA)_3$) and palladium(II) *meso*-tetraphenyltetrabenzoporphyrin (PtTPTBP).

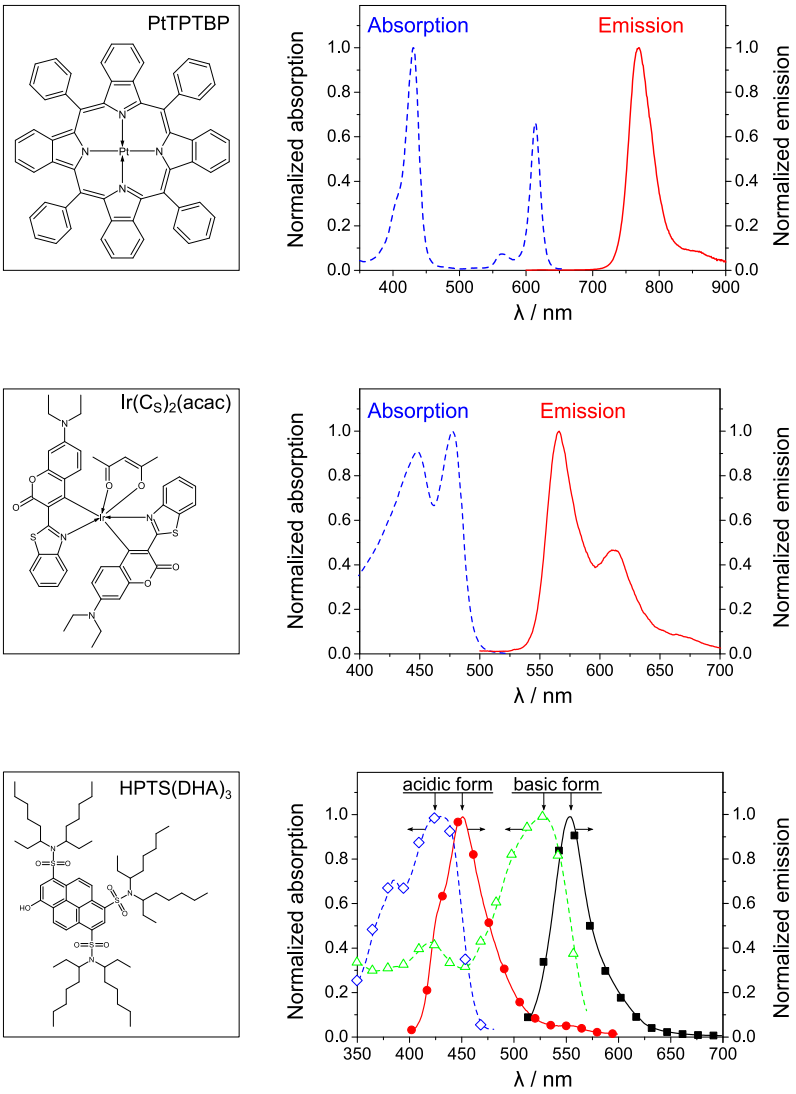

Figure 7.6: Chemical structures and spectral properties of the oxygen sensitive dyes PtTPTBP and $Ir(C_S)_2(acac)$, and the pH-indicator $HPTS(DHA)_3$.

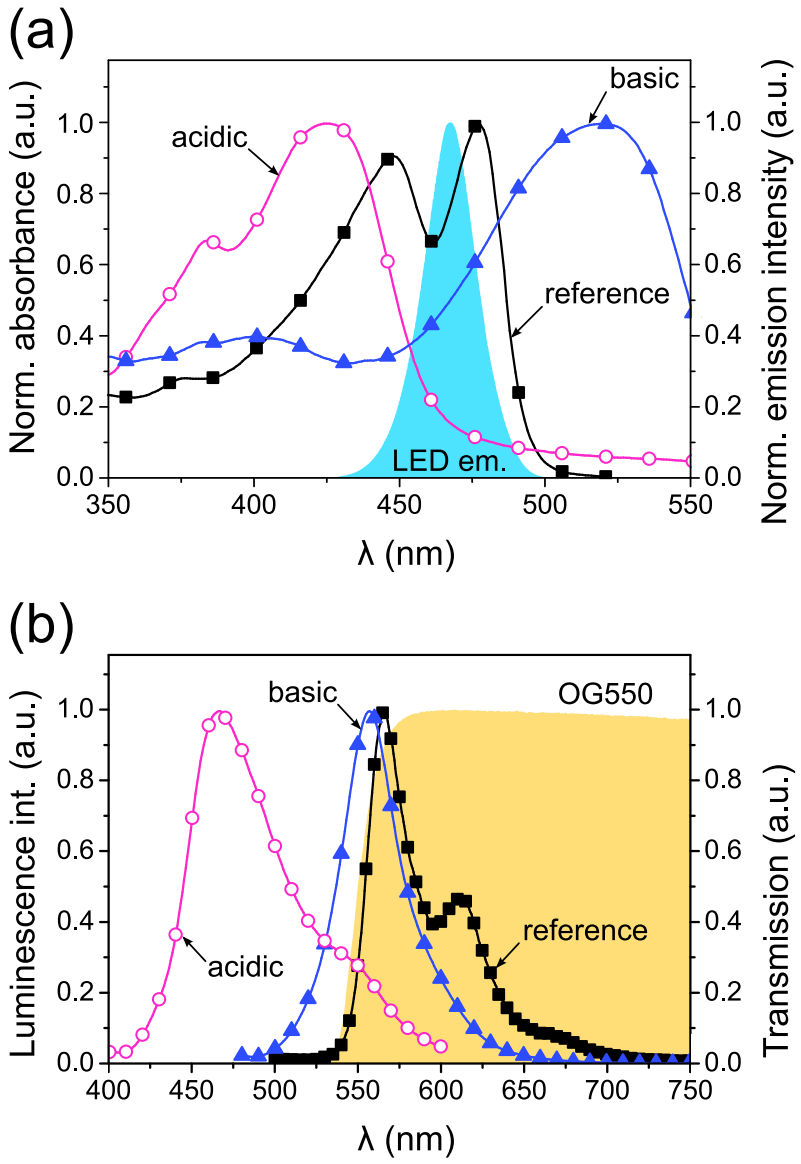

Figure 7.7: (a) Normalized absorption spectra of the acidic and basic form of the pH-indicator, the reference dye ($Ir(C_S)_2(acac)$) and the emission spectrum of the excitation light, a blue LED. (b) Normalized luminescence emission spectra of the pH-indicator (acidic and basic form) and the reference dye plotted together with the transmission spectrum of the OG550 filter. Only the basic form of $HPTS(DHA)_3$ and the reference dye are efficiently excited and detected by the system, while the acidic form does not contribute to the resulting signal. Therefore, the ratio between acidic and basic form can be detected by the combined apparent phase shift of $HPTS(DHA)_3$ (fluorescent, $\phi = 0$) and $Ir(C_S)_2(acac)$ (phosphorescent, $\phi \neq 0$).

7.A.2 Spray-coating of sensor spheres

During the spray-coating procedure, the spheres are continuously shaken to avoid the sticking of the spheres to the dish or to each other.

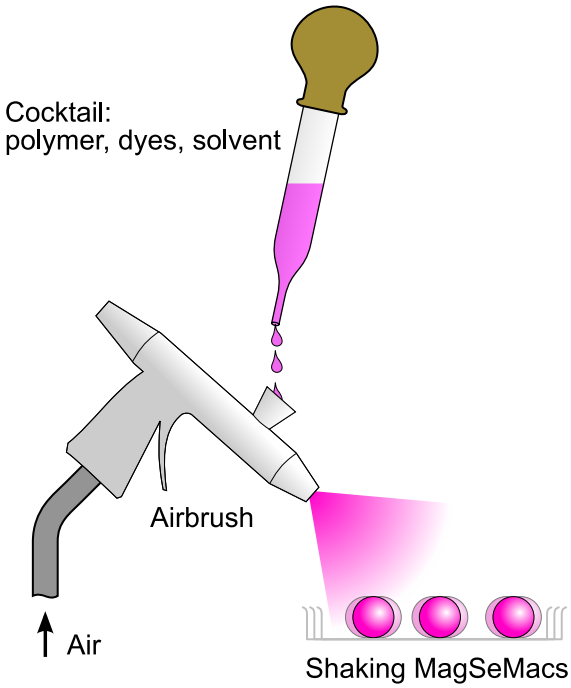

Figure 7.8: The coating of the steel spheres was carried out with a conventional airbrush. During the coating, the spheres were vigorously shaken.

The luminescence image of MagSeMacs coated with PS and $Ir(C_S)_2(acac)$ shows some inhomogeneities (Figure 7.9a). The surface structure of the layers differs depending on the cocktail composition (Figure 7.9c-d).

7.A.3 Modes of operation

A MagSeMac can either be directly mounted to an optical fiber tip, or its position can be remote-controlled through a transparent wall of e.g. a reaction vessel. The remote-controlling of a MagSeMac allows the continuous readout of the analyte concentration at multiple positions with a single sensor. In contrary, a MagSeMac fixed to an optical fiber dip-probe can be moved to any position which is accessible to the fiber and the separator. Separators with barriers to avoid an accidental sweeping of the MagSeMac from the separator are shown in Figure 7.10a-d. These separators protect the MagSeMac and ensure fast analyte exchange close to the MagSeMac.

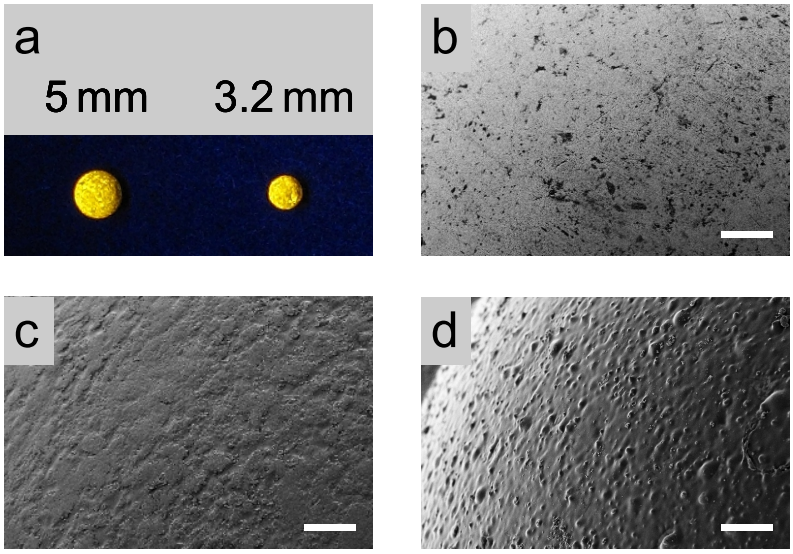

Figure 7.9: (a) Luminescence image of oxygen sensitive MagSeMacs. SEM surface images of an uncoated sphere (b), a PS-coated, oxygen-sensitive sphere (c) and a hydrogel-coated, pH-sensitive sphere (d). The scale bars in all electron micrographs are 100 µm.

7.A.4 Magnetic fixation of sensors for dip-probes

7.A.5 Applications

Potential applications of MagSeMacs are depicted in Figure 7.11. The mobility of the magnetic spheres allows monitoring of analyte gradients in stirred flasks (a) or plug-flow reactors (c). Due to the strong magnetic retention of the sphere, it is also possible to follow analyte levels in shaking (d) or rotating flasks (b) (Movie ac902393u_si_002.avi). In case of a dip-probe, the MagSeMac is magnetically fixed at the optical fiber tip with a modified magnetic separator (Figure 7.10b-d). The probe is applied as conventional dip-probe (f). After usage, the MagSeMac can be replaced by a new sphere.

Even the application in magnetically stirred solutions was possible. The difference in magnetic field strength between the separator and the magnetic stirring bar was high enough to allow trapping of the sphere separately from the stirring bar. In case the MagSeMac stuck to the stirring bar, shortly increasing the steering speed disrupted the weak attraction between the bar and the sphere. However, this happened rarely.

Finally, we modified a SensorDish-Reader for 24-well culture plates with magnets in order to capture the magnetic sphere in front of the optical readout-unit. The thin layer of magnets focused the magnetic spheres reliably in front of the optical read-out unit. In this experiment, the MagSeMacs performed similarly to the other tested systems. However, they were the most convenient sensors to work with. A dosing device for MagSeMacs can be seen as a schematic drawing (Figure 7.12) and in a short movie (Movie ac902393u_si_003.avi). After the measurement, the spheres were either magnetically retained in the plate for a washing step or withdrawn from the medium by a magnet.

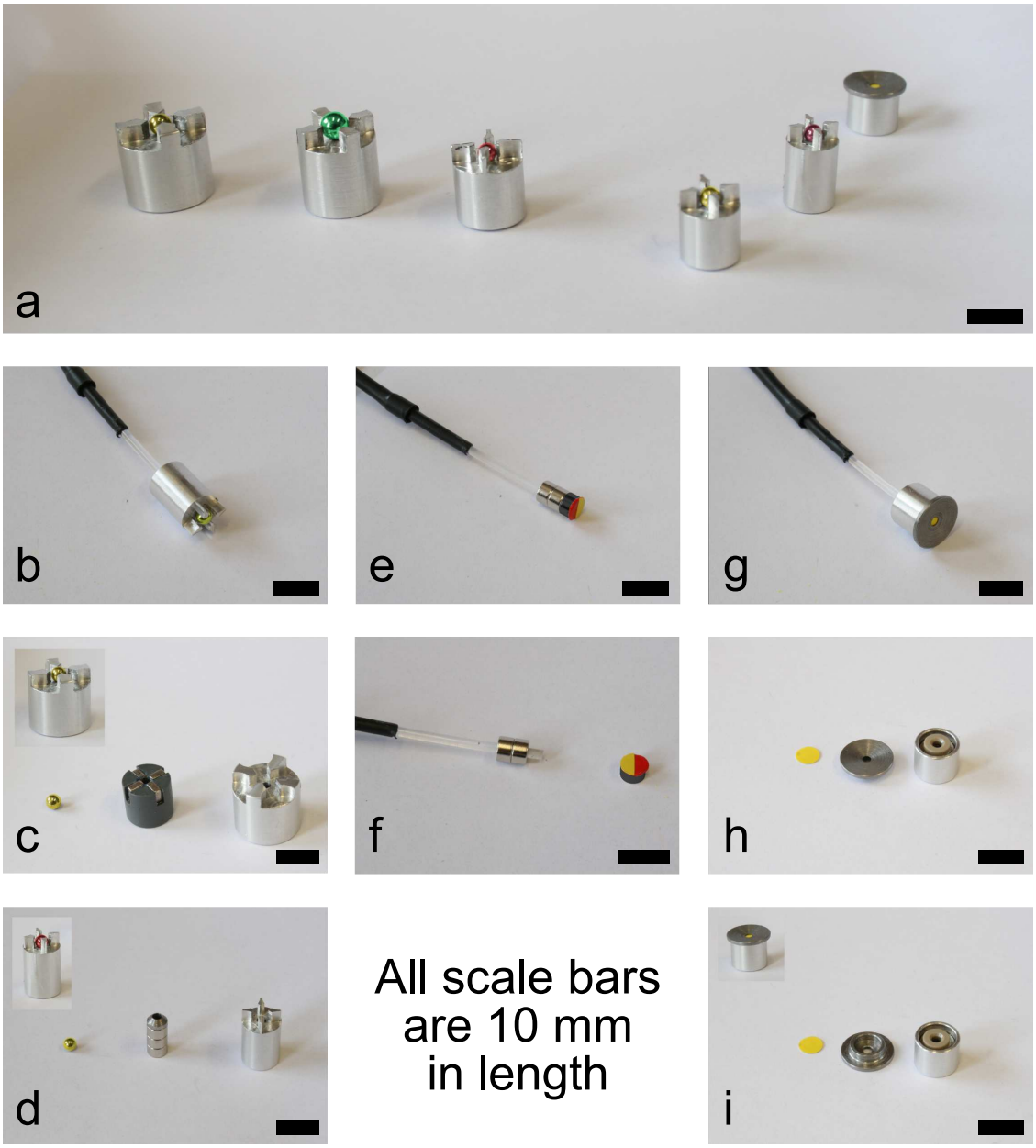

Figure 7.10: Magnetic separators for fixing a MagSeMac in front of an optical fiber tip. In (b-d) a separator for a MagSeMac is shown with its barriers protecting the spherical sensor. Figures (e-f) show a conventional sensor patch glued to an iron ring which can then be magnetically fixed to magnetic rings to form a dip-probe. Finally, it is possible to use a plain sensor patch with the magnetic cap shown in Figures (g-i). Here, the circular sensor foil is clamped between magnetic rings around the fiber and a steel cap.

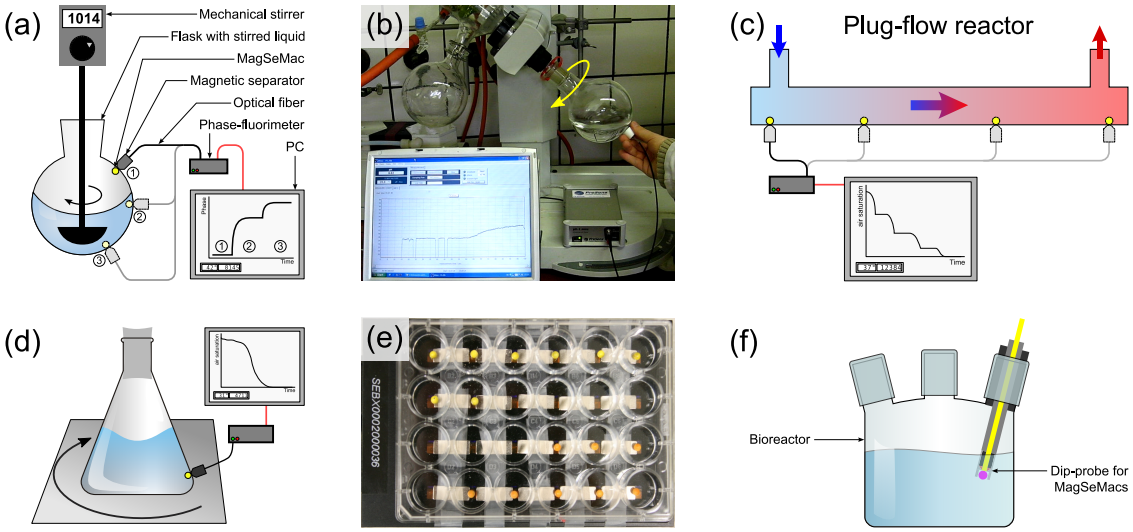

Figure 7.11: Applications of MagSeMacs. Due to the unique properties they can be utilized for process monitoring in (a) stirred flasks, (b) rotating flasks, (c) plug-flow reactors, (d) shake flasks, (e) multi-well plates, or even as exchangeable sensor caps for dip-probes (f).

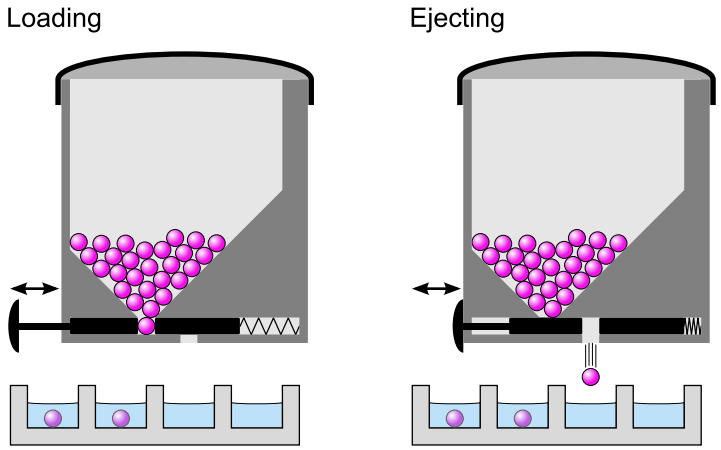

Figure 7.12: Schematic representation of a dosing device for MagSeMacs. Each time the button is pushed, a sphere from the reservoir is ejected.

8 Multifunctional magnetic optical sensor particles with tunable sizes for monitoring metabolic parameters and as basis for nanotherapeutics

This chapter was published as *Full Paper* in

Advanced Functional Materials, 2010, in Press

doi: 10.1002/adfm.201000321

Authors: Günter Mistlberger*, Klaus Koren, Elisabth Scheucher, Daniel Aigner, Sergey M. Borisov, Armin Zankel, Peter Pölt, and Ingo Klimant

Abstract Magnetic optical sensor particles with multifunctional cores and shells are synthesized via a facile nano-precipitation method and the subsequent modification of the particle-shell. The hydrophobic particle core includes optical oxygen indicators, a light harvesting system, photosensitizers and magnetic nanoparticles. Further functionalities are introduced by modifying the shell with enzymes, antibodies, multiple layers of polyelectrolytes, stimuli responsive polymers and luminescent indicator dyes. The hydrodynamic diameter is tunable by varying different precipitation parameters.

8.1 Introduction

Real-time monitoring and imaging of physiologically important parameters in biological samples is of high interest in both bioengineering and life science.[279–283] Optical sensor particles represent a convenient tool for real-time monitoring of these parameters. Recently, the concept of optical sensor particles was enhanced by the incorporation of magnetic nanoparticles. This enables the operator to trap the sensors at a distinct spot and to guide them to a desired position within the measurement setup.[2,13,101] Thereby, the signal intensity is increased and optical interferences with the medium are reduced. Furthermore, it was shown that a particle "swarm" follows a moving magnetic separator faster than single particles and that less sensor particles were required to achieve the signal intensity of dispersed sensor particles.[13,14,136]

A large number of laboratories is nowadays working on the development of multifunctional particles as nanotherapeutics and imaging components. Most of these particles respond to stimuli such as changes in pH, temperature, light, magnetic field, etc.[284–286] They might also be loaded with optical labeling components, such as quantum dots for imaging purposes.[41,84,116,126,287,288] Another common modification is the introduction of magnetic nanoparticles for purposes, such as magnetic guiding, enrichment, thermotherapy by AC magnetic fields and the particles' use as MRI-contrast agent.[77,289,290] While optical sensor particles can be utilized for monitoring changes in oxygenation, pH, temperature, ion concentrations and ammonia,[224,228,229,291–298] multifunctional nanoparticles were reported as tools for drug delivery, biosensors, cancer thermotherapy, magnetic drug targeting and magnetically induced thermal drug release.[6,8,83,290,299–301] Obviously, a smart combination of both principles (optical sensing and the use of multifunctional polymeric nanoparticles) would lead to novel tools for research and life science.

Here, we present a facile route to multifunctional magnetic optical sensor particles (MF-MOSePs) with tunable hydrodynamic diameters between 50 and 180 nm. The particle cores were equipped with oxygen indicators (in visible and NIR-range), magnetic nanoparticles and a photosensitizer. Furthermore, we modified the surface of MOSePs with an enzyme, polyelectrolytes, a pH-indicator and a stimuli responsive polymer. Such a nanodevice can, for example, carry and enzyme its surface and monitor the enzymatic reaction with the help of an incorporated optical sensor.

Different applications require different particle sizes. Whenever the position of particles has to be magnetically controllable in a reasonable time, particles with sizes above 100 nm are preferable. On the contrary, smaller magnetic nanoparticles (< 60 nm) might enable diagnostic and therapeutic applications (MRI imaging, thermotherapy, temperature induced drug release, etc).

8.2 Results and discussion

8.2.1 Synthesis and particle structure

The synthetic route to the MF-MOSePs is outlined in Figure 8.1 and relies on an emulsifier-free nano-precipitation method.[180,295,302–304] After dissolving the polymer (poly(styrene-co-maleic anhydride), PSMA) and an indicator dye in tetrahydrofuran (THF), lipophilic magnetic nanoparticles (L-MNPs) were dispersed in the "cocktail". Upon the addition of water, which is miscible with THF but not a solvent and dispersant for the polymer and the magnetic nanoparticles, respectively, spherical particles formed spontaneously. The unique properties of THF (solvent and dispersant for the "cocktail" components and miscibility with the precipitant) were crucial for the success of this synthetic route. The polarity of other tested solvents was either too high to obtain a homogeneous dispersion of the L-MNP (acetone, dimethylformamide) or too low to allow water miscibility (chloroform, toluene). Notably, no surfactants are used in the process and, consequently, no additional cleaning steps are required to remove emulsifiers that would influence biological systems. After the precipitation, the solvent was evaporated and the particles shrank to their final size. In Figure 8.2a the spherical shape of MOSePs is shown. During the precipitation process, the L-MNPs were irreversibly trapped inside the polymeric matrix (Figure 8.2b).

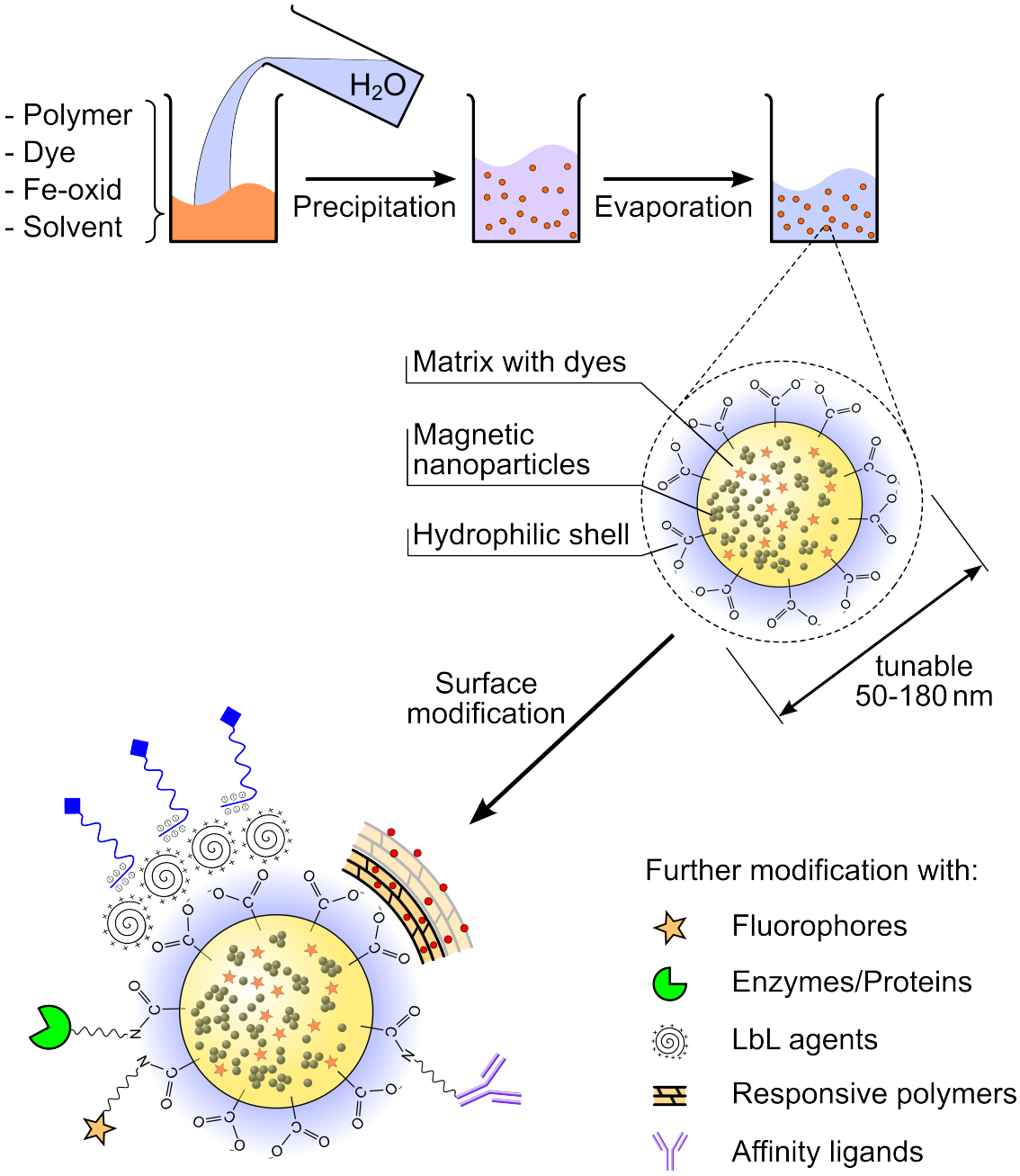

Figure 8.1: Synthetic route to multifunctional magnetic optical sensor particles (MF-MOSePs) via a nano precipitation technique. After particle formation the surface was modified with fluorophores, enzymes, layer-by-layer agents or stimuli responsive polymers.

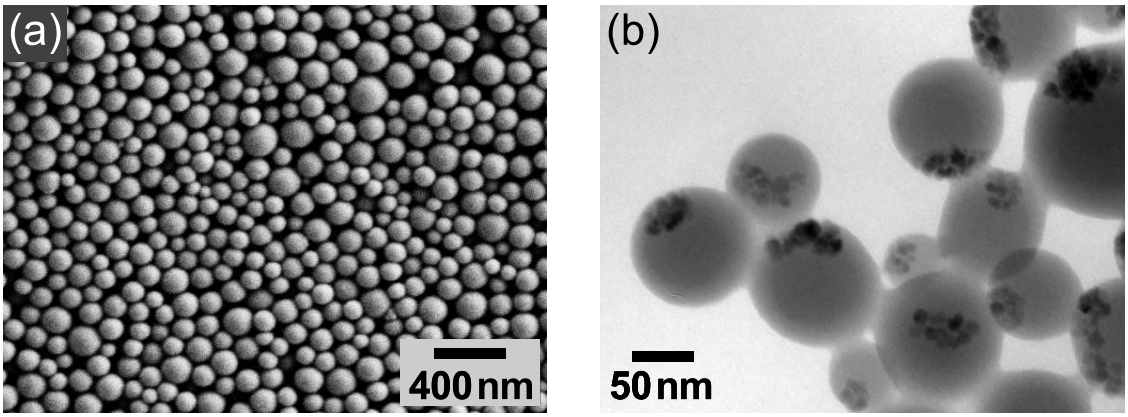

Figure 8.2: (a) SEM image of MOSePs (2 % PSMA93, 20 % magnetite, z-average = 185 nm). (b) TEM image of the core MOSePs used for the layer-by-layer experiment (0.5 % EF-80, 20 % magnetite).

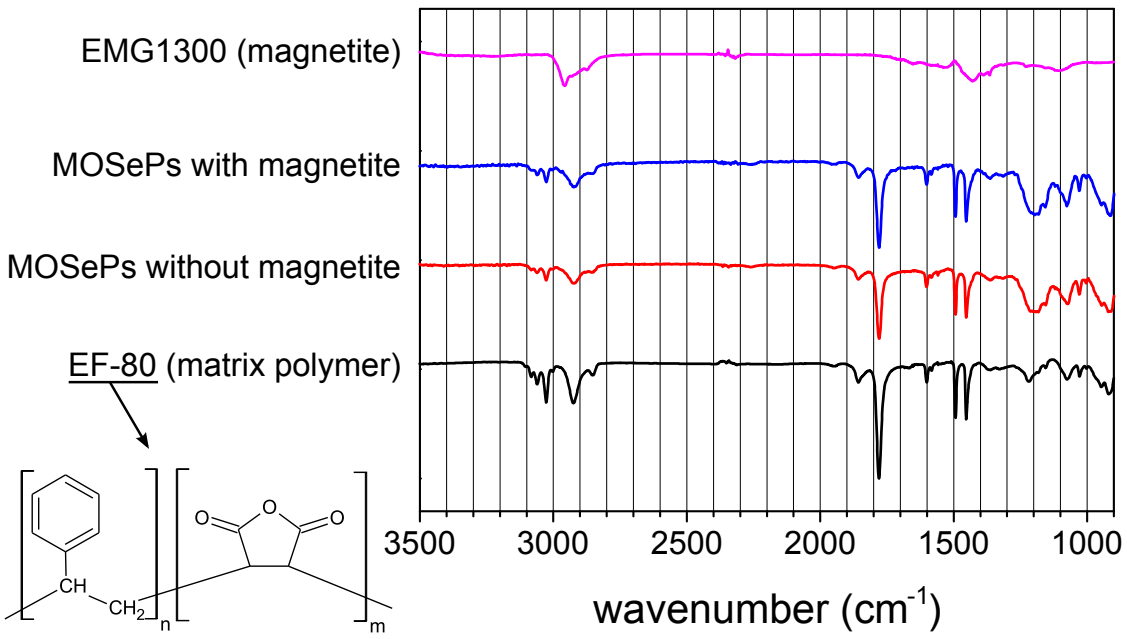

Figure 8.3: IR-spectra of the magnetic nanoparticles (EMG1300), MOSePs with magnetite, MOSePs without magnetite and the matrix polymer EF-80 (chemical structure in bottom left corner). No hydrolyzed anhydride groups can be seen in the MOSePs' spectra. This confirms the low 5-aminofluorescein binding rate (2.2 µmol g^{-1} particles).

During precipitation, anhydride groups on the surface react with water and form carboxyl groups. This results in a negative zeta potential of -35 mV at pH > 5 and ensures highly stable dispersions of MOSePs in aqueous media. In contrast, acidifying a particle dispersion resulted in spontaneous aggregation and sedimentation of the particles. Binding 5-aminofluorescein to the surface via a zerolength crosslinking method[305] with 1-ethyl-3-[3-dimethylaminopropyl]carbodiimide hydrochloride (EDC) elucidated a ratio of 2.0 ± 0.5 bound fluorescein molecules per 1000 maleic anhydride (MA) molecules or 2.2±0.5 µmol per gram particles. This means that an average of ≈10,000 fluorescein molecules is bound to a 250 nm particle (the z-average of the modified batch). The applied assay returns the number of accessible carboxyl groups, which is more relevant for covalent surface modifications than the total number of hydrolyzed anhydrides. FT-IR-spectra confirmed the low total carboxy-concentration in the particles (Figure 8.3). The unmodified matrix polymer EF-80 showed characteristic signals at 2925 cm^{-1} and a double peak at 1453 and 1493 cm^{-1} for the aromatic vibrations of the styrene. At 1780 cm^{-1} the typical signal for the carbonyl bond of the anhydride group can be found.[306] The broad OH-peak at 3000 cm^{-1} for a hydrolyzed anhydride group is missing in both MOSeP-samples, with and without L-MNP included. Furthermore, a shift of the carbonyl peak would be expected during hydrolysis.

While a hydrophilic surface ensures highly stable aqueous dispersions, the particle core needs to be hydrophobic in order to retain the apolar components inside the matrix. Both the dye and the L-MNPs are trapped via hydrophobic interactions in the polymer. A polar matrix would result in rapid leaching of the dye and the magnetic particles out of the core into the medium. Because of the amphiphilic character of the matrix polymer in MOSePs no leaching of the dye or the magnetic particles was observed over a period of several months.

8.2.2 Precipitation parameters influencing the particle sizes

Fine-tuning of the particle sizes by varying different precipitation parameters enables the control of certain size-dependent properties, such as separation speed, sensor response and dispersion stability.

Particularly, the polymer concentration was found to be a critical parameter for adjusting the particle size as can be seen in Figure 8.4a. The values of z-average measured through dynamic light scattering of four consecutive precipitations under the same conditions resulted in a relative standard deviation below 2 % and an average polydispersity index (PDI) of 0.04. The highest concentration of PSMA93 was above the limit for efficient particle production with this method.

The employed polymer type had an effect on both the size of the particles and the upper limit of polymer concentration. The two polymers, EF-80 and PSMA93, differ in the average molecular weight and their MA content, which influences the polarity of the matrix. EF-80, the polymer with shorter chains (Mw = 14,400 vs. 224,000 g mol^{-1} of PSMA93) and higher MA content (11 % vs. 7 % w/w of PSMA93), resulted in particles which were approximately 30 nm smaller over the whole range of tested concentrations (Figure 8.4a, Table 8.1). The lower the molecular weight the lower was the viscosity of the cocktail and this favored the formation of smaller particles. Also the higher polymer

Table 8.1: Overview of various precipitation parameters and resulting values for z-average and PDI. The polymer concentration (w_P) is given in w/w solvent. Concentrations of additives such as magnetite (w_M) and dyes are presented in w/w polymer.

Sample	w_P [%]	w_M [%]	Polymer	Dir.	Vortex [min^{-1}]	Flowrate [$mL\,s^{-1}$]	Precip.	z-av (±s) [nm]	PDI (±s)
CE1	0.2	20	EF-80	CiP	1200	0.5	H_2O	71.5 (±1.2)	0.045 (±0.019)
CE2	0.4	20	EF-80	CiP	1200	0.5	H_2O	90.1 (±1.6)	0.027 (±0.007)
CE3	0.6	20	EF-80	CiP	1200	0.5	H_2O	108.5 (±1.6)	0.029 (±0.009)
CE4	0.8	20	EF-80	CiP	1200	0.5	H_2O	123.0 (±0.8)	0.040 (±0.013)
CE5	0.0	20	EF-80	CiP	1200	0.5	H_2O	134.0 (±0.5)	0.039 (±0.005)
CE6	1.2	20	EF-80	CiP	1200	0.5	H_2O	147.2 (±0.5)	0.076 (±0.005)
CP1	0.2	20	PSMA93	CiP	1200	0.5	H_2O	105.4 (±1.0)	0.022 (±0.006)
CP2	0.4	20	PSMA93	CiP	1200	0.5	H_2O	121.5 (±1.2)	0.035 (±0.007)
CP3	0.6	20	PSMA93	CiP	1200	0.5	H_2O	134.8 (±1.2)	0.035 (±0.011)
CP4	0.8	20	PSMA93	CiP	1200	0.5	H_2O	146.2 (±0.9)	0.059 (±0.012)
CP5	1.0	20	PSMA93	CiP	1200	0.5	H_2O	162.9 (±1.9)	0.079 (±0.002)
CP6	1.2	20	PSMA93	CiP	1200	0.5	H_2O	180.0 (±4.2)	0.198 (±0.058)
PP	0.6	20	PSMA93	CiP	1200	0.5	H_2O	132.2 (±1.7)	0.072 (±0.012)
PE	0.6	20	EF-80	CiP	1200	0.5	H_2O	115.6 (±2.3)	0.068 (±0.007)
M1	0.6	0	EF-80	CiP	1200	0.5	H_2O	135.6 (±1.9)	0.049 (±0.006)
M2	0.6	5	EF-80	CiP	1200	0.5	H_2O	132.9 (±3.7)	0.037 (±0.006)
M3	0.6	10	EF-80	CiP	1200	0.5	H_2O	123.7 (±1.9)	0.051 (±0.014)
M4	0.6	20	EF-80	CiP	1200	0.5	H_2O	115.4 (±0.8)	0.044 (±0.011)
M5	0.6	30	EF-80	CiP	1200	0.5	H_2O	110.1 (±1.4)	0.042 (±0.020)
D1	0.6	20	EF-80	CiP	1200	0.04	H_2O	132.9 (±1.0)	0.050 (±0.025)
D2	0.6	20	EF-80	CiP	1200	0.5	H_2O	126.6 (±1.9)	0.046 (±0.024)
D3	0.6	20	EF-80	CiP	1200	2.0	H_2O	110.3 (±2.1)	0.076 (±0.007)
V1	0.6	20	EF-80	CiP	600	0.5	H_2O	120.2 (±2.5)	0.034 (±0.024)
V2	0.6	20	EF-80	CiP	1200	0.5	H_2O	116.8 (±1.5)	0.040 (±0.007)
V3	0.6	20	EF-80	CiP	1800	0.5	H_2O	118.3 (±2.5)	0.063 (±0.025)
PD1	0.6	20	EF-80	CiP	1200	0.5	H_2O	113.9 (±1.6)	0.052 (±0.015)
PD2	0.6	20	EF-80	PiC	1200	0.5	H_2O	135.0 (±2.5)	0.029 (±0.023)
PR1	0.6	20	EF-80	CiP	1200	0.5	H_2O	115.4 (±0.8)	0.044 (±0.011)
PR2	0.6	20	EF-80	CiP	1200	0.5	MeOH	99.6 (±5.8)	0.027 (±0.009)
PR3	0.6	20	EF-80	CiP	1200	0.5	EtOH	74.9 (±3.9)	0.028 (±0.015)
PDT[a]	2.0	20	PSMA93	PiC	1200	0.5	H_2O	171.1 (±1.2)	0.089 (±0.012)
GOX	1.0	20	PSMA93	CiP	1200	0.5	H_2O	186.0 (±1.7)	0.029 (±0.024)
FLU[b]	0.6	0	EF-80	CiP	—	0.5	H_2O	256.8 (±4.8)	0.274 (±0.063)
SR	0.5	20	EF-80	CiP	1200	0.5	H_2O	100.5 (±0.5)	0.021 (±0.004)
LBL	0.5	20	EF-80	CiP	1200	0.5	H_2O	105.9 (±0.6)	0.077 (±0.012)
SEM	2.0	20	PSMA93	PiC	600	0.5	H_2O	185.4 (±3.6)	0.093 (±0.012)
IrC	1.0	20	PSMA93	CiP	1200	0.5	H_2O	186.0 (±1.7)	0.029 (±0.024)
PdBP	0.6	20	PSMA93	CiP	1200	0.5	H_2O	124.9 (±3.2)	0.100 (±0.024)
PtBP	0.6	20	PSMA93	CiP	1200	0.5	H_2O	110.3 (±2.1)	0.180 (±0.044)

[a] Includes 1 % (w/w polymer) PdTPTBP dye. Particles were filtered through a 0.8 μm syringe filter after precipitation.

[b] In this batch a total of 100 mL cocktail containing 1 % polymer was precipitated with 200 mL water without additional mixing. These undefined conditions resulted in large particles with a higher PDI. Considering the large amount of particles required for the binding experiments these properties were acceptable.

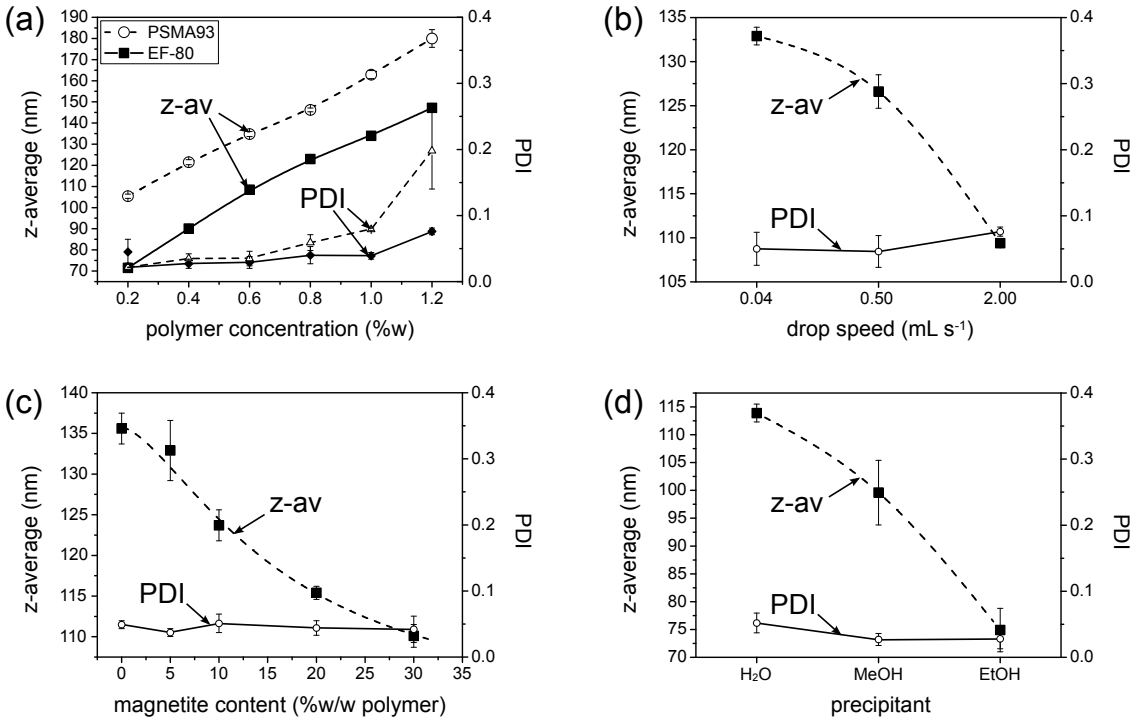

Figure 8.4: Influences of the polymer concentration and -type (a), drop speed (b), the magnetite content (c) and the precipitant (d) on the resulting hydrodynamic diameters. All PDIs, except for 1.2 % PSMA93, are below 0.1.

polarity might have contributed to the formation of smaller particles due to increased precipitant-polymer interactions. Size determination from electron microscopic images resulted in smaller values because the z-average resembles the hydrodynamic diameter of particles in an aqueous dispersion while the particles in the electron microscope were completely dry (Figure 8.5 on the next page and Figure 8.14 on page 152). Moreover, the z-average represents a statistic value that depends on both the particle volume and number. While high polymer concentrations increased the particle size and distribution width, a narrow size distribution was achieved at low polymer concentrations (Figure 8.5).

The effect of the precipitation direction, i.e. "cocktail into precipitant" (CiP) or "precipitant into cocktail" (PiC), can be seen in Figure 8.13 on page 151 in the Supporting Information. Adding the cocktail to the precipitant (CiP) ensures a fast solvent displacement and consequently, smaller particles are formed. In the opposite direction (PiC), the solvent concentration in the cocktail is decreasing slowly which gives the polymer cocktail more time to form particles with a lower surface/volume ratio. This effect can be explained by the decreased contact area between polymer and aqueous phase.

Another parameter influencing the particle size was the flow rate at which the cocktail was injected into the precipitant (Figure 8.4b and Figure 8.15 on page 153). Here, a higher flow rate ($2\,\mathrm{mL\,s^{-1}}$) decreased the particle sizes by 25 nm compared to the drop-wise addition of the cocktail ($0.04\,\mathrm{mL\,s^{-1}}$).

The effect of a varying magnetite concentration indicated the role of the L-MNPs in

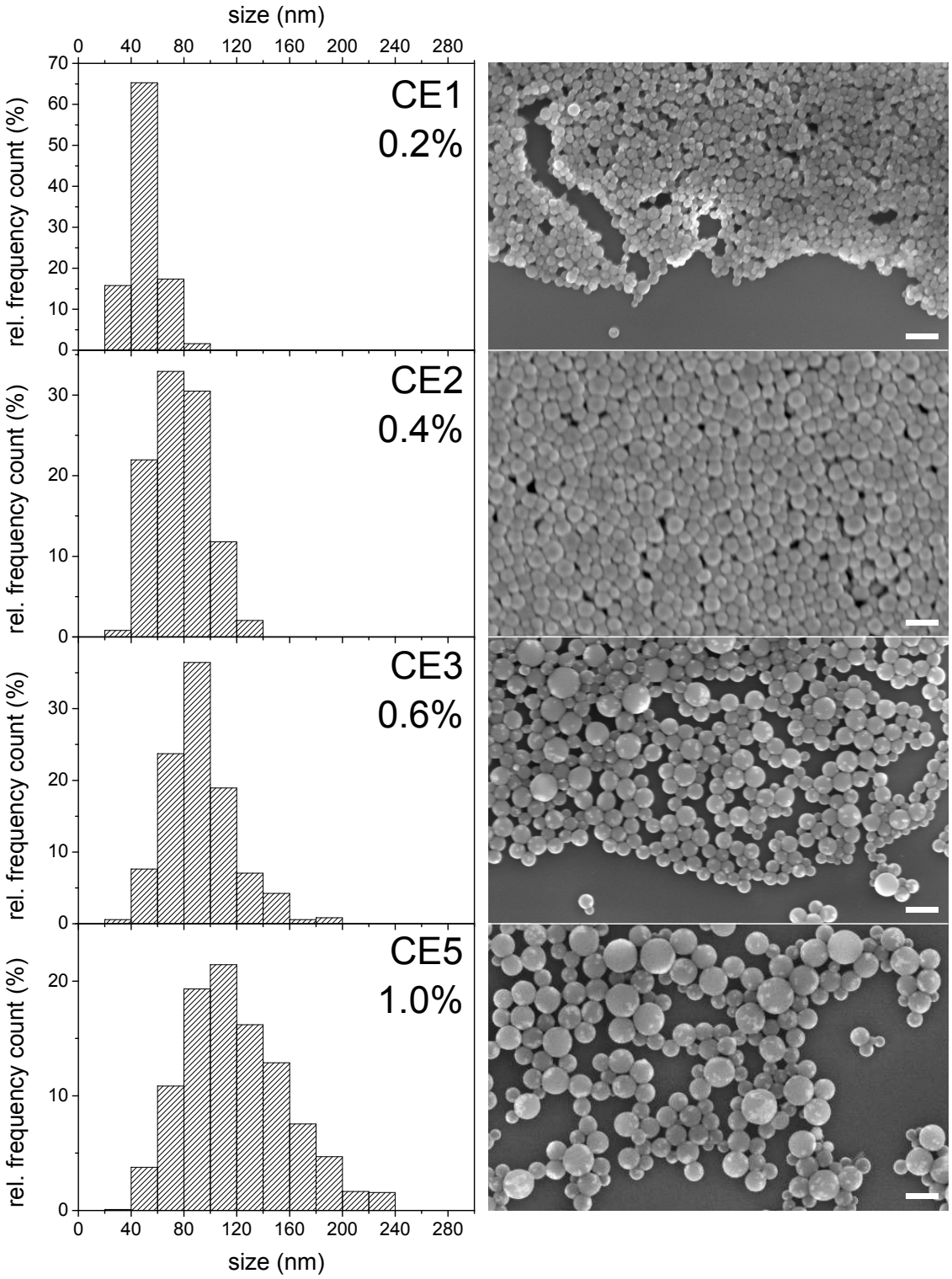

Figure 8.5: Size histograms from SEM images of EF-80 particles with varying polymer concentration in the cocktail (see Tab. 1). The scale bar is 200 nm in all images.

the particle formation process. Increasing the magnetite concentration from 0 to 30 % (w/w polymer) resulted in a stepwise reduction of the particles' z-average from 136 to 110 nm (Figure 8.4 on page 137c, Figure 8.16 on page 154 and Table 8.1). The TEM-image in Figure 8.2b also shows the inorganic particles close to the surface. The L-MNPs might act as seeds for the polymeric particles. The higher the magnetite concentration is, the more seeds are available and therefore the particle size decreases.

Finally, the particle size can be influenced by the polarity of the precipitant. We investigated the z-average of particles resulting from precipitations where the cocktail was injected into water, methanol and ethanol. Figure 8.4 on page 137d and Figure 8.17 on page 155 in the Supporting Information show a significant drop in particle size with decreasing precipitant polarity. However, a precipitation with n-propanol resulted in separated precipitation of the magnetic nanoparticles and the polymeric nanoparticles. Acetone did not act as precipitant and resulted in a clear, non-scattering dispersion of the L-MNPs in the polymer solution.

Changing the vortex speed from 600 to 1800 min^{-1} did not change the particle sizes significantly. Apparently, the mixing due to cocktail injection was sufficient for fast solvent displacement. Swelling of 110 nm EF-80 MOSePs in mixtures of THF and water resulted in a 7, 15, 20 and 26 % increase of particle diameter for 20, 30, 40 and 50 % (v/v) THF in water. The swelling was reversible and the particles returned to the original size after THF evaporation.

In conclusion, the particle sizes can be adjusted to fit the required properties within a certain range. This is necessary as different particle properties are required for different applications. Larger particles (> 100 nm) usually separate faster in a magnetic field but have higher polydispersity indices. Very small particles (< 60 nm) are difficult to separate from dispersion but have higher surface-to-volume ratios, ensure higher dispersion stability and might be suitable for in vivo applications such as thermotherapy, thermal drug release, magnetic particle tracking and MRI imaging.

8.2.3 Functionalities included in the particle core

Magnetism Magnetic nanoparticles included in the core make MOSePs magnetically controllable. The in situ production of a sensor spot, for instance, increases the signal intensity of optical sensor particles and the response speed to a changing magnetic field.[13] We used this technique for sensor characterization. MOSePs dispersed in a buffer solution were collected at the side-wall of the vessel by a magnetic separator with an optical window. An optical fiber pointed through the center of the separator directly onto the particle spot (Figure 8.6a). By this, the required amount of sensor particles is significantly reduced compared to a plain sensor dispersion.

The separation speed is a function of various factors, including particle size, magnetite content of the particles and volume of the dispersion from where the particles are separated. Fine-tuning of these parameters allows to set the priority to separation speed or dispersion stability. On the one hand, the hydrophilic surface ensures highly stable aqueous dispersions. On the other hand, if a fast separation is required, MOSePs (z-av = 192 nm, 20 % magnetite) were quantitatively separated from a 3 mL aqueous dispersion (5 $\mathrm{mg\,mL}^{-1}$) with the aid of a strong magnet within 30 min (Figure 8.6b). The separation

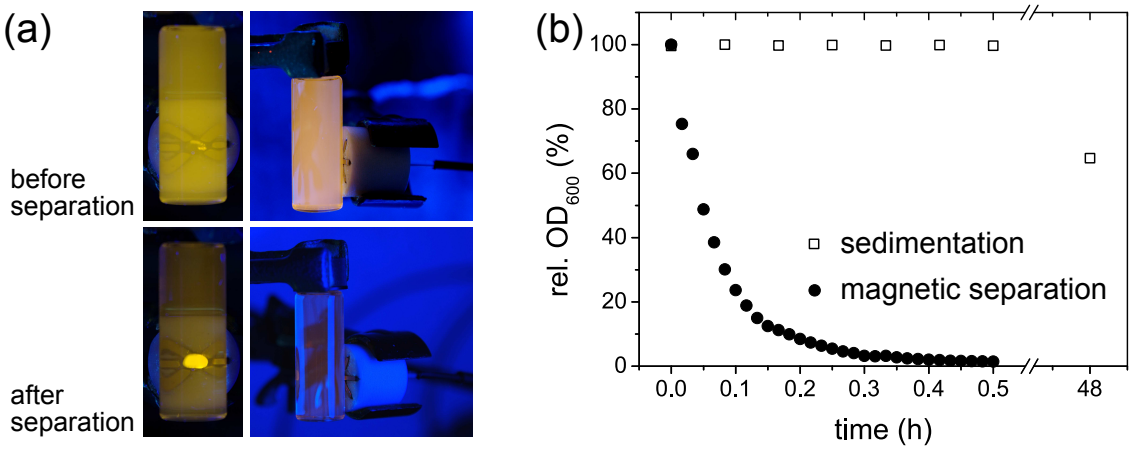

Figure 8.6: (a) Fluorescence image of MOSePs (0.6 % EF-80 in the cocktail, 20 % magnetite, 1 % $Ir(C_S)_2(acac)$, both w/w polymer, z-average = 105 nm) dispersed in water before and after being capture in front of an optical fiber with a specially designed magnetic separator. (b) Sedimentation and magnetic separation speed of MOSePs (2 % PSMA93 in the cocktail, 20 % magnetite w/w polymer, z-average = 192 nm) in an aqueous dispersion followed by measuring the optical density at 600 nm.

inside micro fluidic devices is certainly faster, because of the reduced volume and distances. The time required for separating MOSePs is significantly higher than for particles in the micrometer range[14] but acceptable for biological applications such as the investigation of the surface oxygenation of biofilms.

Besides magnetic guiding, the magnetic properties of MOSePs might enhance the contrast of MRI images and allow the thermal therapy of cancer via AC-magnetic fields.[206,289,300,307–315] The location of magnetic particles is also detectable inside biological tissues by using sensitive SQUID devices.[125] This multifunctionality of the magnetic nanoparticles enables the application of MOSePs with sizes below 60 nm, which would prohibit a separation in a reasonable time frame for conventional sensor applications.

Optical sensing To demonstrate the flexibility of this particular method for incorporating lipophilic indicator dyes into the core, we tested a range of different oxygen-sensitive indicator dyes. For the production of magnetically controllable optical sensor particles, we incorporated oxygen indicators such as iridium(III) acetylacetonato-bis(3-(benzothiazol-2-yl)-7-(diethylamino)-coumarin) ($Ir(C_S)_2(acac)$), palladium(II) and platinum(II) *meso*-tetra(4-fluorophenyl) tetrabenzoporphyrin (PdTPTBPF, PtTPTBPF) and palladium(II) meso-tetraphenyltetrabenzoporphyrin (PdTPTBP). While Ir(CS)2(acac) proved to be an ultra bright oxygen optode for the production of sensors with a high dynamic range (pO_2 = 0-1000 hPa),[14,198] the benzoporphyrin dyes PtTPTBPF, PdTPTBP and PdTPTBPF efficiently absorb red light and emit in the NIR-range. This is especially useful for biological applications because of the increased penetration depth and reduced background due to scattering and autofluorescence.

Fitting the Stern-Volmer plot of $Ir(C_S)_2(acac)$ stained MOSePs ("IrC", Table 8.1) with

the simplified two-site model (Equation 2),[223,230] where one part of the dye is assumed to be unquenchable, i.e. its K_{SV2} =0 hPa^{-1}, resulted in a K_{SV1} =0.0038 hPa^{-1} with a quenchable fraction of $P = 0.94$ (Figure 8.7a).

$$\frac{\tau}{\tau_0} = \frac{P}{1 + K_{SV1} * pO_2} + \frac{1 - P}{1 + K_{SV2} * pO_2} \tag{8.1}$$

$$K_{SV2} = 0 \Longrightarrow \frac{\tau}{\tau_0} = \frac{P}{1 + K_{SV1} * pO_2} + 1 - P \tag{8.2}$$

The almost linear correlation between τ_0/τ vs. pO_2 is useful for practical applications (calibration, dynamic range). High signal intensities are important for oxygen imaging with thin particle layers and small sensor spots, respectively. Moreover, the high brightness of the incorporated dye overcomes the problem of the highly light absorbing L-MNPs. In the case of weak fluorescent dyes and excitation in the UV, the dark color of the magnetite can cause problems by absorbing both excitation and emission light.[316]8]

Finally, due to the small particle sizes, the response to a changing oxygen concentration is fast which enables real-time monitoring of dissolved oxygen. The response time of a particle spot to a rapid change in oxygen concentration was measured with t_{90} of 1.4 s (Figure 8.8 on page 143). This time is, however, limited by the diffusion inside the dense particle layer, whereas the response of single particles is most probably much faster. Nevertheless, a t_{90} of 1.4 s enables real-time monitoring of most biological processes.

For long-term oxygen monitoring in biological samples, benzoporphyrin dyes such as PtTPTBPF and PdTPTBPF can outperform the iridium coumarin dyes due to their higher photostability and phosphorescence emission in the near-infrared range of the spectrum.[317] Moreover, the absorption of the incorporated magnetite nanoparticles is significantly lower in the red part of the spectrum and therefore, the emission intensity is further increased. We produced MOSePs with PtTPTBPF for oxygen monitoring from 0 – 100 % air saturation (K_{SV1} =0.016 hPa^{-1}, $P = 0.92$, Figure 8.7b, "PdBP" in Table 8.1) and MOSePs with PdTPTBPF for trace oxygen monitoring (K_{SV1} =0.067 hPa^{-1}, $P = 0.89$, Figure 8.7c, "PtBP" in Table 8.1).

Recently, the suitability of light harvesting systems to enhance the brightness of optical sensors was reported.[199] Due to the efficient absorption of excitation light by the harvesting dyes, the fraction of light lost due to magnetite absorption is further reduced. The incorporation of the oxygen indicator platinum(II) *meso*(2,3,4,5,6-pentafluoro)phenyl porphyrin (PtTFPP) together with an antenna dye (macrolex yellow) in the MOSeP-core resulted in oxygen sensor particles with an improved excitation spectrum (Figure 8.9). It was possible to increase the emission intensity at 650 nm significantly by changing the excitation wavelength from 505 nm to 465 nm. Besides the signal enhancement due to increased absorption by the acceptor dye compared to the magnetite, this light harvesting system is suitable for the excitation with extremely bright blue LEDs.

Singlet oxygen production Besides the oxygen sensing function of palladium and platinum porphyrins, such dyes are known as efficient singlet oxygen producers. PdTPTBP for instance has a high molar absorption coefficient ($\lambda_{max}(\epsilon) = 629$ nm (173,000 $M^{-1}\,cm^{-1}$) and moderate quantum yield (0.21).[317] Its phosphorescence is almost completely quenched

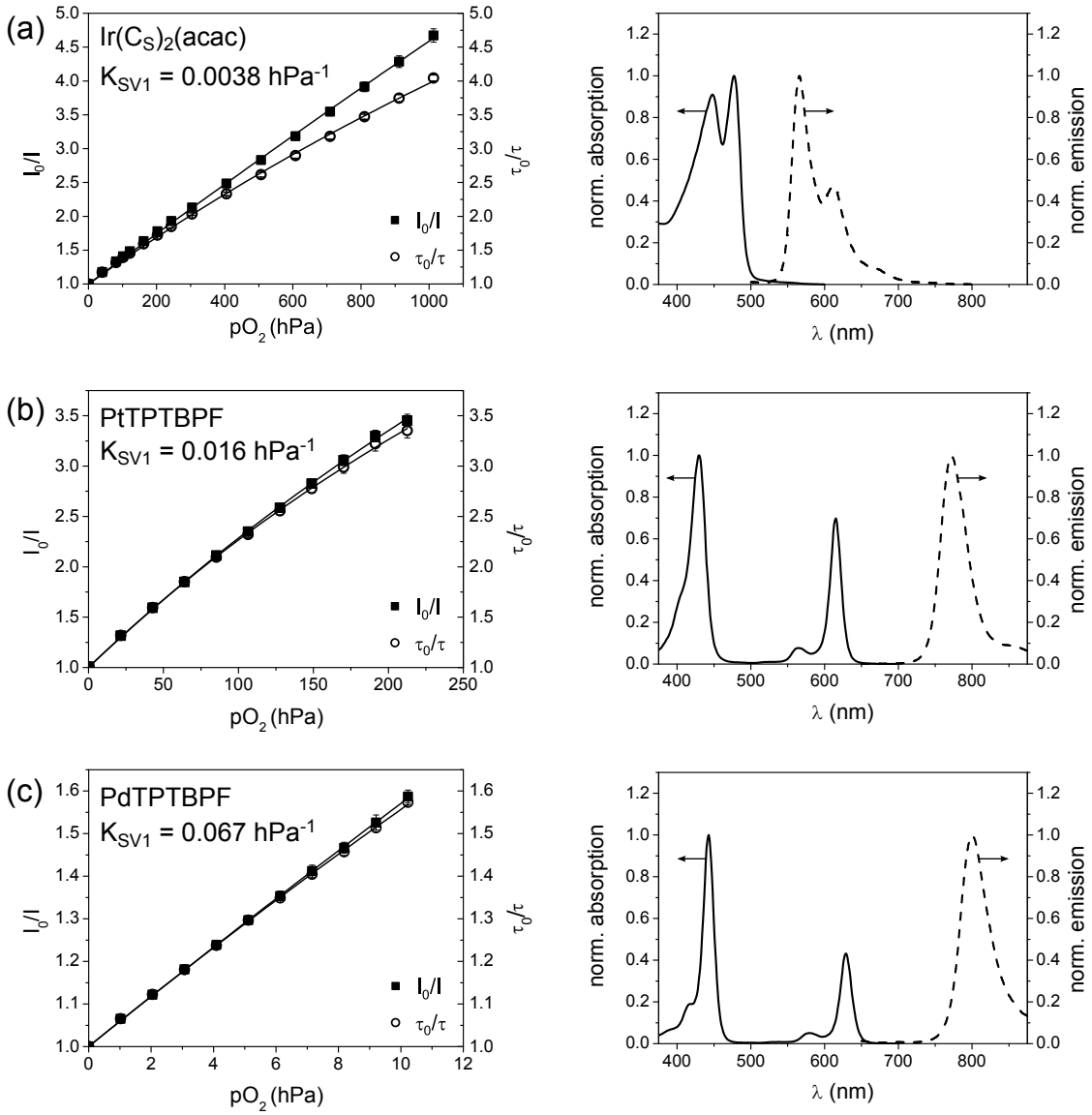

Figure 8.7: Stern-Volmer plots and absorption and emission spectra of oxygen indicators with different dynamic ranges and spectral properties. Chemical structures of the dyes can be seen in Figure 8.19 on page 156 in the Supporting Information.

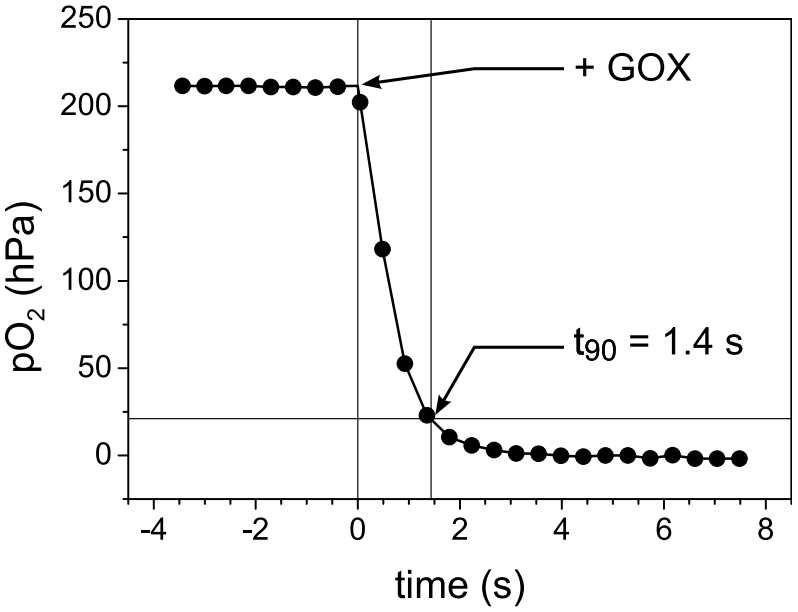

Figure 8.8: Response time of $Ir(C_S)_2(acac)$ stained MOSePs (1 % w/w PSMA93, 20 % magnetite, 1 % dye both w/w polymer, z-average = 186 nm) in a solution of 100 mM glucose upon addition of 400 U mL^{-1} GOX.

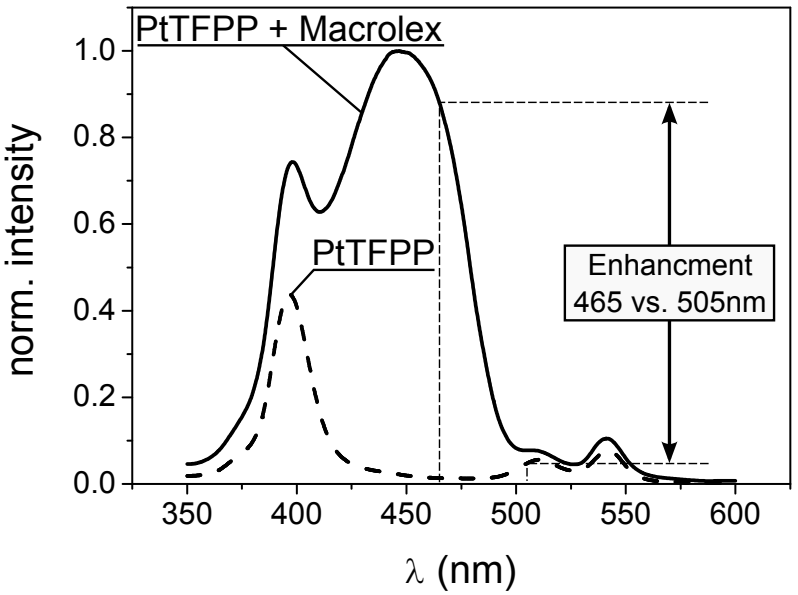

Figure 8.9: Excitation spectra of PtTFPP (1 % w/w polymer) and a light harvesting system consisting of macrolex yellow (2 %) and PtTFPP (1 % w/w polymer) incorporated in MOSePs (λ_{em} = 650 nm).

at air saturation as shown in Figure 8.10a and the quantum yield for singlet oxygen production of platinum- and palladium porphyrins is usually close to unity.[318,319] An efficient singlet oxygen production, however, also depends on an efficient contact of the photosensitizer in its excited state with oxygen. Moreover, the produced singlet oxygen requires rapid transport to the surface in order to avoid deactivation inside the polymer matrix. Small particle diameters result in a high specific surface area and short diffusion distances of both triplet and singlet oxygen.

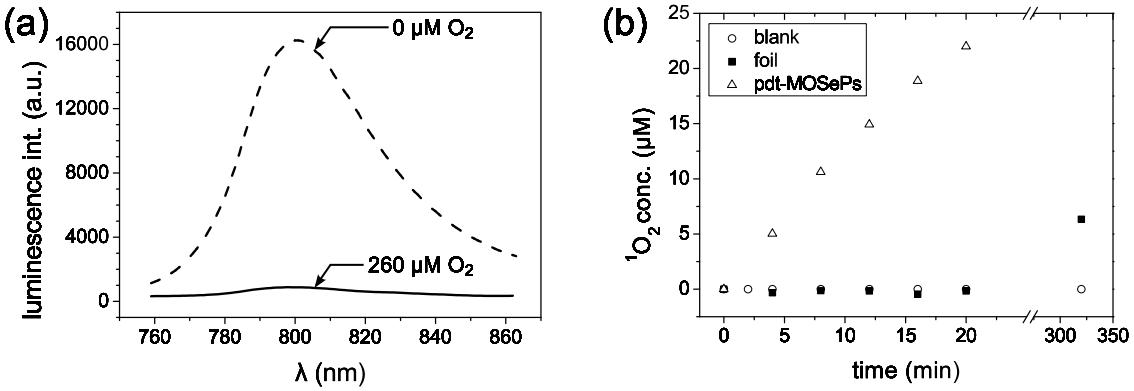

Figure 8.10: (a) Luminescence spectra of PdTPTBP stained MOSePs ("PDT", Table 8.1) in oxygen free and air saturated medium. (b) Singlet oxygen production of the same MOSePs compared to a 1 µm foil containing the same amount of dye.

Lai et al. recently reported on the successful utilization of iridium complexes for the generation of singlet oxygen while simultaneously imaging the localization of the particles and utilizing the magnetic properties of the composite particles for MRI imaging.[84] We investigated the singlet oxygen production efficiency of PdTPTBP doped MOSePs ("PDT", Table 8.1) upon illumination with a xenon lamp filtered trough a 590 nm long pass filter. In comparison to a 1 µm thick foil with the same amount of dye, matrix material and light intensity, the PdTPTBP doped MOSePs resulted in a 60 times higher production rate (Figure 8.10b). Red light excitation is beneficial for a potential application in biological samples. The incorporation of PdTPTBP as trace oxygen sensor and singlet oxygen producer in the MOSeP-cores results in particles capable of simultaneous photodynamic therapy and oxygen monitoring. Oxygenation is a prerequisite for an efficient photodynamic therapy but at the same time the oxygenation is also a parameter characterizing the metabolic state of a tissue.

8.2.4 Modifications of the shell

As mentioned above, MOSePs possess a number of carboxyl groups at the surface. Besides the stabilization of aqueous particle dispersions, carboxyl groups offer the possibility of surface modifications.

Covalently bound indicator dyes or fluorescent labels Polar indicator dyes, such as pH-indicators require a proton permeable matrix. In addition, if leaching of the dye

occurs, a covalent attachment might be favored over the simple enclosure in the polymer network. As an example, we bound amino fluorescein to surface carboxyl groups after activation by EDC. The spectra of the modified MOSePs at varying pH can be seen in Figure 8.11a. Plotting the emission at 519 nm in correlation with the pH value resulted in an apparent pKa of 7.3 (Figure 8.11b), a value for sensors commonly used in physiological applications. An inclusion of lipophilic fluorescein derivatives in the lipophilic core – a common technique for the production of pH sensors in hydrogel particles – would prohibit the interaction of protons with the indicator.

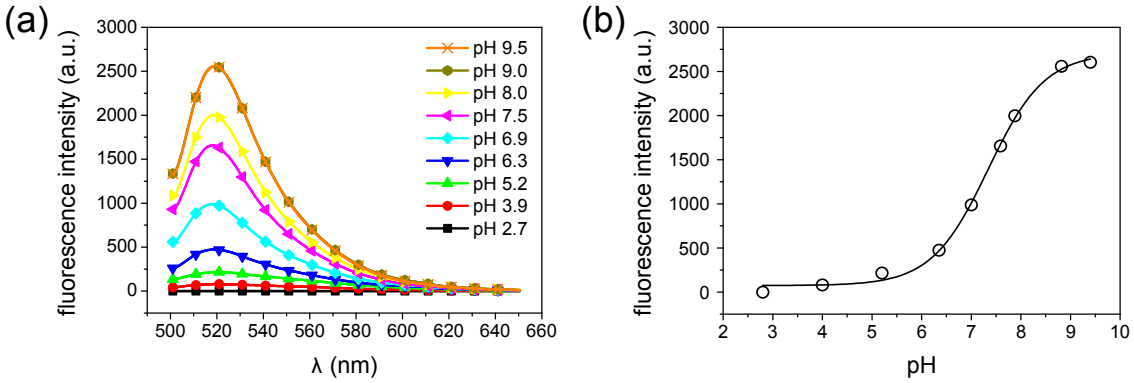

Figure 8.11: MOSePs coated with 5-aminofluorescein resulted in particles with a changing fluorescence emission at 519 nm ($\lambda_{ex} = 480$ nm). The observed pKa of this system is 7.3.

Binding of enzymes and other proteins Through the same zerolength crosslinking method used for the fluorescein binding, it is possible to link an enzyme or protein with an accessible amino group to the MOSePs' surface. Here, we used glucose oxidase (GOX) as a model enzyme to demonstrate the linking of an enzyme in its active form to oxygen-sensitive MOSePs. To prove that the GOX retained its activity after the immobilization, we monitored the oxygen consumption at different glucose concentrations (Figure 8.12a). The modified MOSePs were capable of consuming glucose and oxygen while simultaneously monitoring the change in oxygenation with the incorporated indicator ($Ir(C_S)_2(acac)$). For this experiment, the particles were collected in front of an optical fiber in a glass tube with the help of a magnetic separator with an optical window [13] and they were flushed with different glucose solutions. Binding of other proteins for increased biocompatibility or the introduction of recognition patterns can be carried out in a similar manner.

Surface modification by the Layer-by-Layer (LbL) technique The initially negatively charged surface of the MOSeP at neutral pH allows for surface modifications with charged species (LbL-technique). For a proof of concept, we coated the surface alternately with four layers of poly(diallyldimethylammoniumchloride) (+) and four layers of polystyrene sulfonate (−). The zeta potentials and sizes were measured after every step and elucidated the alternating charges from -32 mV to +37 mV (Figure 8.12b). Throughout the coating procedure the hydrodynamic diameters increased slightly from 105 to 130 nm, compared to blank diameters which increased from 105 to 115 nm. The increasing blank diameter is

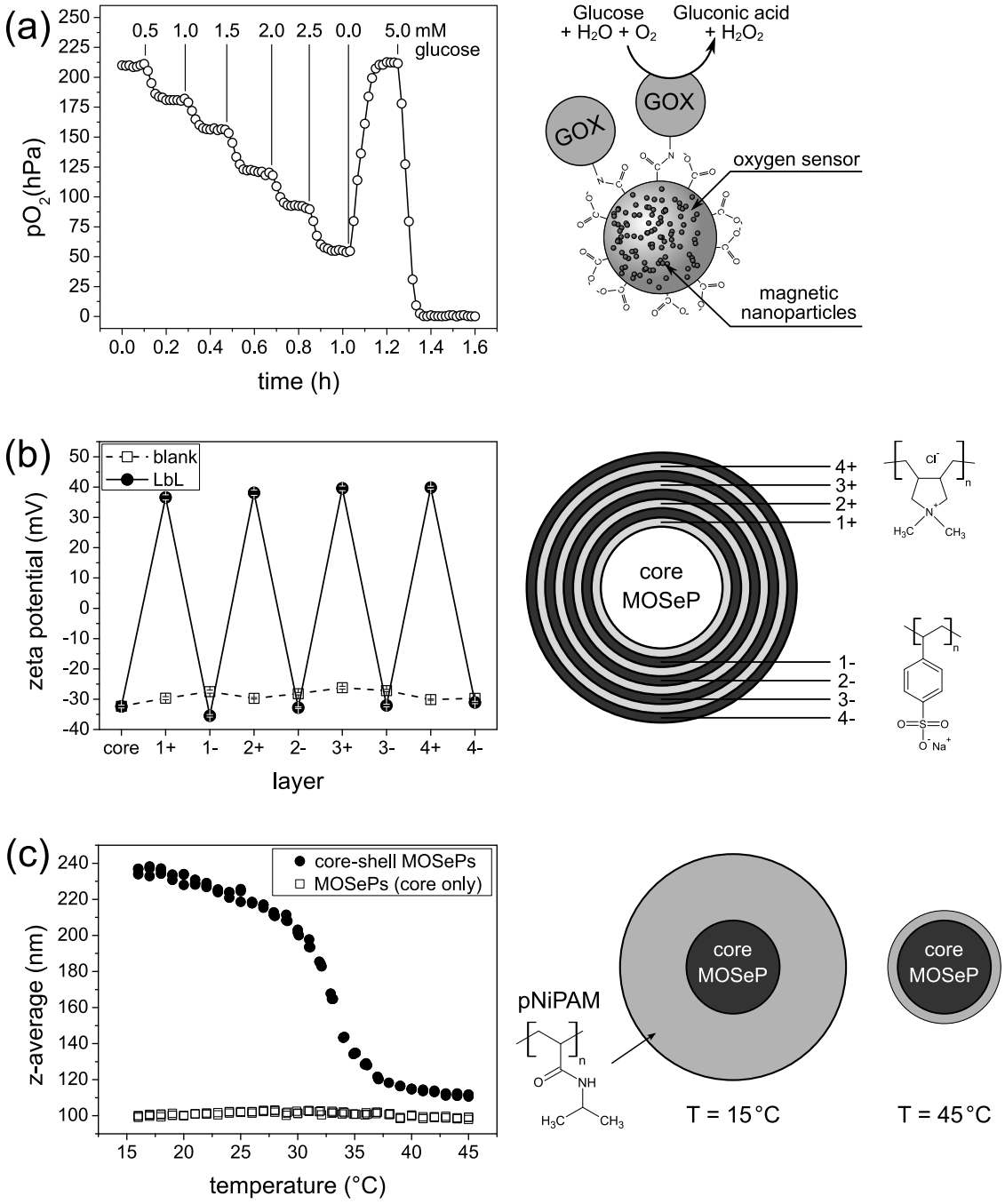

Figure 8.12: Surface modifications of MOSePs. (a) Coupling glucose oxidase to oxygen-sensitive MOSePs basically resulted in magnetic glucose sensors. In (b), the zeta potentials during coating of four positive and four negative polyelectrolyte layers were plotted. (c) The modification of MOSePs with a pNIPAM shell resulted in temperature sensitive core-shell particles.

due to a slight aggregation occurring during the repeated separation and washing steps. However, the SEM image of coated MOSePs shows spherical particles without significant aggregation or change of particle shape (Figure 8.18 on page 155).

Particle coating with stimuli responsive polymers These polymers generally respond to changing physical parameters such as pH and temperature,[54,284,320] but also to light, radiation or chemical stimulators. We chose the hydrogel poly-*N*-isopropylacrylamide (pNIPAM) as one of the most studied representatives of stimuli responsive polymers to prove the possibility of producing stimuli responsive MOSePs (SR-MOSePs). The polymerization was accomplished by polymerizing *N*-isopropylacrylamide and *N,N'*-methylenebisacrylamide in the presence of MOSePs as seeds. The resulting particles were magnetic, oxygen-sensitive ($Ir(C_S)_2(acac)$, $\tau_0/\tau_{air} = 1.5$), and they reversible changed their size with the temperature (Figure 8.12c). Such stimuli responsive MOSePs would provide an optimal basis for magnetic drug carriers[321] releasing a drug at a distinct position and simultaneously measuring the effect of this event in real-time at the very place of the release.

In analogy to the modifications mentioned above (point 1-4), MOSePs represent a basis for the modification with biodegradable polymers or affinity ligands. Biodegradable polymers in combination with magnetic particles are used for targeted drug delivery.[6,322,323] Tumor specific antibodies bound to the surface might reduce the damaging of healthy cells due to drug delivery, PDT or hyperthermia inducible by MOSePs.

8.3 Conclusions

A polymeric multifunctional optical nanosensor platform was developed. We successfully demonstrated the application of MF-MOSePs as real-time oxygen sensors, in situ optical biosensors, magnetic PDT agents, magnetic pH-sensors and stimuli responsive magnetic optical sensors, and proposed other potential applications. Due to the versatility of the platform, the presented particles can be easily modified to match the requirements of a wide range of scientific and clinical applications. For in vivo applications, a further size reduction might be necessary to allow renal excretion. For in vitro applications, however, the here presented MOSePs represent a ready-to-use, multipurpose platform.

8.4 Experimental

Materials: Poly(styrene-co-maleic anhydride) (PSMA93; 7 % maleic anhydride; molecular weight = 224,000 g mol^{-1}), glucose oxidase (GOX, from Aspergillus niger, lyophilized powder), poly(diallyldimethylammonium chloride) (20 % in water), poly(sodium 4-styrenesulfonate) (20 % in water), *N*-isopropylacrylamide, *N,N'*-methylenebisacrylamide, potassium peroxodisulfate, 5-aminofluorescein, *N,N*-dimethyl-4-nitrosoanilin, imidazol and sodium dodecylsulfate were purchased from Sigma (www.sigmaaldrich.com). 1-Ethyl-3-[3-dimethylaminopropyl]carbodiimide hydrochloride (EDC) was purchased from TCI Europe (www.tcieurope.eu). Poly(styrene maleic anhydride) with 11 % maleic anhydride and a molecular weight of 14,400 g mol^{-1} (EF-80) was generously provided by Sartomer

Europe (www.sartomereurope.com). Lipophilic magnetic nanoparticles (L-MNP, polymer coated magnetite nanoparticles "EMG1300" from MNP-kit) were purchased from FerroTec GmbH (www.ferrofluidics.de). Tetrahydrofurane (THF), sodium chloride, phosphate buffer solutions and glucose were obtained from Carl Roth GmbH (www.carl-roth.de). Platinum(II) *meso*(2,3,4,5,6-pentafluoro)phenyl porphyrin (PtTFPP) was bought from Frontier Scientific (www.frontiersci.com) and Macrolex Yellow from Simon & Werner GmbH (Flörsheim, Germany). Nitrogen, oxygen, synthetic air and test gas with 1 % oxygen (all of 99.999 % purity) were purchased from Air Liquide (www.airliquide.at). Iridium(III) acetylacetonato-bis(3-(benzothiazol-2-yl)-7-(diethylamino)-coumarin) ($Ir(C_S)_2(acac)$), palladium(II) *meso*-tetra(4-fluorophenyl) tetrabenzoporphyrin (PdTPTBPF) and platinum(II) *meso*-tetra(4-fluorophenyl) tetrabenzoporphyrin (PtTPTBPF) were prepared in our lab as reported elsewhere.[198,317] Palladium(II) *meso*-tetraphenyltetrabenzoporphyrin (PdTPTBP) was prepared according to Finikova et al.[324]

Absorption spectra were measured at a Cary 50 UV–vis spectrophotometer (Varian Inc., USA). Emission spectra were acquired on a Hitachi F-7000 fluorescence spectrometer (Hitachi Inc., www.inula.at) equipped with a red-sensitive photomultiplier R 928 from Hamamatsu (www.hamamatsu.com). The phase shifts for the oxygen measurements were recorded with a 2 mm optical fibre and a fibre optic phase fluorimeter (www.presens.de) equipped with a blue LED (470 nm) for excitation and a 550 nm long-pass filter for the emission. The modulation frequency was adjusted to 20 kHz. Alternatively, for PdTPTBPF and PtTPTBPF a 630 nm LED (Roithner Laser Technik, www.roithner-laser.com) was modulated with a two-phase lock-in amplifier (SR830, Stanford Research Inc., www.thinksrs.com). A bifurcated fiber bundle was used to guide the excitation light (filtered through a Calflex filter, Linos) to the sample and the luminescence back to the detector after being filtered through an RG9 (Schott) glass filter. Luminescence was detected with a PMT (H5701-02, Hamamatsu, www.sales.hamamatsu.com). The modulation frequencies were adjusted to 5 kHz for PtTPTBPF and 0.7 kHz for PdTPTBPF. For the calibrations the suspensions were purged with different ratios of nitrogen and oxygen, synthetic air or test gas (1 % O_2) adjusted by a gas mixing device (www.mksinst.com) at a flow rate of 200 mL min^{-1}. Particle sizes and zeta potentials were measured with a particle size analyzer Zetasizer Nano ZS (www.malvern.de). FT-IR-spectra were recorded with a Perkin-Elmer Spectrum One instrument (www.perkinelmer.com) equipped with an ATR-unit. SEM images were recorded on a Zeiss Ultra 55 (www.zeiss.com) equipped with a field emission gun (FEG). A drop of MOSeP suspension was placed on a silicon wafer. After evaporation of the dispersant the samples were coated with a thin chromium layer to avoid specimen charging. TEM images were recorded on a Philips CM 20 microscope equipped with a LaB6 filament. A drop of MOSeP suspension was placed on a standard copper grid and the dispersant was evaporated under a slight stream of air.

Synthesis of magnetic optical sensor particles (MOSePs "CE3", for other diameters parameters were adjusted as stated in Table 8.1): In a typical synthesis EF-80 (3 mg), L-MNP (0.6 mg) and dye (0.03 mg) were dissolved/dispersed in dry THF (0.5 g) under ultrasonication. This "cocktail" was then added to deionized water (4.5 mL) under vortexing (1200 min^{-1}). Particle precipitation occurred immediately. Under a stream

of air, THF was evaporated from the mixture during 25 min and the resulting particles were washed twice with deionized water by magnetic separation. Occasionally occurring aggregates were removed by filtration through a syringe filter (Rotilabo, 0.8 µm). The particles obtained under these conditions had a hydrodynamic diameter of 109 nm (Table 8.1).

Singlet oxygen assay: The assay was based on the procedure published by Kraljic and Mohsni[325] Briefly, a phosphate buffer solution (2.5 mL, pH 7.4, ionic strength = 0.05 M) containing *N,N*-dimethyl-4-nitrosoanilin (5×10^{-5} M), and imidazol (8×10^{-3} M) with a 10 µm foil (2.5 cm × 1.4 cm) containing 55 µg PdTPTBP ("foil") or a 5.5 mg PdTPTBP (1 %, w/w) stained MOSePs ("PDT-MOSePs","PDT" in Table 8.1) were illuminated with a xenon lamp filtered through a 590 nm long pass filter (excitation via the Q-Band only) for up to 300 min. As blank, only the assay components were illuminated. The production of singlet oxygen was controlled by measuring the absorption at 440 nm of the supernatant every 5 min after separating the MOSePs and sensor foil, respectively.

Surface modification of MOSePs with GOX: MOSePs (5 mg) were dispersed in phosphate buffer (2 mL, 0.05 M, pH 7.0). The dispersion was then incubated with EDC (2 mg) for 10 min to activate the carboxyl groups. For binding, GOX (5 mg) was added and the binding reaction was carried out for five hours on a rotation mixer at $50\,\mathrm{min}^{-1}$. The resulting particles were magnetically separated and washed 4 times with phosphate buffer for further investigation.

Surface modification of MOSePs with 5-aminofluorescein: MOSePs (200 mg, "FLU" in Table 1) were dispersed in MES buffer (10 mL, 0.1 M, pH 4.5). The dispersion was then incubated with EDC (30 mg) and 5-aminofluorescein (10 mg) in a rotation mixer for 2 h. The resulting particles were magnetically separated and washed four times with ethanol, three times with water and redispersed in water for further investigation.

Layer-by-layer coating of MOSePs: In a glas vial, MOSePs (5 mg, "LBL", Table 8.1, zeta potential = -32.4 ± 0.6 mV) were incubated with a 0.8 % (w/w) solution of the two different polyelectrolytes poly(diallyldimethylammonium chloride) and poly(sodium 4-styrenesulfonate) (2 mL) in alternating manner. After each incubation step, the particles were magnetically separated and washed three times with deionized water in the ultrasonic bath.

Coating of MOSePs with a pNIPAM shell (SR-MOSePs): In a typical procedure, MOSePs (15 mg, "SR", Table 8.1), *N*-isopropylacrylamide (50 mg), *N,N'*-methylenebisacrylamide (1.7 mg), and sodium-dodecylsulfate (3.6 mg) were dissolved in deionized (9 mL) water and heated to 65 °C under nitrogen. After the addition of potassiumperoxodisulfate (9.0 mg dissolved in 1 mL of water), the NIPAM was allowed to polymerize under continued stirring for 3 h. Afterwards, the particles were cleaned repeatedly with deionized water and dispersed in water for further investigations.

Measurement of the 5-aminofluorescein binding capacity: 5-aminofluorescein modified MOSePs (100 mg, "FLU", see Table 8.1) were dissolved in THF (3 mL) and the concentration was calculated using the absorption and extinction coefficient at 483 nm.

Acknowledgement

We gratefully thank DI S. Fladischer and DI C. Gspan from the FELMI-ZFE Graz for their help to record the TEM images. We also acknowledge F. Adanitsch and J. Flock for their excellent technical support and Dr. Ute Daschiel for her help performing FT-IR measurements. This work was supported by the Austrian Science Fund FWF (project P 21192-N17). Supporting Information is available online from Wiley InterScience or from the author.

8.A ESI for the manuscript: Multifunctional magnetic optical sensor particles with tunable sizes for monitoring metabolic parameters and as basis for nanotherapeutics

This chapter was published as *Supporting Information for the Full Paper* in

Advanced Functional Materials, 2010, in Press

doi: 10.1002/adfm.201000321

Authors: Günter Mistlberger*, Klaus Koren, Elisabth Scheucher, Daniel Aigner, Sergey M. Borisov, Armin Zankel, Peter Pölt, and Ingo Klimant

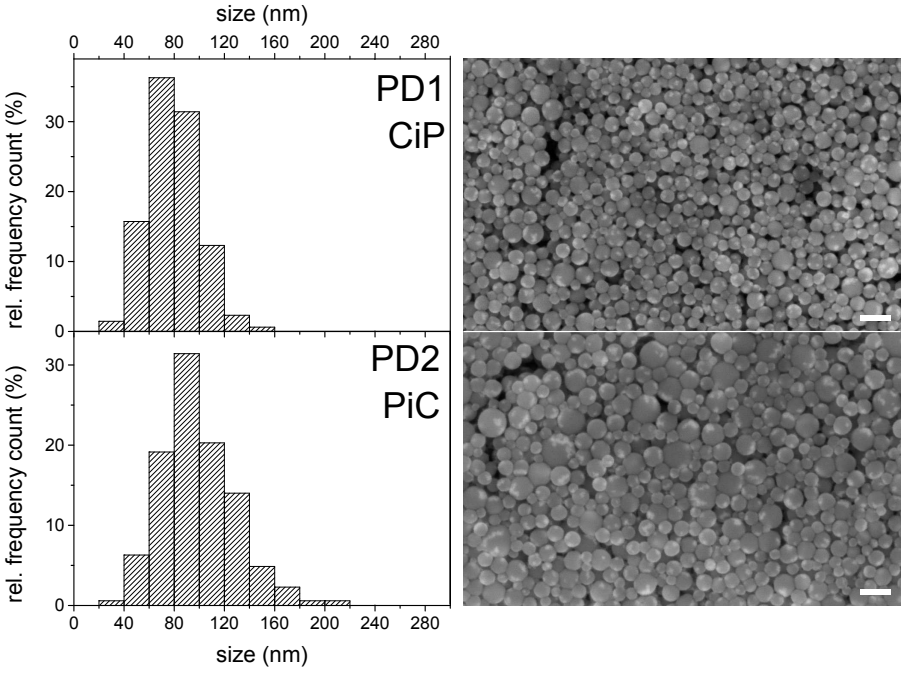

Figure 8.13: Size histograms from SEM images of EF-80 particles when changing the precipitation direction from "cocktail-into-precipitant" (PD1) to "precipitant-into-cocktail" (PD2). Other precipitation parameters are listed in Table 8.1 on page 136. The scale bar is 200 nm in all images.

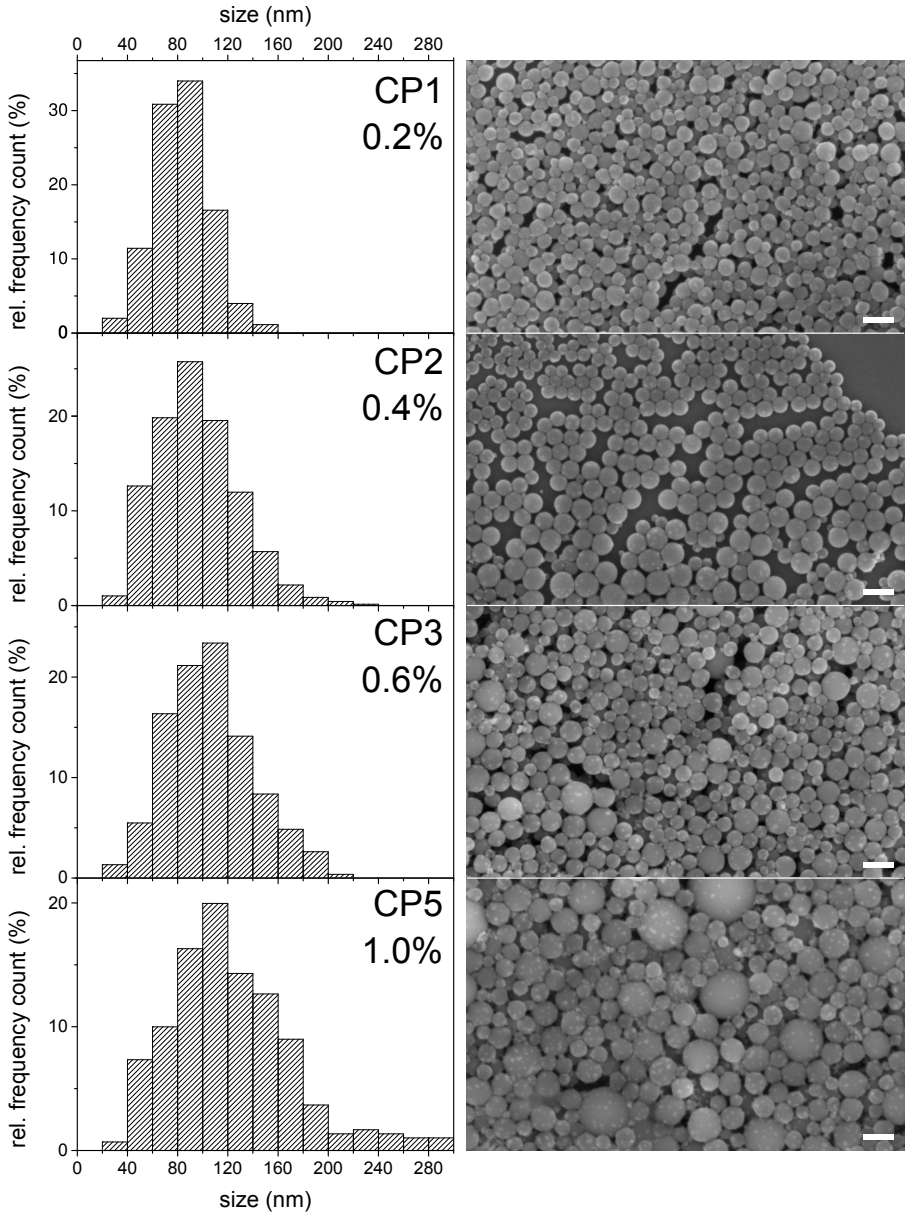

Figure 8.14: Size histograms from SEM images of PSMA93 particles with varying polymer concentration in the cocktail (see Table 8.1 on page 136). The scale bar is 200 nm in all images.

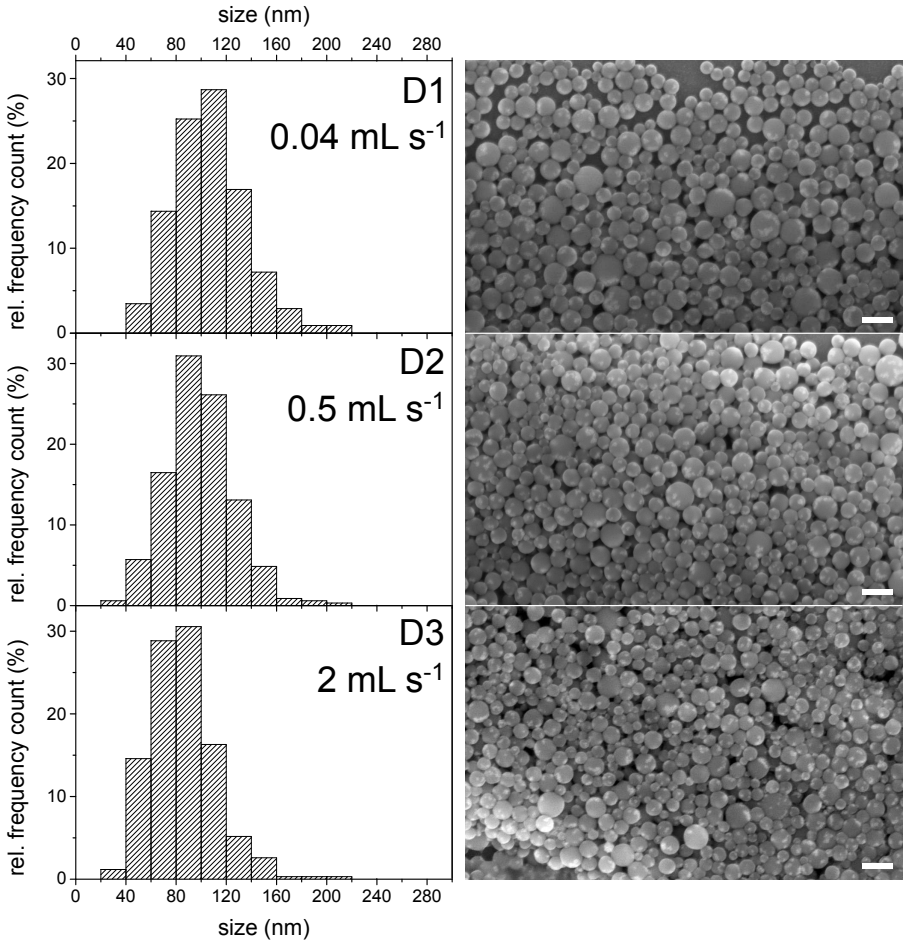

Figure 8.15: Size histograms from SEM images of MOSePs produced by different cocktail flow rates (see Table 8.1 on page 136). The scale bar is 200 nm in all images.

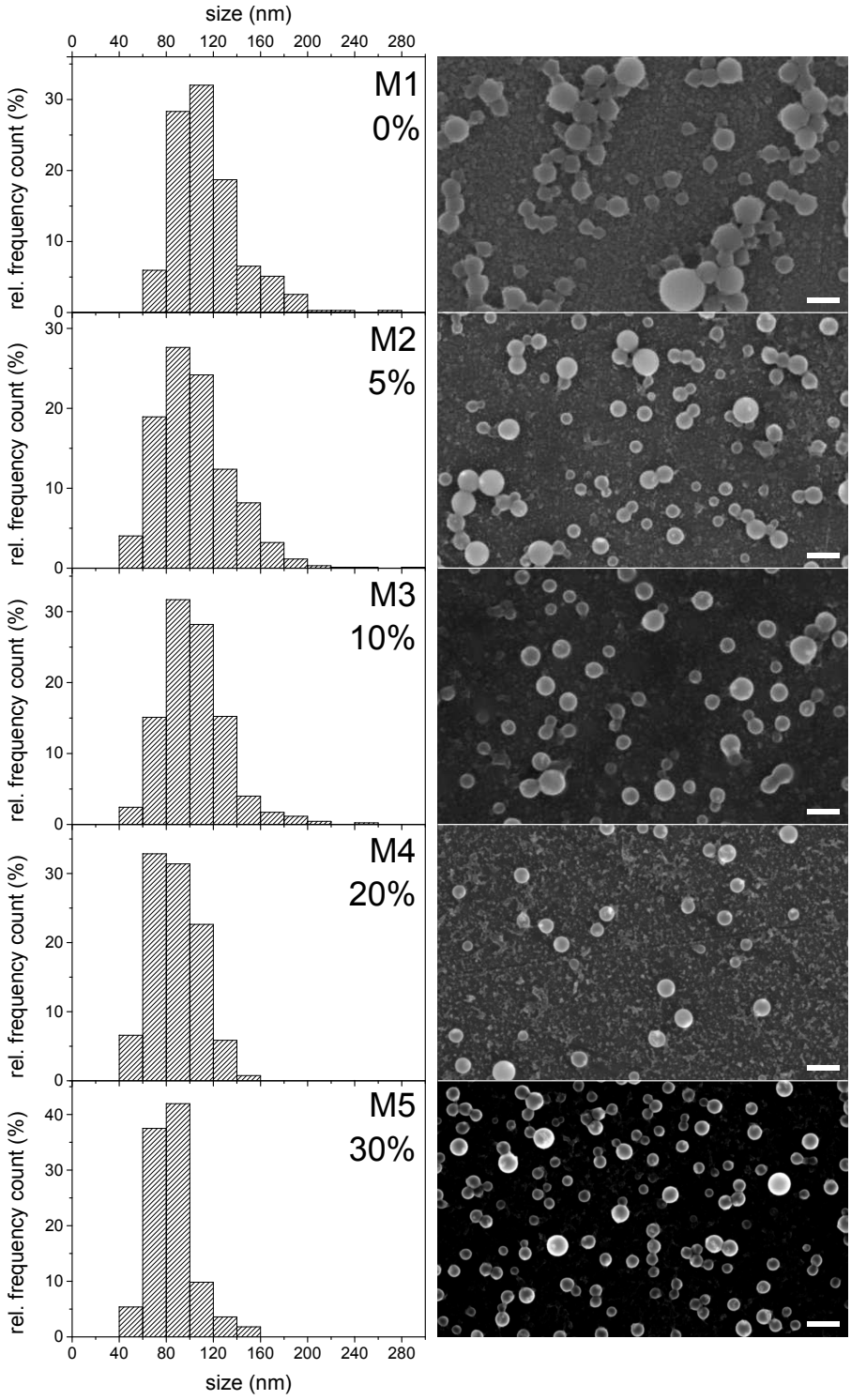

Figure 8.16: Size histograms from SEM images of MOSePs with different concentrations of magnetic nanoparticles (see Table 8.1 on page 136). The scale bar is 200 nm in all images.

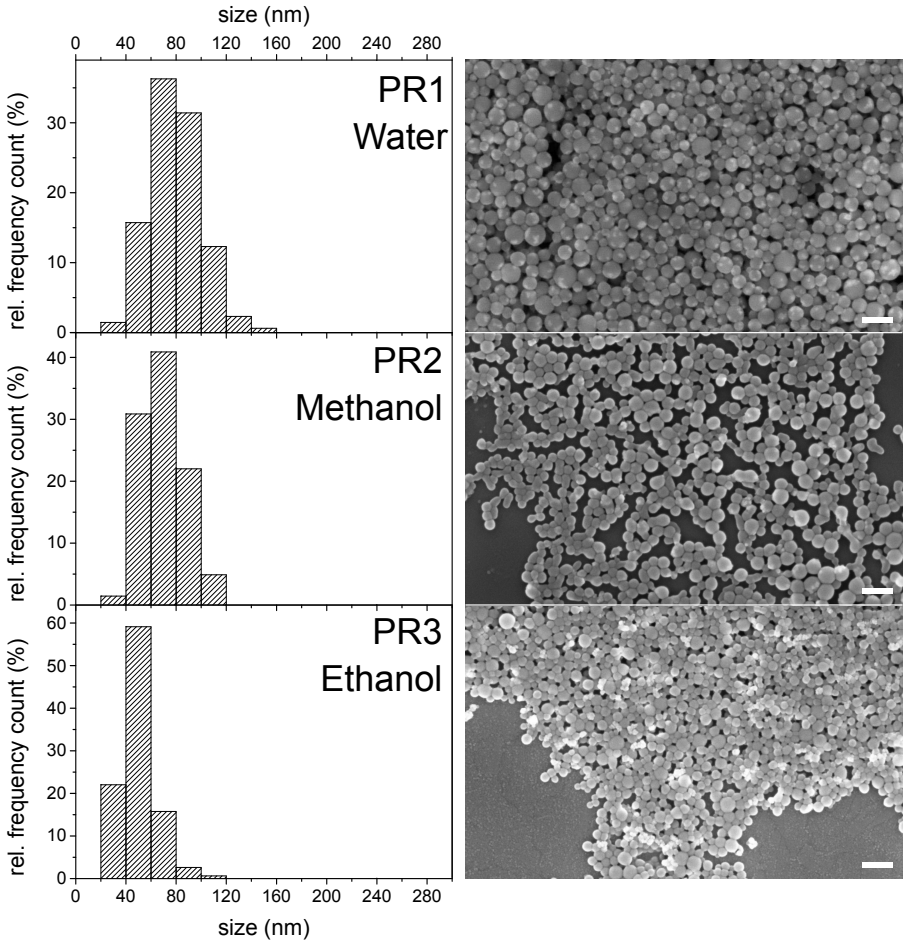

Figure 8.17: Size histograms from SEM images of MOSePs precipitated with different precipitants: water (PR1), methanol (PR2) and ethanol (PR3). Other precipitation parameters are listed in Table 8.1 on page 136. The scale bar is 200 nm in all images.

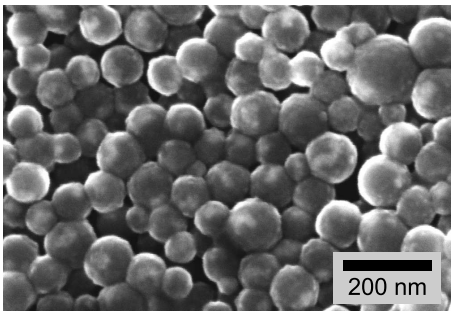

Figure 8.18: SEM image of MOSePs ("LBL") coated with eight alternating layers of positive and negative polyelectrolytes (see Table 8.1 on page 136).

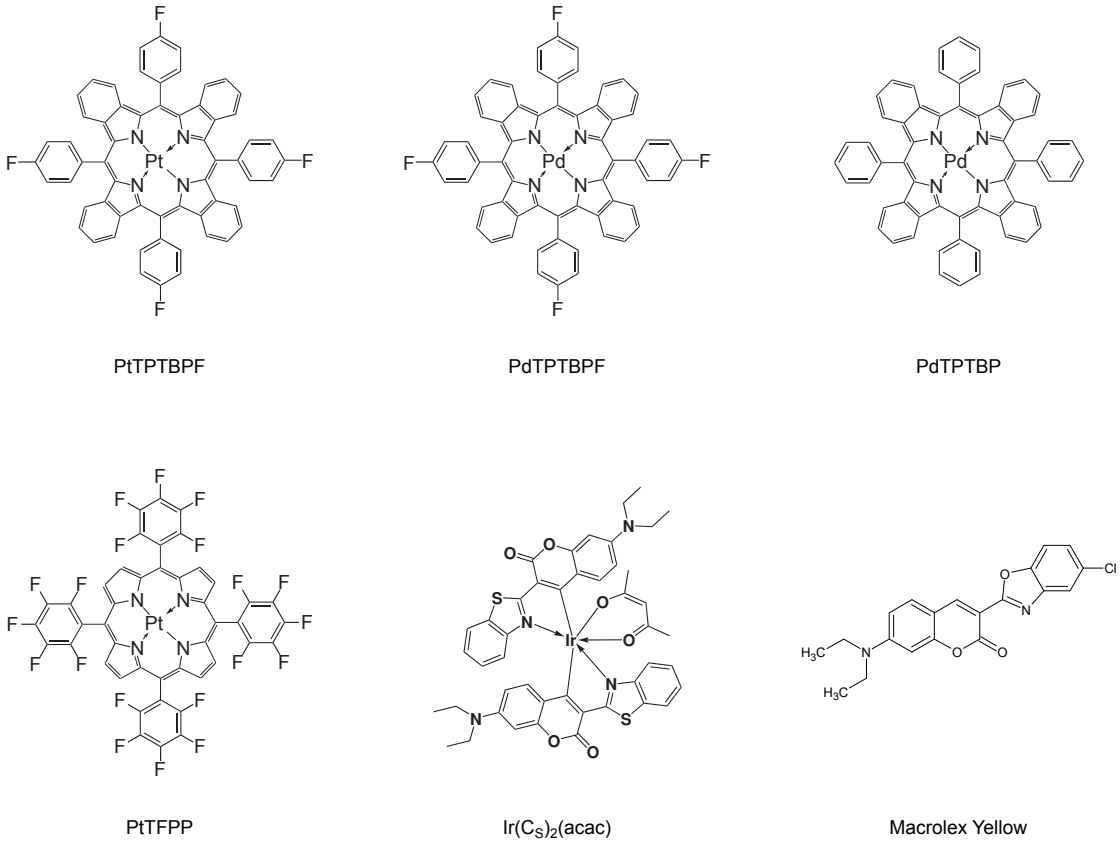

Figure 8.19: Chemical structure of the dyes incorporated in the MOSePs' cores.

Part III

Future prospects and conclusions

9 Production of magnetic nanosensors by miniemulsion solvent-evaporation

The main limitations of nanoprecipitation as method for the production of nanometer-sized MOSePs are the restriction to special solvent-precipitant combinations and the relativeley low throughput. For this reason, several other approaches towards the synthesis of nanoparticles were tested. One of them was solvent-evaporation. This method has previously been used for the formation of magnetic nanoparticles and consists of the following steps:

1. Fabrication of a cocktail in a solvent immiscible with water.
2. Production of an oil-in-water emulsion of the cocktail in an aqueous continuous phase with the help of emulsifiers and ultrasonication.
3. Evaporation of the solvent from the droplets, also referred to as "particle curing".

These steps are schematically shown in figure 9.1.

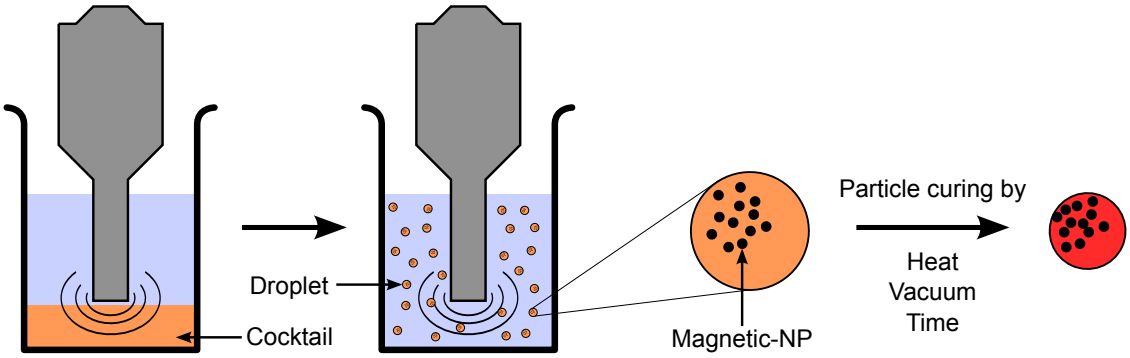

Figure 9.1: Production of nano-MOSePs *via* a combined miniemulsion solvent evaporation technique.

Due to the possibility of using solvents that are immiscible with water, a wide variety of organic polymers, dyes and magnetic particles is suitable for this method. In a cooperation with the University of Granada, we were able to demonstrate the production of oxygen and pH sensitive, magnetic nanospheres with all types of lipophilic indicator dyes. The polymers included polystyrene, poly(styrene-co-maleic anhydride), hydrathane D4 (a polyurethane based hydrogel) and Eudragit RL100® (a copolymer of acrylic and methacrylic esters with quarternary ammonium groups).

Status

Data acquisition is finished and a manuscript is in preparation.

10 Luminescent oxygen imaging with micro- and nano-MOSePs

As mentioned in the main section of the thesis, MOSePs represent an excellent tool for the investigation of biological materials, such as biofilms or single cells. Some possibilities are outlined in figure 10.1. They can be used for monitoring at distinct positions (1), on the whole surface (2) or in the surrounding medium (3).

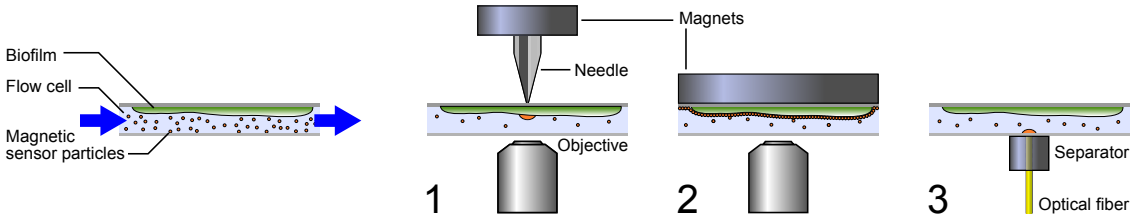

Figure 10.1: Applications of MOSePs for the investigation of biofilms. Analyte monitoring can be carried out at distinct positions (1), on the whole surface (2) or in the surrounding medium (3).

First promising results with micro-MOSePs produced *via* spray-drying (chapter 4 on page 69) were achieved during a research stay in the laboratory of Prof. Michael Kühl at the University of Copenhagen. A biofilm was grown on a microscope cover slip which was then used as a lid for a custom-made flow cell. The flow cell enabled to image the surface of the biofilm with an inverse fluorescence microscope. By the application of a magnet on top of the flow cell, oxygen sensitive micro-MOSePs were deposited on the surface of the biofilm. The intensity of the luminescent signal changed in dependency on the nutrient content in the feeding solution. When glucose was added, the microorganisms in the biofilm consumed oxygen. The reduced concentration of oxygen, which is a quencher for the oxygen sensitive dye in the MOSePs, resulted in a higher luminescence intensity.

In a later work in our lab, we reproduced some of these measurements with a lifetime imaging technique and by using both, micro- and nano-MOSePs. Thereby, the dependency of the signal on parameters, such as the thickness of the sensing layer or other imaging artefacts was greatly reduced. This work was carried out together with DI Birgit Ungerböck and Dr. Torsten Mayr from the Applied Sensors group at the Institute of Analytical Chemistry and Food Chemistry, Graz University of Technology. First results of a calibration carried out with spray-dried MOSePs on the surface of an immobilized GOX layer can be seen in figure 10.2 on the next page.

Due to the relatively large macro-sizes of these particles it is impossible to achieve an image of the oxygen concentration with high spatial resolution. For this reason, we carried out the same experiment again with nano-MOSePs. Figure 10.3 on page 163 shows a plain intensity image and two oxygen distribution images achieved *via* rapid lifetime

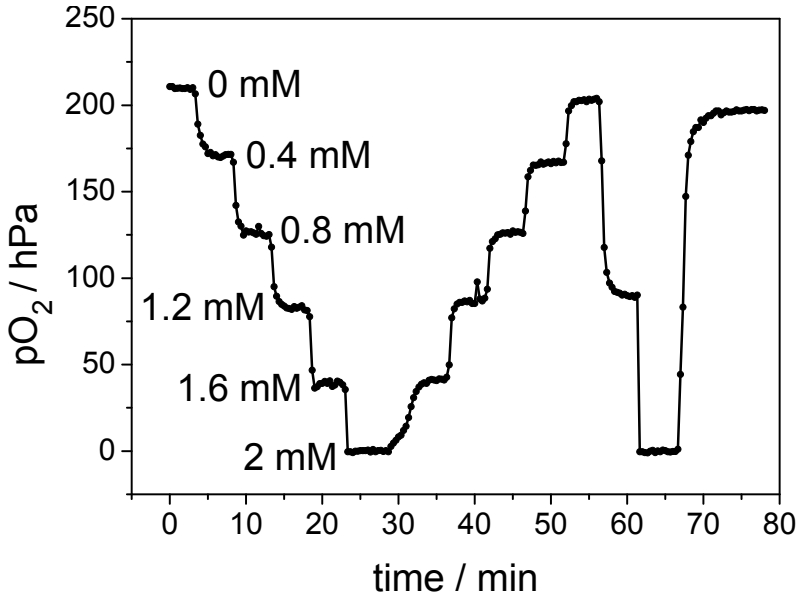

Figure 10.2: Monitoring the oxygen concentration on the surface of an immobilized GOX layer with micro-MOSePs. Spray-dried MOSePs were captured with a magnet and the flow cell was flushed with solutions containing different glucose concentrations (0 – 2 mM). One image was acquired every 20 seconds.

imaging. Compared to the plain intensity image, the strong variation in signal was almost completely eliminated in decay-time derived oxygen maps, except for areas in which the sensor concentration was too low for the calculation (lower left corner of the images).

This concept was also applied to a microfluidic chip where bacteria cells were immobilized (figure 10.4 on the next page). The oxygen concentration was significantly lower at regions where the bacteria cells were located.

Status

Data acquisition is almost finished. A manuscript about the methodology of oxygen imaging and monitoring on surfaces of biological materials is in preparation.

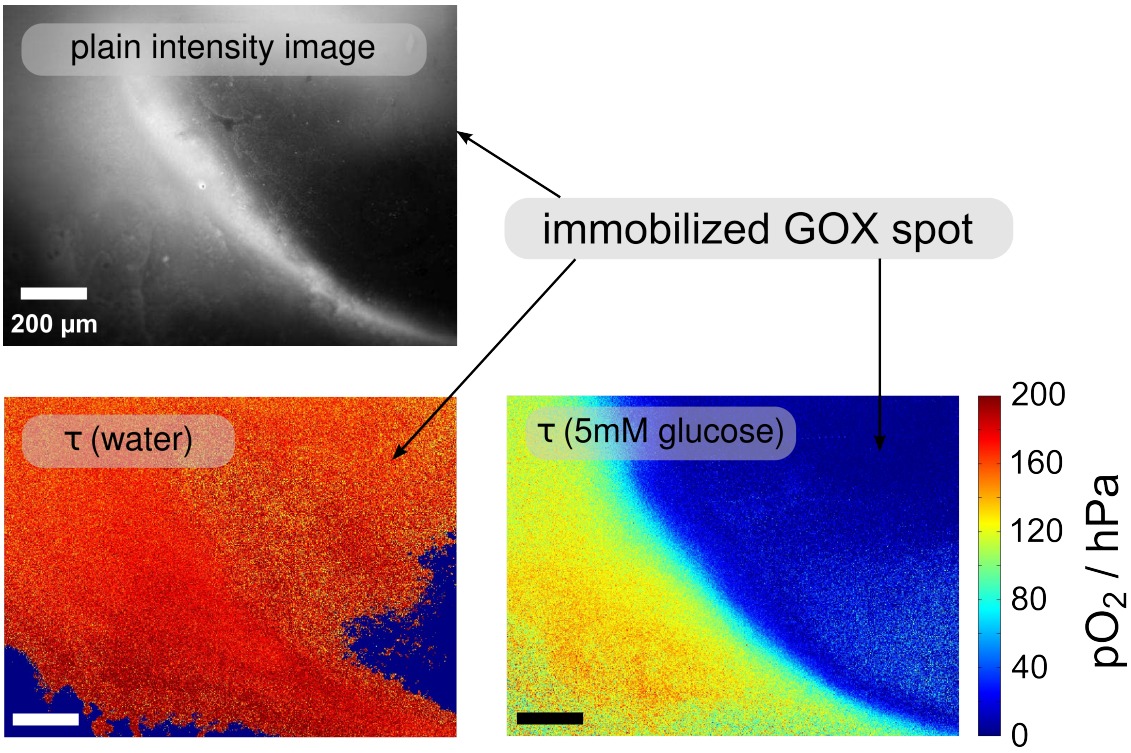

Figure 10.3: Monitoring the oxygen concentration on the surface of an immobilized GOX layer with nano-MOSePs. The sensor particles formed a layer on the GOX spot. Although the distribution was inhomogeneous, the oxygen image derived from the decay-time measurement was relatively uniform. Upon flushing with a glucose solution, deoxygenation above the GOX spot occured.

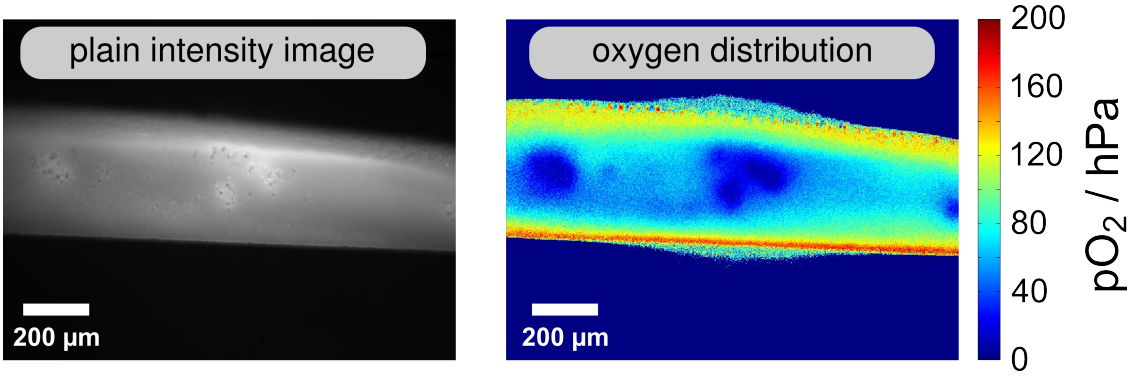

Figure 10.4: Monitoring the oxygen concentration around bacteria cells in a microfluidic channel with nano-MOSePs achieved *via* a nano-precipitation method (see chapter 8 on page 131).

11 Doubling the number of optical sensors on magnetic spheres

A recent discovery led to an attractive extension of the MagSeMac concept presented in chapter 7 on page 115. If the sphere is permanent magnetic rather than ferromagnetic, the orientation in a magnetic field is fully predictable. Therefore, it is possible to coat both hemispheres with a different sensing layer. The magnetic sphere optically separates the two sensing layers and enables a separate read-out without spectral interferences (figure 11.1). In this way, the number of sensors on a single sphere can be doubled.

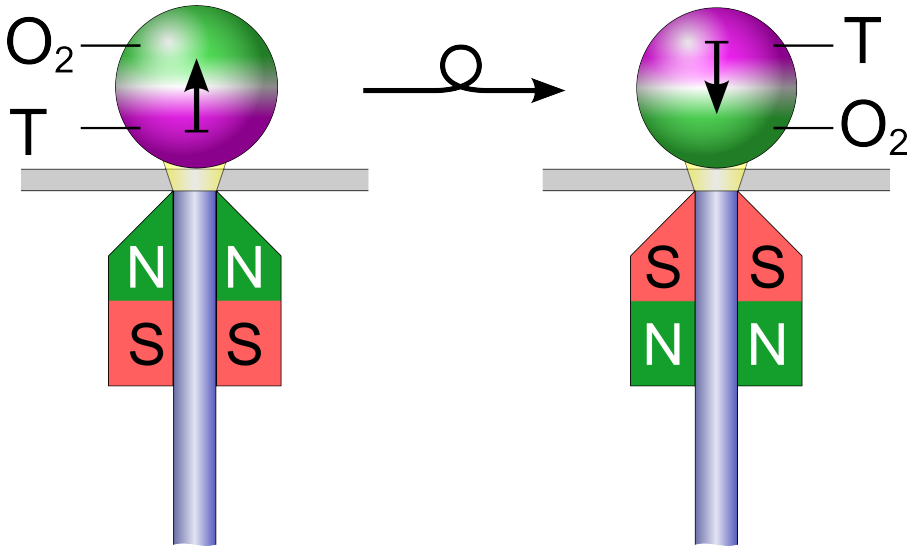

Figure 11.1: Sensing layers coated onto the two different hemispheres of a permanent magnetic sphere enable the separate read-out of both sensors without spectral interferences.

Switching back and forth from side one to side two can be accomplished with an electromagnet, i.e. a coil around an optical fiber. A device was constructed for exchanging the poles of the electromagnet and, consequently, turning the sphere upside down. The frequency can be adjusted from 0.2 to 3 Hz either manually or remote-controlled *via* an RS232-interface. In an upcoming bachelor work, Stefan Scheer will try to find a solution to integrate the device into the currently available LabView software for controlling the lock-in amplifiers and the photomultiplier boxes. Finally, the software should be able to correlate the data acquisition with the orientation of the magnetic field for a separate output of the two analytical signals.

Currently, the following sensor spheres are in development:

- a combined oxygen and temperature sensor (same matrix material can be used for both sensors),
- a combined oxygen and pH sensor (oxygen sensor in PS-DVB and the pH sensor in a hydrogel), and
- a sphere with double sensors on both sides (temperature and salinity on one side, oxygen and pH on the other side).

While the chemistry is already established for these sensors, we do expect some difficulties due to the increased stress for the coating by the continuous switching of the sphere. However, first tests with a similar method as described in chapter 7 on page 115 were promising and we have several other ideas to overcome the problem of limited adhesion between the sensor layer and the surface of the sphere.

Status

First promising results were recently achieved. Further optimizations of the coating procedure and the electromagnetic separators are currently in progress. Afterwards the double and quadruple sensors will be extensively tested and analytically characterized.

12 Micro respirometry of adherent cell cultures

This work is carried out at the University College Cork (UCC, Ireland) in the group of Prof. Dmitri Papkovsky. They received magnetic nano- and microsensors with oxygen sensitive porphyrin complexes. The particles were designed to match the spectral requirements of the measurement setup currently available at the UCC. The group has experience in respirometric measurements of different cell lines with optical sensors and is currently evaluating the suitability of MOSePs for this type of investigation. The magnetism facilitates the fixation of the sensors on the cell surfaces. Nanoparticles might even allow intra-cellular measurements. According to Prof. Papkovsky, micro-MOSePs are currently evaluated with adherent cell cultures and the first results were promising.

Status

This topic is currently elaborated the UCC.

13 Applications of MOSePs in marine biology

An interesting application of MOSePs was developed together with Prof. Michael Kühl at the Marine Biology Laboratory (University of Copenhagen, Denmark). His group is specialized in the investigation of all types of aquatic microorganisms. The bigger size of some organisms living in marine cultures facilitates the application of magnetic sensors, because magnetic sensor particles of 10 to approximately 100 µm can be employed.

Recently, magnetic microparticles were used to investigate the oxygen production of a coral upon irradiation with light. Under the supervision of Prof. Michael Kühl, Jon Fabricius-Dyg developed a setup (figure 13.1) for these measurements during his bachelor thesis. A scleractinian coral (*Caulastrea furcata*) was fixed in a flow cell and illuminated with different light doses. By imaging the oxygen concentration with the help of micro-MOSePs and a lifetime imaging system, they were able to identify zones of different respiratory and photosynthetic activities. Exemplaric data is shown in figure 13.2 on the following page.

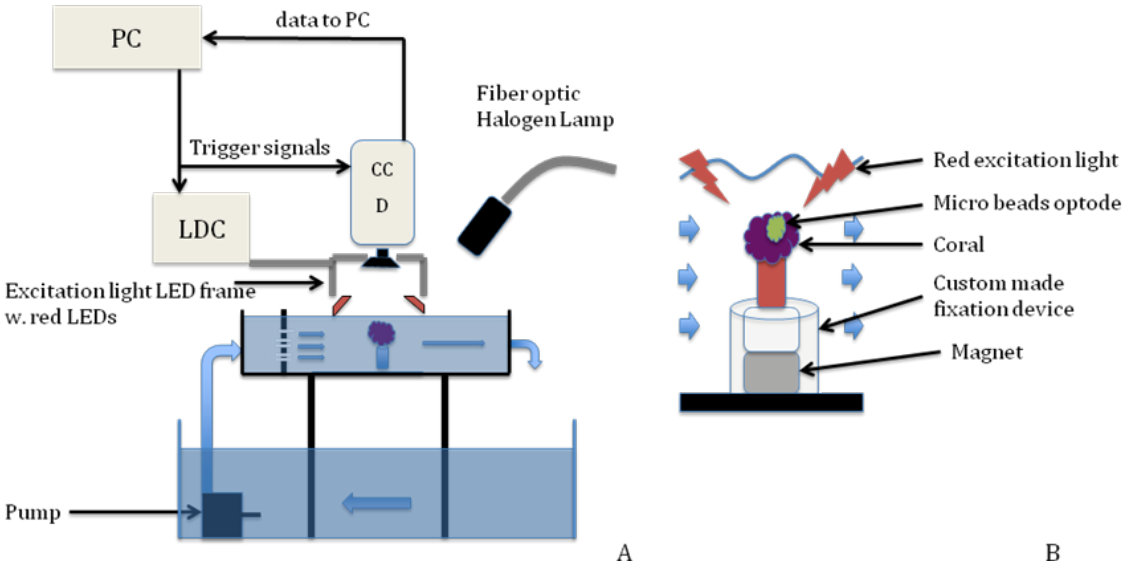

Figure 13.1: Setup for oxygen imaging on corals with MOSePs. Micrometer sized particles were attracted by a magnet under the coral. The oxygen concentration was determined by lifetime imaging of the oxygen sensitive dye in the MOSePs.

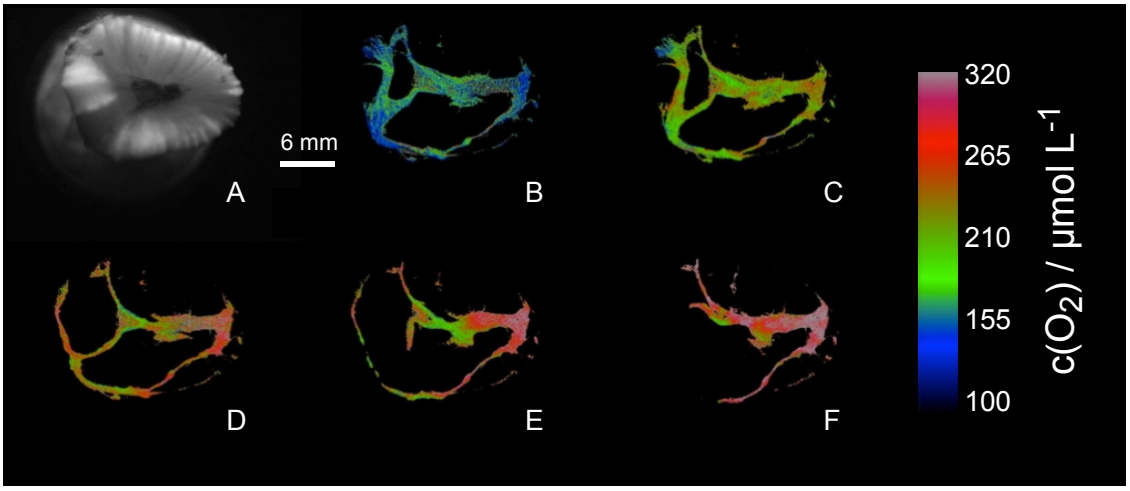

Figure 13.2: Oxygen imaging on an immobilized coral cell. Zones of different photosynthetic and respiratory activities can be seen in the oxygen images (B-F). The light doses were increased from B to F: 63, 149, 309, 596, 1229 µmol photons $m^{-2}\,s^{-1}$.

Status

A draft of a manuscript for a technical note in the journal "Marine Biology" is available.

14 Upcoming cooperations

14.1 Magnetic nanoparticles for facilitating single-particle surface plasmon resonance imaging

The cooperation with Dr. Alexander Zybin from the ISAS Dortmund (Germany) was established during this year's Europtrode conference in Prag. The working group of Dr. Zybin recently published interesting work on the detection of single nano-particles with an SPR imaging technique. Dr. Zybin is currently working with non-magnetic nanoparticles but expects a significant improvement of his technique by the application of magnetic polymer based nanoparticles. Preliminary experiments on the modification of nano-MOSePs with antibodies were carried out together with Dr. Andreas Winkler at the Institute of Biochemistry (Graz University of Technology) and showed promising results. However, further optimization of the binding parameters is required. The cooperation with Dr. Zybin might be a promising platform for employing the magnetic particles developed in our lab in applications other than optical sensing.

Status

A potential cooperation-strategy was discussed. Further details will be elaborated in an upcoming meeting.

14.2 Magnetic optical ion sensors

Due to the limited experience with ionsensors in our working group, we established a cooperation with one of the top researchers in this field, Prof. Eric Bakker. During a short research stay in his lab at the Nanochemistry Research Institute in Perth (Australia), I was introduced by Dr. Pengchao Si and Prof. Eric Bakker to the techniques available for the production of highly monodisperse, ionsensitive microparticles. Furthermore, I was able to incorporate magnetic nanoparticles in this type of sensors. The characterization of the resulting sensor particles is still in progress, but first results showed that the produced particles are both magnetic and ionsensitive.

Status

This cooperation will be continued at the University of Geneva, where I will join Prof. Bakkers new research group as postdoctoral fellow in August 2010.

15 Summary and conclusion

In summary, different magnetic optical sensor systems were developed during this thesis. In most cases, the application determins the required particle size. While nanoparticles are necessary for imaging with high spatial resolution and for certain *in vivo* applications, micrometer sized particles can be used for analyte monitoring with both fiber optical and imaging devices. Magnetic sensor macrospheres with diameters of up to 5 mm are strongly magnetic and follow any movement of a magentic separator in real-time.

The work during my thesis resulted in five first-author and four co-author publications in peer-reviewed journals, and seven oral presentations at conferences and in companies. This underlines the importance of the research in this field and attests the high quality of the work. The extensive literature search for the review article on applications and structures of luminescent magnetic particles (LuMaPs), also elucidated the increasing importance of this topic. The number of publications per year is still increasing. Research groups around the world try to solve biological and analytical problems by using magnetic luminescent multimodal imaging probes. Furthermore, the application of modified LuMaPs as nanotherapeutics is an especially promising field for future research. The combination of optical magnetic sensors with a drug delivery vehicle results in a device, which is capable of monitoring the organism's response to a drug *in situ*.

Part IV

Appendix

A Curriculum vitæ

Günter Mistlberger

Date of Birth	October 9, 1979
in	Wels, Upper Austria
Marriage Status	engaged
Nationality	Austrian
Current address	Schörgelgasse 9 8010 Graz Austria
Permanent address	Markt 12 4654 Bad Wimsbach-Nh. Austria g.mistlberger@gmail.com

Education	1994–1999	HTBLA for Chemical Engineering in Wels
	1999	A Levels (passed with distinction)

Employment

- Ferialjobs at the division of Research and Development at Biochemie Kundl (now Sandoz)
- Scientific co-worker at the Institute of Analytical Chemistry and Radiochemistry (Graz University of Technology)
- Students assistent at the Institute of Analytical Chemistry and Radiochemistry (Graz University of Technology)
- Scientific assistent at the Institute of Analytical Chemistry and Food Chemistry (Graz University of Technology)

Languages: German, English, Swedish (beginner), Spanish (beginner)

Studies

2000–2006	Master student in Chemical Engineering at Graz University of Technology.
2004–2005	ERASMUS - Exchange student in Lund (Sweden), Master thesis at the Department of Pure and Applied Biochemistry, Lund Institute of Technology (LTH), supervised by Prof. Dr. Bengt Danielsson

	and Prof. Dr. Ingo Klimant at Graz University of Technology. Topic: Probing lectin-carbohydrate interactions with atomic force microscopy - Modifications of surfaces and AFM-tips.
March 30, 2006	Diploma in Chemical Engeneering (passed with distinction)
2006–2010	PhD student in the sensor group at the Institute of Analytical Chemistry and Food Chemistry, Graz University of Technology. Supervisor: Prof. Dr. Ingo Klimant

Publications

Publications in peer reviewed journals

2010/1 Koren, K.; **Mistlberger, G.***; Aigner, D.; Borisov, S.; Zankel, A.; Pölt, P.; Klimant, I. *Characterization of micrometer-sized magnetic optical sensor particles produced via spray-drying*, Monatshefte für Chemie = Chemical monthly, **2010**, In press.

2010/2 Medina-Castillo, A. L.; **Mistlberger, G.***; Fernandez-Sanchez, J. F.*; Segura-Carretero, A.; Klimant, I.; Fernandez-Gutierrez, A. *Novel strategy to design magnetic, molecular imprinted polymers with well controlled structure for the application in optical sensors*, Macromolecules, **2010**, 43(1), 55–61.

2010/3 **Mistlberger, G.***; Koren, K.; Borisov, S. & Klimant, I. *Magnetically Remote-Controlled Optical Sensor Spheres for Monitoring Oxygen or pH*, Analytical Chemistry, **2010**, 82(5), 2124–2128.

2010/4 **Mistlberger, G.***; Koren, K.; Scheucher, E.; Aigner, D.; Borisov, S.; Zankel, A.; Pölt, P. & Klimant, I. *Multi-functional magnetic optical sensor particles with tunable sizes for monitoring metabolic parameters and as basis for nanotherapeutics*, Advanced Functional Materials, **2010**, In press

2010/5 **Mistlberger, G.*** & Klimant, I. *Luminescent Magnetic Particles: multimodal imaging (luminescence and MRI) and analytical applications*, Bioanalytical Reviews, **2010**, invited.

2009/1 **Mistlberger, G.***; Borisov, S. M. & Klimant, I. *Enhancing performance in optical sensing with magnetic nanoparticles*, Sensors and Actuators B: Chemical, **2009**, 139(1), 174–180.

2009/2 Mayr, T.*; Borisov, S.; Abel, T.; Enko, B.; Waich, K.; **Mistlberger, G.**; Klimant, I. *Light Harvesting as a Simple and Versatile Way to Enhance Brightness of Luminescent Sensors*, Analytical Chemistry, **2009**, 15, 6541–6545.

2009/3 Borisov, S.*; Mayr, T.; **Mistlberger, G.**; Waich, K.; Koren, K.; Chojnacki, P.; Klimant, I. *Precipitation as a simple and versatile*

method for preparation of optical nanochemosensors, Talanta, **2009**, 79(5), 1322–1330.

2008 **Mistlberger, G.***; Chojnacki, P. & Klimant, I. *Magnetic sensor particles: an optimized magnetic separator with an optical window*, Journal of Physics, D: Applied Physics, **2008**, 41(8), 085003.

2007 Chojnacki, P.; **Mistlberger, G.** & Klimant, I.* *Separable magnetic sensors for the optical determination of oxygen.*, Angewandte Chemie Int. Ed., **2007**, 46(46), 8850-8853.

Patents

2010/1 **Mistlberger, G.***; Wiesbauer, J.; Borisov, S.M.; Klimant, I. *Selbstreinigende Sensoren*, patent pending.

Oral presentations

2009/01 Koren, K.*; **Mistlberger, G.** & Klimant, I.: *Magnetic Sensor Spheres as Versatile Tools in Optical Sensing* Euroanalysis XV, Innsbruck, Austria, 2009

2009/02 Mayr, T.*; Abel, T.; Ungerböck, B.; Koren, K.; **Mistlberger, G.**; Borisov, S. & Klimant, I. *Optical Sensor for Microscale Devices* Society for General Microbiology - Meeting, Edingburgh, UK., 2009

2009/03 Mayr, T.*; Ungerböck, B.; **Mistlberger, G.**; Richter, L.; Charwat, V.; Ertl, P.; Klimant, I. *Optical sensors for bioprocess monitoring in microfluidic devices* International Graz Congress for Pharmaceutical Engineering, Graz, 17.09., 2009

2009/04 **Mistlberger, G.*** *Multi-functional magnetic optical sensor systems or "how to convert a boring experiment into an award-winning idea"* Austrian Chemistry Days, Vienna, Austria, 2009

2009/05 **Mistlberger, G.***; Koren, K.; Borisov, S. & Klimant, I. *Magnetic Sensor Macrospheres as Easy-to-Use, Remote-Controlled, Optical Sensors in Bioprocess Monitoring* IEEE Sensors Conference, Christchurch, New Zealand, 2009

2009/06 **Mistlberger, G.***; Koren, K.; Mayr, T.; Borisov, S. & Klimant, I. *Multifunctional Magnetic Optical Sensor Particles* International Graz Congress for Pharmaceutical Engineering, 2009

2008/05 Mayr, T.*; Zenkl, G.; **Mistlberger, G.**; Koren, K.; Borisov, S. & Klimant, I. *Nanometer sized sensor particles: Versatile tools for biotechnology and life science* NanoSens 2008, Wien, 29.09.08, 2008

2008/04 **Mistlberger, G.***; Koren, K.; Mayr, T.; Borisov, S. & Klimant, I. *Magnetic optical sensor particles: a versatile tool for bioprocess monitoring and life science.* Millipore Corp, R&D Seminary, Millipore Corp. / Boston, 26.06.08, 2008

2008/03 **Mistlberger, G*.**; Borisov, S. & Klimant, I. *Magnetic Optical Sensor Particles: A Versatile Tool for Life Science* Scientific and Clinical Applications of Magnetic Carriers, UBC, Vancouver, 20.05.08, 2008

2008/02 **Mistlberger, G.***; Chojnacki, P.; Borisov, S. & Klimant, I. *Magnetic Sensor Particles: A tool for 'in situ' sensor spot formation* Europtrode IX, Dublin, 30.03.08, 2008

2008/01 Staal, M. J.*; **Mistlberger, G.**; Borisov, S.; Rickelt, L. F.; Kühl, M. & Klimant, I. *3D oxygen imaging in microbial systems employing confocal microscopy and luminescent nano sensors* Europtrode IX, Dublin, 30.03.08, 2008

2007 **Mistlberger, G.***; Chojnacki, P. & Klimant, I. *Magnetically separable beads for optical chemosensing of dissolved oxygen and pH* ICMAT2007-International Conference on Materials for Advanced Technologies, Singapore, Suntec Convention Center, 01.07.07, 2007

Poster presentations

2010/01 Medina-Castillo, A. L.; **Mistlberger, G.**; Fernandez-Sanchez, J. F.; Segura-Carretero, A.; Klimant, I.; Fernandez-Gutierrez, A. *Novel strategy to design magnetic, molecular imprinted polymers with well controlled structure for the application in optical sensors* Europtrode X, Prague, Czech Republic, 2010

2010/02 Medina-Castillo, A. L.; **Mistlberger, G.**; Fernandez-Sanchez, J. F.; Segura-Carretero, A.; Klimant, I.; Fernandez-Gutierrez, A. *Magnetic nanoparticles prepared by miniemulsion-solvent-evaporation: a straightforward methodology to prepare O2 and pH-sensitive optical sensing films* Europtrode X, Prague, Czech Republic, 2010

2010/03 **Mistlberger, G.**; Koren, K.; Borisov, S.; Klimant, I. *Magnetically Remote-Controlled, Optical Sensor Macrospheres* Europtrode X, Prague, Czech Republic, 2010

2010/04 Scheucher, E.; **Mistlberger, G.**; Koren, K.; Borisov, S.; Zankel, A.; Pölt, P.; Klimant, I. *Magnetic optical sensor particles with tunable size and multifunctional shells* Europtrode X, Prague, 2010

2010/05 Ungerböck, B.; **Mistlberger, G.**; Klimant, I.; Mayr, T. *Oxygen Imaging in Microfluidic Devices with Integrated Sensors Applying Color Cameras* Europtrode X, Prague, Czech Republic, 2010

2009/01 Borisov, S.; Zenkl, G.; Mayr, T.; **Mistlberger, G.**; Klimant, I. *Advanced Luminescent Metal Complexes and their Application in Optical Sensing* MAF11, 11th Conference on Methods and Applications of Fluorescenc, 2009

2009/02 Koren, K.; **Mistlberger, G.** & Klimant, I. *Magnetic sensor macrospheres as versatile tools for optical sensing and process monitoring*

	International Graz Congress for Pharmaceutical Engineering, Graz, Austria, 2009
2009/03	Koren, K.; **Mistlberger, G.**; Zankel, A.; Pölt, P. & Klimant, I. *Characterization of highly versatile micrometer sized sensor particles using different microscopical techniques* Microscopy 2009, Graz, 2009
2009/04	**Mistlberger, G.**; Koren, K. & Klimant, I. *Synthesis and application of magnetic optical sensor systems from "nano-" to "macro-" scale* MAF 11, 11th Conference on Methods and Applications of Fluorescence, Budapest, Hungary, 2009
2009/05	**Mistlberger, G.**; Koren, K. & Klimant, I. *Magnetic optical sensor systems in life science* Austrian Chemistry Days, Vienna, Austria, 2009
2009/06	**Mistlberger, G.**; Koren, K.; Zenkl, G.; Mayr, T.; Zankel, A.; Pölt, P.; Borisov, S. & Klimant, I. *Production and application of polymeric nanoparticles for the optical determination of physiological parameters* Microscopy 2009, Graz, 2009
2008	**Mistlberger, G.**; Koren, K. & Klimant, I. *Multi-functional magnetic optical sensor particles* Gordon Research Conference on Bioanalytical Sensors, Bryant University, Boston, MA, USA, 2008
2007	**Mistlberger, G.** & Klimant, I. *Optimized magnetic separation of chemically sensitive microspheres* ICMAT2007-International Conference on Materials for Advanced Technologies, Singapore, Suntec Convention Center, 2007

Internships and cooperations

2009	Internship for two weeks at the Nanochemistry Research Institute (Perth, Australia) supervised by Prof. Dr. Eric Bakker. Topic: Production of magnetic ion sensor particles.
2008	Internship for 1.5 months at the Analytical Chemistry department (University of Granada) supported by the program "Acciones Integradas 2007-2008, Project No. ES 13/2007". Topic: Synthesis and characterization of magnetic, molecular imprinted optical sensor particles and novel magnetic nano materials for sensing applications.
2007	Internship for two weeks at the Institute of Marine Biology (University of Copenhagen, Helsingborg, Denmark) supervised by Prof. Dr. Michael Kühl. Topic: 3D-oxygen-imaging in biological samples

Awards

2009/01	Winner of the "idea-storm-competition" presented by the Science Park Graz. The presented idea was ranked No. 1 out of over 100 competitors.

2009/02	Best Student Paper Award (runner up) presented by the IEEE Sensors Council during the IEEE Sensors conference in Christchurch, New Zealand.
2009/03	Best Poster Award for the poster with the title "Magnetic optical sensor systems in life science" presented by the Austrian Chemical Society at the Austrian Chemistry Days in Vienna.
2008	Winner of the price for the best group work at the "ASCOS Advanced Study Course on Optical Chemical Sensors 2008".
2007	Best Poster Award for the poster with the title "Optimized magnetic separation of chemically sensitive microspheres", presented by the MRS Material Research Society in Singapore at the ICMAT conference.

Graz, April 20, 2010

B List of Figures

C List of Tables

D Bibliography

[1] H. Baharvand. *Journal of Applied Polymer Science*, 109(3):1823–1828, 2008.

[2] P. Chojnacki, G. Mistlberger, and I. Klimant. *Angewandte Chemie (International Ed. in English)*, 46(46):8850–8853, 2007.

[3] J. Guo, C. Wang, W. Mao, W. Yang, C. Liu, and J. Chen. *Nanotechnology*, 19(31), 2008.

[4] V. Holzapfel, M. Lorenz, C. K. Weiss, H. Schrezenmeier, K. Landfester, and V. Mailaender. *Journal Of Physics – Condensed Matter*, 18(38, Sp. Iss. SI):S2581–S2594, 2006.

[5] J. Kim, J. Lee, J. Lee, J. Yu, B. Kim, K. An, Y. Hwang, C. Shin, J. Park, J. Kim, and T. Hyeon. *Journal of the American Chemical Society*, 128(3):688–689, 2006.

[6] J. Kim, J. E. Lee, S. H. Lee, J. H. Yu, J. H. Lee, T. G. Park, and T. Hyeon. *Advanced Materials*, 20(3):478+, 2008.

[7] H.-J. Kim, K.-J. Shin, M. K. Han, K. An, J.-K. Lee, I. Honma, and H. Kim. *Scripta Materialia*, 61(12):1137–1140, 2009.

[8] R. Kopelman, Y.-E. Lee Koo, M. Philbert, B. A. Moffat, G. Ramachandra Reddy, P. McConville, D. E. Hall, T. L. Chenevert, M. S. Bhojani, S. M. Buck, A. Rehemtulla, and B. D. Ross. *Journal of Magnetism and Magnetic Materials*, 293(1):404–410, 2005.

[9] L. Li, D. Chen, Y. Zhang, Z. Deng, X. Ren, X. Meng, F. Tang, J. Ren, and L. Zhang. *Nanotechnology*, 18(40), 2007.

[10] X. Li, L. Wang, C. Zhou, T. Guan, J. Li, and Y. Zhang. *Clinica Chimica Acta*, 378 (1-2):168–174, 2007.

[11] L. Li, C.-K. Tsung, T. Ming, Z. Sun, W. Ni, Q. Shi, G. D. Stucky, and J. Wang. *Advanced Functional Materials*, 18(19):2956–2962, 2008.

[12] J. Liu, Y. Zhang, T. Yang, Y. Ge, S. Zhang, Z. Chen, and N. Gu. *Journal of Applied Polymer Science*, 113(6):4042–4051, 2009.

[13] G. Mistlberger, P. Chojnacki, and I. Klimant. *Journal of Physics D: Applied Physics*, 41(8):085003 (9pp), 2008.

[14] G. Mistlberger, S. M. Borisov, and I. Klimant. *Sensors and Actuators, B: Chemical*, 139(1):174 – 180, 2009.

[15] G. Mistlberger, K. Koren, E. Scheucher, D. Aigner, S. M. Borisov, A. Zankel, P. Pölt, and I. Klimant. *Advanced Functional Materials*, In Press, 2010.

[16] K. Ozawa and K. Ishii. *Physical Chemistry Chemical Physics*, 11(7):1019–1022, 2009.

[17] T. Sathe, A. Agrawal, and S. Nie. *Analytical Chemistry*, 78(16):5627–5632, 2006.

[18] J. E. Smith, C. D. Medley, Z. Tang, D. Shangguan, C. Lofton, and W. Tan. *Analytical Chemistry*, 79(8):3075–3082, 2007.

[19] W. Tan and Y. Zhang. *Advanced Materials*, 17(19):2375+, 2005.

[20] C. Tu, Y. Yang, and M. Gao. *Nanotechnology*, 19(10), 2008.

[21] G. Wang, E. Song, H. Xie, Z. Zhang, Z. Tian, C. Zuo, D. Pang, D. Wu, and Y. Shi. *Chemical Communications*, (34):4276–4278, 2005.

[22] L. Wang and J. Sun. *Journal of Materials Chemistry*, 18(34):4042–4049, 2008.

[23] G. Wang, C. Wang, W. Dou, Q. Ma, P. Yuan, and X. Su. *Journal of Fluorescence*, 19(6):939–946, 2009.

[24] J. Wu, Z. Ye, G. Wang, and J. Yuan. *Talanta*, 72(5):1693–1697, 2007.

[25] H. Xie, C. Zuo, Y. Liu, Z. Zhang, D. Pang, X. Li, J. Gong, C. Dickinson, and W. Zhou. *Small*, 1(5):506–509, 2005.

[26] M. Xie, J. Hu, Y.-M. Long, Z.-L. Zhang, H.-Y. Xie, and D.-W. Pang. *Biosensors & Bioelectronics*, 24(5, Sp. Iss. SI):1311–1317, 2009.

[27] C. H. Yang, K. S. Huang, Y. S. Lin, K. Lu, C. C. Tzeng, E. C. Wang, C. H. Lin, W. Y. Hsu, and J. Y. Chang. *Lab on a Chip*, 9(7):961–965, 2009.

[28] P. Zhang, H. Dou, W. Li, K. Tao, B. Xing, and K. Sun. *Chemistry Letters*, 36(12): 1458–1459, 2007.

[29] B. Zhang, J. Cheng, X. Gong, X. Dong, X. Liu, G. Ma, and J. Chang. *Journal of Colloid and Interface Science*, 322(2):485–490, 2008.

[30] H. Yan, J. C. Zhang, B. W. Yu, and Y. Shen. *Acta Materialia*, 58(2):726–733, 2010.

[31] D. Thakur, S. Deng, T. Baldet, and J. O. Winter. *Nanotechnology*, 20(48), 2009.

[32] J. N. Anker and R. Kopelman. *Applied Physics Letters*, 82(7):1102–1104, 2003.

[33] J. N. Anker, C. J. Behrend, H. Huang, and R. Kopelman. *Journal of Magnetism and Magnetic Materials*, 293(1):655–662, 2005.

[34] C. Behrend, J. Anker, B. McNaughton, M. Brasuel, M. Philbert, and R. Kopelman. *Journal of Physical Chemistry B*, 108(29):10408–10414, 2004.

[35] T. G. Roberts, J. N. Anker, and R. Kopelman. *Journal of Magnetism and Magnetic Materials*, 293(1):715–724, 2005.

[36] R. He, X. You, J. Shao, F. Gao, B. Pan, and D. Cui. *Nanotechnology*, 18(31), 2007.

[37] L. Levy, Y. Sahoo, K. Kim, E. J. Bergey, and P. N. Prasad. *Chemistry of Materials*, 14(9):3715–3721, 2002.

[38] H. Lu, G. Yi, S. Zhao, D. Chen, L. Guo, and J. Cheng. *Journal of Materials Chemistry*, 14(8):1336–1341, 2004.

[39] Z. Y. Ma, D. Dosev, M. Nichkova, S. J. Gee, B. D. Hammock, and I. M. Kennedy. *Journal of Materials Chemistry*, 19(27):4695–4700, 2009.

[40] G. Qiu, Y. Xu, B. Zhu, and G. Oiu. *Biomacromolecules*, 6(2):1041–1047, 2005.

[41] S. Santra, H. Yang, P. H. Holloway, J. T. Stanley, and R. A. Mericle. *Journal of the American Chemical Society*, 127(6):1656–1657, 2005.

[42] D. K. Yi, S. T. Selvan, S. S. Lee, G. C. Papaefthymiou, D. Kundaliya, and J. Y. Ying. *Journal of the American Chemical Society*, 127(14):4990–4991, 2005.

[43] S. T. Selvan, P. Patra, C. Ang, and J. Ying. *Angewandte Chemie International Edition*, 46(14):2448–2452, 2007.

[44] Y. Sahoo, A. Goodarzi, M. Swihart, T. Ohulchanskyy, N. Kaur, E. Furlani, and P. Prasad. *Journal of Physical Chemistry B*, 109(9):3879–3885, 2005.

[45] D. Wang, J. He, N. Rosenzweig, and Z. Rosenzweig. *Nano Letters*, 4(3):409–413, 2004.

[46] Y. Lalatonne, C. Paris, J. M. Serfaty, P. Weinmann, M. Lecouvey, and L. Motte. *Chemical Communications*, (22):2553–2555, 2008.

[47] O. Veiseh, C. Sun, J. Gunn, N. Kohler, P. Gabikian, D. Lee, N. Bhattarai, R. Ellenbogen, R. Sze, A. Hallahan, J. Olson, and M. Zhang. *Nano Letters*, 5(6):1003–1008, 2005.

[48] H. Kim, M. Achermann, L. P. Balet, J. A. Hollingsworth, and V. I. Klimov. *Journal of the American Chemical Society*, 127(2):544–546, 2005.

[49] M. Nichkova, D. Dosev, S. J. Gee, B. D. Hammock, and I. M. Kennedy. *Analytical Biochemistry*, 369(1):34–40, 2007.

[50] T. Zhou, M. Lu, Z. Zhang, H. Gong, W. S. Chin, and B. Liu. *Advanced Materials*, 22(3):403, 2010.

[51] P. Yang, M. Ando, and N. Murase. *New Journal of Chemistry*, 33(7):1457–1461, 2009.

[52] M. Zhang, S. Shi, J. Meng, X. Wang, H. Fan, Y. Zhu, X. Wang, and Y. Qian. *Journal Of Physical Chemistry C*, 112(8):2825–2830, 2008.

[53] S. Buathong, D. Ung, T. J. Daou, C. Ulhaq-Bouillet, G. Pourroy, D. Guillon, L. Ivanova, I. Bernhardt, S. Begin-Colin, and B. Donnio. *Journal Of Physical Chemistry C*, 113(28):12201–12212, 2009.

[54] Y. Deng, C. Wang, X. Shen, W. Yang, L. Jin, H. Gao, and S. Fu. *Chemistry A European Journal*, 11(20):6006–6013, 2005.

[55] M. Funovics, X. Montet, F. Reynolds, R. Weissleder, and L. Josephson. *Neoplasia (New York, N.Y.)*, 7(10):904–911, 2005.

[56] L. Stelter, J. G. Pinkernelle, R. Michel, R. Schwartlaender, N. Raschzok, M. H. Morgul, M. Koch, T. Denecke, J. Ruf, H. Baeumler, A. Jordan, B. Hamm, I. M. Sauer, and U. Teichgraeber. *Molecular Imaging and Biology*, 12(1):25–34, 2010.

[57] K. M. L. Taylor, W. J. Rieter, and W. Lin. *Journal of the American Chemical Society*, 130(44):14358–14359, 2008.

[58] N. Nitin, L. LaConte, O. Zurkiya, X. Hu, and G. Bao. *Journal of Biological Inorganic Chemistry*, 9(6):706–712, 2004.

[59] M. Chu, X. Song, D. Cheng, S. Liu, and J. Zhu. *Nanotechnology*, 17(13):3268–3273, 2006.

[60] B. Liu, D. Wang, W. Huang, M. Yu, and A. Yao. *Materials Research Bulletin*, 43 (11):2904–2911, 2008.

[61] P. Sun, H. Zhang, C. Liu, J. Fang, M. Wang, J. Chen, J. Zhang, C. Mao, and S. Xu. *Langmuir*, 26(2):1278–1284, 2010.

[62] S. Wu, Y. Lin, Y. Hung, Y. Chou, Y. Hsu, C. Chang, and C. Mou. *ChemBioChem*, 9(1):53–57, 2008.

[63] J. Yang, J. Lee, J. Kang, C.-H. Chung, K. Lee, J.-S. Suh, H.-G. Yoon, Y.-M. Huh, and S. Haam. *Nanotechnology*, 19(7), 2008.

[64] T. Yoon, J. Kim, B. Kim, K. Yu, M. Cho, and J. Lee. *Angewandte Chemie, International Edition*, 44(7):1068–1071, 2005.

[65] Y. Zhang, S.-N. Wang, S. Ma, J.-J. Guan, D. Li, X.-D. Zhang, and Z.-D. Zhang. *Journal Of Biomedical Materials Research Part A*, 85A(3):840–846, 2008.

[66] J. Kim, H. S. Kim, N. Lee, T. Kim, H. Kim, T. Yu, I. C. Song, W. K. Moon, and T. Hyeon. *Angewandte Chemie, International Edition*, 47(44):8438–8441, 2008.

[67] B. Liu, W. Xie, D. Wang, W. Huang, M. Yu, and A. Yao. *Materials Letters*, 62 (17-18):3014–3017, 2008.

[68] X. Huang, J. Zhuang, D. Chen, H. Liu, F. Tang, X. Yan, X. Meng, L. Zhang, and J. Ren. *Langmuir*, 25(19):11657–11663, 2009.

[69] J. H. Jang and H. B. Lim. *Microchemical Journal*, 94(2):148–158, 2010.

[70] D. Ma, J. Guan, S. Dénommée, G. Enright, T. Veres, and B. Simard. *Chemistry of Materials*, 18(7):1920–1927, 2006.

[71] C. Ren, J. Li, Q. Liu, J. Ren, X. Chen, Z. Hu, and D. Xue. *Nanoscale Research Letters*, 3(12):496–501, 2008.

[72] Q. Wang, Y. Liu, C. Lin, and H. Yan. *Nanotechnology*, 18(40), 2007.

[73] L. Zhang, B. Liu, and S. Dong. *Journal of Physical Chemistry B*, 111(35):10448–10452, 2007.

[74] M. Liong, J. Lu, M. Kovochich, T. Xia, S. G. Ruehm, A. E. Nel, F. Tamanoi, and J. I. Zink. *ACS NANO*, 2(5):889–896, 2008.

[75] Y. Ichiyanagi, S. Moritake, S. Taira, and M. Setou. *Journal of Magnetism and Magnetic Materials*, 310(2, Part 3):2877–2879, 2007.

[76] A. Abou-Hassan, R. Bazzi, and V. Cabuil. *Angewandte Chemie (International Ed. in English)*, 48(39):7180–7183, 2009.

[77] J.-L. Bridot, A.-C. Faure, S. Laurent, C. Rivière, C. Billotey, B. Hiba, M. Janier, V. Josserand, J.-L. Coll, L. V. Elst, R. Muller, S. Roux, P. Perriat, and O. Tillement. *Journal of the American Chemical Society*, 129(16):5076–5084, 2007.

[78] J.-L. Bridot, D. Dayde, C. Riviere, C. Mandon, C. Billotey, S. Lerondel, R. Sabattier, G. Cartron, A. Le Pape, G. Blondiaux, M. Janier, P. Perriat, S. Roux, and O. Tillement. *Journal of Materials Chemistry*, 19(16):2328–2335, 2009.

[79] O. Ergeneman, G. Dogangil, M. Kummer, J. Abbott, M. Nazeeruddin, and B. Nelson. *IEEE Sensors Journal*, 8(1):29–37, 2008.

[80] G. Mistlberger, K. Koren, S. M. Borisov, and I. Klimant. *Analytical Chemistry*, 82 (5):2124–2128, 2010.

[81] A.-C. Faure, S. Dufort, V. Josserand, P. Perriat, J.-L. Coll, S. Roux, and O. Tillement. *Small*, 5(22):2565–2575, 2009.

[82] Y. Ge, Y. Zhang, S. He, F. Nie, G. Teng, and N. Gu. *Nanoscale Research Letters*, 4 (4):287–295, 2009.

[83] A. T. Heitsch, D. K. Smith, R. N. Patel, D. Ress, and B. A. Korgel. *Journal of Solid State Chemistry*, 181(7):1590–1599, 2008.

[84] C.-W. Lai, Y.-H. Wang, C.-H. Lai, M.-J. Yang, C.-Y. Chen, P.-T. Chou, C.-S. Chan, Y. Chi, Y.-C. Chen, and J.-K. Hsiao. *Small*, 4(2):218–224, 2008.

[85] Z. Liu, G. Yi, H. Zhang, J. Ding, Y. Zhang, and J. Xue. *Chemical Communications*, (6):694–696, 2008.

[86] Y. Lu, Y. Yin, B. Mayers, and Y. Xia. *Nano Letters*, 2(3):183–186, 2002.

[87] C. Lu, Y. Hung, J. Hsiao, M. Yao, T. Chung, Y. Lin, S. Wu, S. Hsu, H. Liu, C. Mou, C. Yang, D. Huang, and Y. Chen. *Nano Letters*, 7(1):149–154, 2007.

[88] K. M. Yeo, C. J. Gao, K.-H. Ahn, and I. S. Lee. *Chemical Communications*, (38): 4622–4624, 2008.

[89] T. Yoon, K. Yu, E. Kim, J. Kim, B. Kim, S. Yun, B. Sohn, M. Cho, J. Lee, and S. Park. *Small*, 2(2):209–215, 2006.

[90] J. Kim, J. E. Lee, J. Lee, Y. Jang, S.-W. Kim, K. A. an, H. H. Yu, and T. Hyeon. *Angewandte Chemie, International Edition*, 45(29):4789–4793, 2006.

[91] N. Insin, J. B. Tracy, H. Lee, J. P. Zimmer, R. M. Westervelt, and M. G. Bawendi. *ACS NANO*, 2(2):197–202, 2008.

[92] Y. Maeda, T. Yoshino, and T. Matsunaga. *Journal of Materials Chemistry*, 19(35): 6361–6366, 2009.

[93] B. Fernandez, N. Galvez, R. Cuesta, A. B. Hungria, J. J. Calvino, and J. M. Dominguez-Vera. *Advanced Functional Materials*, 18(24):3931–3935, 2008.

[94] J. Gao, W. Zhang, P. Huang, B. Zhang, X. Zhang, and B. Xu. *Journal of the American Chemical Society*, 130(12):3710+, 2008.

[95] H. Gu, R. Zheng, X. Zhang, and B. Xu. *Journal of the American Chemical Society*, 126(18):5664–5665, 2004.

[96] S.-H. Hu, K.-T. Kuo, W.-L. Tung, D.-M. Liu, and S.-Y. Chen. *Advanced Functional Materials*, 19(21):3396–3403, 2009.

[97] D. Ma, Z. J. Jakubek, and B. Simard. *Journal of Nanoscience and Nanotechnology*, 6(12):3677–3684, 2006.

[98] Q. Chang, L. Zhu, C. Yu, and H. Tang. *Journal of Luminescence*, 128(12):1890–1895, 2008.

[99] X. Hong, J. Li, M. Wang, J. Xu, W. Guo, J. Li, Y. Bai, and T. Li. *Chemistry of Materials*, 16(21):4022–4027, 2004.

[100] H. Liu, J. Guo, L. Jin, W. Yang, and C. Wang. *Journal of Physical Chemistry B*, 112(11):3315–3321, 2008.

[101] O. Kreft, A. M. Javier, G. B. Sukhorukov, and W. J. Parak. *Journal of Materials Chemistry*, 17(42):4471–4476, 2007.

[102] J. Guo, W. Yang, Y. Deng, C. Wang, and S. Fu. *Small*, 1(7):737–743, 2005.

[103] N. Gaponik, I. Radtchenko, G. Sukhorukov, and A. Rogach. *Langmuir*, 20(4): 1449–1452, 2004.

[104] L. Li, H. Li, D. Chen, H. Liu, F. Tang, Y. Zhang, J. Ren, and Y. Li. *Journal of Nanoscience and Nanotechnology*, 9(4):2540–2545, 2009.

[105] O. Kreft, M. Prevot, H. Möhwald, and G. Sukhorukov. *Angewandte Chemie International Edition*, 46(29):5605–5608, 2007.

[106] B.-S. Kim and T. A. Taton. *Langmuir*, 23(4):2198–2202, 2007.

[107] Y. T. Lim, J. K. Kim, Y.-W. Noh, M. Y. Cho, and B. H. Chung. *Small*, 5(3): 324–328, 2009.

[108] S. Yang, H. Liu, and Z. Zhang. *New Journal of Chemistry*, 33(3):620–625, 2009.

[109] Z. Wang, L. Wu, M. Chen, and S. Zhou. *Journal of the American Chemical Society*, 131(32):11276+, 2009.

[110] B. Zebli, A. S. Susha, G. B. Sukhorukov, A. L. Rogach, and W. J. Parak. *Langmuir*, 21(10):4262–4265, 2005.

[111] V. Roullier, F. Grasset, F. Boulmedais, F. Artzner, O. Cador, and V. Marchi-Artzner. *Chemistry of Materials*, 20(21):6657–6665, 2008.

[112] S. Mandal, N. Lequeux, B. Rotenberg, M. Tramier, J. Fattaccioli, J. Bibette, and B. Dubertret. *Langmuir*, 21(9):4175–4179, 2005.

[113] K. Vuu, J. Xie, M. McDonald, M. Bernardo, F. Hunter, Y. Zhang, K. Li, M. Bednarski, and S. Guccione. *Bioconjugate Chemistry*, 16(4):995–999, 2005.

[114] M. Lansalot, M. Sabor, A. Elaissari, and C. Pichot. *Colloid and Polymer Science*, 283(12):1267–1277, 2005.

[115] P. A. Jarzyna, T. Skajaa, A. Gianella, D. P. Cormode, D. D. Samber, S. D. Dickson, W. Chen, A. W. Griffioen, Z. A. Fayad, and W. J. M. Mulder. *Biomaterials*, 30(36): 6947–6954, 2009.

[116] J.-H. Lee, Y.-W. Jun, S.-I. Yeon, J.-S. Shin, and J. Cheon. *Angewandte Chemie (International Ed. in English)*, 45(48):8160–8162, 2006.

[117] W. J. Rieter, J. Kim, K. Taylor, H. An, W. Lin, T. Tarrant, and W. Lin. *Angewandte Chemie International Edition*, 46(20):3680–3682, 2007.

[118] R. Koole, M. M. van Schooneveld, J. Hilhorst, K. Castermans, D. P. Cormode, G. J. Strijkers, C. d. M. Donega, D. Vanmaekelbergh, A. W. Griffioen, K. Nicolay, Z. A. Fayad, A. Meijerink, and W. J. M. Mulder. *Bioconjugate Chemistry*, 19(12): 2471–2479, 2008.

[119] F. Bertorelle, C. Wilhelm, J. Roger, F. Gazeau, C. Menager, and V. Cabuil. *Langmuir*, 22(12):5385–5391, 2006.

[120] J. LeFort. *Comptes Rendus de l'Académie des sciences*, 34:480, 1852.

[121] W. C. Elmore. *Physical Review*, 54(4):309, 1938.

[122] R. Massart. *IEEE Transactions on Magnetics*, 17(2):1247 – 1248, 1981.

[123] U. Schwertmann and R. M. Cornell. *Iron Oxides in the Laboratory: Preparation and Characterization*. Wiley-VCH, 2 edition, 2000.

[124] H. Zhao, K. Saatchi, and U. O. Häfeli. *Journal of Magnetism and Magnetic Materials*, 321(10):1356–1363, 2009.

[125] Q. Pankhurst, J. Connolly, S. Jones, and J. Dobson. *Journal of Physics D: Applied Physics*, 36(13):R167–R181, 2003.

[126] A. Quarta, R. D. Corato, L. Manna, A. Ragusa, and T. Pellegrino. *IEEE Transactions on NanoBioscience*, 6(4):298–308, 2007.

[127] C. Fang and M. Zhang. *Journal of Materials Chemistry*, 19(35):6258–6266, 2009.

[128] A. D. Lehmann, W. J. Parak, F. Zhang, Z. Ali, C. Röcker, G. U. Nienhaus, P. Gehr, and B. Rothen-Rutishauser. *Small*, 9999(9999):NA, 2010.

[129] K. Lee, H.-Y. Moon, C. Park, O. R. Kim, E. Ahn, S. Y. Lee, H. E. Park, S.-H. Ihm, K.-B. Seung, K. Chang, T.-J. Yoon, C. Lee, C. Cheong, and K. S. Hong. *Current Applied Physics*, 9(Sp. Iss. SI Suppl. 1):S15–S18, 2009.

[130] J. Gao, G. Liang, B. Zhang, Y. Kuang, X. Zhang, and B. Xu. *Journal of the American Chemical Society*, 129(5):1428–1433, 2007.

[131] J. H. Choi, F. T. Nguyen, P. W. Barone, D. A. Heller, A. E. Moll, D. Patel, S. A. Boppart, and M. S. Strano. *Nano Letters*, 7(4):861–867, 2007.

[132] D. Dosev, M. Nichkova, R. K. Dumas, S. J. Gee, B. D. Hammock, K. Liu, and I. M. Kennedy. *Nanotechnology*, 18(5), 2007.

[133] K. M. L. Taylor, A. Jin, and W. Lin. *Angewandte Chemie International Edition*, 47 (40):7722–7725, 2008.

[134] N. Galvez, B. Fernandez, P. Sanchez, J. Morales-Sanfrutos, F. Santoyo-Gonzalez, R. Cuesta, R. Bermejo, M. Clemente-Leon, E. Coronado, A. Soriano-Portillo, and J. M. Dominguez-Vera. *Solid State Sciences*, 11(4):754–759, 2009.

[135] M. F. Kircher, U. Mahmood, R. S. King, R. Weissleder, and L. Josephson. *Cancer Research*, 63(23):8122–8125, 2003.

[136] J. N. Anker, Y.-E. Koo, and R. Kopelman. *Sensors and Actuators B: Chemical*, 121 (1):83–92, 2007.

[137] Z.-L. Chen, Y. Sun, P. Huang, X.-X. Yang, and X.-P. Zhou. *Nanoscale Research Letters*, 4(5):400–408, 2009.

[138] H. Gu, K. Xu, Z. Yang, C. K. Chang, and B. Xu. *Chemical Communications*, (34): 4270–4272, 2005.

[139] X. Michalet, F. Pinaud, L. Bentolila, J. Tsay, S. Doose, J. Li, G. Sundaresan, A. Wu, S. Gambhir, and S. Weiss. *Science*, 307(5709):538–544, 2005.

[140] S. Mulvaney, H. Mattoussi, and L. Whitman. *BioTechniques*, 36(4):602+, 2004.

[141] P. Yang, Z. Quan, Z. Hou, C. Li, X. Kang, Z. Cheng, and J. Lin. *Biomaterials*, 30 (27):4786–4795, 2009.

[142] S. Gai, P. Yang, C. Li, W. Wang, Y. Dai, N. Niu, and J. Lin. *Advanced Functional Materials*, pages NA–NA, 2010.

[143] Y. I. Park, J. H. Kim, K. T. Lee, K. Jeon, H. B. Na, J. H. Yu, H. M. Kim, N. Lee, S. H. Choi, S. Baik, H. Kim, S. P. Park, B. Park, Y. W. Kim, S. H. Lee, S. Yoon, I. C. Song, W. K. Moon, Y. D. Suh, and T. Hyeon. *Advanced Materials*, 21(44): 4467–4471, 2009.

[144] A. Kumar, P. K. Jena, S. Behera, R. F. Lockey, S. Mohapatra, and S. Mohapatra. *Nanomedicine: Nanotechnology, Biology and Medicine*, 6(1):64–69, 2010.

[145] S. Dubus, J. Gravel, B. L. Drogoff, P. Nobert, T. Veres, and D. Boudreau. *Analytical Chemistry*, 78(13):4457–4464, 2006.

[146] M. Liong, S. Angelos, E. Choi, K. Patel, J. F. Stoddart, and J. I. Zink. *Journal of Materials Chemistry*, 19(35):6251–6257, 2009.

[147] K. Patel, S. Angelos, W. R. Dichtel, A. Coskun, Y. Yang, J. I. Zink, and J. F. Stoddart. *Journal of the American Chemical Society*, 130(8):2382–2383, 2008.

[148] S. Saha, K. Leung, T. Nguyen, J. Stoddart, and J. Zink. *Advanced Functional Materials*, 17(5):685–693, 2007.

[149] S. Angelos, E. Choi, F. Vögtle, L. D. Cola, and J. I. Zink. *The Journal of Physical Chemistry C*, 111(18):6589–6592, 2007.

[150] C. Ren, J. Sun, Y. Zhang, X. Chen, and Z. Hu. *Journal of Nanoscience and Nanotechnology*, 9(4):2664–2670, 2009.

[151] T. Mayr, C. Moser, and I. Khmant. *Analytica Chimica Acta*, 597(1):137–144, 2007.

[152] C. Moser, T. Mayr, and I. Klimant. *Analytica Chimica Acta*, 558(1-2):102–109, 2006.

[153] E. Schellenberger, F. Rudloff, C. Warmuth, M. Taupitz, B. Hamm, and J. Schnorr. *Bioconjugate Chemistry*, 19(12):2440–2445, 2008.

[154] G. H. Du, Z. L. Liu, Q. H. Lu, X. Xia, L. H. Jia, K. L. Yao, Q. Chu, and S. M. Zhang. *Nanotechnology*, 17(12):2850–2854, 2006.

[155] T. Rajh, L. X. Chen, K. Lukas, T. Liu, M. C. Thurnauer, and D. M. Tiede. *The Journal of Physical Chemistry B*, 106(41):10543–10552, 2002.

[156] S. A. Corr, A. O. Byrne, Y. K. Gun'ko, S. Ghosh, D. F. Brougham, S. Mitchell, Y. Volkov, and A. Prina-Mello. *Chemical Communications*, (43):4474–4476, 2006.

[157] Y.-S. Lin and C. L. Haynes. *Chemistry of Materials*, 21(17):3979–3986, 2009.

[158] Z. Zhang, S. Chen, and S. Jiang. *Biomacromolecules*, 7(12):3311–3315, 2006.

[159] S. Chen and S. Jiang. *Advanced Materials*, 20(2):335–338, 2008.

[160] Y. Namba, M. Usami, and O. Suzuki. *Analytical Sciences*, 15(11):1087–1093, 1999.

[161] A. Wellman and M. Sepaniak. *Analytical Chemistry*, 78(13):4450–4456, 2006.

[162] Z. Li, B. Tan, M. Allix, A. I. Cooper, and M. J. Rosseinsky. *Small*, 4(2):231–239, 2008.

[163] Y. S. Kim, B. C. Kim, J. H. Lee, J. Kim, and M. B. Gu. *Biotechnology and Bioprocess Engineering*, 11(5):449–454, 2006.

[164] A. Danielli, A. Arie, N. Porat, and M. Ehrlich. *Optics Express*, 16(23):19253–19259, 2008.

[165] 2010. URL http://www.bangslabs.com/products/fluorescent_microspheres.

[166] URL http://www.chemicell.com/products/fluorescent/index.html.

[167] URL http://www.magnamedics.com/index.php/magsi-fluor.

[168] URL http://www.micromod.de.

[169] URL http://www.polysciences.com.

[170] URL http://www.spherotech.com/fluor_mag_par.htm.

[171] Y. Okamoto, F. Kitagawa, and K. Otsuka. *Analytical Chemistry*, 79(8):3041–3047, 2007.

[172] Y. Yeung and K. Wittrup. *Biotechnology Progress*, 18(2):212–220, 2002.

[173] A. Elaissari. *Colloidal Polymers*. Marcel Dekker, 1 edition, 2003.

[174] W. Stöber, A. Fink, and E. Bohn. *Journal of Colloid and Interface Science*, 26(1): 62–69, 1968.

[175] R. Wilson, D. G. Spiller, I. A. Prior, R. Bhatt, and A. Hutchinson. *Journal of Materials Chemistry*, 17(41):4400–4406, 2007.

[176] R. Wilson, D. G. Spiller, I. A. Prior, K. J. Veltkamp, and A. Hutchinson. *ACS Nano*, 1(5):487–493, 2007.

[177] L. Li, E. S. G. Choo, Z. Liu, J. Ding, and J. Xue. *Chemical Physics Letters*, 461 (1-3):114–117, 2008.

[178] K. Koren, G. Mistlberger, D. Aigner, S. Borisov, A. Zankel, P. Pölt, and I. Klimant. *Monatshefte für Chemie / Chemical Monthly*, In Press, 2010.

[179] G. Mistlberger, A. L. Medina-Castillo, J. F. Fernandez-Sanchez, A. Segura-Carretero, A. Fernandez-Gutierrez, and I. Klimant. *unpublished results*, 2010.

[180] S. M. Borisov, T. Mayr, G. Mistlberger, K. Waich, K. Koren, P. Chojnacki, and I. Klimant. *Talanta*, 79:1322–1330, 2009.

[181] P. Kumar and K. L. Mittal. *Handbook of microemulsion science and technology.* CRC Press, 1999.

[182] J. Guo, W. Yang, C. Wang, J. He, and J. Chen. *Chemistry of Materials*, 18(23): 5554–5562, 2006.

[183] J.-T. Kwon, S.-K. Hwang, H. Jin, D.-S. Kim, A. Mina-Tehrani, H.-J. Yoon, M. Chop, T.-J. Yoon, D.-Y. Han, Y.-W. Kang, B.-I. Yoon, J.-K. Lee, and M.-H. Cho. *Journal of Occupational Health*, 50(1):1–6, 2008.

[184] Y. K. Lee, R. Smith, and R. Kopelman. 2009.

[185] Y.-S. Lin, S.-H. Wu, Y. Hung, Y.-H. Chou, C. Chang, M.-L. Lin, C.-P. Tsai, and C.-Y. Mou. *Chemistry of Materials*, 18(22):5170–5172, 2006.

[186] S. Tu, M. Golden, P. Andreotti, L. Yu, and P. Irwin. *Journal of rapid methods and automation in microbiology*, 9(2):71–84, 2001.

[187] A. Fan, C. Lau, and J. Lu. *Analytical Chemistry*, 77(10):3238–3242, 2005.

[188] A. Scheffold, S. Miltenyi, and A. Radbruch. *Immunotechnology*, 1(2):127–137, 1995.

[189] K. Kim and J. Park. *Lab on a Chip*, 5(6):657–664, 2005.

[190] K. C. Ahn, P. Lohstroh, S. J. Gee, N. A. Gee, B. Lasley, and B. D. Hammock. *Analytical Chemistry*, 79(23):8883–8890, 2007.

[191] Y. Kwon, C. A. Hara, M. G. Knize, M. H. Hwang, K. S. Venkateswaran, E. K. Wheeler, P. M. Bell, R. F. Renzi, J. A. Fruetel, and C. G. Bailey. *Analytical Chemistry*, 80(22):8416–8423, 2008.

[192] W.-S. Chang, H. Shang, R. M. Perera, S.-m. Lok, D. Sedlak, R. J. Kuhn, and G. U. Lee. *Analyst*, 133(2):233–240, 2008.

[193] P. Hazarika, S. Jickells, K. Wolff, and D. Russell. *Angewandte Chemie*, 120(52): 10321–10324, 2008.

[194] E. P. Dupont, E. Labonne, C. Vandevyver, U. Lehmann, E. Charbon, and M. A. M. Gijs. *Analytical Chemistry*, 82(1):49–52, 2010.

[195] D. Dressman, H. Yan, G. Traverso, K. Kinzler, and B. Vogelstein. *Proceedings of the National Academy of Sciences of the United States of America*, 100(15):8817–8822, 2003.

[196] S. H. Lim, F. Bestvater, P. Buchy, S. Mardy, and A. D. C. Yu. *Sensors*, 9(7): 5590–5599, 2009.

[197] G. Wang, C. Wang, Q. Ma, and X. Su. *Journal of Nanoscience and Nanotechnology*, 10(3, Sp. Iss. SI):1956–1963, 2010.

[198] S. Borisov and I. Klimant. *Analytical Chemistry*, 79(19):7501–7509, 2007.

[199] T. Mayr, S. M. Borisov, T. Abel, B. Enko, K. Waich, G. Mistlberger, and I. Klimant. *Analytical Chemistry*, 81(15):6541–6545, 2009.

[200] E. Scheucher, G. Mistlberger, and I. Klimant. *AIP Conference Proceedings*, in preparation, 2010.

[201] J. N. Anker, C. Behrend, and R. Kopelman. *Journal of Applied Physics*, 93(10): 6698, 2003.

[202] M. Ettenauer, T. Posnicek, M. Brandl, V. Weber, and D. Falkenhagen. *Biomacromolecules*, 8(12):3693–3696, 2007.

[203] M. C. Frost and M. E. Meyerhoff. *Current Opinion in Chemical Biology*, 6(5): 633–641, 2002.

[204] X. Gao, L. Yang, J. Petros, F. Marshal, J. Simons, and S. Nie. *Current Opinion in Biotechnology*, 16(1):63–72, 2005.

[205] Y.-S. Yun, J. I. Park, and J. M. Park. *Process Biochemistry*, 40(3-4):1301–1306, 2005.

[206] M. Shinkai and A. Ito. *Advances in Biochemical Engineering / Biotechnology*, 91: 191–220, 2004.

[207] R. Y. Cheung, Y. Ying, A. M. Rauth, N. Marcon, and X. Y. Wu. *Biomaterials*, 26 (26):5375–5385, 2005.

[208] C. Grüttner and J. Teller. *Journal of Magnetism and Magnetic Materials*, 194(1): 8–15, 1999.

[209] M. A. M. Gijs. *Microfluidics and Nanofluidics*, 1(1):22–40, 2004.

[210] J. A. Ritter, A. D. Ebner, K. D. Daniel, and K. L. Stewart. *Journal of Magnetism and Magnetic Materials*, 280(2-3):184–201, 2004.

[211] G. Iacob, O. Rotariu, N. J. C. Strachan, and U. O. Häfeli. *Biorheology*, 41(5): 599–612, 2004.

[212] G. Friedman and B. Yellen. *Current Opinion in Colloid and Interface Science*, 10 (3-4):158–166, 2005.

[213] C. Hoffmann and M. Franzreb. *IEEE Transactions on Magnetics*, 40(2 I):456–461, 2004.

[214] C. Hoffmann and M. Franzreb. *IEEE Transactions on Magnetics*, 40(2 I):462–468, 2004.

[215] M. Takayasu, E. Maxwell, and D. Kelland. *IEEE Transactions on Magnetics*, 20(5): 1186–1188, 1984.

[216] D. C. Meeker. Finite element method magnetics, v3.2.4. http://femm.foster-miller.net, 2005.

[217] I. Klimant and O. Wolfbeis. *Analytical Chemistry*, 67(18):3160–3166, 1995.

[218] B. Valeur. *Molecular Fluorescence: Principles and Applications*. Wiley-VCH Verlag GmbH, Weinheim (Germany), 2001.

[219] M. Fitzgerald, D. B. Papkovsky, M. Smiddy, J. P. Kerry, C. K. O'Sullivan, D. J. Buckley, and G. G. Guilbault. *Journal of Food Science*, 66:105–110, 2001.

[220] W. Wang and P. Vadgama. *Journal of the Royal Society, Interface*, 1(1):109–117, 2004.

[221] X. Ge, Y. Kostov, and G. Rao. *Biosensors and Bioelectronics*, 18(7):857–865, 2003.

[222] L. Ramírez and K. Landfester. *Macromolecular Chemistry and Physics*, 204(1): 22–31, 2003.

[223] E. R. Carraway, J. N. Demas, B. A. DeGraff, and J. R. Bacon. *Analytical Chemistry*, 63(4):337–342, 1991.

[224] C. McDonagh, C. S. Burke, and B. D. MacCraith. *Chemical Reviews*, 108(2):400–422, 2008.

[225] O. S. Wolfbeis. *Analytical Chemistry*, 80(12):4269–4283, 2008.

[226] O. S. Wolfbeis. *Journal of Materials Chemistry*, 15(27-28):2657–2669, 2005.

[227] I. Klimant, M. Kuhl, R. Glud, and G. Holst. *Sensors and Actuators B: Chemical*, 38(1-3):29–37, 1997.

[228] S. Borisov, T. Mayr, and I. Klimant. *Analytical Chemistry*, 80(3):573–582, 2008.

[229] S. M. Borisov and I. Klimant. *Analyst*, 133(10):1302–1307, 2008.

[230] I. Klimant, F. Ruckruh, G. Liebsch, A. Stangelmayer, and O. Wolfbeis. *Mikrochimica Acta*, 131(1-2):35–46, 1999.

[231] J. Park, K. An, Y. Hwang, J.-G. Park, H.-J. Noh, J.-Y. Kim, J.-H. Park, N.-M. Hwang, and T. Hyeon. *Nature Materials*, 3:891–895, 2004.

[232] B. Sellergren. *Molecularly Imprinted Polymers, Volume 23: Man-Made Mimics of Antibodies and their Application in Analytical Chemistry*. Elsevier Science, 1 edition, 2001.

[233] F. H. Dickey. *Proceedings of the National Academy of Sciences of the United States of America*, 35(5):227–229, 1949.

[234] F. H. Dickey. *The Journal of Physical Chemistry*, 59(8):695–707, 1955.

[235] L. Pauling. *Journal of the American Chemical Society*, 62(10):2643–2657, 1940.

[236] A. Katz and M. E. Davis. *Nature*, 403(6767):286–289, 2000.

[237] A. Mayes and M. Whitcombe. *Advanced Drug Delivery Reviews*, 57(12):1742–1778, 2005.

[238] G. Masci, F. Aulenta, and V. Crescenzi. *Journal of Applied Polymer Science*, 83 (12):2660–2668, 2002.

[239] F. L. Dickert, H. Besenböck, and M. Tortschanoff. *Advanced Materials*, 10(2): 149–151, 1998.

[240] F. Dickert, P. Achatz, and K. Halikias. *Fresenius' Journal of Analytical Chemistry*, 371(1):11–15, 2001.

[241] N. Kirsch, J. P. Hart, D. J. Bird, R. W. Luxton, and D. V. McCalley. *The Analyst*, 126(11):1936–1941, 2001.

[242] I. Sánchez-Barragán, J. M. Costa-Fernández, R. Pereiro, A. Sanz-Medel, A. Salinas, A. Segura, A. Fernández-Gutiérrez, A. Ballesteros, and J. M. González. *Analytical Chemistry*, 77(21):7005–7011, 2005.

[243] A. Valero-Navarro, A. Salinas-Castillo, J. F. Fernandez-Sanchez, A. Segura-Carretero, R. Mallavia, and A. Fernandez-Gutierrez. *Biosensors and Bioelectronics*, 24(7): 2305–2311, 2009.

[244] X. Wang, X. Ding, Z. Zheng, X. Hu, X. Cheng, and Y. Peng. *Macromolecular Rapid Communications*, 27(14):1180–1184, 2006.

[245] Y. Zhang, R. Liu, Y. Hu, and G. Li. *Analytical Chemistry*, 81(3):967–976, 2009.

[246] W. Zheng, F. Gao, and H. Gu. *Journal of Magnetism and Magnetic Materials*, 288: 403–410, 2005.

[247] C. Baggiani, L. Anfossi, P. Baravalle, C. Giovannoli, and G. Giraudi. *Analytical and Bioanalytical Chemistry*, 389(2):413–422, 2007.

[248] F. Montagne, O. Mondain-Monval, C. Pichot, and A. Elaïssari. *Journal of Polymer Science Part A: Polymer Chemistry*, 44(8):2642–2656, 2006.

[249] J. Berg, D. Sundberg, and B. Kronberg. *Journal of Microencapsulation: Micro and Nano Carriers*, 6(3):327, 1989.

[250] Y. Chen, V. Dimonie, and M. S. El-Aasser. *Journal of Applied Polymer Science*, 42 (4):1049–1063, 1991.

[251] T. Gong, D. Yang, J. Hu, W. Yang, C. Wang, and J. Q. Lu. *Colloids and Surfaces A: Physicochemical and Engineering Aspects*, 339(1-3):232–239, 2009.

[252] G. Odian. *Principles of Polymerization*. John Wiley & Sons, Inc., Hoboken, NJ, USA, 2004.

[253] X. Liu, Y. Guan, Z. Ma, and H. Liu. *Langmuir*, 20(23):10278–10282, 2004.

[254] J. Ugelstad, L. Söderberg, A. Berge, and J. Bergström. *Nature*, 303(5912):95–96, 1983.

[255] H. Xu, L. Cui, N. Tong, and H. Gu. *Journal of the American Chemical Society*, 128 (49):15582–15583, 2006.

[256] A. L. Medina-Castillo, J. F. Fernandez-Sanchez, A. Segura-Carretero, and A. Fernandez-Gutierrez. *Biosensors and Bioelectronics*, 25(2):442–449, 2009.

[257] M. Jaroniec and R. Madey. *Physical Adsorption on Heterogeneous Solids*. Elsevier Publishing Company, 1988.

[258] R. J. Umpleby, S. C. Baxter, M. Bode, J. K. Berch, R. N. Shah, and K. D. Shimizu. *Analytica Chimica Acta*, 435(1):35–42, 2001.

[259] E. Corton, J. García-Calzón, and M. Díaz-García. *Journal of Non-Crystalline Solids*, 353(8-10):974–980, 2007.

[260] J. A. García-Calzón and M. E. Díaz-García. *Sensors and Actuators B: Chemical*, 123(2):1180–1194, 2007.

[261] A. M. Rampey, R. J. Umpleby, G. T. Rushton, J. C. Iseman, R. N. Shah, and K. D. Shimizu. *Analytical Chemistry*, 76(4):1123–1133, 2004.

[262] R. Sips. *The Journal of Chemical Physics*, 18(8):1024, 1950.

[263] D. A. Spivak. *Advanced Drug Delivery Reviews*, 57(12):1779–1794, 2005.

[264] D. B. Papkovsky. *Methods Enzymol.*, 381:715–735, 2004.

[265] T. C. O'Riordan, D. Buckley, V. Ogurtsov, R. O'Connor, and D. B. Papkovsky. *Analytical Biochemistry*, 278(2):221–227, 2000.

[266] F. G. Gao, J. M. Fay, G. Mathew, A. S. Jeevarajan, and M. M. Anderson. *Journal of Biomedical Optics*, 10(5):054005, 2005.

[267] T. Anderlei and J. Büchs. *Biochemical Engineering Journal*, 7(2):157–162, 2001.

[268] M. A. Hanson, X. Ge, Y. Kostov, K. A. Brorson, A. R. Moreira, and G. Rao. *Biotechnology and Bioengineering*, 97(4):833–841, 2007.

[269] L. Tolosa, Y. Kostov, P. Harms, and G. Rao. *Biotechnology and Bioengineering*, 80 (5):594–597, 2002.

[270] D. Weuster-Botz, R. Puskeiler, A. Kusterer, K. Kaufmann, G. John, and M. Arnold. *Bioprocess and Biosystems Engineering*, 28(2):109–119, 2005.

[271] C. Wittmann, H. M. Kim, G. John, and E. Heinzle. *Biotechnology Letters*, 25(5): 377–380, 2003.

[272] B. König, O. Kohls, G. Holst, R. Glud, and M. Kühl. *Marine Chemistry*, 97(3-4): 262–276, 2005.

[273] I. Klimant, V. Meyer, and M. Kuhl. *Limnology and Oceanography*, 40(6):1159–1165, 1995.

[274] S. M. Borisov, D. L. Herrod, and I. Klimant. *Sensors and Actuators B: Chemical*, 139(1):52–58, 2009.

[275] C. Borek, K. Hanson, P. Djurovich, M. Thompson, K. Aznavour, R. Bau, Y. Sun, S. Forrest, J. Brooks, L. Michalski, and J. Brown. *Angewandte Chemie, International Edition*, 46(7):1109–1112, 2007.

[276] J. R. Lakowicz, I. Gryczynski, and Z. Gryczynski. *Journal of Biomolecular Screening*, 5(3):123–132, 2000.

[277] C. Huber, I. Klimant, C. Krause, and O. S. Wolfbeis. *Analytical Chemistry*, 73(9): 2097–2103, 2001.

[278] E. Pines, D. Pines, Y.-Z. Ma, and G. R. Fleming. *ChemPhysChem*, 5(9):1315–1327, 2004.

[279] Y.-E. Koo, Y. Cao, R. Kopelman, S. Koo, M. Brasuel, and M. Philbert. *Analytical Chemistry*, 76(9):2498–2505, 2004.

[280] F. C. O'Mahony, C. O'Donovan, J. Hynes, T. Moore, J. Davenport, and D. B. Papkovsky. *Environmental Science and Technology*, 39(13):5010–5014, 2005.

[281] S. M. Borisov and O. S. Wolfbeis. *Chemical Reviews*, 108(2):423–461, 2008.

[282] H. Xu, J. W. Aylott, R. Kopelman, T. J. Miller, and M. A. Philbert. *Analytical Chemistry*, 73(17):4124–4133, 2001.

[283] J. W. Aylott. *Analyst*, 128(4):309–312, 2003.

[284] S. Giri, B. G. Trewyn, M. P. Stellmaker, and V. S.-Y. Lin. *Angewandte Chemie International Edition in English*, 44(32):5038–5044, 2005.

[285] A. P. Herrera, M. Rodriguez, M. Torres-Lugo, and C. Rinaldi. *Journal of Materials Chemistry*, 18(8):855–858, 2008.

[286] Y. Deng, C. Deng, D. Yang, C. Wang, S. Fu, and X. Zhang. *Chemical Communications (Cambridge, United Kingdom)*, pages 5548–5550, 2005.

[287] J. S. Kim, W. J. Rieter, K. M. L. Taylor, H. An, W. Lin, and W. Lin. *Journal of the American Chemical Society*, 129(29):8962–8963, 2007.

[288] J. Rao, A. Dragulescu-Andrasi, and H. Yao. *Current Opinion in Biotechnology*, 18 (1):17–25, 2007.

[289] X. Ji, R. Shao, A. Elliott, R. Stafford, E. Esparza-Coss, J. Bankson, G. Liang, Z.-P. Luo, K. Park, J. Markert, and C. Li. *The Journal of Physical Chemistry C*, 111(17): 6245–6251, 2007.

[290] J. Kim, S. Park, J. E. Lee, S. M. Jin, J. H. Lee, I. S. Lee, I. Yang, J.-S. Kim, S. K. Kim, M.-H. Cho, and T. Hyeon. *Angewandte Chemie International Edition in English*, 45(46):7754–7758, 2006.

[291] Y. Cao, Y. E. Koo, and R. Kopelman. *Analyst*, 129(8):745–750, 2004.

[292] P. J. Cywinski, A. J. Moro, S. E. Stanca, C. Biskup, and G. J. Mohr. *Sensors and Actuators B: Chemical*, 135(2):472–477, 2009.

[293] T. Doussineau, M. Smaihi, and G. J. Mohr. *Advanced Functional Materials*, 19(1): 117–122, 2009.

[294] R. Kopelman and R. Tjalkens. *Analytical Chemistry*, 71(21):4837–4843, 1999.

[295] K. Waich, T. Mayr, and I. Klimant. *Talanta*, 77(1):66–72, 2008.

[296] K. Wygladacz, Y. Qin, W. Wroblewski, and E. Bakker. *Analytica Chimica Acta*, 614(1):77–84, 2008.

[297] C. Xu, K. Wygladacz, R. Retter, M. Bell, and E. Bakker. *Analytical Chemistry*, 79 (24):9505–9512, 2007.

[298] G. Zenkl, T. Mayr, and I. Klimant. *Macromolecular Bioscience*, 8(2):146–152, 2008.

[299] M. Kettering, J. Winter, M. Zeisberger, S. Bremer-Streck, H. Oehring, C. Bergemann, C. Alexiou, R. Hergt, K. J. Halbhuber, W. A. Kaiser, and I. Hilger. *Nanotechnology*, (17):175101, 2007.

[300] N. Nasongkla, E. Bey, J. Ren, H. Ai, C. Khemtong, J. S. Guthi, S.-F. Chin, A. D. Sherry, D. A. Boothman, and J. Gao. *Nano Letters*, 6(11):2427–2430, 2006.

[301] W. S. Seo, J. H. Lee, X. Sun, Y. Suzuki, D. Mann, Z. Liu, M. Terashima, P. C. Yang, M. V. McConnell, D. G. Nishimura, and H. Dai. *Nature Materials*, 5(12): 971–976, 2006.

[302] V. Bychkova and A. Shvarev. *Analytical Chemistry*, 81(6):2325–2331, 2009.

[303] J. M. Kürner, I. Klimant, C. Krause, H. Preu, W. Kunz, and O. S. Wolfbeis. *Bioconjugate Chemistry*, 12(6):883–889, 2001.

[304] A. Pfister, G. Zhang, J. Zareno, A. F. Horwitz, and C. L. Fraser. *ACS Nano*, 2(6): 1252–1258, 2008.

[305] Z. Grabarek and J. Gergely. *Analytical Biochemistry*, 185(1):131–135, 1990.

[306] G. Sokrates. *Infrared characteristic Group Frequencies*. John Wiley & Sons, Chichester, 2nd edition, 1998.

[307] M. Babincova, V. Altanerova, C. Altaner, P. Cicmanec, and P. Babinec. *Medical Physics*, 31(8):2219–2221, 2004.

[308] M. De, P. S. Ghosh, and V. M. Rotello. *Advanced Materials*, 20(9999):1–17, 2008.

[309] C. Dennis, A. Jackson, J. Borchers, R. Ivkov, A. Foreman, P. Hoopes, R. Strawbridge, Z. Pierce, E. Goerntiz, J. Lau, and C. Gruettner. *Journal of Physics D: Applied Physics*, 41(13):134020, 2008.

[310] D.-H. Kim, D. Nikles, D. Johnson, and C. Brazel. *Journal of Magnetism and Magnetic Materials*, 320(19):2390–2396, 2008.

[311] C.-W. Lu, Y. Hung, J.-K. Hsiao, M. Yao, T.-H. Chung, Y.-S. Lin, S.-H. Wu, S.-C. Hsu, H.-M. Liu, C.-Y. Mou, C.-S. Yang, D.-M. Huang, and Y.-C. Chen. *Nano Letters*, 7(1):149–154, 2007.

[312] Z. Medarova, W. Pham, C. Farrar, V. Petkova, and A. Moore. *Nature Medicine*, 13 (3):372–377, 2007.

[313] J. Motoyama, T. Hakata, R. Kato, N. Yamashita, T. Morino, T. Kobayashi, and H. Honda. *BioMagnetic Research and Technology*, 6(1):4, 2008.

[314] C. Sun, J. S. Lee, and M. Zhang. *Advanced Drug Delivery Reviews*, 60(11):1252–1265, 2008.

[315] D.-L. Zhao, X.-W. Zeng, Q.-S. Xia, and J.-T. Tang. *Journal of Alloys and Compounds*, 469(1-2):215–218, 2009.

[316] A. L. Medina-Castillo, G. Mistlberger, J. F. Fernandez-Sanchez, A. Segura-Carretero, I. Klimant, and A. Fernandez-Gutierrez. *Macromolecules*, 43(1):55–61, 2010.

[317] S. Borisov, G. Nuss, W. Haas, R. Saf, M. Schmuck, and I. Klimant. *Journal of Photochemistry and Photobiology, A: Chemistry*, 201(2-3):128–135, 2009.

[318] N. Rubio, F. Prat, N. Bou, J. I. Borrell, J. Teixido, A. Villanueva, A. Juarranz, M. Canete, J. C. Stockert, and S. Nonell. *New Journal of Chemistry*, 29(2):378–384, 2005.

[319] F. Wilkinson, W. P. Helman, and A. B. Ross. *Journal of Physical and Chemical Reference Data*, 22(1):113–262, 1993.

[320] Z. M. Rzaev, S. Dincer, and E. Piskin. *Progress in Polymer Science*, 32(5):534–595, 2007.

[321] D. Schmaljohann. *Advanced Drug Delivery Reviews*, 58(15):1655–1670, 2006.

[322] M. Hans and A. Lowman. *Current Opinion in Solid State and Materials Science*, 6 (4):319–327, 2002.

[323] W. Wan, L. Yang, and D. Padavan. *Nanomedicine*, 2(4):483–509, 2007.

[324] O. Finikova, A. Cheprakov, I. Beletskaya, P. Carroll, and S. Vinogradov. *Journal of Organic Chemistry*, 69(2):522–535, 2004.

[325] I. Kraljic and S. E. Mohsni. *Photochemistry and Photobiology*, 28(4-5):577–581, 1978.